Spatial and Temporal Protein Oxidation and Redox Signaling in Mechanisms of Structural Birth Defects

by

Samantha Lapehn

A dissertation submitted in partial fulfillment
of the requirements for the degree of
Doctor of Philosophy
(Toxicology)
in The University of Michigan
2021

Doctoral Committee:

Professor Emeritus Craig Harris, Co-Chair
Professor Yoichi Osawa, Co-Chair
Assistant Professor Justin A. Colacino
Professor Alexey Nesvizhskii
Professor Emeritus Rudy J. Richardson

Samantha Lapehn
slapehn@umich.edu
ORCID iD: 0000-0001-6299-7633

DEDICATION

To Mom, Dad, Allison, and Dillon

ACKNOWLEDGMENTS

There are many people that I would like to thank for their help and encouragement throughout my time at the University of Michigan. Firstly, I would like to thank my advisor, Dr. Craig Harris, whose guidance in planning my experiments, improving my writing, and supporting my research interests has been critical to my success. I would also like to thank Dr. Harris for pushing me outside my comfort zone in trying new experimental techniques and helping me to persevere through the steep learning curve of my proteomics research. I would also like to thank my dissertation committee, Dr. Yoichi Osawa, Dr. Rudy Richardson, Dr. Justin Colacino, and Dr. Alexey Nesvizhskii for their guidance and suggestions that have helped me to greatly improve the analysis and communication of my research findings. I am also grateful to my undergraduate research advisor, Dr. Motoko Mukai, for developing my research skills and inspiring my interest in Toxicology and Environmental Health Sciences.

I would like to acknowledge former Harris Lab members, Andrea Cruz, Joseph Skulsky, Kristen Ball, Cole Zingas, and Makenzie Zima for technical assistance in completing some of the experiments included in Chapter 2. In addition, I wish to recognize our collaborators from the Hansen Lab at Brigham Young University, specifically Dr. Jason Hansen and Ted Piorczynski who provided experimental and analytical assistance of the PCR and western blotting work. The

Proteomics Resource Facility at University of Michigan has been an invaluable resource to me in navigating my proteomics experiments. I am very thankful for the support from Dr. Venky Basrur and Kevin Conlon for performing LC-MS/MS and protein identification for my data. Dr. Justin Colacino and Dr. Alexey Nesvizhskii have also provided extensive guidance in analyzing my proteomics data. This work would not have been possible without the support of the administrative staff of the EHS department. I would specifically like to thank Cecilia Young and Sue Crawford for their assistance in navigating my time in EHS.

I have several funding sources to acknowledge for their support in funding my dissertation research and providing financial support for my studies at University of Michigan. These sources include: the Environmental Epidemiology and Toxicology Program Training Grant (NIH T32 ES007062), Rackham Student Research Grants (Pre-Candidate & Candidate), CEW+ Riecker Graduate Student Research Fund, Rackham One-Term Dissertation Writing Fellowship, and Dr. Craig Harris‘s faculty grant through the University of Michigan Office of Research (UMOR).

The support of my family and friends has been essential to my success at University of Michigan. I would specifically like to thank my parents, Laura & Richard, my sister, Allison, and my fiancé, Dillon. Thank you for always believing in me and supporting my goals. I could not have accomplished any of this without your love and support.

TABLE OF CONTENTS

LIST OF TABLES

LIST OF FIGURES

LIST OF ABBREVIATIONS

AF- amniotic fluid
ANOVA- analysis of variance
CE- convergent extension
Ctl- control
Cys- cysteine
CySS- cystine
D3T- 1, 2-dithiole-3-thione
EEF- extra embryonic fluid
EMB- embryo proper
FDR- false discovery rate
GABA- gamma aminobutyric acid
GD- gestational day
GO- gene ontology
GSEA- gene set enrichment analysis
GSH- glutathione
GSSG- glutathione disulfide
HDAC- histone deacetylase
Hr- hour
HPLC- high performance liquid chromatography
IodoTMT- iodoacetyl tandem mass tags
LC-MS/MS- liquid chromatography, tandem mass spectrometry
LC-MS^3- liquid chromatography, multinotch MS3 mass spectrometry
MEHP- mono ethyl hexyl phthalate
Nrf2- nuclear factor erythroid 2–related factor 2
NTC- neural tube closure
NTD- neural tube defect
PCR- polymerase chain reaction
PCP- planar cell polarity
PTM- post-translational modification
Redox- reduction-oxidation
RT-qPCR- reverse transcriptase quantitative polymerase chain reaction
TBHQ- tert-butylhydroquinone
TF- transcription factor
TMT- tandem mass tags
TOR- target of rapomycin
VPA- valproic acid
YSF- yolk sac fluid
VYS- visceral yolk sac

ABSTRACT

Neural tube defects (NTDs) are birth defects that arise from failed neural tube closure resulting in morphological abnormality of the brain and spinal cord. NTD risk has been associated with genetic mutations, a maternal diet low in folic acid, as well as gestational exposure to anti-epileptic medications such as valproic acid (VPA). Though VPA exposure during pregnancy has been associated with a 20-fold increase in the risk of NTDs, there is not an accepted mechanism for VPA-induced NTDs. The reduction-oxidation (redox) environment is a critical component of development with evidence to suggest that redox signaling at the cellular and protein level is a key factor in developmental progression. VPA exposure has previously been associated with several biomarkers of oxidation leading to the hypothesis that VPA may act through a redox-regulated mechanism to cause NTDs. The objective of this dissertation was to identify spatial and temporal redox mechanisms of VPA teratogenesis across the period of early organogenesis in the CD-1 mouse conceptus. This was accomplished by carrying out three aims designed to identify changes in cellular redox potential, reversible oxidative post-translational modifications (PTMs) of proteins, and protein abundance that may be implicated in failed neural tube closure.

Aim 1 evaluated the cellular redox environment through measurement of the glutathione (GSH) and cysteine (Cys) redox couples in four distinct compartments of the mouse conceptus over 24 hours of organogenesis following VPA exposure. This analysis demonstrated that VPA's actions as a cellular oxidant are not universal, but are, instead, specific to time and tissue. Aim 2

utilized a systems biology proteomics approach to assess changes in the developmental mouse proteome in terms of protein oxidation and protein abundance. Measurement of whole conceptus reversible oxidative PTMs at Cys residues indicated that VPA causes an initial decrease in Cys-oxidation compared to the control with an increase in oxidation building over time. Several target pathways relevant to nervous system development, cell polarity, and cytoskeletal organization were identified as being differentially oxidized after VPA exposure. Tissue-specific assessment of protein abundance following VPA exposure identified divergent patterns of temporal sensitivity to VPA between the visceral yolk sac (VYS) and embryo (EMB). It also identified time and tissue-specific patterns of alterations in development and oxidation-reduction pathways including differentiation, growth, and Wnt signaling. Aim 3 integrated the data from previous chapters to construct a timeline of mechanistic VPA perturbation events. This timeline highlighted the time and tissue specific recurrence of developmentally relevant pathways such as differentiation, growth, Wnt signaling, cell polarity, and nervous system development that are likely to have mechanistic roles in VPA teratogenesis.

Overall, this dissertation has significantly increased the breadth of knowledge related to VPA-associated redox and developmental events across mouse organogenesis. It demonstrated that both the temporality of sampling and exposure length exert meaningful effects on outcomes related to redox and protein abundance, thereby emphasizing the importance of time course evaluation of developmental toxicants. Tissue specific compartmentalization of protein oxidation-associated perturbations of developmental pathways and their related protein abundance demonstrate an important role for the VYS during early neurulation and in specific neurulation/developmental pathways throughout organogenesis. Future studies should build on

these results to analyze VPA's effects at the cell, tissue, and organ levels by focusing on the role of specific oxidative PTMs on protein form and function as it relates to neural tube closure.

Chapter 1

Introduction

Overview

The link between gestational exposure to anti-epileptic medication, valproic acid (VPA) and neural tube defects (NTDs) is well established. However, the molecular mechanisms through which these defects arise is still not understood. Progression of development is known to be dependent on and reactive to changes in the reduction and oxidation (redox) environment over time. VPA has been shown to cause an increase in the production of cellular reactive oxygen species (ROS), thus, altering the redox environment and leading to the hypothesis that VPA's mechanism of action in causing NTDs may be through disruption of the embryonic redox balance through an increase in production of ROS (Tung & Winn, 2011). Confirmation of increased cellular oxidation and determination of the magnitude of damage is often measured *indirectly* through changes in concentrations of ROS, antioxidants (oxidized and reduced ratios), their precursors, lipid peroxidation byproducts, and a myriad of other means (Cipak Gasparovic et al., 2017; Sies et al., 2017). These methods are largely qualitative and far removed from the actual mechanistic pathways but are often used as the sole basis for making the assessment that any given chemical or environmental insult is causing its effects through "oxidative stress" (Costantini, 2019; Jones, 2006). Recent advances in the quantitation of the most prevalent cellular antioxidants such as GSH/GSSG and Cys/CySS have improved the ability to determine

and quantify changes in cellular redox states, likely through increased production of ROS, by using their respective half-cell redox potentials as a means of comparison (Jones, 2006; Schafer & Buettner, 2001). The ultimate determination of oxidation as a causative factor in mechanisms of toxicity cannot be made through indirect means and require specific molecular and global measures of cellular oxidation. Spatial identification of specific oxidized proteins (oxidative post-translational modifications (PTMs)) within their respective mechanistic pathways will be necessary to supply the burden of proof necessary to confirm the mechanistic involvement of ROS. The objective of this dissertation is to explore VPA's role as an oxidant across the period of neural tube closure (NTC) during mouse organogenesis. To accomplish this goal, a systems biology-based framework was utilized to evaluate the hypothesis that VPA will increase cellular oxidation across this time period and produce tissue specific patterns of cellular oxidation alongside specific oxidative PTMs that may be involved in VPA's disruption of the NTC pathway.

Neural Tube Defects

NTDs comprise a group of birth defects that result from failed neural tube closure (NTC) during early organogenesis and cause malformations to the brain and spinal cord. In the United States, NTDs affect approximately 3000 pregnancies each year with higher incidence globally (CDC, 2004; Seidahmed et al., 2014; Zaganjor et al., 2016). NTDs range in severity depending on the timing and location of the failed closure along the developing neural tube (Juriloff & Harris, 2018; Nakatsu et al., 2000). NTDs that affect brain development such as anencephaly are the most serious and life threatening with high levels of perinatal mortality, while those conditions that affect the spine such as spina bifida can result in a survivable, but serious handicap with average associated lifetime healthcare costs of approximately $800,000 in 2014

(Copp & Greene, 2010; Grosse et al., 2016). The cause of NTDs is multifactorial and complex with several known risk factors including genetic predisposition, prenatal folic acid consumption, maternal hyperglycemia, hyperthermia, and chemical exposure, including the use of certain anti-epileptic medications during pregnancy (De Marco et al., 2011).

Neurulation is the developmental process of creating the central nervous system which occurs through two distinct phases. Phase one consists of primary neurulation and involves the establishment of the neural plate, elevation, and closure of the neural tube, which will later develop into the brain and spinal cord. The second phase of neurulation is an internal process of condensation and epithelialization that forms the medullary cord and notochord (Copp et al., 2013; Nikolopoulou et al., 2017). In mice, neural tube closure (NTC) takes place over the course of gestational days (GD) 8 and 9 with closure in humans occurring during early organogenesis at 3-4 weeks post-fertilization (Copp et al., 2013; Sakai, 1989). The molecular mechanisms of NTC are primarily driven by the non-canonical Wnt/PCP gene pathway which is highly conserved in vertebrates with secondary mechanisms being orchestrated by up to 300 additional related genes (Nikolopoulou et al., 2017). The primary role of PCP in neurulation is in establishing directional asymmetries and tissue organization of the neural epithelium that allows designated cells to migrate and change shape to assist in the bending and folding of the neural plate (Figure 1-1) (Butler & Wallingford, 2017). The PCP pathway generates force for cellular movement through contraction of mediolateral cellular junctions with intercalation of cells guided by actin protrusions (Figure 1-1a) (Butler & Wallingford, 2017). This mechanism has specifically been noted in neural epithelia where anteroposterior junctions are transformed into mediolateral junctions through sequential resolution and elongation (Figure 1-1b) (Butler & Wallingford, 2017). NTC is accomplished through convergent extension (CE), where the two sides of the open

neural tube converge and fuse to form a closed tube (Figure 1-2) (Blom et al., 2006). Mutation of the core PCP pathway genes has been shown to result in abnormal NTC through affecting the process of CE in a variety of vertebrate species emphasizing the importance of these genes for development (Nikolopoulou et al., 2017). Fusion of the neural tube through CE takes place at several locations along the embryonic mid-line with points of closure including caudal, forebrain, midbrain, and hindbrain (Copp et al., 2013). The timing, location, and developmental stage as indicated by somite number for mouse NTC are illustrated in Figure 1-3 (Sakai, 1989). Different mouse strains, as well as different species exhibit unique sequences and patterns of neural tube fusion.

There is substantial evidence of genetic influences on NTD outcomes. When one sibling has an NTD condition, there is a 2-5% chance that other siblings will be affected which is much higher than levels in the general population and provides evidence for a genetic component to NTD development (Copp & Greene, 2010; Rampersaud et al., 2006). Evidence supporting a possible genetic cause for NTDs has led to extensive studies to determine genes associated with NTD occurrence leading to identification of over 200 genes whose mutations lead to NTDs in mice with confirmation of several of these associations in humans (Copp & Greene, 2010; De Marco et al., 2011). Due to the large number of NTD associated mutations and genes, it is believed that the genetic cause of NTDs is largely multifactorial and depends on the presence or absence of several individual genetic factors. Additionally, there continue to be diagnoses of NTDs where there is no known familial history or observed genetic cause, highlighting the importance of understanding the non-genetic risk factors for NTD occurrence and their use in prevention of NTD occurrence.

Prenatal folic acid consumption has been a successful primary prevention method for NTDs in the United States that has been recommended since the early 1990's (Junod, 2001). While first limited to women considered high risk due to previous NTD-affected pregnancies, the recommendation for prenatal folic acid supplementation is now universal to all women of childbearing age. To promote equitable access to folic acid supplementation, the Food and Drug Administration (FDA) approved the fortification of certain grain products in 1998 (Crider et al., 2011; Junod, 2001; Werler et al., 1993; Willett, 1992). A study of the U.S. prevalence of two NTD conditions, spina bifida and anencephaly, from the pre-folic acid fortification period of 1995-1996 to the mandatory folic acid fortification period of late 1998-1999 demonstrated that spina bifida prevalence decreased by 31% and anencephaly prevalence decreased by 16% (Williams et al., 2002). These observations supported the use of folic acid fortification for the successful prevention of NTDs. Following the success of folic acid fortification in the United States, similar recommendations and fortification efforts have been established in other countries (Crider et al., 2011; Zaganjor et al., 2016).

The number of infants born with NTDs in the United States has been in a steady decline due to folic acid fortification, improving pre-natal diagnostic capabilities including *in utero* surgeries, and the understanding of the link between anti-epileptics such as valproic acid (VPA) and NTD outcomes (Sutton, 2008). However, NTDs are still prevalent in countries without high quality pre-natal care and a diet high in folic acid (Blencowe et al., 2018). Additionally, due to the closure of the neural tube occurring within the first month of pregnancy, women who take VPA that are experiencing either an unplanned pregnancy or cannot reduce or eliminate their use of the medication due to the risks of their underlying seizure disorder are still at risk of having an infant affected by a costly and debilitating NTD condition. It is therefore critical that a

mechanism of action for VPA's teratogenicity be determined in order to aid in the prevention of this type of birth defect for women of childbearing age.

Valproic Acid

Valproic acid (VPA) is a short-chain fatty acid that is most commonly used as an anti-seizure medication (Figure 1-4). Although VPA's original intended use was as an anti-convulsant, there continues to be new research describing additional therapeutic uses for VPA including the treatment of conditions such as bipolar disorder, cancer, and HIV, among others (Chateauvieux et al., 2010). VPA's widening utility as a therapeutic, however, also exposes a greater number of people to its many side effects, the most well-known being liver toxicity and increased risk of NTDs following gestational exposure (Jentink et al., 2010; Ornoy, 2009). The teratogenicity of VPA was first predicted following a case study in 1979 of a pregnant patient who began taking VPA during their third trimester. This study demonstrated VPA's ability to cross the placenta and be present in the infant's bloodstream after birth (Dickinson et al., 1979). Following this case report, there were several noted instances of gestational VPA exposure that led to morphological abnormalities associated with NTDs (Dalens et al., 1980; Gomez, 1981; Robert, 1983). It is now well established that taking VPA during pregnancy, especially during the sensitive time period of organogenesis during the first trimester increases the risk of having an infant with a NTD (Jentink et al., 2010; Ornoy, 2009). In a review of eight cohort studies of first trimester exposure to VPA with birth dates ranging from 1972 to 2005, NTD malformation rates of exposed infants ranged from 6.2 to 17.4% of births with a significant increase in malformation rates compared to unexposed controls for six NTD related conditions (Jentink et al., 2010).

Despite the frequent, widespread use of VPA as a therapeutic agent and its known, dangerous side effects, VPA's mechanism of action is not well understood (Zhu et al., 2017). Dosing of VPA varies widely across patient populations due to the lack of a known correlation between dose and plasma concentration which for therapeutic purposes should fall between 50-100 μg/mL (Zhu et al., 2017). VPA is metabolized by the liver through three main pathways including glucuronidation, ß-oxidation, and the cytochrome P450 pathway with the two former serving as the primary metabolic routes (Zhu et al., 2017). To date, there are three established mechanisms of VPA action including acting as a histone de-acetylase (HDAC) inhibitor, increasing γ-aminobutyric acid (GABA) levels, and blocking voltage-gated ion channels, none of which can be directly linked to mechanisms of birth defects (Ghodke-Puranik et al., 2013; Phiel et al., 2001).

Histones are proteins that are wrapped with DNA to maintain chromosome compaction. Post-translational modification (PTM) of histone proteins controls the tightness of DNA winding and the level of transcriptional activity of the wrapped DNA (Park & Kim, 2020). Acetylation of histone proteins unwind chromatin DNA to a relaxed state that is available for transcription. Histone de-acetylases (HDACs) remove the acetyl moiety and thereby maintain chromatin in its condensed form reducing access for transcription (Park & Kim, 2020). As an HDAC inhibitor, VPA is capable of preventing de-acetylation and thereby promoting gene expression. There are four classes of HDAC inhibitors with classes I, II, and IV being zinc-dependent and class III being NAD+ dependent (Hull et al., 2016). VPA inhibits class I HDACs which include HDAC1, HDAC2, HDAC3, and HDAC8 (Göttlicher et al., 2001; Park & Kim, 2020). In addition to inhibition of class I HDAC activity, VPA has also been shown to specifically degrade HDAC2

(Kramer, 2003). HDAC inhibitors are frequently investigated for use as anti-cancer therapeutics due to the ability to maintain target gene expression levels (Park & Kim, 2020).

GABA is an inhibitory neurotransmitter that is increased with exposure to VPA in a biphasic manner (Biggs et al., 1992). GABA has been associated with inhibition of neurological disorders related to neurodegeneration, cognitive impairment, memory loss, neuronal responses, memory, and depression (Ngo & Vo, 2019). In addition to increasing GABA levels, VPA is also known to increase responses of the GABA-A and GABA-B receptors (Romoli et al., 2019). VPA acts on ion-gated channels through reducing high frequency firing in some sodium, potassium and calcium channels (Romoli et al., 2019). A combination of all three of these mechanisms is likely responsible for VPA's anti-epileptic properties, however it's unknown how these mechanisms may contribute to VPA's teratogenicity.

Redox Balance and Development

Reduction and oxidation (redox) are essential cellular mechanisms for maintaining homeostasis, cellular signaling, and responding to distress cues during development and throughout the lifespan. When external oxidants, such as VPA, disrupt the homeostatic redox balance of a system, there can be physiological consequences if antioxidant prevention mechanisms are unable to react sufficiently to the insult with enough force. While the concept of "oxidative stress" is often used as a catchall term to describe any disruption to the cellular redox system, there are actually many components of the cellular redox system that can be affected through independent mechanisms underlining the importance of specificity in studying and describing redox events (Sies et al., 2017).

The Keap1/Nrf2 antioxidant pathway is one of the first lines of defense for the cell following insult by external oxidants. Nrf2 is an oxidation responsive transcription factor that

resides in a protein-protein interaction with Keap1 in the cytoplasm. Under homeostatic conditions where Keap1 exists in a reduced state, Nrf2 is continuously ubiquitinated and subsequently degraded (Tonelli et al., 2018). Following detection of oxidation through Keap1's reactive cysteine sites, Nrf2 is translocated to the nucleus where it binds to the antioxidant response element (ARE) and induces the transcription of genes that play a role in GSH biosynthesis, thioredoxin activity, and NADPH regulation (Tonelli et al., 2018). Despite VPA's association with increased cellular oxidation it does not induce the Nrf2 antioxidant pathway (Palsamy et al., 2014). 1,2-dithiole-3-thione (D3T) is an inducer of the Nrf2 antioxidant pathway that can act as a modulator of antioxidant status (Figure 1-5) (Dong et al., 2008). D3T has previously been demonstrated to function as an antioxidant, anti-teratogenic compound against ethanol by reducing ROS generation and apoptosis in a mouse model of fetal alcohol spectrum disorders (Dong et al., 2008). *In utero* exposure to D3T prior to VPA treatment has also shown promise in reducing birth defect outcomes through reducing the number of offspring affected by NTDs from 58% to 5.5% in CD-1 mice (Piorczynski et al., Under Review). Evidence of lower VPA-induced NTD outcomes following D3T exposure adds to the growing body of evidence that cites increased markers of oxidation in NTD cases and following VPA exposure, indicating that VPA's mechanism of action in preventing NTC may be through oxidation at the cellular or protein level.

Glutathione (GSH) is the most abundant cellular antioxidant making it an essential part of the cellular antioxidant defense system (Figure 1-6). GSH is a tripeptide comprised of cysteine (Cys), glutamic acid (Glu), and glycine (Gly). GSH's cysteine thiol group (-SH) grants its reducing power through donating electrons and forming a self-dimer to convert to GSH's oxidized counterpart, glutathione disulfide (GSSG) (Kalinina et al., 2014). The concentration of

cellular glutathione can be used to calculate its redox potential (E_h), a measure of the ratio of GSH:GSSG calculated through the Nernst equation, $E_h = E_0 + (\frac{RT}{nF}) \ln (\frac{[GSH]^2}{[GSSG]})$. Glutathione's abundance and critical role in redox homeostasis makes its E_h a reliable metric to understand the oxidation balance of a particular tissue or cell type following oxidation events (Harris & Hansen, 2012). GSH's other mechanism of action prevents oxidation through the process of S-glutathionylation which involves post-translational modification of protein Cys residues by binding GSH to prevent further irreversible oxidation and degradation of the protein (Grek et al., 2013).

As a precursor of GSH synthesis, Cys concentrations and redox potential of the Cys-Cystine (CySS) redox couple can complement GSH measurements in understanding cellular redox dynamics. Cys residues are redox active due to the thiol group and can be reversibly oxidized to sulfenic (-SOH) or sulfinic acid ($-SO_2H$), or irreversibly oxidized to sulfonic ($-SO_3H$) acid as a post-translational protein modification (Go et al., 2015) (Figure 1-6). Cysteines are commonly found in conserved locations of functional importance to proteins including active sites, transporters, receptors, protein-protein interfaces, and RNA/DNA binding sites. It is therefore predicted that the oxidation states of cysteines could act as regulatory signals by cycling through oxidation states in response to environmental cues (Go et al., 2015). Selective oxidation of specific cysteine residues has, for example, been shown to lead to direct cellular events with the evidence suggesting that oxidation of Cys 139 and Cys 147 on the cytoskeletal protein cofilin leads to activation of the protein triggering apoptotic signaling and that oxidation of Cys 50 on peroxiredoxin redirects H_2O_2 detoxification to other antioxidant systems (Go et al., 2015). Oxidation of Cys 377 on catalase, an antioxidant enzyme that reduces H_2O_2, has been shown to decrease its enzyme activity potentially leading to further oxidation due to decreased

ability to reduce H_2O_2 (Ghosh et al., 2006). These examples demonstrate the importance of understanding redox dynamics not only from a more global cellular perspective, but also at the proteome and individual protein level to evaluate the mechanism and effects of increased oxidation in a particular system.

The *Redox Theory of Development* explains the need for tight regulation of oxygen concentrations throughout embryonic development to support proper progression of developmental events for morphological and physiological function (Figure 1-8) (Hansen et al., 2020). It also supports the notion that conclusions of "oxidative stress" should be more carefully defined to specify affected oxidation targets and their functional downstream consequences such as the effects of post-translational protein modifications on physiological function (Hansen et al., 2020). Between the time periods of blastocyst implantation into the uterine wall through development and functioning of the placenta, development takes place under hypoxic conditions with oxygen concentrations less than 2% (15 mmHg) to support the totipotent state of the early embryo as differentiation and organogenesis take place (Hansen et al., 2020). Disruption of the hypoxic embryonic environment during this time can therefore lead to oxidative damage with the capacity to affect morphological development. Fluctuations in developmental GSH:GSSG E_h have been linked to developmental progression by acting as a "molecular switch" where a highly reduced E_h supports cellular proliferation with increasing levels of E_h oxidation leading to differentiation, apoptosis, and eventually necrosis (Figure 1-9) (Schafer & Buettner, 2001). The necessity of the first three of these processes, proliferation, differentiation, and apoptosis, to development suggests that fluctuations in the GSH:GSSG E_h are essential for development and that not all oxidation events should be viewed as aberrant. The importance of redox homeostasis to development has been further supported by the association of many teratogenic compounds

including thalidomide, nicotine, and paraquat with imbalances in developmental redox homeostasis (Hansen, 2006). It is possible, therefore that the link between gestational VPA exposure and NTDs may also be linked to disruption of developmental redox homeostasis.

Valproic Acid and Redox

In addition to other well-established mechanistic hypotheses for VPA, there is also evidence that VPA affects the redox balance of cells and tissues. For example, it has been hypothesized that some of VPA's hepatotoxic effects may be linked to its ability to increase cellular oxidation through increases in the measurement of ROS, cellular glutathione, lipid peroxidation, and DNA oxidation (Chang & Abbott, 2006). VPA has also been shown to inhibit the actions of the transcription factor, nuclear factor erythroid-2 related factor 2 (Nrf2) following oxidative insult which can exacerbate the effects of oxidative damage by blocking the activation of downstream Nrf2 antioxidant pathways (Palsamy et al., 2014). Epidemiological evidence of VPA's oxidative capabilities demonstrates that obese children with epilepsy that are treated with VPA show increased markers of lipid peroxidation and decreased Vitamin E antioxidant levels (Verrotti et al., 2008). There is also more limited, conflicting research that portrays VPA as an antioxidant in rodent models of sepsis and in human neuroblastoma cell co-treated with other oxidants (Cui et al., 2007; Lai et al., 2006; Liu et al., 2014; Shi et al., 2019). Together this body of research demonstrates that there is strong evidence that VPA affects redox balance. However, it is not yet clear why there is conflicting evidence regarding the increased or decreased direction of VPA's oxidative manipulations and whether this apparent dichotomy may be related to specific factors such as dose, exposure length, age, species, or tissue.

Redox and Proteomics

Proteomics is the study of proteins at a systems level. The advantage of discovery-based shotgun proteomics is that multiple hypotheses can be tested and generated from a single experiment rather than individually investigating single hypotheses. Protein identification is most commonly completed through liquid chromatography followed by tandem mass spectrometry (LC-MS/MS) with protein identification determined through software that matches peptides against a species-specific protein database. While the most straightforward use of proteomics is simply in noting the presence of specific proteins in a sample, advancements to the field have allowed for relative protein quantitation and even identification of specific post-translational modifications (PTMs) to specific amino acids. Identification of PTMs can be especially helpful in the field of toxicology to understand how a toxicant exposure modifies the proteome compared to the control state.

Tandem Mass Tags (TMT) are sets of proteomic labels that are amine reactive for use in global proteome identification. Labeling consists of tagging each experimental group with a specific TMT label. Each label is of isobaric mass to allow for simultaneous elution in liquid chromatography, but also contains a unique reporter and balancing group to allow for differentiation of samples through mass spectrometry (McAlister et al., 2012; Thompson et al., 2003). Abundance values of each unique reporter mass can then be used to calculate a ratio relative to a control experimental group to determine relative abundance of proteins across experimental treatments.

The technology of TMT labeling has also been modified to allow for identification of reversible oxidative cysteine PTMs, as Iodoacetyl TMT (IodoTMT). In IodoTMT labeling, the standard TMT tag is modified with an iodoacetyl group that is reactive to cysteine thiols (-SH)

(Shakir et al., 2017). Through sequential labeling and reduction steps, it is possible to label reduced cysteine thiols followed by formerly oxidized cysteine thiols. The abundance values of these experimental groups that are identified through LC-MS/MS identification of the unique reporter group can be used to calculate the percent oxidation of a given protein.

While IodoTMT labels are able to quantitatively identify reversible cysteine oxidation, it is unable to differentiate across species of oxidative cysteine PTMs (Figure 1-7). Several other proteomic labeling procedures have been developed for this purpose with protein identification through a combination of western blotting and LC-MS/MS. Some of these other labeling strategies include dimedone or DCP-Bio1 for sulfenic acid labeling and biotinylated glutathione ethyl ester (BioGEE) for S-glutathionylation detection (Klomsiri et al., 2010; Pople & Chalker, 2021).

The Mouse Conceptus as a Developmental Model

While many teratogens are first noted through epidemiological studies of human populations following evidence of birth defects, it is preferred that these compounds are eliminated from potential use through pre-approval teratogenicity screens in animal models. Segment II teratogenicity screens are considered the gold standard in the United States, but are very costly to complete due to the requirement for use of multiple species and dose groups (Webster et al., 1997). Whole embryo culture (WEC) is therefore an excellent tool for use as a preliminary assessment that can test potentially teratogenic agents and visualize morphological differences without the high costs and heavy usage of animals required for a full segment II screening (New, 1978; Webster et al., 1997). Additionally, WEC can be useful for evaluations of mechanisms of action for known teratogens. In WEC methods, mouse embryos can be cultured from GD 8-10 encompassing the highly dynamic period of early organogenesis. A host of

morphological and physiological events occur during this time period that can be visualized through light microscopy including NTC, limb bud development, otic vesicle and optic cup formation, axial rotation, and heartbeat activation with yolk sac circulation (Harris, 2012). WEC is most commonly used as a form of *in vitro* chemical screening with chemical agents being dosed directly in the culture serum; however, these techniques can also be used following *in vivo* gestational exposures to monitor morphological and physiological changes in real time.

In addition to the practical benefits of using mouse WEC to study birth defect endpoints, mouse conceptus dissection also allows for separate assessment of distinct developmental tissues and compartments including the visceral yolk sac (VYS), embryo proper (EMB), yolk sac fluid (YSF), and amniotic fluid (AF) (Figure 1-10) (Jilek et al., 2015). While many teratogenic studies focus exclusively on morphological and biochemical changes in the embryo proper, the other tissue and fluid compartments are equally important for development and can also be affected by teratogenic exposures (Beckman et al., 1990). The visceral yolk sac (VYS) is a tissue of embryonic origin that encases the amniotic sac and embryo proper. The purpose of the VYS during early development is to provide the embryo proper with nutrients through histiotrophic uptake prior to the formation and function of the placenta which carries out hemotrophic nutrition (Jollie, 1990). The VYS accomplishes this through its three primary functions of digestion, absorption and distribution of nutrients to the embryo proper (Jollie, 1990; Lloyd et al., 1998). Disturbance of these VYS functions by teratogen exposure during early development can therefore disrupt embryonic development due to decreased nutrient uptake which can result in morphological birth defects (Jollie, 1990; Lloyd et al., 1998). The essential role of the VYS during early development and its potential to be targeted by teratogen exposure makes it imperative that its role not be ignored or conflated with the embryo proper during study of the

organogenesis-stage mouse conceptus. Separately evaluating mouse conceptal tissue and fluid compartments can therefore be a meaningful way to understand the spatial dynamics of morphological, physiological, and biochemical processes of organogenesis. In this dissertation, mouse WEC will be a critical technique used to study the mechanism of VPA teratogenesis, allowing for easy sampling of separate conceptal tissue and fluids components over time.

Specific Aims

The summarized research suggests that early periods of development, including NTC, show sensitivity to oxidation that could be responsible for VPA induced NTDs. To determine a mechanism of VPA induced NTDs, spatial and temporal redox profiles of control and perturbed neurulation in CD-1 mouse conceptuses will be combined with a proteomics analysis of oxidative protein modifications and protein abundance. This strategy is designed to identify specific proteins and pathways affected by VPA with respect to oxidation state or abundance across time and space. These data will then be used develop mechanistic hypotheses for VPA induced NTD formation. **These studies will elucidate the role of protein oxidation and redox environment on NTDs in a mouse embryo model, where it is hypothesized that VPA increases generation of ROS and disrupts cellular redox balance. These changes in turn lead to specific oxidative post-translational protein modifications that result in alterations in pathways critical to neurulation**. These goals will be accomplished through the following specific aims:

Aim 1: Characterize the spatial, temporal, and stage-specific redox status of early, mid- and late neurulation in control and treated gestational day (GD) 8-9 mouse conceptuses.

- Conceptuses will be exposed to VPA and redox modulator, D3T, over the course of neurulation for measurement of redox active thiol concentrations in fluids and tissues.
- Hypothesis: VPA exposure will cause increased oxidation across all tissues and fluids with D3T co-treatment fully or partially alleviating these effects.

Aim 2: Identify redox sensitive pathways and specific redox active proteins associated with neural tube defect formation in response to VPA treatment during GD 8-9 in mouse embryo and visceral yolk sac tissue and in whole mouse conceptuses.

- Redox-proteomic label, IodoTMT (reversible Cys oxidation) and quantitative-proteomic label, TMT, will be measured by LC-MS/MS to identify conceptal protein abundance and oxidation as affected by VPA treatment across early organogenesis.
- Hypothesis: VPA exposure will lead to select changes in oxidative post-translational modifications and protein abundance that may be involved in NTD formation.

Aim 3: Develop an integrative omics analysis incorporating data on protein quantity and redox modifications across developmental time and space.

- Identify key proteins in the VPA mechanistic pathway through integrating proteomic data measuring protein oxidation and protein abundance with measures of cellular redox across time and space and develop a timeline of VPA's perturbation events across early organogenesis.
- Hypothesis: Developing an integrative omics analysis will aid in identifying key proteins and oxidation events related to VPA's mechanism of action during early development.

Figures

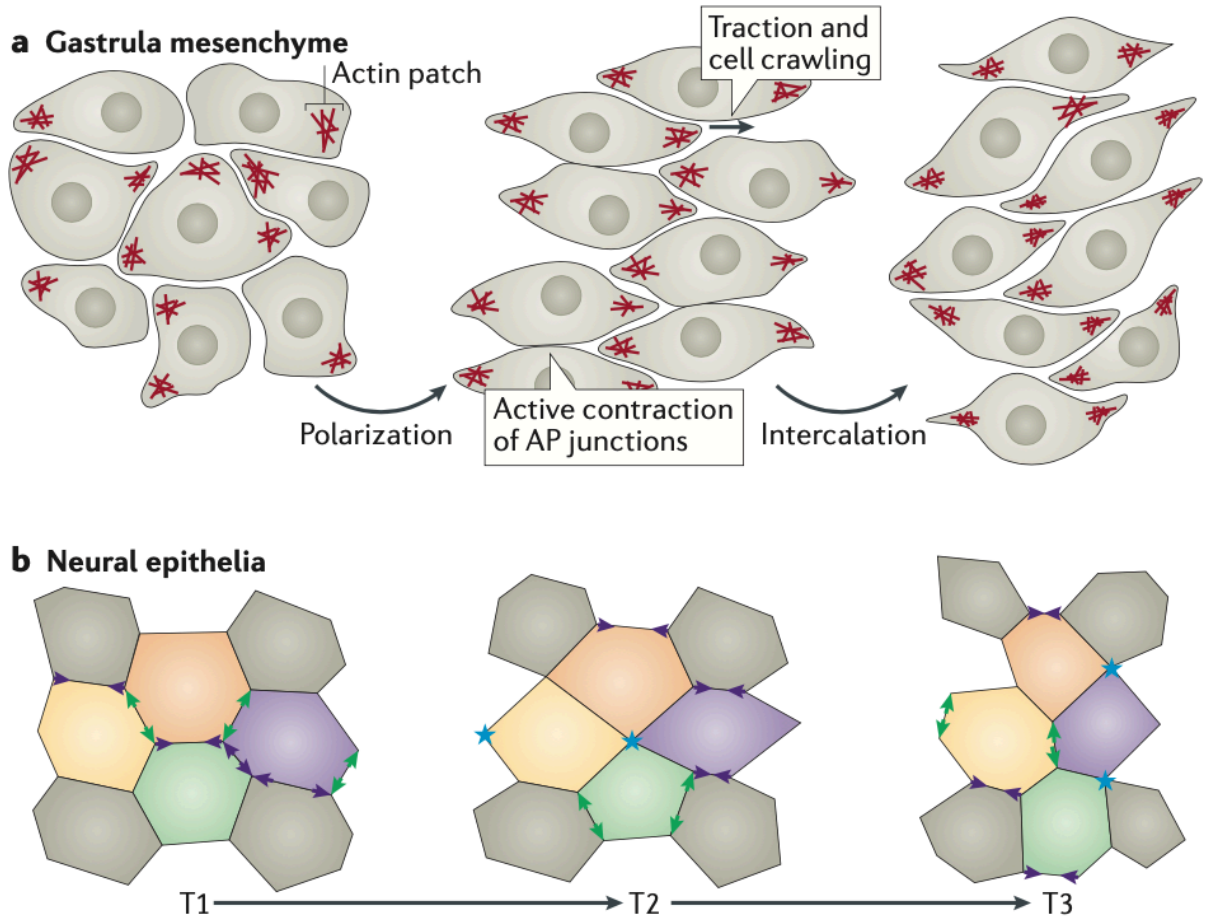

Figure 1-1 Role of the PCP pathway in neurulation: (Butler & Wallingford, 2017)- The planar cell polarity (PCP) pathway establishes cellular asymmetries which is important for developmental tissue organization including the convergent extension process of neurulation. a: The PCP pathway drives cellular intercalation through contraction of mediolateral junctions and movement through actin cell protrusions. b: Intercalation of the neural epithelia moves through transition phases (T1-T3) with a sequence of anteroposterior junction resolution followed by mediolateral junction elongation. Reprinted by permission from Springer Nature: Nature Reviews Molecular Cell Biology. "Planar cell polarity in development and disease" Butler M.T. & Wallingford J.B., Copyright 2017. License Number: 4991081071034.

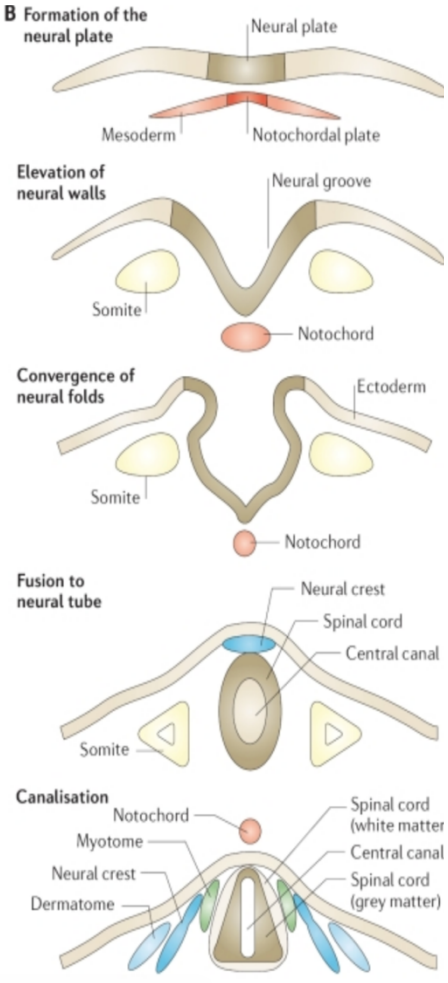

Figure 1-2 Primary and secondary neurulation: (Blom et al. 2006)- Neurulation consists of two stages: primary and secondary. Primary neurulation consists of Neural Tube Closure (NTC) which occurs through the process of convergent extension (CE) involving the formation and elevation of the neural plate to fold, converge, and fuse into the neural tube. Secondary neurulation involves the internal processes of forming the notochord and the medullary cord/secondary neural tube which develop into the spine (Blom et al., 2006; Nikolopoulou et al., 2017). Reprinted by permission from Springer Nature: Nature Reviews Neuroscience. "Neural tube defects and folate: case far from closed," Blom H.J., Shaw G. M., den Heijer M., & Finnell R. H. Copyright 2006. License Number: 4991090843938.

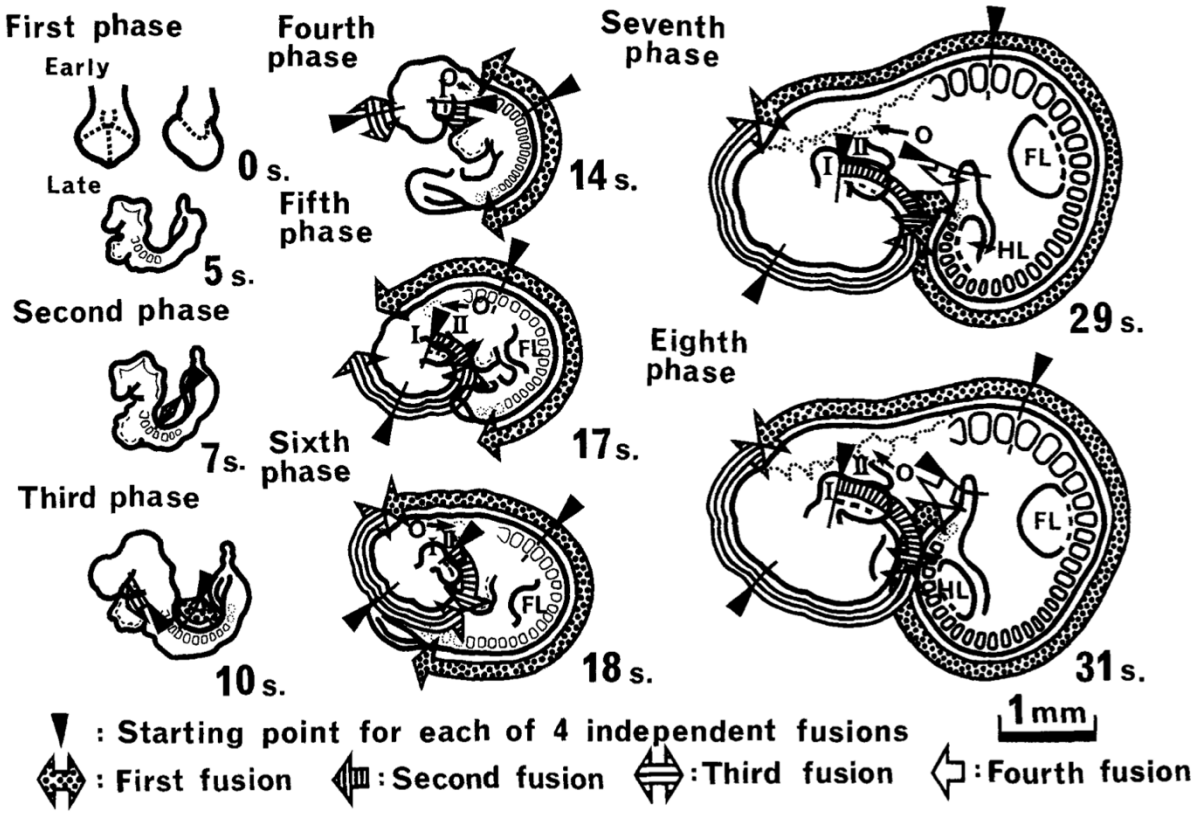

Figure 1-3 Fusion points of mouse neural tube closure: (Sakai, 1989)- Mouse neural tube closure (NTC) occurs from gestational days (GDs) 8-9 and involves coordinated closure at 4 points along the embryonic mid-line. This figure illustrates the direction and sequence of NTC alongside developmental timing indicated through mouse somite number (Sakai, 1989). Reprinted by permission from John Wiley and Sons: The Anatomical Record: Advances in Integrative Anatomy and Evolutionary Biology. "Neurulation in the mouse: Manner and timing of neural tube closure," Yoshio S. Copyright 2005. License Number: 4991091096852.

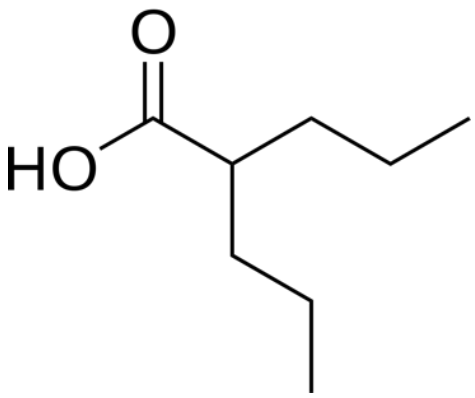

Figure 1-4 Chemical structure of valproic acid (VPA): Structure of anti-epileptic medication, valproic acid. When taken during pregnancy, VPA increases the risk of neural tube defects (NTDs) in exposed offspring.

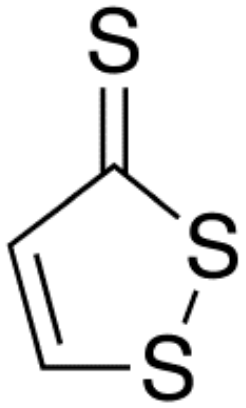

Figure 1-5 Chemical structure of 1,2-dithiole-3-thione: Structure of 1,2-dithiole-3-thione (D3T), a chemotherapeutic agent and known inducer of the Nrf2 antioxidant pathway will be utilized alongside VPA to manipulate the mouse conceptal redox environment.

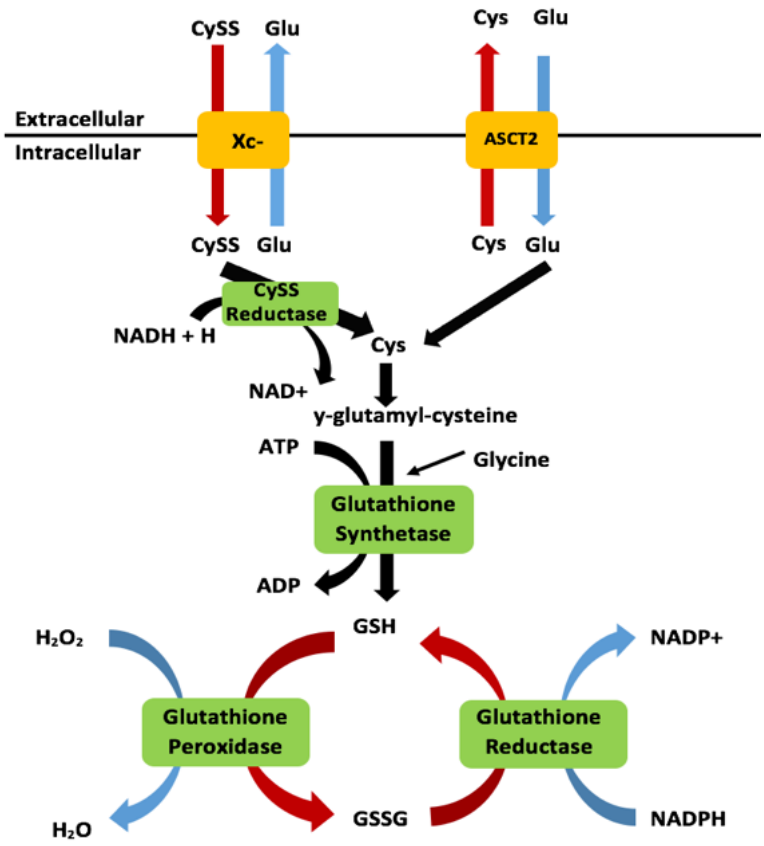

Figure 1-6 Glutathione synthesis and redox cycle: Glutathione (GSH) is an antioxidant tripeptide consisting of cysteine, glycine, and glutamic acid. The enzyme glutathione synthetase is responsible for its synthesis. GSH's antioxidant properties are derived from its ability to cycle between its reduced state of GSH to its oxidized self-dimerized counterpart glutathione disulfide (GSSG). The GSH redox cycle is controlled by enzymes glutathione peroxidase and glutathione reductase.

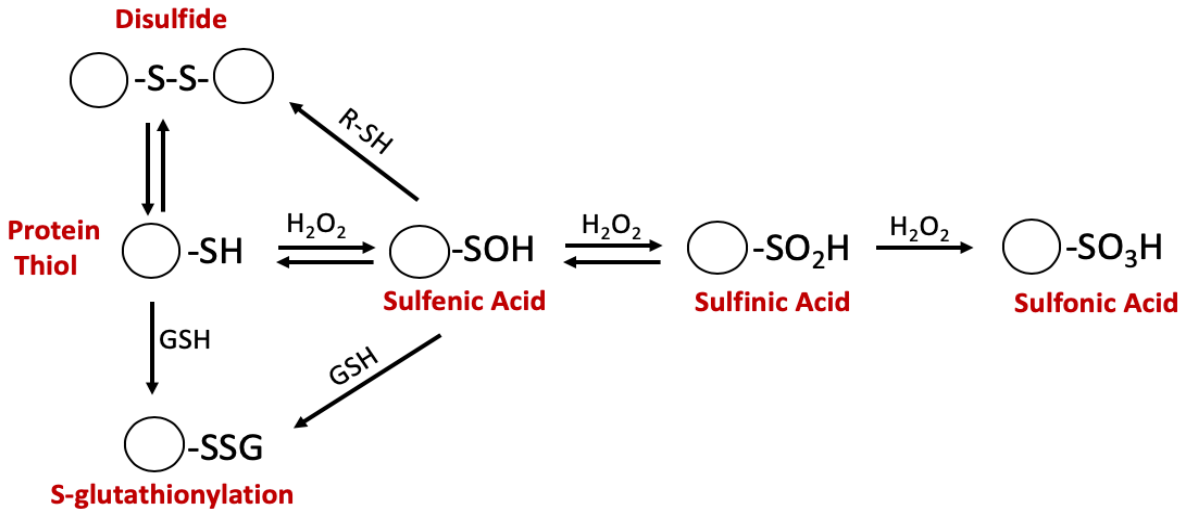

Figure 1-7 Oxidative modifications of cysteine sulfhydryl groups: The sulfhydryl (-SH) group on Cys residues is highly reactive to oxidation and can exist in several reversible and irreversible states. Reversible cysteine modifications, especially sulfenic acid and s-glutathionylation, are hypothesized to act as cellular signaling mechanisms.

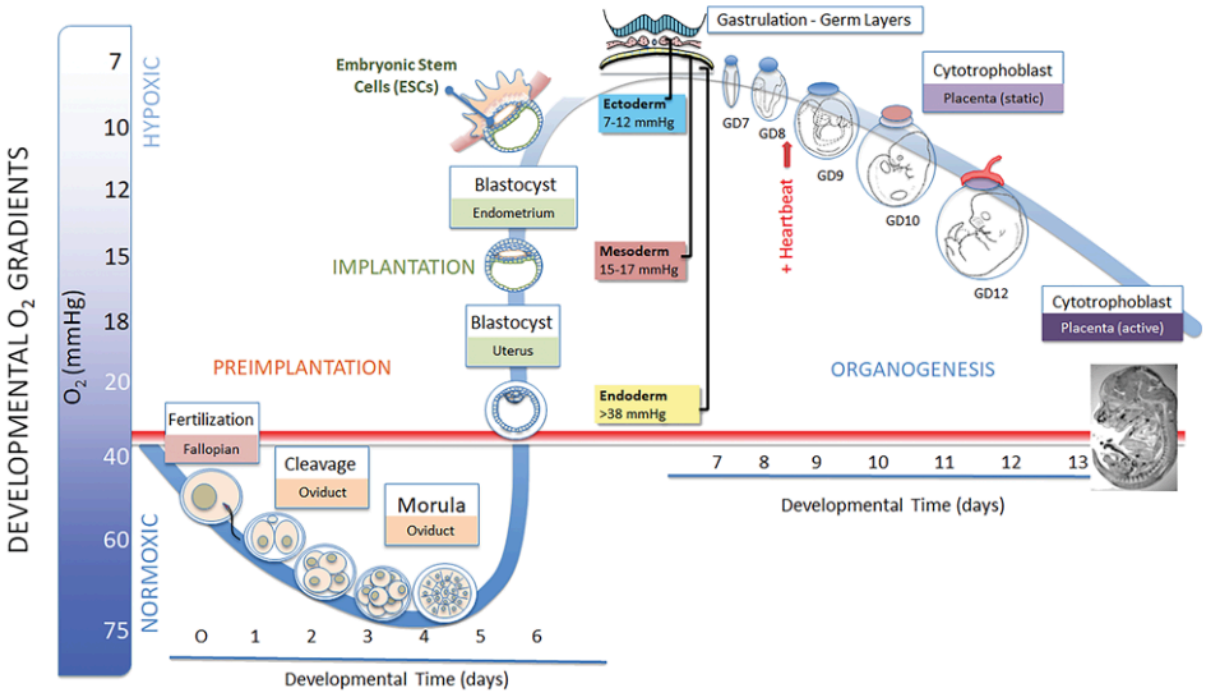

Figure 1-8 Oxygen gradients of early development: (Hansen et al., 2020)- The O_2 concentrations of early development are tightly regulated progressing from normoxic conditions preimplantation to highly hypoxic during the period of organogenesis. It is hypothesized that the hypoxic conditions of organogenesis make this time period particularly susceptible to oxidative insults that may result in structural birth defects. Reprinted by permission from: Mary Ann Liebert Inc.: Antioxidants & Redox Signaling. "The Redox Theory of Development" Hansen J.M., Jones D.P., Harris C. Copyright 2020.

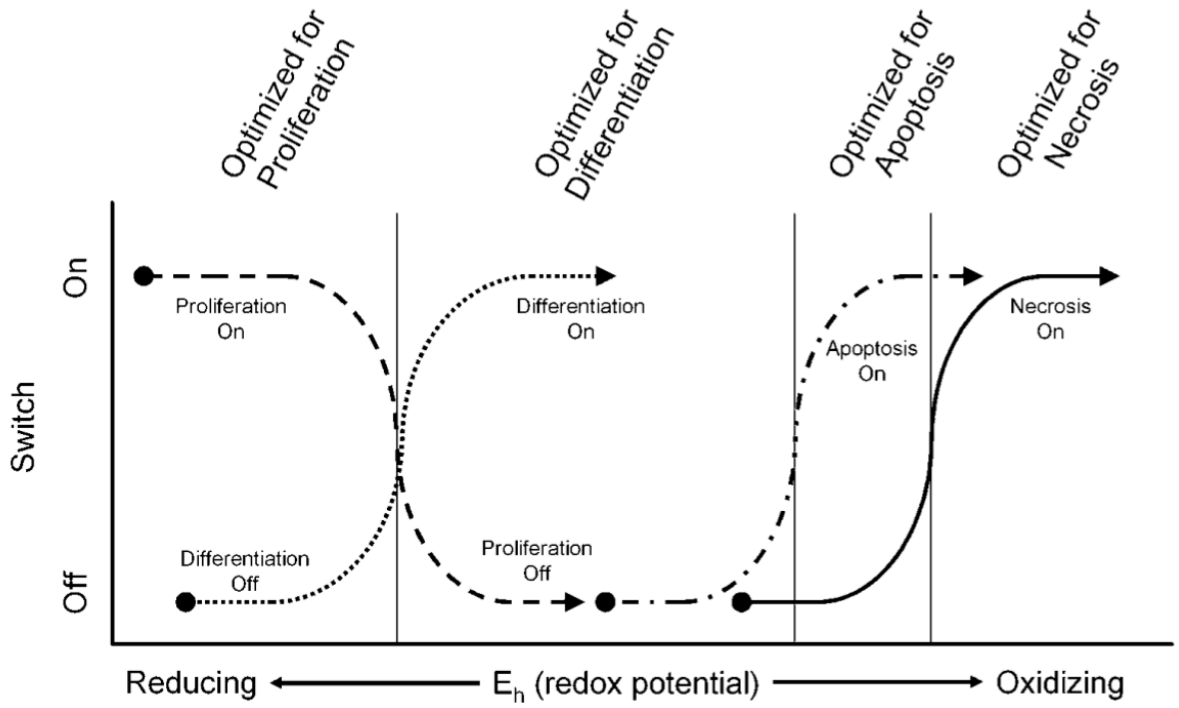

Figure 1-9 Glutathione redox potential as a redox signal: (Hansen, 2006)- The GSH:GSSG redox potential (E_h) acts as a "molecular switch" where a highly reduced E_h supports cellular proliferation with increasing levels of E_h oxidation leading to differentiation, apoptosis, and finally necrosis (Schafer & Buettner, 2001). Reprinted by permission from John Wiley and Sons: Birth Defects Research Part C: Embryo Today: Reviews "Oxidative stress as a mechanism of teratogenesis," Hansen J.M. Copyright 2007. License Number: 4991090433429.

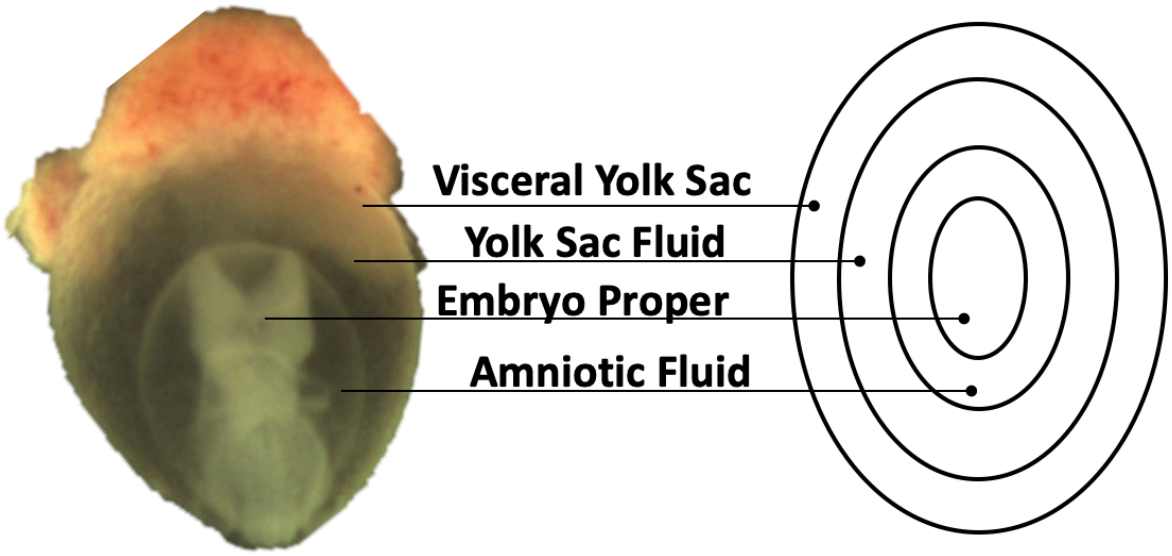

Figure 1-10 Compartmental anatomy of the GD 8 mouse conceptus: Compartments of a GD 8/9 mouse conceptus include the visceral yolk sac (VYS), embryo proper (EMB), yolk sac fluid (YSF), and amniotic fluid (AF). Individual assessment of these conceptal compartments can help evaluate spatial differences in the embryo.

References

Beckman, D. A., Koszalka, T. R., Jensen, M., & Brent, R. L. (1990). Experimental manipulation of the rodent visceral yolk sac. *Teratology*, *41*(4), 395–404. https://doi.org/10.1002/tera.1420410405

Biggs, C. S., Pearce, B. R., Fowler, L. J., & Whitton, P. S. (1992). The effect of sodium valproate on extracellular GABA and other amino acids in the rat ventral hippocampus: An in vivo microdialysis study. *Brain Research*, *594*(1), 138–142. https://doi.org/10.1016/0006-8993(92)91038-G

Blencowe, H., Kancherla, V., Moorthie, S., Darlison, M. W., & Modell, B. (2018). Estimates of global and regional prevalence of neural tube defects for 2015: A systematic analysis: Worldwide neural tube defects: estimates for 2015. *Annals of the New York Academy of Sciences*, *1414*(1), 31–46. https://doi.org/10.1111/nyas.13548

Blom, H. J., Shaw, G. M., den Heijer, M., & Finnell, R. H. (2006). Neural tube defects and folate: Case far from closed. *Nature Reviews Neuroscience*, *7*(9), 724–731. https://doi.org/10.1038/nrn1986

Butler, M. T., & Wallingford, J. B. (2017). Planar cell polarity in development and disease. *Nature Reviews Molecular Cell Biology*, *18*(6), 375–388. https://doi.org/10.1038/nrm.2017.11

CDC. (2004). Spina Bifida and Anencephaly Before and After Folic Acid Mandate—United States, 1995–1996 and 1999—2000. *MMWR*, *53*(17), 362–365.

Chang, T. K. H., & Abbott, F. S. (2006). Oxidative Stress as a Mechanism of Valproic Acid-Associated Hepatotoxicity. *Drug Metabolism Reviews*, *38*(4), 627–639. https://doi.org/10.1080/03602530600959433

Chateauvieux, S., Morceau, F., Dicato, M., & Diederich, M. (2010). Molecular and Therapeutic Potential and Toxicity of Valproic Acid. *Journal of Biomedicine and Biotechnology*, *2010*, 1–18. https://doi.org/10.1155/2010/479364

Cipak Gasparovic, A., Zarkovic, N., Zarkovic, K., Semen, K., Kaminskyy, D., Yelisyeyeva, O., & Bottari, S. P. (2017). Biomarkers of oxidative and nitro-oxidative stress: Conventional and novel approaches: Redox signalling and nitro-oxidative stress. *British Journal of Pharmacology*, *174*(12), 1771–1783. https://doi.org/10.1111/bph.13673

Copp, A. J., & Greene, N. D. (2010). Genetics and development of neural tube defects: Genetics and development of neural tube defects. *The Journal of Pathology*, *220*(2), 217–230. https://doi.org/10.1002/path.2643

Copp, A. J., Stanier, P., & Greene, N. D. E. (2013). Neural tube defects: Recent advances, unsolved questions, and controversies. *The Lancet. Neurology*, *12*(8), 799–810. https://doi.org/10.1016/S1474-4422(13)70110-8

Costantini, D. (2019). Understanding diversity in oxidative status and oxidative stress: The opportunities and challenges ahead. *The Journal of Experimental Biology*, *222*(13), jeb194688. https://doi.org/10.1242/jeb.194688

Crider, K. S., Bailey, L. B., & Berry, R. J. (2011). Folic Acid Food Fortification—Its History, Effect, Concerns, and Future Directions. *Nutrients*, *3*(3), 370–384. https://doi.org/10.3390/nu3030370

Cui, J., Shao, L., Young, L. T., & Wang, J.-F. (2007). Role of glutathione in neuroprotective effects of mood stabilizing drugs lithium and valproate. *Neuroscience*, *144*(4), 1447–1453. https://doi.org/10.1016/j.neuroscience.2006.11.010

Dalens, B., Raynaud, E.-J., & Gaulme, J. (1980). Teratogenicity of valproic acid. *The Journal of Pediatrics*, *97*(2), 332–333. https://doi.org/10.1016/S0022-3476(80)80517-8

De Marco, P., Merello, E., Cama, A., Kibar, Z., & Capra, V. (2011). Human neural tube defects: Genetic causes and prevention. *BioFactors*, *37*(4), 261–268. https://doi.org/10.1002/biof.170

Dickinson, R. G., Harland, R. C., Lynn, R. K., Smith, W. B., & Gerber, N. (1979). Transmission of valproic acid (Depakene) across theplacenta: Half-life of the drug in mother and baby. *The Journal of Pediatrics*, *94*(5), 832–835. https://doi.org/10.1016/S0022-3476(79)80172-9

Dong, J., Sulik, K. K., & Chen, S. (2008). Nrf2-Mediated Transcriptional Induction of Antioxidant Response in Mouse Embryos Exposed to Ethanol *in vivo*: Implications for the Prevention of Fetal Alcohol Spectrum Disorders. *Antioxidants & Redox Signaling*, *10*(12), 2023–2033. https://doi.org/10.1089/ars.2007.2019

Ghodke-Puranik, Y., Thorn, C. F., Lamba, J. K., Leeder, J. S., Song, W., Birnbaum, A. K., Altman, R. B., & Klein, T. E. (2013). Valproic acid pathway: Pharmacokinetics and pharmacodynamics. *Pharmacogenetics and Genomics*, *23*(4), 236–241. https://doi.org/10.1097/FPC.0b013e32835ea0b2

Ghosh, S., Janocha, A. J., Aronica, M. A., Swaidani, S., Comhair, S. A. A., Xu, W., Zheng, L., Kaveti, S., Kinter, M., Hazen, S. L., & Erzurum, S. C. (2006). Nitrotyrosine Proteome Survey in Asthma Identifies Oxidative Mechanism of Catalase Inactivation. *The Journal of Immunology*, *176*(9), 5587–5597. https://doi.org/10.4049/jimmunol.176.9.5587

Go, Y.-M., Chandler, J. D., & Jones, D. P. (2015). The cysteine proteome. *Free Radical Biology and Medicine*, *84*, 227–245. https://doi.org/10.1016/j.freeradbiomed.2015.03.022

Gomez, M. R. (1981). Possible teratogenicity of valproic acid. *The Journal of Pediatrics*, *98*(3), 508–509. https://doi.org/10.1016/S0022-3476(81)80743-3

Göttlicher, M., Minucci, S., Zhu, P., Krämer, O. H., Schimpf, A., Giavara, S., Sleeman, J. P., Lo Coco, F., Nervi, C., Pelicci, P. G., & Heinzel, T. (2001). Valproic acid defines a novel class of HDAC inhibitors inducing differentiation of transformed cells. *The EMBO Journal*, *20*(24), 6969–6978. https://doi.org/10.1093/emboj/20.24.6969

Grek, C. L., Zhang, J., Manevich, Y., Townsend, D. M., & Tew, K. D. (2013). Causes and Consequences of Cysteine *S* -Glutathionylation. *Journal of Biological Chemistry*, *288*(37), 26497–26504. https://doi.org/10.1074/jbc.R113.461368

Grosse, S. D., Berry, R. J., Mick Tilford, J., Kucik, J. E., & Waitzman, N. J. (2016). Retrospective Assessment of Cost Savings From Prevention. *American Journal of Preventive Medicine*, *50*(5), S74–S80. https://doi.org/10.1016/j.amepre.2015.10.012

Hansen, J. M. (2006). Oxidative stress as a mechanism of teratogenesis. *Birth Defects Research Part C: Embryo Today: Reviews*, *78*(4), 293–307. https://doi.org/10.1002/bdrc.20085

Hansen, J. M., Jones, D. P., & Harris, C. (2020). The Redox Theory of Development. *Antioxidants & Redox Signaling*, *32*(10), 715–740. https://doi.org/10.1089/ars.2019.7976

Harris, C. (2012). Rodent Whole Embryo Culture. In C. Harris & J. M. Hansen (Eds.), *Developmental Toxicology* (Vol. 889, pp. 215–237). Humana Press. https://doi.org/10.1007/978-1-61779-867-2_13

Harris, C., & Hansen, J. M. (2012). Oxidative Stress, Thiols, and Redox Profiles. In C. Harris & J. M. Hansen (Eds.), *Developmental Toxicology* (Vol. 889, pp. 325–346). Humana Press. https://doi.org/10.1007/978-1-61779-867-2_21

Hull, E. E., Montgomery, M. R., & Leyva, K. J. (2016). HDAC Inhibitors as Epigenetic Regulators of the Immune System: Impacts on Cancer Therapy and Inflammatory Diseases. *BioMed Research International*, *2016*, 8797206. https://doi.org/10.1155/2016/8797206

Jentink, J., Loane, M. A., Dolk, H., Barisic, I., Garne, E., Morris, J. K., & de Jong-van den Berg, L. T. W. (2010). Valproic Acid Monotherapy in Pregnancy and Major Congenital Malformations. *New England Journal of Medicine*, *362*(23), 2185–2193. https://doi.org/10.1056/NEJMoa0907328

Jilek, J. L., Sant, K. E., Cho, K. H., Reed, M. S., Pohl, J., Hansen, J. M., & Harris, C. (2015). Ethanol Attenuates Histiotrophic Nutrition Pathways and Alters the Intracellular Redox Environment and Thiol Proteome during Rat Organogenesis. *Toxicological Sciences*, *147*(2), 475–489. https://doi.org/10.1093/toxsci/kfv145

Jollie, W. P. (1990). Development, morphology, and function of the yolk-sac placenta of laboratory rodents. *Teratology*, *41*(4), 361–381. https://doi.org/10.1002/tera.1420410403

Jones, D. P. (2006). Redefining Oxidative Stress. *Antioxidants & Redox Signaling*, *8*(9–10), 1865–1879. https://doi.org/10.1089/ars.2006.8.1865

Junod, S. W. (2001). Folic Acid Fortification: Fact and Folly. *FDA Update*, *4, 5, 6*.

Juriloff, D., & Harris, M. (2018). Insights into the Etiology of Mammalian Neural Tube Closure Defects from Developmental, Genetic and Evolutionary Studies. *Journal of Developmental Biology*, *6*(3), 22. https://doi.org/10.3390/jdb6030022

Kalinina, E. V., Chernov, N. N., & Novichkova, M. D. (2014). Role of glutathione, glutathione transferase, and glutaredoxin in regulation of redox-dependent processes. *Biochemistry (Moscow)*, *79*(13), 1562–1583. https://doi.org/10.1134/S0006297914130082

Klomsiri, C., Nelson, K. J., Bechtold, E., Soito, L., Johnson, L. C., Lowther, W. T., Ryu, S.-E., King, S. B., Furdui, C. M., & Poole, L. B. (2010). Use of Dimedone-Based Chemical Probes for Sulfenic Acid Detection. In *Methods in Enzymology* (Vol. 473, pp. 77–94). Elsevier. https://doi.org/10.1016/S0076-6879(10)73003-2

Kramer, O. H. (2003). The histone deacetylase inhibitor valproic acid selectively induces proteasomal degradation of HDAC2. *The EMBO Journal*, *22*(13), 3411–3420. https://doi.org/10.1093/emboj/cdg315

Lai, J. S., Zhao, C., Warsh, J. J., & Li, P. P. (2006). Cytoprotection by lithium and valproate varies between cell types and cellular stresses. *European Journal of Pharmacology*, *539*(1–2), 18–26. https://doi.org/10.1016/j.ejphar.2006.03.076

Liu, Z., Li, Y., Chong, W., Deperalta, D. K., Duan, X., Liu, B., Halaweish, I., Zhou, P., & Alam, H. B. (2014). Creating a Prosurvival Phenotype Through a Histone Deacetylase Inhibitor in a Lethal Two-Hit Model: *Shock*, *41*(2), 104–108. https://doi.org/10.1097/SHK.0000000000000074

Lloyd, J. B., Beckman, D. A., & Brent, R. L. (1998). Nutritional role of the visceral yolk sac in organogenesis-stage rat embryos. *Reproductive Toxicology*, *12*(2), 193–195. https://doi.org/10.1016/S0890-6238(97)00148-2

McAlister, G. C., Huttlin, E. L., Haas, W., Ting, L., Jedrychowski, M. P., Rogers, J. C., Kuhn, K., Pike, I., Grothe, R. A., Blethrow, J. D., & Gygi, S. P. (2012). Increasing the Multiplexing Capacity of TMTs Using Reporter Ion Isotopologues with Isobaric Masses. *Analytical Chemistry*, *84*(17), 7469–7478. https://doi.org/10.1021/ac301572t

Nakatsu, T., Uwabe, C., & Shiota, K. (2000). Neural tube closure in humans initiates at multiple sites: Evidence from human embryos and implications for the pathogenesis of neural tube defects. *Anatomy and Embryology*, *201*(6), 455–466. https://doi.org/10.1007/s004290050332

New, D. A. T. (1978). WHOLE-EMBRYO CULTURE AND THE STUDY OF MAMMALIAN EMBRYOS DURING ORGANOGENESIS. *Biological Reviews*, *53*(1), 81–122. https://doi.org/10.1111/j.1469-185X.1978.tb00993.x

Ngo, D.-H., & Vo, T. S. (2019). An Updated Review on Pharmaceutical Properties of Gamma-Aminobutyric Acid. *Molecules*, *24*(15), 2678. https://doi.org/10.3390/molecules24152678

Nikolopoulou, E., Galea, G. L., Rolo, A., Greene, N. D. E., & Copp, A. J. (2017). Neural tube closure: Cellular, molecular and biomechanical mechanisms. *Development*, *144*(4), 552–566. https://doi.org/10.1242/dev.145904

Ornoy, A. (2009). Valproic acid in pregnancy: How much are we endangering the embryo and fetus? *Reproductive Toxicology*, *28*(1), 1–10. https://doi.org/10.1016/j.reprotox.2009.02.014

Palsamy, P., Bidasee, K. R., & Shinohara, T. (2014). Valproic acid suppresses Nrf2/Keap1 dependent antioxidant protection through induction of endoplasmic reticulum stress and Keap1 promoter DNA demethylation in human lens epithelial cells. *Experimental Eye Research*, *121*, 26–34. https://doi.org/10.1016/j.exer.2014.01.021

Park, S.-Y., & Kim, J.-S. (2020). A short guide to histone deacetylases including recent progress on class II enzymes. *Experimental & Molecular Medicine*, *52*(2), 204–212. https://doi.org/10.1038/s12276-020-0382-4

Phiel, C. J., Zhang, F., Huang, E. Y., Guenther, M. G., Lazar, M. A., & Klein, P. S. (2001). Histone Deacetylase Is a Direct Target of Valproic Acid, a Potent Anticonvulsant, Mood Stabilizer, and Teratogen. *Journal of Biological Chemistry*, *276*(39), 36734–36741. https://doi.org/10.1074/jbc.M101287200

Piorczynski, T.B., Lapehn, S., Ringer, K.P., Allen, S.A., Johnson, G.A., Call, K., Lucas, S.M., Harris, C., & Hansen, J.M. Inhibition of valproic acid-induced murine neural tube defects through Nrf2 signaling. *Under Review*

Pople, J. M. M., & Chalker, J. M. (2021). A critical evaluation of probes for cysteine sulfenic acid. *Current Opinion in Chemical Biology*, *60*, 55–65. https://doi.org/10.1016/j.cbpa.2020.07.011

Rampersaud, E., Melvin, E., & Speer, M. (2006). Nonsyndromic neural tube defects: Genetic basis and genetic investigations. In *Neural Tube Defects: From Origin to Treatment* (pp. 165–175). Oxford University Press.

Robert, E. (1983). Valproic Acid in Pregnancy-Association with Spina Bifida: A Preliminary Report. *Clinical Pediatrics*, *22*(5), 336–336. https://doi.org/10.1177/000992288302200502

Romoli, M., Mazzocchetti, P., D'Alonzo, R., Siliquini, S., Rinaldi, V. E., Verrotti, A., Calabresi, P., & Costa, C. (2019). Valproic Acid and Epilepsy: From Molecular Mechanisms to Clinical Evidences. *Current Neuropharmacology*, *17*(10), 926–946. https://doi.org/10.2174/1570159X17666181227165722

Sakai, Y. (1989). Neurulation in the mouse: Manner and timing of neural tube closure. *The Anatomical Record*, *223*(2), 194–203. https://doi.org/10.1002/ar.1092230212

Schafer, F. Q., & Buettner, G. R. (2001). Redox environment of the cell as viewed through the redox state of the glutathione disulfide/glutathione couple. *Free Radical Biology and Medicine*, *30*(11), 1191–1212. https://doi.org/10.1016/S0891-5849(01)00480-4

Seidahmed, M. Z., Abdelbasit, O. B., Shaheed, M. M., Alhussein, K. A., Miqdad, A. M., Khalil, M. I., Al-Enazy, N. M., & Salih, M. A. (2014). Epidemiology of neural tube defects. *Saudi Medical Journal*, *35 Suppl 1*, S29-35.

Shakir, S., Vinh, J., & Chiappetta, G. (2017). Quantitative analysis of the cysteine redoxome by iodoacetyl tandem mass tags. *Analytical and Bioanalytical Chemistry*, *409*(15), 3821–3830. https://doi.org/10.1007/s00216-017-0326-6

Shi, X., Liu, Y., Zhang, D., & Xiao, D. (2019). Valproic acid attenuates sepsis-induced myocardial dysfunction in rats by accelerating autophagy through the PTEN/AKT/mTOR pathway. *Life Sciences*, *232*, 116613. https://doi.org/10.1016/j.lfs.2019.116613

Sies, H., Berndt, C., & Jones, D. P. (2017). Oxidative Stress. *Annual Review of Biochemistry*, *86*(1), 715–748. https://doi.org/10.1146/annurev-biochem-061516-045037

Sutton, L. N. (2008). Fetal surgery for neural tube defects. *Best Practice & Research Clinical Obstetrics & Gynaecology*, *22*(1), 175–188. https://doi.org/10.1016/j.bpobgyn.2007.07.004

Thompson, A., Schäfer, J., Kuhn, K., Kienle, S., Schwarz, J., Schmidt, G., Neumann, T., & Hamon, C. (2003). Tandem Mass Tags: A Novel Quantification Strategy for Comparative Analysis of Complex Protein Mixtures by MS/MS. *Analytical Chemistry*, *75*(8), 1895–1904. https://doi.org/10.1021/ac0262560

Tonelli, C., Chio, I. I. C., & Tuveson, D. A. (2018). Transcriptional Regulation by Nrf2. *Antioxidants & Redox Signaling*, *29*(17), 1727–1745. https://doi.org/10.1089/ars.2017.7342

Tung, E. W. Y., & Winn, L. M. (2011). Valproic Acid Increases Formation of Reactive Oxygen Species and Induces Apoptosis in Postimplantation Embryos: A Role for Oxidative Stress in Valproic Acid-Induced Neural Tube Defects. *Molecular Pharmacology*, *80*(6), 979–987. https://doi.org/10.1124/mol.111.072314

Verrotti, A., Scardapane, A., Franzoni, E., Manco, R., & Chiarelli, F. (2008). Increased oxidative stress in epileptic children treated with valproic acid. *Epilepsy Research*, *78*(2–3), 171–177. https://doi.org/10.1016/j.eplepsyres.2007.11.005

Webster, W. S., Brown-Woodman, P. D., & Ritchie, H. E. (1997). A review of the contribution of whole embryo culture to the determination of hazard and risk in teratogenicity testing. *The International Journal of Developmental Biology*, *41*(2), 329–335.

Werler, M. M., Shapiro, S., & Mitchell, A. A. (1993). Periconceptional folic acid exposure and risk of occurrent neural tube defects. *JAMA*, *269*(10), 1257–1261.

Willett, W. C. (1992). Folic acid and neural tube defect: Can't we come to closure? *American Journal of Public Health*, *82*(5), 666–668. https://doi.org/10.2105/AJPH.82.5.666

Williams, L. J., Mai, C. T., Edmonds, L. D., Shaw, G. M., Kirby, R. S., Hobbs, C. A., Sever, L. E., Miller, L. A., Meaney, F. J., & Levitt, M. (2002). Prevalence of spina bifida and anencephaly during the transition to mandatory folic acid fortification in the United States. *Teratology*, *66*(1), 33–39. https://doi.org/10.1002/tera.10060

Zaganjor, I., Sekkarie, A., Tsang, B. L., Williams, J., Razzaghi, H., Mulinare, J., Sniezek, J. E., Cannon, M. J., & Rosenthal, J. (2016). Describing the Prevalence of Neural Tube Defects Worldwide: A Systematic Literature Review. *PLOS ONE*, *11*(4), e0151586. https://doi.org/10.1371/journal.pone.0151586

Zhu, M.-M., Li, H.-L., Shi, L.-H., Chen, X.-P., Luo, J., & Zhang, Z.-L. (2017). The pharmacogenomics of valproic acid. *Journal of Human Genetics*, *62*(12), 1009–1014. https://doi.org/10.1038/jhg.2017.91

Chapter 2

Spatiotemporal Evaluation of the Mouse Embryonic Redox Environment and Histiotrophic Nutrition Following Treatment with Valproic Acid during Early Organogenesis

Abstract

Redox regulation during metazoan development ensures that coordinated metabolic reprogramming and developmental signaling are orchestrated with high fidelity in the hypoxic embryonic environment. Valproic acid (VPA), an anti-seizure medication, is known to increase markers of oxidation and increase the risk of neural tube defects (NTDs) when taken during pregnancy. It is unknown, however, whether oxidation plays a direct role in failed neural tube closure (NTC). Spatial and temporal fluctuations in total glutathione (GSH) and total cysteine (Cys) redox steady states were seen during a 24hr period of CD-1 mouse organogenesis in untreated conceptuses and following exposure to VPA and the Nrf2 antioxidant pathway inducer, 1,2-dithiole-3-thione (D3T). Glutathione, glutathione disulfide (GSSG), and Cys, cystine (CySS) concentrations, measured in conceptal tissues (embryo/visceral yolk sac) and fluids (yolk sac fluid/amniotic fluid) showed that VPA did not cause extensive and prolonged oxidation during the period of NTC. Instead, VPA produced transient periods of oxidation, as assessed by GSH:GSSG redox potentials, which revealed oxidation in all four conceptal compartments at 4, 10, and 14 hrs, corresponding to the period of heartbeat activation and NTC. Other changes were tissue and time specific. VPA treatment also reduced total FITC-Ab clearance from the

medium over 3 hrs, indicating potential disruption of nutritive amino acid supply. Overall, these results indicate that VPA's ability to affect cellular redox status may be limited to tissue-specific windows of sensitivity during the period of NTC. The safety evaluation of drugs used during pregnancy should therefore consider time and tissue specific redox factors.

Introduction

The *redox theory of development* describes the strict maintenance of developmental oxygen concentrations required for the regulation of proper redox signaling and control of morphological growth and development (Hansen et al., 2020). Redox signaling is impacted by changes in the concentration of cellular glutathione (GSH), its oxidation state, and other antioxidant levels as well as the direct post-translational modification of protein cysteine (Cys) residues that can affect protein form, abundance, and function (Hansen et al., 2020). Changes to the GSH and glutathione disulfide (GSSG) redox potential (E_h), a measure of cell and tissue-level oxidation, have been shown to correlate with the cellular activities of proliferation, differentiation, apoptosis and necrosis, indicating that redox fluxes in early development have the capacity to act as signaling mechanisms for developmental stage progression (Schafer & Buettner, 2001). The organogenesis stage of development occurs under conditions of hypoxia where oxygen concentrations (O_2) range between 7-18 mmHg and encompass the period during which the developing embryo is most susceptible to morphological birth defects, such as those relating to neural tube closure, limb abnormalities and heart defects (Greene & Copp, 2014).

This study describes the redox response to VPA, a commonly prescribed anti-epileptic drug that when taken during pregnancy, can lead to an increased risk of the infant developing a neural tube defect (NTD) (Vajda et al., 2013). NTDs are a group of morphological birth defects that result from incomplete neural tube closure (NTC) during early embryonic development that

range in severity depending on the timing and location of the failed closure (Greene & Copp, 2014). In the United States, the occurrence of NTDs is significant with 3,000 cases per year, but in the developing world incidence can be up to 100 times higher (CDC, 2004; Shibuya & Murray, 1998). Risk factors for NTD occurrence have been identified to include genetic mutations, gestational exposure to anti-epileptic and other drugs, and a maternal diet deficient in folic acid during pregnancy, among others (Bruckner et al., 1983; De Marco et al., 2011; Grosse et al., 2016). Despite this evidence, the mechanism of action for spontaneous or VPA-induced NTDs remains unknown, although there is significant evidence from cell, animal, and human studies that VPA exposure causes increases in oxidation markers and is associated with oxidative endpoints (Ahangar et al., 2017; Chaudhary et al., 2015; Komulainen et al., 2015; Palsamy et al., 2014; Tung & Winn, 2011).

Therapeutic and environmental chemicals with pro-oxidant properties have also been implicated in reduced nutrient uptake during organogenesis, where amino acid starvation has been shown to be associated with increased cellular oxidation (Harris et al., 2015; Jilek et al., 2015; Sant et al., 2016a). Prior to the development of a functioning placenta, rodent and human embryonic nutrition rely on nutrient uptake via a process of histiotrophic nutrition which involves the uptake of proteins and nutrients by the visceral yolk sac (VYS) through receptor mediated endocytosis, followed by proteolysis and utilization of liberated amino acids for protein synthesis (Burton et al., 2002). In addition to serving as a nutritional pathway preceding placental development, histiotrophic nutrition helps to maintain the necessary hypoxic environment during organogenesis by eliminating the need for direct contact with maternal blood and high rates of oxygen delivery (Burton et al., 2001). Decreases in histiotrophic nutrition during organogenesis could promote delayed growth or morphological abnormalities, as well as

changes in redox status since histiotrophic nutrition supplies the amino acids needed for synthesis of GSH and other antioxidant compounds (Jilek et al., 2015; Sant et al., 2016a). Developmental exposure to ethanol in rat embryos, for example, caused significantly decreased histiotrophic uptake of nutrients and led to altered GD9 morphology (Jilek et al., 2015). It is unknown whether VPA acts as an inhibitor of histiotrophic nutrition or whether oxidation may play a role in the decreased histiotrophic uptake seen with other pro-oxidant developmental toxins (Jilek et al., 2015; Sant et al., 2016a).

Due to the rapidly changing and dynamic continuum of developmental events, it is important to understand the spatiotemporal fluctuations in cellular redox states under normal developmental conditions during organogenesis in order to contrast them with the redox profile following perturbations with pro-oxidant agent and commonly prescribed medication, VPA, and the antioxidant response-inducing compound, 1,2-dithiole-3-thione (D3T). D3T is a synthetic chemotherapeutic agent and known inducer of the Nrf2 antioxidant response that has previously been demonstrated to act as an anti-teratogenic compound through reduction of ethanol-induced reactive oxygen species (ROS) generation and apoptosis in pre-treated mouse embryos (Dong et al., 2008). Nrf2 is an oxidation responsive transcription factor that resides in a protein-protein interaction with Keap1 and is continuously degraded through ubiquitination under homeostatic conditions (Tonelli et al., 2018). In conditions of elevated oxidation where Keap1 is oxidized at reactive cysteine sites, Nrf2 is translocated to the nucleus where it binds to the antioxidant response element (ARE) and induces the transcription of genes that play a role in glutathione (GSH), thioredoxin, and NADPH regulation (Tonelli et al., 2018). Although VPA exposure has been associated with oxidation endpoints, it suppresses the Nrf2 antioxidant response which could lead to greater oxidative damage (Palsamy et al., 2014). We hypothesized that pre-

treatment of mouse embryos with D3T would increase GSH concentrations and elicit a more negative, protective, GSH/GSSG redox potential (E_h) across the time period of neural tube closure from gestational days (GD) 8-9. To assess this, a 24-hour time course of VPA and D3T exposure was performed in organogenesis-stage mouse conceptuses measured in 4 conceptal tissues and fluid compartments including the embryo proper (EMB), visceral yolk sac (VYS), yolk sac fluid (YSF), and amniotic fluid (AF). A histiotrophic nutrition assay was also performed at 1 and 3 hours after VPA or VPA+D3T exposure to determine whether potential decreases in histiotrophic nutrient uptake may correlate with changes to spatial or temporal redox status. Evaluating redox and nutritional dynamics across developmental time and space will help to generate a road map of spatiotemporal organogenesis redox dynamics during organogenesis under normal and VPA-challenged conditions that will help to identify periods of embryonic oxidant-sensitivity and potentially help to illuminate a mechanism for VPA induced teratogenesis.

Materials and Methods

Animals

Experiments were conducted using mouse whole embryo culture (mWEC) to culture conceptuses from gestational days (GD) 8-9 in time-mated, pregnant CD-1 mice (Charles River Laboratories, Raleigh, NC). The morning following mating with discovery of a vaginal plug was designated as gestational day 0 (GD 0). Animals were housed in groups of 6 or fewer in ventilated cages prior to explant and allowed access to feed and water *ad libitum*. All animal protocols were approved by the University of Michigan Institutional Animal Care and Use Committee and followed the NIH Guide for the Care and Use of Laboratory Animals.

Culture Conditions

Pregnant GD 8 dams were euthanized by CO_2 asphyxiation and uteri were removed and placed in Tyrode's solution (pH 7.4; HiMedia; Mumbai, India). Intact conceptuses were dissected free from decidual implantation sites with watchmaker's forceps and iridectomy scissors. Maternal tissues including the parietal yolk sac and Reichert's membrane were removed to complete preparation of the conceptus for culture. Conceptuses were cultured in groups of 2-6 per bottle of 2 mL of immediately centrifuged female rat serum with 4.3 µl/mL penicillin, streptomycin (10,000 units penicillin and 10 mg streptomycin per mL, Sigma Aldrich; St. Louis, MO). All culture conditions were at 37 °C with gas concentrations at 5% O_2, 5% CO_2, 90% N_2 for 6 hrs then 20% O_2, 5% CO_2, 75% N_2 for the remainder of the culture period (Harris, 2012).

Time Course Exposures and Sampling for Redox HPLC

Pre-treatment of D3T (10 µM, <0.01% DMSO v/v, Santa Cruz Biotechnology; Dallas, TX) was administered *in vitro* directly in the female rat serum at the start of the culture period. After two hours, VPA (600 µM in H_2O, Sigma-Aldrich; St. Louis, MO) was added *in vitro* to the female rat serum for the VPA and VPA+D3T groups. Samples were collected every 2 hours following the administration of D3T up to 26 hours. Conceptuses were rinsed twice in Hank's Balanced Salt Solution (HBSS, pH 7.4; Thermo Fisher Scientific; Waltham, MA) then pipetted in groups of 2-3 into a 150 µL drop of HBSS in a petri dish where the visceral yolk sac (VYS) was torn and agitated, releasing yolk sac fluid (YSF). The drop of HBSS and YSF was added to a microcentrifuge tube containing 2x HPLC Buffer [10% perchloric acid v/v, 0.4 M boric acid, and 20 µM γ-glutamylglutamate (γ-EE)]. A second 150 µL drop of HBSS was pipetted over the VYS and embryo (EMB) in the petri dish, which were then separated to release amniotic fluid into the

HBSS. EMB and VYS were added to separate tubes containing 1x HPLC Buffer and amniotic fluid (AF) was added to a tube with 2x HPLC buffer. All samples were snap frozen in liquid nitrogen and stored at -80 °C prior to sample processing. Positive control samples were dosed with mono-ethyl hexyl phthalate (MEHP 100 and 250 µg/mL in DMSO <0.1% v/v, Sigma-Aldrich; St. Louis, MO) or tertbutyl hydroquinone (TBHQ 50 and 100 µM, DMSO <0.1% v/v, Sigma-Aldrich; St. Louis, MO) 2 hours following the start of culture and were processed as described above.

Sample preparation and reverse-phase HPLC

EMB, VYS, YSF, and AF samples were sonicated to homogenize tissues then derivatized following the protocol outlined by Jones (Jones, 2002) and modified by Harris and Hansen (Harris & Hansen, 2012). The bicinchoninic acid (BCA) assay using bovine serum albumin as a standard was performed to determine protein content of samples.

GSH, GSSG, Cys and cystine (CySS) concentrations were determined through reverse-phase HPLC analysis using a Waters 2695 Alliance Separations Module (Milford, MA) fitted with a Supelcosil LC-NH_2 column (Sigma-Aldrich; St. Louis, MO). Mobile phase A consisted of 80% methanol and 20% ddiH_2O v/v and mobile phase B consisted of 62.5% methanol, 12.5% glacial acetic acid v/v, and 214 mg/ml sodium acetate trihydrate in ddiH_2O. Samples were run at a gradient flow rate of 1 ml/min. Detection of peaks was determined using a Waters 2474 fluorescence detector (excitation 335 nm and emission at 518 nm) with data analysis on Empower 3 software (Waters; Milford, MA).

Redox potential, soluble and bound thiol concentration calculations

The Nernst equation was used to calculate the redox potential from concentrations of soluble, GSH, GSSG and Cys, CySS (Harris & Hansen, 2012; Jones, 2002). VYS and EMB calculations utilized BCA protein concentration data for normalization and YSF and AF samples utilized fluid compartment volume estimations. Fluid compartments volumes were estimated utilizing conceptus images and calculating the volume of spheres ($4\pi r^3$) and subtracting nested compartments. Fluid compartment volumes for 0-12 hrs and 14-24 hrs were 3 µL and 5.9 µL for YSF and 1.1 µL and 2.4 µL for AF. Total Glutathione and total cysteine were calculated as the sum of reduced thiol partner and two times the oxidized thiol partner (GSH + 2GSSG and Cys + 2CySS).

Histiotrophic Nutrition

Conceptuses were cultured as described above except with 75% female rat serum/25% Tyrode's as the culture serum to reduce the protein content of the culture medium. Following 2 hr pre-incubation with D3T, FITC-Ab (100 µg/ml) was added to the culture medium in each culture bottle (Ambroso & Harris, 2012). Culture bottles were then incubated for 1 or 3 hours with treatment groups Control, D3T (10µM), VPA (600 µM) or VPA + D3T (600 µM + 10 µM). Following incubation, conceptuses were rinsed in 50 mM sodium phosphate buffer then pipetted into a 250 µL drop where the VYS and EMB were separated allowing the extraembryonic fluid (EEF) to release into the sodium phosphate buffer. VYS and EMB were separately rinsed then added to tubes containing 250 µL 0.1% Triton X-100 v/v. All samples were homogenized and then had a 20 µl aliquot saved for BCA assay to determine protein content. Protein was precipitated through acidification with 750 µL 6% TCA w/v for 1 hr followed by centrifugation and separation of the pellet and supernatant. TCA-soluble supernatants were combined with 1 ml

of 500 mM Tris (4 °C) and 150 µL of 1 N NaOH to bring to pH of 8.8. TCA-insoluble pellets were dissolved with 150 µL of 1 N NaOH, vortexed and incubated for 1 hour. 1 ml 500 mM Tris (4 °C), 150 µL 1 N NaOH, and 750 µL 6% TCA w/v were then added to both the acid soluble and insoluble samples. Culture media aliquots were collected in 250µL of 0.1% Triton X-100 v/v, 750µL of 6% TCA w/v with 1% SDS w/v and 150 µL of 1 N NaOH and processed as described above into TCA soluble and insoluble fractions. Fluorescence intensities of all samples and blanks were measured in black polypropylene 96-well plate and read at an excitation wavelength of 495nm with 520nm emission on a SpectraMax Gemini XS (Molecular Devices; San Jose, CA). A standard curve of a 1:10000 dilution of FITC-Ab balanced for pH with 500 mM Tris (4 °C) and 6% TCA w/v was used for quantification.

Statistical Analysis

To determine statistical significance for the histiotrophic nutrition assay and whole conceptus HPLC a one-way ANOVA was calculated within each timepoint across treatment groups. A confidence level of 95% (α=0.05) was utilized as a threshold for statistical significance. Significant ANOVA results underwent Tukey's post-hoc test to determine significant groups. Statistics were performed in Excel using the Real Statistics Resource Pack add-in and where applicable are reported as mean ± standard error. The whole conceptus oxidation analysis had a sample size of 2 per time point and condition for whole conceptus and 3 per time point and condition for VYS and EMB. Histiotrophic nutrition had a sample size of 6 per time point and condition.

RNA Extraction and qPCR

Treatment groups for qPCR and Western Blots included: Control, D3T (*in vitro*, 10 µM), D3T (*in vivo*, 5 mg/kg), VPA (600 µM), and VPA + D3T (600 µM + *in vitro* 10 µM and 600 µM + *in vivo* 5mg/kg). *In Vivo* D3T dosing was administered on GD 7.5 through an IP injection of 100 µL with a soybean oil vehicle. *In vivo* dosing and culture conditions were performed as described above. Conceptuses were rinsed twice in HBSS before separation of embryo and visceral yolk sac. Tissues were saved in groups of 5 in 50 µL RNALater (Invitrogen; Carlsbad, CA). RNA extraction was performed using the RNeasy kit according to manufacturer's instructions (Qiagen; Hilden, Germany). RNA concentration and quality were verified by Nanodrop (Thermo Fisher Scientific; Waltham, MA). RNA was synthesized into cDNA using the iScript cDNA Synthesis Kit (Bio-Rad; Hercules, CA) and prepared for quantitative real-time PCR using SYBR Green Detection Master Mix (SABiosciences; Frederick, MD) per the manufacturer's instructions in a StepOnePlus real-time PCR cycler (Applied Biosystems; Foster City, CA). All primers were purchased from Integrated DNA Technologies (Coralville, IA). β-actin was measured as a housekeeping gene for normalization purposes. Samples were analyzed using the ΔΔCt method and analyzed relative to the 0 hr control. Samples were run in triplicate, n = 3. Genes of interest included Glutamate-cysteine ligase catalytic subunit (GCLC), Heme Oxygenase 1 (HO1), and NADPH dehydrogenase (quinone 1) (NQ01) which are all known downstream gene targets of Nrf2 activation (Alam et al., 1999; Venugopal & Jaiswal, 1996; Wild et al., 1999). The ß-actin (4970S) primary antibody was purchased from Cell Signaling Technology (Danvers, MA). NQO1 (ab28947), GCLC (ab190685), and HO1 (ab13248) primary antibodies were purchased from Abcam (Cambridge, UK). The secondary antibodies used were Alexa Fluor 680 donkey anti-mouse (175774) and 800 goat anti-rabbit (ab216773).

Western Blots

Conceptuses were rinsed twice in 1x HBSS before separation of embryo and visceral yolk sac. Tissues were saved in 100 µL 1x RIPA buffer in groups of 4-6 then sonicated. Protein concentration was determined through BCA assay and equal amounts of protein were separated by 10% SDS-polyacrylamide gel electrophoresis using a PowerPac Basic electrophoresis unit (Bio-Rad; Hercules, CA) run at 80 V and transferred onto nitrocellulose membranes. ß-actin (4970S) primary antibody was purchased from Cell Signaling Technology (Danvers, MA). NQO1 (ab28947), GCLC (ab190685), and HO1(ab13248) antibodies were purchased from Abcam (Cambridge, UK). The membranes were blocked with LiCor blocking buffer (LiCor Biosciences; Lincoln, NE) for 60 minutes at room temperature and then probed with the denoted primary antibodies diluted 1:500 in PBS with 0.1% Tween 20 (Thermo Fisher Scientific; Waltham, MA) at 4°C overnight. The next day, membranes were probed with fluorescent Alexa Fluor secondary antibodies (LiCor Biosciences; Lincoln, NE) at room temperature for 90 minutes. Membranes were imaged on an Odyssey CLx scanner (LiCor Biosciences; Lincoln, NE) and quantified by expression of the desired protein relative to the actin loading control. Data are expressed as the mean ± SEM. Prism v7.00 software (Graphpad Software Inc.; San Diego, CA) was used for the statistical analysis. Statistical comparisons were made using a one-way analysis of variance (ANOVA) followed by Dunnett's post hoc test with statistical significance denoted as a $p < 0.05$. Asterisks (*) denote statistical significance compared to the control, and hashtags (#) denote statistical significance compared to the VPA treated group.

Results

The described experiments were conducted to evaluate the spatial and temporal baseline redox steady states of the organogenesis stage mouse conceptus under control and VPA and/or D3T perturbed conditions. Measurements of GSH, GSSG, Cys, and CySS across embryonic time and space were used to calculate total glutathione (GSH + 2GSSG) and total cysteine (Cys + 2CySS) as well as the corresponding redox potential (E_h) for each thiol pair. Finally, the histiotrophic nutrition assay measured protein uptake via receptor-mediated endocytosis in the VYS across early organogenesis to determine whether an association exists between reduced GSH or Cys concentrations and decreased histiotrophic nutrition under VPA-treated conditions.

Total Glutathione and Total Cysteine

Total glutathione (GSH + 2GSSG) and total cysteine (Cys + 2CySS) concentrations in tissue and fluid compartments are displayed for each 2 hr interval across the 24 hr time course as heat maps in order to provide a qualitative context of changes in soluble thiol levels over developmental time (Figure 2-1, Figure 2-2). This analysis shows only concentrations of total (oxidized and reduced) thiols. Changes in oxidation states for the respective redox pairs are shown below as their respective redox potentials (E_h) as bubble diagrams in Figure 2-3.

Concentrations of total glutathione fluctuate naturally in the control VYS between 1400 and 5600 μM across the time course with highs at 6 hr and 14 hr and a low at 16 hr. Control EMB total glutathione drops to its lowest levels at 10 and 12 hrs followed by a peak at 14 hr. Total glutathione concentrations in the YSF and AF compartments are considerably lower compared to tissues with a much narrower range of variation, fluctuating between 5 μM and 120 μM, showing their highest concentrations during the first 8-10 hrs with peaks at 4 hr (Figure 2-1). In contrast to the control values of total glutathione, VPA treatment caused noticeably higher

levels of total glutathione from 2-4, 8-10, and 18 hrs in the VYS and 4, 16, and 22 hrs in the EMB. The only noticeable increase in total glutathione in the fluid compartments following VPA treatment was at 18 hrs in the AF.

Total cysteine concentrations range from 127-936 μM in control EMB and 107-1152 μM in the VYS. Similar to glutathione, the concentration of total cysteine in the fluid compartments is much lower than in the tissues with a control concentration of 7-199 μM in YSF and 13-218 μM in the AF. In the tissues, VPA causes elevated levels of total cysteine compared to the control at 12 and 22 hrs in the VYS and 4 and 22 hrs in the embryo. The fluid compartments show greater sensitivity to VPA with more periods of increased total cysteine from 2, 20, and 24 hrs in the YSF and 8, 16, and 22-24 hrs in the AF.

Thiol Pair Redox Potentials

Redox potential (E_h) measures the steady state balance between oxidized and reduced counterparts of a redox active thiol couple such as GSH and GSSG or Cys and CySS. Figure 2-3 visualizes E_h values as a heat map across developmental time and space for each of these redox pairs. Across all treatment groups, the YSF and AF compartments exhibited a more oxidized E_h than the tissue compartments for both GSH:GSSG and Cys:CySS. In the control, compartmental GSH E_h ranged from -168 to -208 mV in the VYS, -172 to -229 mV in the EMB, -98 to -136 mV in the YSF and -118 to -149 mV in the AF. VPA treatment caused a distinct oxidation event in all tissues and fluid compartments in the GSH:GSSG redox potential at 4, 10 and 14 hrs compared to the control, but at 6, 8, and 20 hrs, nearly identical redox profiles were seen across all tissues. Co-treatment with D3T and VPA did not maintain a control level oxidation profile, and in some cases, such as at 20 hrs, the co-treatment led to more oxidation than seen in any of the other treatment groups with a compartmental range of -111 to -156 mV compared to -129 to -

229 mV in the control. Across the 24 hours of sampling, all VYS showed a trend toward becoming increasingly reduced. EMB fluctuated between -180 to -220 mV with a low of -230 and a high of -155 mV both at 20 hrs in the control and VPA + D3T group respectively for the GSH:GSSG redox potential. AF and YSF GSH:GSSG redox potential trended toward becoming more reduced by the end of the time course. Thus, in spite of considerable variation in steady state E_h during the GD 8 segment of the time course, all tissues and fluids show progressive reduction as growth and development proceeds during organogenesis.

The Cys:CySS redox potential was consistently more oxidized than the GSH:GSSG redox potential (Figure 2-3). This more oxidized Cys:CySS redox potential was expected due to Cys being predominately found in its oxidized form, CySS, in extracellular spaces compared to the reduced form which is found at much lower concentrations intracellularly (McBean, 2017). Control values of the Cys:CySS redox potential ranged from -72 to -147 mV in the VYS, -45 to -149 mV in the EMB, -31 to -91 mV in the YSF, and -49 to -113 mV in the AF. At 12 hrs, most treatment groups showed a reduction in the VYS Cys:CySS redox potential followed by a reversion to oxidation at 14 hrs. At 24 hrs, all tissues and fluids showed a highly oxidized Cys:CySS redox potential. Compared to the control, VPA treatment lead to visible reduction in all tissues at 18 and 22 hrs which was also seen in most tissues in the VPA + D3T group at the same time points.

Whole conceptus redox potential measurements for GSH:GSSG were more reduced than those of isolated EMBs and VYSs at the corresponding time points (Figure 2-4). The pattern of reduction and oxidation over time, however, is similar between whole conceptus, EMB, and VYS, which indicates that while the time-sensitive manipulation of conceptuses to separate

tissues may cause slight artifactual oxidation, the patterns of increased and decreased oxidation remain consistent.

MEHP and TBHQ treatments were administered as positive controls at 4 and 22 hrs. Both compounds have shown the capacity to act as oxidants in developmental models of mouse or zebrafish embryos (Sant, et al., 2016b; Sant et al., 2017). In the VYS and EMB, the VPA GSH:GSSG redox potential was statistically more reduced ($p<0.05$) following 4 and 22 hrs of treatment than either dose of MEHP or TBHQ (Figure 2-5). The YSF and AF showed no statistical difference in GSH:GSSG redox potential between VPA, MEHP, or TBHQ at 4 or 22 hours. In all tissues and fluid compartments, the low and high dose of MEHP or TBHQ showed no statistical difference from each other in their effect on GSH:GSSG redox potential.

Nrf2 Pathway Activation by D3T

To determine whether D3T was properly inducing the Nrf2 antioxidant response during the 2-hour *in vitro* pre-treatment, RT-qPCR gene expression of three downstream marker genes of Nrf2 was measured (Figure 2-6). NQO1, a Nrf2-induced antioxidant, increased significantly in gene expression following both *in vitro* and *in vivo* D3T treatment in the embryo and in EMB and VYS in combination with *in* vitro VPA. HO1, another Nrf2 induced antioxidant, showed a significant increase in gene expression in the EMB for all groups treated with D3T and in the VYS in all groups treated with D3T except *in vivo* D3T alone. GCLC, a rate-limiting enzyme for glutathione synthesis, showed no significant increases in gene expression, although the *in vivo* and *in vitro* VPA + D3T combination treatments were trending toward significance in both tissues. There was no difference between VPA treated and control EMB or VYS in any of the three genes.

To complement gene expression data, western blots were performed to evaluate protein expression of the same three downstream Nrf2 targets (Figure 2-7). NQO1 protein expression was increased in the EMB following *in vivo* D3T dosing as well as in EMB and VYS following *in vivo* or *in vitro* D3T in combination with *in vitro* VPA. HO1 protein expression was significantly elevated in EMB and VYS following *in vitro* D3T dosing and in the EMB only after both VPA+D3T combination treatments. GCLC showed elevated protein expression in the VYS and EMB following *in vitro* D3T, *in vivo* D3T and *in* vitro VPA + D3T dosing, but only showed elevated protein expression in the VYS following *in vivo* D3T + *in vitro* VPA. Unlike in the gene expression data, VPA alone caused moderate increases in protein expression of NQO1 and HO1.

Histiotrophic Nutrition

The total histiotrophic clearance rate of FITC-Ab was decreased compared to the control after 1 and 3 hrs exposure to VPA and VPA+D3T (Figure 2-8). After 1 hr, control clearance was 102 µL media/mg/hr compared to 62 and 52 µL/mg/hr in VPA and VPA+D3T respectively. Similarly, at 3 hrs control clearance was 40 µL media/mg/hr with VPA and VPA+D3T clearance at 32 and 25 µL/mg/hr. Total FITC-Ab clearance at 3 hrs was also reduced in VPA and VPA+D3T treated groups with total clearance of 120 µL/mg in the Control compared to 97 and 74 µL/mg in the VPA and VPA+D3T treatment groups. The majority of FITC label was detected in the VYS and the EEF with only trace amounts reaching the embryo. In all treatment groups and time points the total uptake rate of acid soluble (degraded protein) and acid insoluble (intact protein) was roughly equal, but with the majority of acid soluble uptake in the VYS and the majority of insoluble uptake found in the EEF.

Discussion

The aim of the 24-hour time course was to determine whether VPA perturbed the redox environment during the period of mouse NTC in a spatially and temporally specific manner. The stated hypothesis considered that if VPA's mechanism of action involved increased cellular oxidation, it would cause an elevated GSH:GSSG redox potential and deplete GSH concentrations in all tissues and fluids across the time course. Redox profiles based on the GSH:GSSG and Cys:CySS redox couples did not show sustained oxidation by VPA across the time course of early organogenesis. Observed patterns of spatial and temporal fluctuations in soluble thiol antioxidant status may serve to indicate specific targets of chemical and environmental insult. The logic behind using a more generalized visualization of cellular redox states during organogenesis, measured from soluble thiols (GSH and Cys) and their respective redox potentials as heat maps, is based on considerations related to the need to visualize patterns of thiol oxidation and reduction as an ontogeny. Broad experience with developmental toxicology studies and rodent whole embryo culture reveal that any detailed sampling of individual litters will exhibit a spectrum of responses to developmental toxicants, such as VPA, that range from very high sensitivity to very high resistance in terms of malformations, functional deficits and embryo mortality. This is the basis for evaluating developmental toxicant effects by litter, rather than averaging individual embryo effects from litters of varying sensitivity (Hardy & Stedeford, 2008). The randomization method used in these experiments mixes conceptuses from many different litters that, individually, represent the entire range of sensitivity and resistance across a broad population spectrum. This conservative approach is expected to minimize the contribution of a few highly sensitive or resistant litters and show a general ontogeny of redox shifts. Different types of chemical agents such as the positive controls

TBHQ and MEHP are shown to be more responsive when taken from a much smaller total number/subset of litters.

In both whole conceptus and compartmental tissue and fluids, VPA did not consistently demonstrate the capacity to act as an oxidant through alterations of GSH and Cys concentrations. However, there were separate periods of oxidation seen for individual tissues and three time points (4, 10, and 14 hours) where all four embryonic compartments showed an oxidizing GSH:GSSG redox potential compared to the control tissues at the same time (Figure 2-3). These two later time points, 10 and 14 hrs, could be related to the morphological milestones related to neural tube closure that occur during the last quarter of GD 8. In late GD 8 when the embryo is in the stage of 15.4-17.7 somites, neural tube development completes two closures at the telencephalic neuropore followed by the metencephalic neuropore with average timing of about 2 hrs between these events (Sakai, 1989). The oxidation seen across the 4 embryonic compartments at 10 and 14 hrs could be indicative of specific aspects of VPA's disruption of the neural tube closure process, although it is still unknown whether neural fold elevation or apical fusion is involved VPA's mechanism of disruption. The earlier time point of VPA-induced oxidation at 4 hrs occurred during the time period of heartbeat activation which occurs between the 4 and 8 somite stage around mid-GD 8 (Nishii & Shibata, 2006). Therefore, it is possible that some of the timed elevations in the GSH:GSSG redox potential could be linked to other morphological or physiological development milestones during mouse organogenesis.

Positive controls, TBHQ and MEHP, are known oxidants with MEHP also being implicated in NTD outcomes (Sant et al., 2016b). TBHQ and MEHP produced statistically significant levels of oxidation in the EMB and VYS but not in the fluid compartments supporting the idea that oxidation responses in the mouse conceptus may be tissue dependent. The MEHP

results confirm previous results indicating that a 12 hr exposure to MEHP increased GSH E_h in the EMB but not VYS (Sant et al., 2016b). Despite not showing significant evidence for VPA's oxidative potential, this study's 2 hr sampling windows provided more finely timed points of measurement than seen in most redox studies illustrating that thiol concentrations are in constant flux and that stationary measurements from a single time point are not enough to capture the dynamic nature of the redox control of development. When compared to redox profiles of organogenesis stage zebrafish development (18-24 hpf), the control tissues and fluids show a similar pattern of shifting toward a more reduced GSH potential compared to the earlier stages of organogenesis (Timme-Laragy et al., 2013). Redox shifts encompassed in the 24-hour time course could also be significant in understanding physiological and structural birth defects related to the heart, eye, ear and limbs as these organs all achieve significant developmental milestones during the same time period as neural tube closure including heartbeat activation, limb bud development, optic cup and otic vesicle formation (Harris, 2012).

While there is evidence to demonstrate VPA's actions as an oxidant, there are also studies that indicate that under some conditions VPA may have the capacity to act as an antioxidant. In a rat model of sepsis, treatment with VPA reduced oxidative injury as measured by decreased levels of ROS and malondialdehyde (MDA) as well as increased levels of GSH, and superoxide dismutase (SOD) in myocardial tissue (Shi et al., 2019). Similarly, a mouse model of sepsis, found that VPA reduced levels of MDA and myeloperoxidase, while increasing levels of GSH and SOD indicating an overall reduction of oxidation markers in renal tissue (Liu et al., 2014). Human neuroblastoma SH-SY5Y cells treated with VPA for 1 week have been shown to increase glutathione levels compared to controls, while maintaining lactate dehydrogenase levels (LDH) and in some cases reducing oxidation caused by Rotenone and

H_2O_2 (J. Cui et al., 2007; Lai et al., 2006). Finally, VPA was shown to eliminate oxidative protein lesions found in a mouse model mimicking the neurodegenerative condition, X-linked adrenoleukodystrophy through inducing the expression of a peroxisomal transporter related to a transporter that loses function through the disease (Fourcade et al., 2010). Together, these studies could help explain why VPA did not cause consistent oxidation across the developmental time course.

The discordant research findings related to VPA's redox manipulation make it imperative that VPA be evaluated under conditions that most specifically relate to the outcome of interest to determine whether its actions are more pro- or antioxidant in nature. Recent findings related to oxidative post-translational modification of protein Cys in young and old mice has indicated that protein redox changes are often specific to tissue and age (Xiao et al., 2020). This research is particularly relevant to development as it is one of the most dynamic periods of life for programmed oxidation events (Hansen et al., 2020). The hypothesis that VPA would consistently elevate oxidation levels across organogenesis as measured through total thiol concentrations and redox potentials in conjunction with causing morphological abnormalities was not supported. It is possible, however, that these findings may have been masked by the intricate timeline of morphological changes that occur in addition to NTC during this period and the use of the broad developmental tissue and fluid compartments to study the spatiality of redox without the ability to differentiate between the many developing organ systems. Additionally, although VPA is known to suppress the Nrf2 antioxidant system and did not show increases in downstream Nrf2 gene and protein targets, HO1, GCLC, or NQO1 compared to the control, the primary transcription factor regulating basal antioxidant levels throughout development is Nrf1 (Palsamy et al., 2014; Raghunath et al., 2018). As evidenced by the similarities between control and VPA-

treated qPCR and western blot data, the Nrf1 system remains intact. It is therefore possible that basal levels of GSH synthesized through activation of the Nrf1 pathway could be sufficient to react to minor oxidation shifts caused by VPA without noting extended periods of redox imbalance that could be captured by 2 hr windows of the GSH:GSSG E_h. Alternatively, the findings of Xiao, et al. support the idea that naturally occurring and VPA-perturbed developmental redox signaling may be occurring primarily at the protein level independent of GSH redox states through oxidative post-translational modification of Cys residues (Xiao et al., 2020). This same reasoning may also resolve the limited changes in cellular redox profile following pre-treatment of conceptuses with D3T. Potential changes to the oxidation state of the developmental proteome would allow for natural and VPA-perturbed development to proceed with more targeted oxidation events that could be more time specific to protein pathways implicated in development of specific tissues and organs than could be achieved through GSH levels alone.

Pre-treatment of samples with D3T was intended to induce the Nrf2 antioxidant response prior to the challenge with suspected oxidant, VPA. D3T was selected based on numerous previous studies that have demonstrated D3T's ability to increase antioxidant concentrations and decrease markers of oxidative stress in both *in vivo* mouse and *in vitro* mouse cell models (Y. Cui et al., 2018; Dong et al., 2008; Kuo et al., 2017; Wang et al., 2017). Total glutathione concentration showed limited elevation in GSH from 4-10 hrs in the VYS with no apparent change in the other tissues or in redox potential following 2 hr *in vitro* D3T treatment. Despite seeing only limited time and tissue specific changes in total glutathione, *in vitro* D3T dosing did increase gene expression of HO1 in VYS and EMB and NQO1 in the embryo with protein expression showing increased GCLC and HO1 in both VYS and EMB (Figures 2-6 and 2-7). GD

7.5 *in vivo* IP D3T data also proved effective at increasing gene expression of NQO1 and HO1 in the EMB and increasing protein expression of NQO1 in the embryo and GCLC in EMB and VYS but was not more effective than the shorter *in vitro* dosing indicating equivalence between these two dosing regimens. These data suggest that the redox activity of D3T through the Nrf2 pathway is activated through *in vitro* or *in vivo* pre-treatment. However, the downstream consequences of this induction were not revealed through GSH measurements and may indicate the promotion of other downstream Nrf2 pathways. Additionally, the tissue selectivity seen with total glutathione elevation in the VYS that is absent in the EMB as well as the gene expression elevation of NQO1 in the EMB but not the VYS could indicate tissue differences in distribution of Nrf2 ARE targets or differences in Keap1 oxidation patterns that would affect Nrf2 nuclear translocation. There are four classes of ARE enhancer regions with two of these classes (I and II) being induced by Nrf2 as a transcription factor. Within these classes and even between ARE sequences for the same gene, there are known single nucleotide polymorphisms (SNPs) which have been shown to affect Nrf2 binding affinity (Raghunath et al., 2018). Timing of cell and tissue differentiation throughout development and tissue specific distribution of these ARE SNP varieties could therefore lead to differential antioxidant responses through the Nrf2 pathway over developmental time and space. Tissue-specific responses of Nrf2 gene GCLC were also noted in the EMB and VYS of post-implantation rat conceptuses where on both GD 10 and 11 (corresponding to mouse GD 8 and 9), concentrations of GCLC activity was two to three times higher in the VYS (Hansen et al., 2004).

It was predicted that co-treatment with VPA and D3T would decrease the oxidative effects of VPA alone, however as seen through the GSH:GSSG E_h and histiotrophic nutrition, there were several instances where the co-treatment caused an exacerbation of VPA's effects.

Similar results were seen in a study of the oxidative effects of advanced glycation end products (AGE) on SH-SY5Y cells where it was seen that while treatment of the cells with only D3T caused no change in cell viability or ROS production, co-treatment with AGE and D3T led to a decrease in viability and an increase in ROS beyond what was seen with AGE treatment alone (Stochelski et al., 2019). This potentiation effect caused by D3T was attributed to an elevation of the Nrf2 associated gene G6PD and a decrease in glutathione reductase activity (Stochelski et al., 2019). Based on the RT-qPCR and western blot data, VPA + D3T treatment showed a strong Nrf2 induction for HO1, NQO1, and GCLC. Therefore, the combination of VPA and D3T may be acting similarly through a potentiation effect, although unlike AGE, VPA did not show evidence of activating the Nrf2 pathway independently.

Histiotrophic nutrition data suggests that VPA may slow the rate of uptake of proteins and essential amino acids during early organogenesis. Histiotrophic clearance was measured through uptake of FITC-Ab, which was decreased following VPA exposure at both 1 and 3 hrs, which could indicate a delay in uptake of essential amino acids for protein synthesis and redox regulation through glutathione synthesis. This pattern of decreased uptake was seen in both acid soluble and insoluble samples, as well as across the three developmental compartments of EMB, VYS, and EEF. The combination treatment with VPA + D3T had a slower rate of histiotrophic uptake compared to VPA alone, whereas D3T by itself showed little change in rate of uptake. In addition to rate of uptake being slowed in VPA and VPA + D3T treatment groups, the total uptake of FITC-Ab across the 3hr experimental period was also decreased compared to the control and D3T alone. Other developmental toxins, such as ethanol, have also been shown to impact histiotrophic nutrition uptake by leading to significantly reduced clearance following 3 hours of exposure in organogenesis-stage rat conceptuses (Jilek et al., 2015). In mouse

conceptuses, oxidant MEHP has also been shown to reduce histiotrophic clearance after 3 hours at a dose of 250 μg/mL (Sant et al., 2016a). Both of these previous studies measured changes in clearance rate over 3 hrs on GD 9, so the assessment of VPA's effect on its histiotrophic nutrition during early-mid GD 8 is unique. Compared to the MEHP and ethanol studies, there was a much higher proportion of total uptake from the acid insoluble, intact protein, fraction in both control and VPA treated samples, which may be attributable to the earlier time point of analysis.

Comparing histiotrophic uptake rate at 1 and 3 hrs to the total thiol and redox potential at 2 and 4 hrs does not indicate a depletion of glutathione due to lower amino acid supply caused by VPA's slowed histiotrophic uptake. However, there is a slight decrease in total glutathione around 8-10 hrs in the EMB and 10 hrs in the VYS and EMB, which could indicate the delayed effects of decreased amino acid uptake (Figure 2-1). Total cysteine concentrations are lower after 2 hr VPA exposure in the EMB and VYS but higher in the YSF and AF (Figure 2-2). The decreased total cysteine after 2 hr VPA exposure in the tissue compartments could be indicative of a combinatorial effect of reduced amino acid uptake through histiotrophic nutrition as well as increased glutathione synthesis evidenced by higher total glutathione levels at 2 hrs in EMB and VYS compared to the control.

Overall, VPA treatment caused fewer perturbations to the organogenesis-stage mouse total GSH concentrations, total Cys concentrations, and thiol-pair redox potentials than expected. However, there were still distinct periods of oxidation produced by VPA that were time and tissue specific which, along with a potential disruption in histiotrophic nutrition, could affect maintenance of a developmentally appropriate redox state. Additionally, the carefully timed measurement of cellular redox in the control across 24 hrs of organogenesis demonstrated that

even in properly developing conceptuses, redox is in a natural state of fluctuation that differs across developmental time and space thereby underlining the importance of time course evaluation to understand redox mechanisms of development. These results suggest that further testing of VPA and other potentially teratogenic compounds and therapeutic agents for safety during pregnancy should be conducted over time within several embryonic tissue targets. This recommendation is based on the caveat that singular, one time, sampling of whole conceptuses may not be a valid measure of drug safety due to the potential for developmental interruption to be specific to the tissue and timing of exposure. The results of this study indicate that VPA may not act as a consistent oxidant under the traditional dogma of oxidative stress through manipulating cellular total GSH and its redox potential. Nevertheless, there is a growing body of evidence that oxidative post-translational modifications of protein Cys residues may be differentially affected by tissue and age which could be applicable to development and neural tube closure. Further exploration of the relationship between protein redox status and VPA treatment during mouse organogenesis is needed to understand whether VPA may act through pathways of oxidative post-translational protein modifications that could influence protein structure or function and developmental progression.

Figures

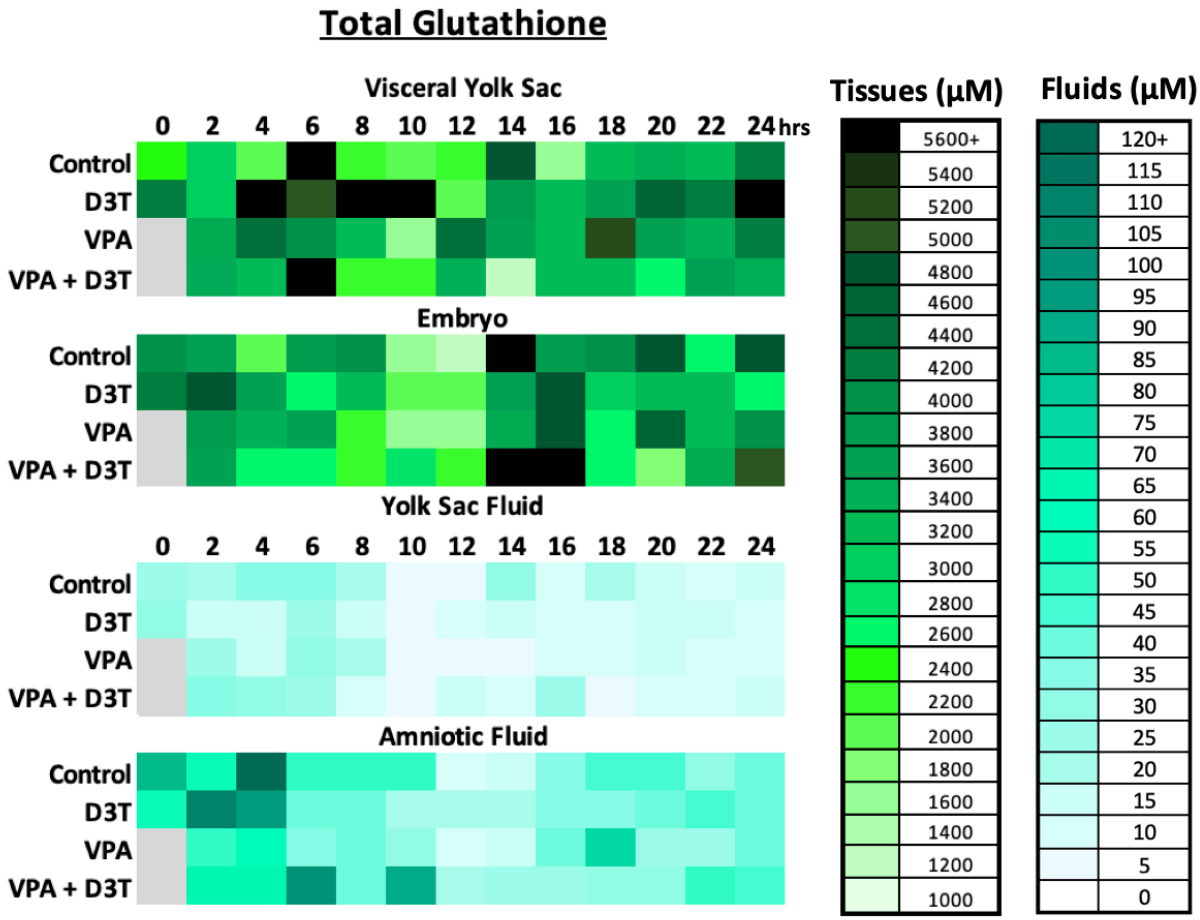

Figure 2-1 Compartmental total glutathione concentrations: Total Glutathione (GSH+2GSSG) concentration was measured by HPLC every 2 hours over 24 hours of mouse neurulation in the embryo (EMB), visceral yolk sac (VYS), yolk sac fluid (YSF), and amniotic fluid (AF) (n=3). D3T (10 µM) pre-treatment began 2 hours prior to dosing of VPA (600 µM) at 0 hours. All dosing was done directly in the culture medium.

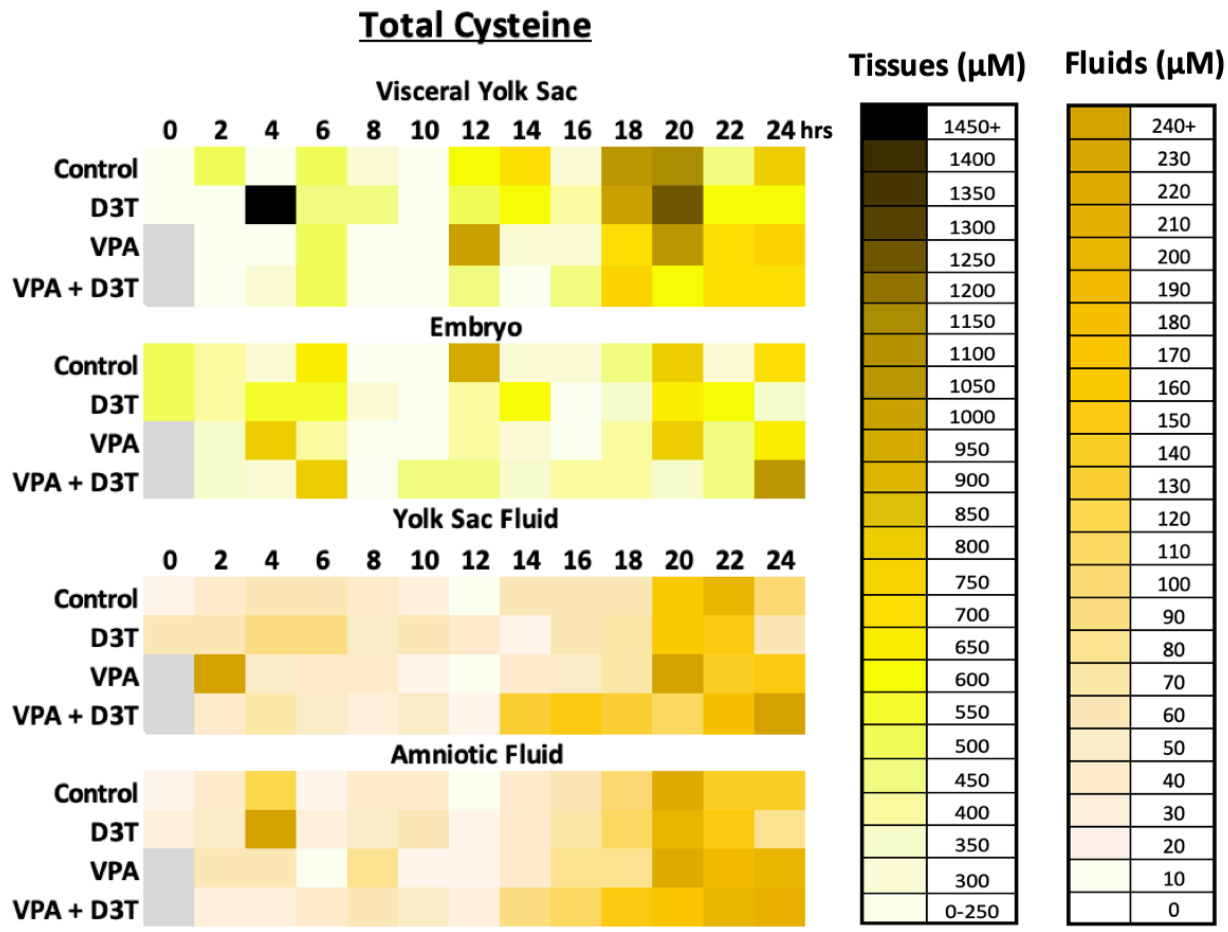

Figure 2-2 Compartmental total cysteine concentrations: Total Cysteine (Cys+2CySS) concentration was measured by HPLC every 2 hours over 24 hours of mouse neurulation in the embryo (EMB), visceral yolk sac (VYS), yolk sac fluid (YSF), and amniotic fluid (AF) (n=3). D3T (10 µM) pre-treatment began 2 hours prior to dosing of VPA (600 µM) at 0 hours. All dosing was done directly in the culture medium.

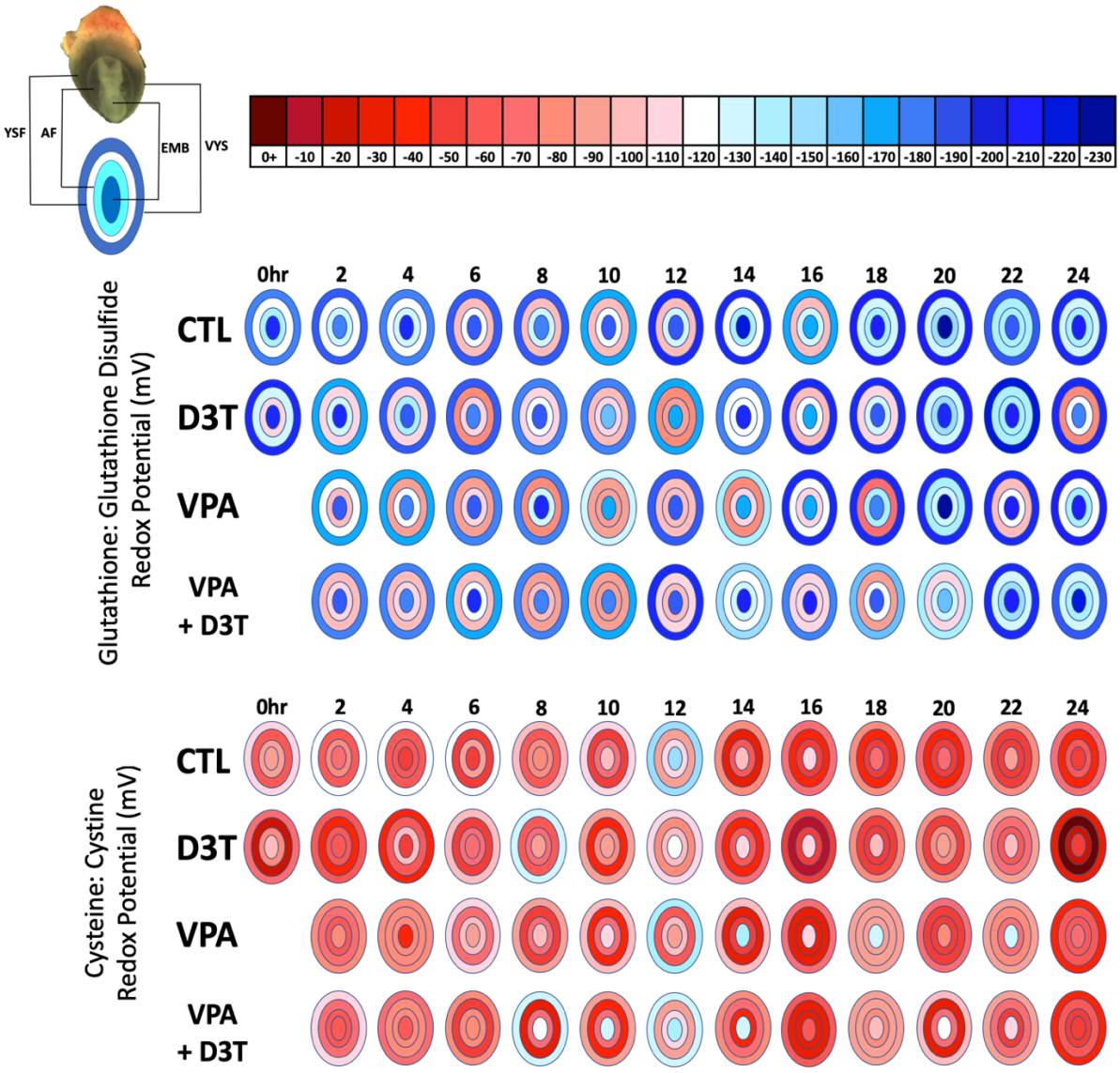

Figure 2-3 Compartmental glutathione and cysteine redox potentials: GSH:GSSG and Cys:CySS redox potentials (E_h) were measured by HPLC every 2 hours across 24 hours of mouse neurulation in the embryo (EMB), visceral yolk sac (VYS), yolk sac fluid (YSF), and amniotic fluid (AF) (n=3). Redox Potential was calculated using the Nernst equation. Negative values are more reducing and positive values are more oxidizing. D3T (10 µM) pre-treatment began 2 hours prior to dosing of VPA (600 µM) at 0 hours. All dosing was directly in the culture medium of female rat serum.

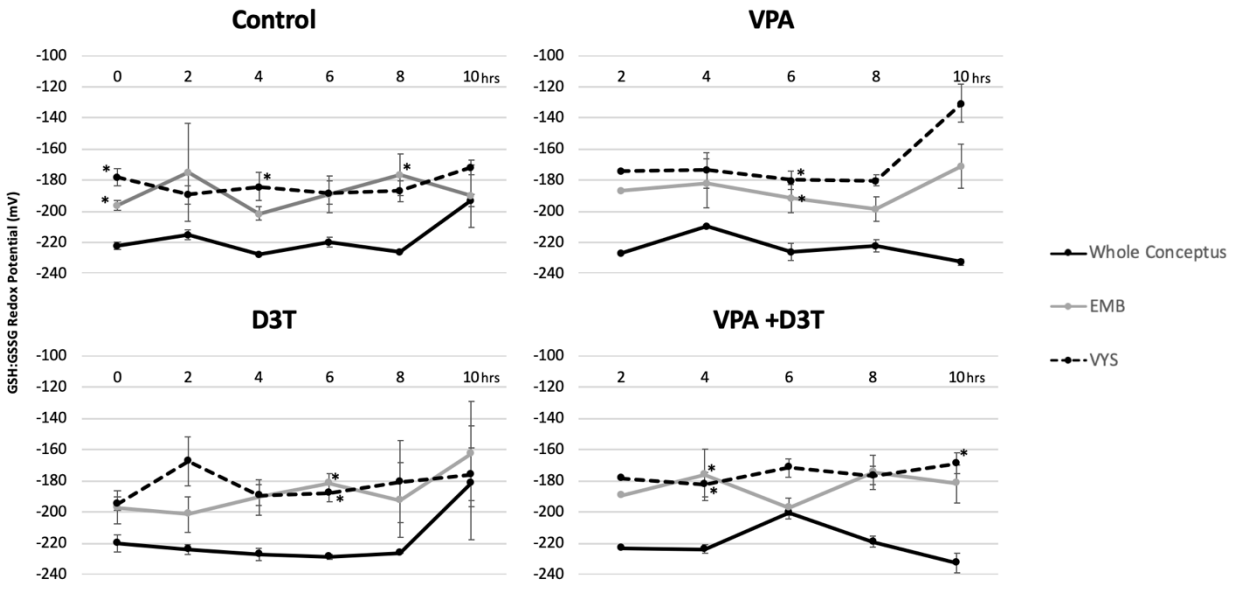

Figure 2-4 Whole conceptus glutathione redox potential: Whole Conceptus (n=2) GSH:GSSG redox potential (E_h) compared to embryo (EMB) and visceral yolk sac (VYS) (n=3) redox potential after 0-10 hours of exposure in Control, D3T (10 µM), VPA (600 µM), and VPA +D3T (600 µM +10 µM) treatment groups. *$p<0.05$ compared to the whole conceptus value.

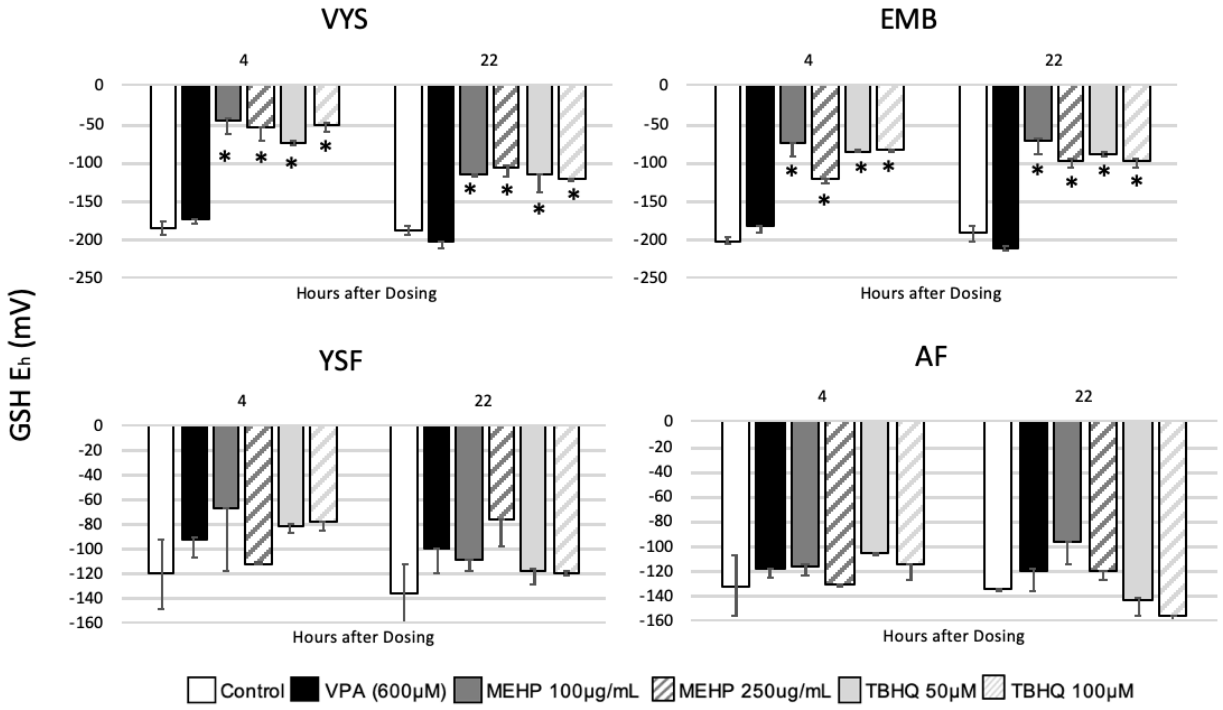

Figure 2-5 Positive control compartmental glutathione redox potential: GSH:GSSG redox potential (E_h) in VYS and EMB following dosing with VPA (600 µM, n=3, MEHP (100 and 250 µg/ml, n=4) or TBHQ (50 and 100 µM, n=4) for 4 and 22 hours. Error bars represent standard error. *$p<0.05$.

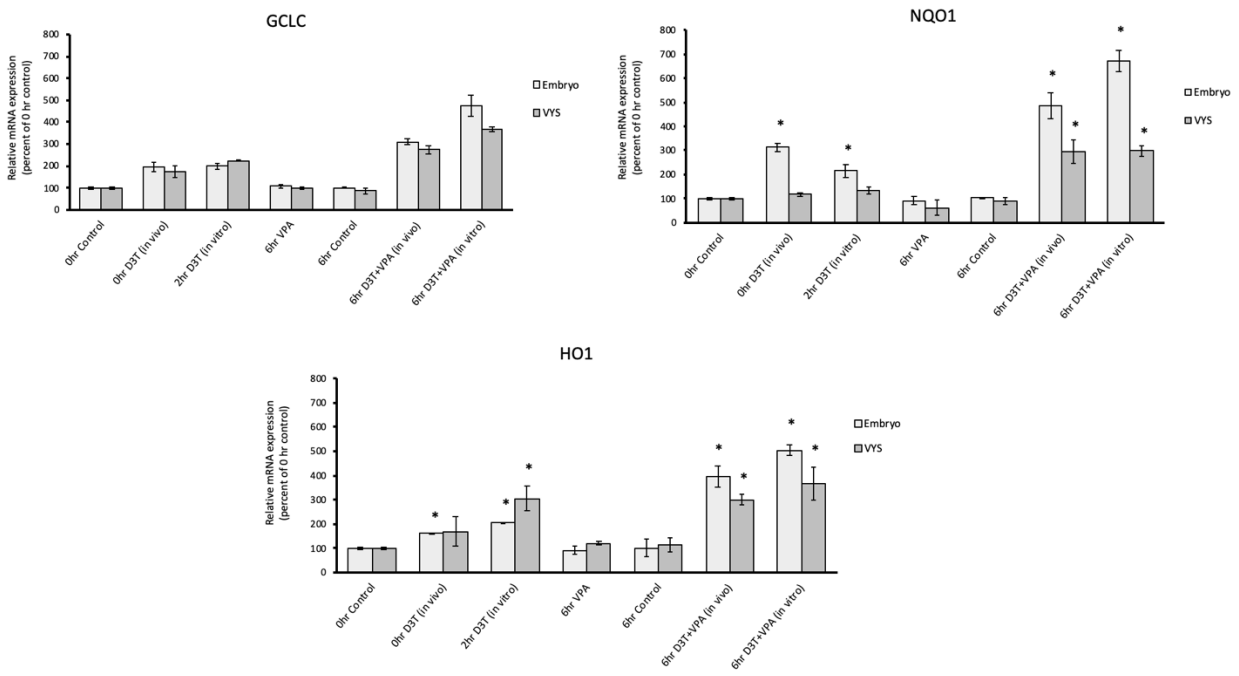

Figure 2-6 Gene expression of Nrf2 pathway genes: RT-qPCR measurement of Nrf2 antioxidant pathway genes *GCLC, H01,* and *NQ01* in the EMB and VYS following treatment with *in vivo* D3T (5 mg/kg), *in vitro* D3T (10 μM) or VPA (600 μM). Results are represented as fold-changes relative to the 0 hr control with normalization based on housekeeping gene *B-actin*. n=3, *p<0.05

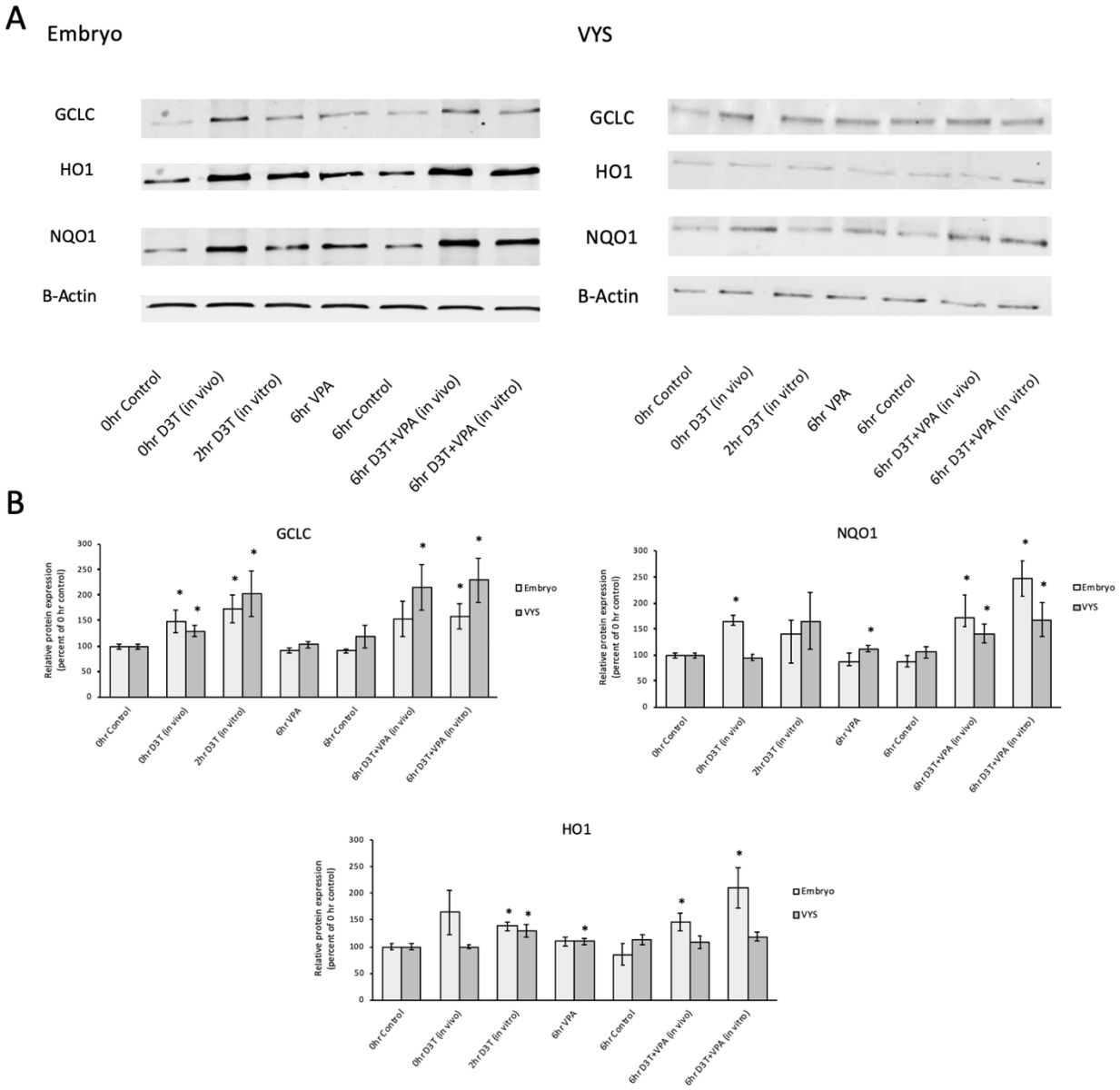

Figure 2-7 Protein expression of Nrf2 pathway proteins: Protein expression of Nrf2 antioxidant pathway proteins *GCLC, H01,* and *NQ01* in the EMB and VYS following treatment with *in vivo* D3T (5 mg/kg), *in vitro* D3T (10 μM) or VPA (600 μM). A: Western Blot Images B: Results are represented as fold-changes relative to the 0 hr control with normalization based on housekeeping gene *B-actin*. n=3, *p<0.05

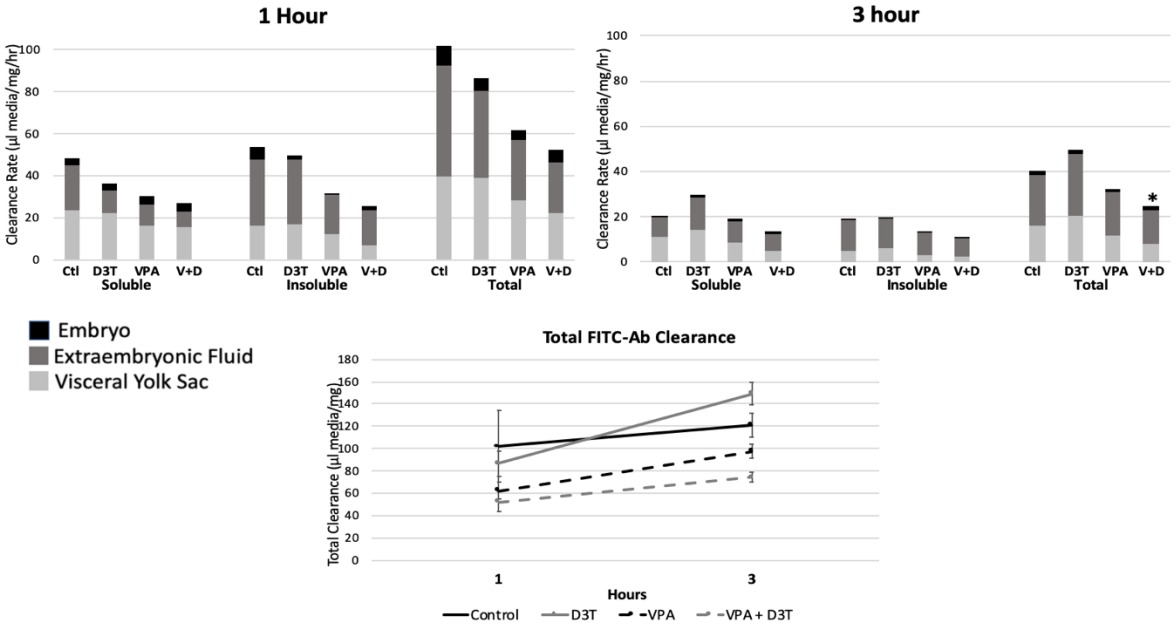

Figure 2-8 Compartmental histiotrophic nutrition assessment: Histiotrophic nutrition evaluated at 1 and 3 hours through FITC-Ab clearance. Total clearance is the sum of FITC-Ab fluorescence across VYS, EMB, and EEF. Acid insoluble and soluble fluorescence represent intact and degraded proteins respectively. n=6, *p<0.05

References

Ahangar, N., Naderi, M., Noroozi, A., Ghasemi, M., Zamani, E., & Shaki, F. (2017). Zinc Deficiency and Oxidative Stress Involved in Valproic Acid Induced Hepatotoxicity: Protection by Zinc and Selenium Supplementation. *Biological Trace Element Research*, *179*(1), 102–109. https://doi.org/10.1007/s12011-017-0944-z

Alam, J., Stewart, D., Touchard, C., Boinapally, S., Choi, A. M. K., & Cook, J. L. (1999). Nrf2, a Cap'n'Collar Transcription Factor, Regulates Induction of the Heme Oxygenase-1 Gene. *Journal of Biological Chemistry*, *274*(37), 26071–26078. https://doi.org/10.1074/jbc.274.37.26071

Ambroso, J., & Harris, C. (2012). Assessment of Histiotrophic Nutrition Using Fluorescent Probes. In C. Harris & J. M. Hansen (Eds.), *Developmental Toxicology* (Vol. 889, pp. 407–423). Humana Press. https://doi.org/10.1007/978-1-61779-867-2_25

Bruckner, A., Lee, Y. J., O'Shea, K. S., & Henneberry, R. C. (1983). Teratogenic effects of valproic acid and diphenylhydantoin on mouse embryos in culture. *Teratology*, *27*(1), 29–42. https://doi.org/10.1002/tera.1420270106

Burton, G.J., Hempstock, J., & Jauniaux, E. (2001). Nutrition of the Human Fetus during the First Trimester—A Review. *Placenta*, *22*, S70–S77. https://doi.org/10.1053/plac.2001.0639

Burton, Graham J., Watson, A. L., Hempstock, J., Skepper, J. N., & Jauniaux, E. (2002). Uterine Glands Provide Histiotrophic Nutrition for the Human Fetus during the First Trimester of Pregnancy. *The Journal of Clinical Endocrinology & Metabolism*, *87*(6), 2954–2959. https://doi.org/10.1210/jcem.87.6.8563

CDC. (2004). Spina Bifida and Anencephaly Before and After Folic Acid Mandate—United States, 1995–1996 and 1999—2000. *MMWR*, *53*(17), 362–365.

Chaudhary, S., Ganjoo, P., Raiusddin, S., & Parvez, S. (2015). Nephroprotective activities of quercetin with potential relevance to oxidative stress induced by valproic acid. *Protoplasma*, *252*(1), 209–217. https://doi.org/10.1007/s00709-014-0670-8

Cui, J., Shao, L., Young, L. T., & Wang, J.-F. (2007). Role of glutathione in neuroprotective effects of mood stabilizing drugs lithium and valproate. *Neuroscience*, *144*(4), 1447–1453. https://doi.org/10.1016/j.neuroscience.2006.11.010

Cui, Y., Ma, S., Zhang, C., Li, D., Yang, B., Lv, P., Xing, Q., Huang, T., Yang, G. L., Cao, W., & Guan, F. (2018). Pharmacological activation of the Nrf2 pathway by 3H-1, 2-dithiole-3-thione is neuroprotective in a mouse model of Alzheimer disease. *Behavioural Brain Research*, *336*, 219–226. https://doi.org/10.1016/j.bbr.2017.09.011

De Marco, P., Merello, E., Cama, A., Kibar, Z., & Capra, V. (2011). Human neural tube defects: Genetic causes and prevention. *BioFactors*, *37*(4), 261–268. https://doi.org/10.1002/biof.170

Dong, J., Sulik, K. K., & Chen, S. (2008). Nrf2-Mediated Transcriptional Induction of Antioxidant Response in Mouse Embryos Exposed to Ethanol *in vivo*: Implications for the Prevention of Fetal Alcohol Spectrum Disorders. *Antioxidants & Redox Signaling*, *10*(12), 2023–2033. https://doi.org/10.1089/ars.2007.2019

Fourcade, S., Ruiz, M., Guilera, C., Hahnen, E., Brichta, L., Naudi, A., Portero-Otín, M., Dacremont, G., Cartier, N., Wanders, R., Kemp, S., Mandel, J. L., Wirth, B., Pamplona, R., Aubourg, P., & Pujol, A. (2010). Valproic acid induces antioxidant effects in X-linked adrenoleukodystrophy. *Human Molecular Genetics*, *19*(10), 2005–2014. https://doi.org/10.1093/hmg/ddq082

Greene, N. D. E., & Copp, A. J. (2014). Neural Tube Defects. *Annual Review of Neuroscience*, *37*(1), 221–242. https://doi.org/10.1146/annurev-neuro-062012-170354

Grosse, S. D., Berry, R. J., Mick Tilford, J., Kucik, J. E., & Waitzman, N. J. (2016). Retrospective Assessment of Cost Savings From Prevention. *American Journal of Preventive Medicine*, *50*(5), S74–S80. https://doi.org/10.1016/j.amepre.2015.10.012

Hansen, J. M., Jones, D. P., & Harris, C. (2020). The Redox Theory of Development. *Antioxidants & Redox Signaling*, *32*(10), 715–740. https://doi.org/10.1089/ars.2019.7976

Hansen, J. M., Lee, E., & Harris, C. (2004). Spatial activities and induction of glutamate-cysteine ligase (GCL) in the postimplantation rat embryo and visceral yolk sac. *Toxicological Sciences: An Official Journal of the Society of Toxicology*, *81*(2), 371–378. https://doi.org/10.1093/toxsci/kfh154

Hardy, M., & Stedeford, T. (2008). Use of the Pup as the Statistical Unit in Developmental Neurotoxicity Studies: Overlooked Model or Poor Research Design? *Toxicological Sciences*, *103*(2), 409–410. https://doi.org/10.1093/toxsci/kfn036

Harris, C. (2012). Rodent Whole Embryo Culture. In C. Harris & J. M. Hansen (Eds.), *Developmental Toxicology* (Vol. 889, pp. 215–237). Humana Press. https://doi.org/10.1007/978-1-61779-867-2_13

Harris, C., & Hansen, J. M. (2012). Oxidative Stress, Thiols, and Redox Profiles. In C. Harris & J. M. Hansen (Eds.), *Developmental Toxicology* (Vol. 889, pp. 325–346). Humana Press. https://doi.org/10.1007/978-1-61779-867-2_21

Harris, C., Jilek, J. L., Sant, K. E., Pohl, J., Reed, M., & Hansen, J. M. (2015). Amino acid starvation induced by protease inhibition produces differential alterations in redox status and the thiol proteome in organogenesis-stage rat embryos and visceral yolk sacs. *The Journal of Nutritional Biochemistry*, *26*(12), 1589–1598. https://doi.org/10.1016/j.jnutbio.2015.07.026

Jilek, J. L., Sant, K. E., Cho, K. H., Reed, M. S., Pohl, J., Hansen, J. M., & Harris, C. (2015). Ethanol Attenuates Histiotrophic Nutrition Pathways and Alters the Intracellular Redox Environment and Thiol Proteome during Rat Organogenesis. *Toxicological Sciences*, *147*(2), 475–489. https://doi.org/10.1093/toxsci/kfv145

Jones, D. P. (2002). Redox potential of GSH/GSSG couple: Assay and biological significance. In *Methods in Enzymology* (Vol. 348, pp. 93–112). Elsevier. https://doi.org/10.1016/S0076-6879(02)48630-2

Komulainen, T., Lodge, T., Hinttala, R., Bolszak, M., Pietilä, M., Koivunen, P., Hakkola, J., Poulton, J., Morten, K. J., & Uusimaa, J. (2015). Sodium valproate induces mitochondrial respiration dysfunction in HepG2 in vitro cell model. *Toxicology*, *331*, 47–56. https://doi.org/10.1016/j.tox.2015.03.001

Kuo, P.-C., Yu, I.-C., Scofield, B. A., Brown, D. A., Curfman, E. T., Paraiso, H. C., Chang, F.-L., & Yen, J.-H. (2017). 3 H -1,2-Dithiole-3-thione as a novel therapeutic agent for the treatment of ischemic stroke through Nrf2 defense pathway. *Brain, Behavior, and Immunity*, *62*, 180–192. https://doi.org/10.1016/j.bbi.2017.01.018

Lai, J. S., Zhao, C., Warsh, J. J., & Li, P. P. (2006). Cytoprotection by lithium and valproate varies between cell types and cellular stresses. *European Journal of Pharmacology*, *539*(1–2), 18–26. https://doi.org/10.1016/j.ejphar.2006.03.076

Liu, Z., Li, Y., Chong, W., Deperalta, D. K., Duan, X., Liu, B., Halaweish, I., Zhou, P., & Alam, H. B. (2014). Creating a Prosurvival Phenotype Through a Histone Deacetylase Inhibitor in a Lethal Two-Hit Model: *Shock*, *41*(2), 104–108. https://doi.org/10.1097/SHK.0000000000000074

McBean, G. (2017). Cysteine, Glutathione, and Thiol Redox Balance in Astrocytes. *Antioxidants*, *6*(3), 62. https://doi.org/10.3390/antiox6030062

Nishii, K., & Shibata, Y. (2006). Mode and determination of the initial contraction stage in the mouse embryo heart. *Anatomy and Embryology*, *211*(2), 95–100. https://doi.org/10.1007/s00429-005-0065-x

Palsamy, P., Bidasee, K. R., & Shinohara, T. (2014). Valproic acid suppresses Nrf2/Keap1 dependent antioxidant protection through induction of endoplasmic reticulum stress and Keap1 promoter DNA demethylation in human lens epithelial cells. *Experimental Eye Research*, *121*, 26–34. https://doi.org/10.1016/j.exer.2014.01.021

Raghunath, A., Sundarraj, K., Nagarajan, R., Arfuso, F., Bian, J., Kumar, A. P., Sethi, G., & Perumal, E. (2018). Antioxidant response elements: Discovery, classes, regulation and potential applications. *Redox Biology*, *17*, 297–314. https://doi.org/10.1016/j.redox.2018.05.002

Sakai, Y. (1989). Neurulation in the mouse: Manner and timing of neural tube closure. *The Anatomical Record*, *223*(2), 194–203. https://doi.org/10.1002/ar.1092230212

Sant, K. E., Dolinoy, D. C., Jilek, J. L., Sartor, M. A., & Harris, C. (2016a). Mono-2-ethylhexyl phthalate disrupts neurulation and modifies the embryonic redox environment and gene expression. *Reproductive Toxicology*, *63*, 32–48. https://doi.org/10.1016/j.reprotox.2016.03.042

Sant, K. E., Dolinoy, D. C., Jilek, J. L., Shay, B. J., & Harris, C. (2016b). Mono-2-ethylhexyl phthalate (MEHP) alters histiotrophic nutrition pathways and epigenetic processes in the developing conceptus. *The Journal of Nutritional Biochemistry*, *27*, 211–218. https://doi.org/10.1016/j.jnutbio.2015.09.008

Sant, K. E., Hansen, J. M., Williams, L. M., Tran, N. L., Goldstone, J. V., Stegeman, J. J., Hahn, M. E., & Timme-Laragy, A. (2017). The role of Nrf1 and Nrf2 in the regulation of glutathione and redox dynamics in the developing zebrafish embryo. *Redox Biology*, *13*, 207–218. https://doi.org/10.1016/j.redox.2017.05.023

Schafer, F. Q., & Buettner, G. R. (2001). Redox environment of the cell as viewed through the redox state of the glutathione disulfide/glutathione couple. *Free Radical Biology and Medicine*, *30*(11), 1191–1212. https://doi.org/10.1016/S0891-5849(01)00480-4

Shi, X., Liu, Y., Zhang, D., & Xiao, D. (2019). Valproic acid attenuates sepsis-induced myocardial dysfunction in rats by accelerating autophagy through the PTEN/AKT/mTOR pathway. *Life Sciences*, *232*, 116613. https://doi.org/10.1016/j.lfs.2019.116613

Shibuya, K., & Murray, C. J. L. (1998). Congenital Abnormalities. In C. J. L. Murray & A. D. Lopez (Eds.), *Health dimensions of sex and reproduction: The global burden of sexually transmitted diseases, HIV, maternal conditions, perinatal disorders, and congenital anomalies* (pp. 455–512). Harvard School of Public Health.

Stochelski, M. A., Wilmanski, T., Walters, M., & Burgess, J. R. (2019). D3T acts as a pro-oxidant in a cell culture model of diabetes-induced peripheral neuropathy. *Redox Biology*, *21*, 101078. https://doi.org/10.1016/j.redox.2018.101078

Timme-Laragy, A. R., Goldstone, J. V., Imhoff, B. R., Stegeman, J. J., Hahn, M. E., & Hansen, J. M. (2013). Glutathione redox dynamics and expression of glutathione-related genes in the developing embryo. *Free Radical Biology and Medicine*, *65*, 89–101. https://doi.org/10.1016/j.freeradbiomed.2013.06.011

Tonelli, C., Chio, I. I. C., & Tuveson, D. A. (2018). Transcriptional Regulation by Nrf2. *Antioxidants & Redox Signaling*, *29*(17), 1727–1745. https://doi.org/10.1089/ars.2017.7342

Tung, E. W. Y., & Winn, L. M. (2011). Valproic Acid Increases Formation of Reactive Oxygen Species and Induces Apoptosis in Postimplantation Embryos: A Role for Oxidative Stress in Valproic Acid-Induced Neural Tube Defects. *Molecular Pharmacology*, *80*(6), 979–987. https://doi.org/10.1124/mol.111.072314

Vajda, F. J., O'Brien, T. J., Graham, J. E., Lander, C. M., & Eadie, M. J. (2013). Dose dependence of fetal malformations associated with valproate. *Neurology*, *81*(11), 999–1003. https://doi.org/10.1212/WNL.0b013e3182a43e81

Venugopal, R., & Jaiswal, A. K. (1996). Nrf1 and Nrf2 positively and c-Fos and Fra1 negatively regulate the human antioxidant response element-mediated expression of NAD(P)H:quinone oxidoreductase1 gene. *Proceedings of the National Academy of Sciences*, *93*(25), 14960–14965. https://doi.org/10.1073/pnas.93.25.14960

Wang, L., Wang, M., Hu, J., Shen, W., Hu, J., Yao, Y., Wang, X., Afzal, C. M., Ma, R., & Li, G. (2017). Protective effect of 3H-1, 2-dithiole-3-thione on cellular model of Alzheimer's disease involves Nrf2/ARE signaling pathway. *European Journal of Pharmacology*, *795*, 115–123. https://doi.org/10.1016/j.ejphar.2016.12.013

Wild, A. C., Moinova, H. R., & Mulcahy, R. T. (1999). Regulation of γ-Glutamylcysteine Synthetase Subunit Gene Expression by the Transcription Factor Nrf2. *Journal of Biological Chemistry*, *274*(47), 33627–33636. https://doi.org/10.1074/jbc.274.47.33627

Xiao, H., Jedrychowski, M. P., Schweppe, D. K., Huttlin, E. L., Yu, Q., Heppner, D. E., Li, J., Long, J., Mills, E. L., Szpyt, J., He, Z., Du, G., Garrity, R., Reddy, A., Vaites, L. P., Paulo, J. A., Zhang, T., Gray, N. S., Gygi, S. P., & Chouchani, E. T. (2020). A Quantitative Tissue-Specific Landscape of Protein Redox Regulation during Aging. *Cell*, *180*(5), 968-983.e24. https://doi.org/10.1016/j.cell.2020.02.012

Chapter 3

Reversible Temporal Oxidation of Protein Cysteines by Valproic Acid During Early Organogenesis in Mouse Conceptuses

Abstract

Reversible oxidative post-translational modifications (PTMs) of cysteine (Cys) residues have been demonstrated to act as signals with the ability to modify protein expression and function. Valproic acid (VPA) is an anti-epileptic medication that increases the risk of neural tube defects (NTDs). While VPA has been associated with biomarkers of elevated oxidation, there is little known about VPA's ability to differentially produce oxidative PTMs and the relationship between this potential mechanism and NTD risk. This study identified proteins and their networks that were differentially oxidized by VPA compared to controls at five time points during early organogenesis in whole mouse conceptuses. The distribution of differentially oxidized proteins indicated that a greater number of proteins had higher control oxidation until 10 hrs of exposure, where VPA-treated proteins began to show greater oxidation. Proteins mapping to pathways with developmental relevance and oxidation-reduction relevance were found to be recurrently enriched and included those related to nervous system development (6, 8, 10 hrs) and planar cell polarity (4 and 10 hrs) pathways with higher oxidation seen in the control and VPA groups, respectively. Proteins, β–actin and Pdc6ip, were identified at each occurrence of nervous system development and planar cell polarity pathway enrichment, respectively.

Redox-relevant pathways were exclusively enriched at 10 hrs with higher control oxidation. Gene set enrichment analysis identified a single developmentally relevant pathway of cytoskeletal organization at 4 hrs. Nervous system development, cytoskeletal organization, and cell polarity are all critical processes involved in neural tube closure with their differential oxidation patterns emphasizing a role for redox regulation of VPA-induced NTDs. Further understanding of specific oxidative Cys PTMs and tissue-specific PTM distribution will be necessary to fully appreciate the associations of Cys oxidation and functional outcomes demonstrated in this study.

Introduction

Valproic acid (VPA) is a branched-chain saturated fatty acid that is used to treat seizure disorders, migraine headaches, and various mood and mental health conditions, including the manic phase of bipolar disorder. Taken during pregnancy, VPA causes an increased risk of neural tube defects (NTDs) in infants (Jentink et al., 2010). NTDs arise when the neural tube fails to close during early organogenesis and can result in several different degrees of severity and types of deformity depending on the timing and location of the failed neural tube closure (NTC) (Greene & Copp, 2014). Clinically, VPA is also known to affect several biological processes including inhibition of histone de-acetylation, increasing γ-aminobutyric acid (GABA) levels, and blocking voltage-gated ion channels, but there is not yet an established mechanism to describe VPA-induced NTDs (Ghodke-Puranik et al., 2013; Phiel et al., 2001).

In addition to VPA's established mechanisms of action, VPA is also known to affect cellular biomarkers of oxidation (Ahangar et al., 2017; Chaudhary et al., 2015; Komulainen et al., 2015; Palsamy et al., 2014; Tung & Winn, 2011). VPA's manipulation of the oxidation environment is particularly interesting in the context of embryonic development, where oxygen concentration

and redox balance are essential for developmental progression (Hansen et al., 2020; Schafer & Buettner, 2001). VPA exposure in a mouse whole embryo culture (WEC) model demonstrated that VPA's effects on the cellular GSH:GSSG redox potential (E_h) differ across time and tissue during the period of organogenesis (Chapter 2). This research found that alterations to GSH concentrations was highly variable over time, but that 4, 10, and 14 hrs after VPA exposure showed the greatest oxidation to the GSH E_h with oxidation in all four embryonic tissue and fluid compartments (Chapter 2). The limited window of sensitivity to oxidation of the GSH redox couple led to the hypothesis that in addition to working through cellular mechanisms, VPA may also be causing oxidative post-translational modifications (PTMs) of proteins that cause changes to protein function relevant to NTC.

Several accessible amino acid residues in proteins are susceptible to oxidation, most notably, cysteine (Cys) and methionine (Met), although histidine, tyrosine, tryptophan, and phenylalanine can also be affected. Cys and Met are specifically susceptible due to the presence of a thiol group (R-SH). Cysteine thiol groups are responsive to the redox environment and can exist in several reversible and irreversible oxidation states (Figure 3-1) (Poole, 2015; Poole et al., 2020). Reversible modification of the Cys thiol group to sulfenic acid (-SOH) has specifically been shown to cause changes to protein function and potentially act as a mechanism for cellular signaling (Go et al., 2015). This has been supported by research showing that Cys sulfenic acid PTMs are specific to tissue type and age in mice (Xiao et al., 2020).

Modern proteomics technology has greatly advanced the field of redox proteomics. Previously, two-dimensional (2-D) gels separated by molecular weight and isoelectric point were the most reliable way to detect oxidative PTMs through comparing gels of control and oxidized conditions to identify differences followed by excision and identification through mass

spectrometry. Limitations of 2-D gels included the tedious workflow, gel-gel variation, and the identification of only excised and digested proteins (Bachi et al., 2013). Advancements in mass spectrometry techniques have led to the practice of shotgun proteomics studies where full protein extracts can be digested and identified through tandem LC-MS/MS. Early use of this technology relied on identifying PTMs through specific peptide mass shifts, however, it is now common practice to utilize labeling systems to tag and enrich samples for specific PTMs (Bachi et al., 2013). One such labeling method for identification of reversible oxidative Cys PTMs is Iodoacetyl Tandem Mass Tags (IodoTMT). IodoTMT labeling utilizes principles of standard TMT labelling to tag samples with an isobaric label containing a unique mass reporter group utilized to measure relative abundance through LC-MS/MS (Thompson et al., 2003). Unlike standard TMT labels that target amine groups, IodoTMT labels target reduced Cys thiols. Therefore, through sequential labeling and reduction steps, a ratio of oxidized to reduced Cys residues can be determined to calculate a protein-specific percent oxidation (Gould et al., 2015; Martínez-Acedo et al., 2014; Shakir et al., 2017).

It is unknown whether VPA affects the oxidation state of the Cys proteome and to date there have not been any whole proteome studies analyzing this question in developing embryos. This study aims to demonstrate that in addition to causing changes to cellular measures of redox balance, that VPA also differentially modifies protein Cys residues through oxidative PTMs. This will be evaluated through a proteome wide quantitative analysis of Cys oxidation levels in whole mouse conceptuses using IodoTMT labeling across five times points during early organogenesis. Pathway analysis of differentially oxidized proteins will then be performed to test the hypothesis that VPA differentially oxidized proteins and pathways of biological relevance to neural tube closure.

Materials & Methods

Animals

Experiments were conducted using mouse whole embryo culture (mWEC) to culture conceptuses from gestational days (GD) 8-9 in time-mated pregnant CD-1 mice (Charles River Laboratories, Raleigh, NC). Gestational day 0 was designated as the morning following mating with a positive vaginal plug. Animals were housed in groups of 6 or fewer in ventilated cages. All animal methodology was approved by the University of Michigan Institutional Animal Care and Use Committee and follows NIH guidelines.

Culture Conditions

Pregnant GD 8 dams were euthanized by CO_2 asphyxiation and uteri were removed and placed in Tyrode's solution (pH 7.4, HiMedia; Mumbai, India). Implantation sites were dissected with watchmaker's forceps and iridectomy scissors. Maternal tissues including the decidua and Reichert's membrane were removed to reveal intact conceptuses. Conceptuses were cultured in groups of 2-6 per bottle of 2 mL of immediately centrifuged female rat serum with 4.3 µl/mL penicillin, streptomycin (10,000 units penicillin and 10 mg streptomycin per mL, Sigma Aldrich; St. Louis, MO). All culture conditions were at 37 °C with gas concentrations at 5% O_2, 5% CO_2, 90% N_2 for 6 hrs then 20% O_2, 5% CO_2, 75% N_2 for the remainder of the culture period (Harris, 2012).

Time Course Exposures and Sampling

VPA (600µM in H_2O) was added *in vitro* to the female rat serum two hours following the start of culture. Samples were collected 2, 4, 6, 8, and 10 hrs following the addition of VPA. At the designated end of culture, conceptuses were rinsed 3 times with 1x Hank's Balanced Salt

Solution (HBSS, pH 7.4). The ecto-placental cone was removed and discarded and then whole conceptuses collected were collected in 200 µL HES buffer (50 mM HEPES, 1 mm EDTA, 0.1% SDS w/v, Thermo Fisher Scientific; Waltham, MA) in pools of ten. Samples were then sonicated to disrupt tissue and homogenize the solution and held on ice before centrifugation for 10 min at 12,000 x g. The supernatant was then frozen at -80 °C before further processing. All timepoints were single replicates, with the exception of 4 hr with a total of 3 replicates collected to measure sample variability. A bicinchoninic acid assay (BCA) was performed with a bovine serum albumin standard to measure protein concentration.

Iodoacetyl Tandem Mass Tag (IodoTMT) Labeling

200 µg protein in 200 µL HES buffer from each sample was combined with the corresponding IodoTMT label dissolved in 10 µL methanol to label reduced Cys residues (Table 3-1). Samples were left to label reduced Cys overnight at room temperature. The following day the remaining label was removed through a methanol/chloroform precipitation followed by 3 washes with ice-cold acetone. The resulting pellet was then re-suspended in 100 µL HES buffer with dithiothreitol (DTT, Thermo Fisher Scientific; Waltham, MA) added at a 50 mM concentration and held at 37 °C for 1 hour. The methanol/chloroform precipitation and acetone washes were repeated followed by resuspending the pellet in 200 µL HES buffer. Samples were combined with the indicated IodoTMT label dissolved in 10 µL methanol and held at room temperature overnight to label previously oxidized Cys residues. The next morning a methanol/chloroform precipitation was performed followed by an overnight trypsin digestion in 200 µL 50 mM ammonium bicarbonate with 5 µg trypsin at 37 °C. The tryptic digestion was completed with the addition of 8 µL 10% trifluoroacetic acid (v/v). All samples of the same timepoint were then combined and separated into two 300 µL aliquots that were dried in a

centrifugal vacuum concentrator. One of the aliquots then underwent enrichment utilizing Immobilized Anti-TMT resin and TMT elution buffer following the manufacturer's instructions (Thermo Fisher Scientific; Waltham, MA). Samples were dried and frozen at -80 °C until analysis by LC-MS^3.

Liquid Chromatography, Mass Spectrometry

Liquid chromatography, mass spectrometry, and protein identification were performed by the Proteomics Resource Facility at University of Michigan. Multinotch-MS3 was utilized to obtain superior accuracy which minimizes the reporter ion ratio distortion resulting from fragmentation of co-isolated peptides during MS analysis (McAlister et al., 2014). Orbitrap Fusion (Thermo Fisher Scientific; Waltham, MA) and RSLC Ultimate 3000 nano-UPLC (Dionex) was used to acquire the data. 2 µl of the sample was resolved on a PepMap RSLC C18 column (75 µm i.d. x 50 cm; Thermo Fisher Scientific; Waltham, MA) at the flow-rate of 300nl/min using 0.1% formic acid/acetonitrile gradient system (2-22% acetonitrile in 150 min; 22-32% acetonitrile in 40 min; 20 min wash at 90% followed by 50 min re-equilibration) and directly sprayed onto the mass spectrometer using an EasySpray source (Thermo Fisher Scientific; Waltham, MA). The mass spectrometer was set to collect one MS1 scan (Orbitrap; 120K resolution; AGC target $2x10^5$; max IT 100ms) followed by data-dependent, "Top Speed" (3 sec) MS2 scans (collision induced dissociation; ion trap; NCE 35; AGC $5x10^3$; max IT 100 ms). For multinotch-MS3, the top 10 precursors from each MS2 were fragmented by HCD followed by Orbitrap analysis (NCE 55; 60K resolution; AGC $5x10^4$; max IT 120 ms, 100-500 m/z scan range).

Protein identification in Proteome Discoverer

Proteome Discoverer (v2.4; Thermo Fisher Scientific; Waltham, MA) was used for data analysis. MS2 spectra were searched against Uniprot mouse protein database (reviewed and unreviewed; 55364 entries; downloaded on 05/06/2020) using the following search parameters: MS1 and MS2 tolerance were set to 10 ppm and 0.6 Da, respectively; IodoTMT modification (+329.227 Da) and carbamidomethylation on Cys residues were considered as variable modifications. Identified proteins and peptides were filtered to retain only those that passed ≤1% FDR threshold. Quantitation was performed using high-quality MS3 spectra (Average signal-to-noise ratio of 10 and <30% isolation interference).

Gene Set Enrichment Analysis

Gene Set Enrichment Analysis (GSEA) was performed to identify pathways that showed differential enrichment between proteins with higher and lower oxidation following VPA (Mootha et al., 2003; Subramanian et al., 2005). Data were input into the GSEA software (v. 4.1.0) as a .rnk file containing Uniprot accession numbers and VPA/Ctl percent oxidation ratios and run as a pre-ranked dataset with 1000 permutations and collapsing redundant accession numbers to a single gene name. Proteins were searched against the Biological Process Gene Ontology (GO) term database (v 7.2). Pathways with an FDR value of less than 25% were included in the results.

Differentially Oxidized Protein Pathway Analysis

Differentially oxidized proteins were categorized by those with increased or decreased oxidation compared to the control and searched for Biological Process Go-term enrichment using String against a background of the *Mus musculus* proteome (Szklarczyk et al., 2019). Pathways

that showed significant (FDR <0.05) were then collapsed in Revigo using the *Mus musculus* database and SimRel semantic similarity measure to reduce redundant pathways (Supek et al., 2011). To be included in downstream pathway analysis or assessment of differential oxidation states, proteins had to have a high confidence false discovery rate (FDR) as defined by Proteome Discoverer (Thermo Fisher Scientific; Waltham, MA). Proteins that did not indicate labeling in both control and VPA-treated samples were excluded from this analysis. Differentially oxidized proteins were defined as proteins that showed a difference of at least 8.6 percentage points between control and VPA percent oxidation values. This threshold was based on the maximum standard deviation of a sample group from the three 4 hr replicates used to measure variability (Table 3-2).

Hierarchical Clustering

Hierarchical clustering of the 102 proteins that appeared in the data set of all five time points was performed by Heatmapper (Babicki et al., 2016). VPA/Ctl oxidation percent ratios were input for each time point and clustering was performed based on Euclidean distance and average linkage.

Results

IodoTMT Data Summary

Table 3-4 summarizes the IodoTMT data across the five time points. The number of proteins identified within each time-specific dataset differed with the highest number of proteins identified at 2 hrs and the lowest at 4 hrs. The average oxidation percent for the controls ranged from 44.7 to 47.5%, while for the VPA samples the average was between 43.9 and 46.9%. The percent of proteins that were differentially oxidized between control and VPA samples are

displayed in Figure 3-2. 2 hrs and 10 hrs had the greatest number of proteins meeting the threshold for differential oxidation. At 2 hrs, the majority of differentially oxidized proteins showed higher oxidation in the control while at 10 hrs the majority of these proteins were more oxidized following VPA treatment (Figure 3-2).

Differentially Oxidized Protein Pathway Analysis

All sets of differentially oxidized proteins showed biological process GO-term enrichment (Figures 3-3 to 3-7). Identified pathways spanned a wide range of biological processes with prominent categories including metabolism, gene/protein expression, response to stimulus, and transport. Pathway enrichment in String and GSEA utilized the mouse proteome as background for consistency across time points and due to the relatively low number of protein IDs within each time point. Due to the tendency of LC-MS/MS methodology to identify proteins of greatest abundance, it is expected that some of these more general pathways within the categories of metabolism and gene/protein expression are prominent.

To specifically address the hypothesis of VPA-induced Cys modification as a potential disruptor to NTC, the results will specifically focus on pathways of developmental or redox relevance. Developmental pathways are enriched with higher control oxidation at 2, 4, 8, 10 hrs and in pathways with higher VPA oxidation at 4, 6, and 10 hrs. The biological process GO-term pathways that make up these categories are summarized in Table 3-5. The majority of the 12 developmental pathways show greater oxidation in control samples compared to VPA-treated samples. There is enrichment of pathways with higher control oxidation at 2, 4, 6, and 8 hrs and enrichment of pathways with higher VPA oxidation only at 4 and 10 hrs. Establishment or maintenance of cell polarity is enriched at two time points for proteins with higher VPA oxidation at 4 and 10 hrs, while nervous system development is enriched for proteins with higher

control oxidation at 6, 8, 10 hrs. At 10 hrs, nervous system development is collapsed within the multicellular organism development pathway. All other pathways only appear at one time point. The specific proteins that make up each of these repeat pathways are identified in Figures 3-8 and 3-9.

Response to stimulus pathways encompass pathways that are relevant to actions of the cell or organism in response to an outside signal such as drugs, stress, a specific molecular compound, environmental cue, or oxidation. Of particular interest to this study are pathways related to oxidation due to VPA's association in previous research with increases in markers of oxidation. Enriched pathways of the most relevance to oxidation included oxidation-reduction process, response to oxidative stress, and response to hydrogen peroxide. These pathways were exclusively enriched at 10 hrs with higher oxidation in the control and are highlighted in Table 3-6.

In addition to these pathways that are directly relevant to development or oxidation other pathways that may play a role in the process of NTC were also identified. These pathways included the following: actin cytoskeletal organization (4 hr higher VPA oxidation), cortical cytoskeleton organization (6 and 10 hr higher VPA oxidation), response to axon injury (10 hr higher Ctl oxidation), and positive regulation of NF-kappa B transcription factor activity (10 hr higher Ctl oxidation). The proteins within each of these enriched pathways and their corresponding VPA/Ctl oxidation ratio are listed in Table 3-7.

Gene Set Enrichment Results

GSEA was performed to identify pathways that showed directional oxidation enrichment without the need for a predetermined threshold for inclusion. The pre-ranked GSEA identified only a small number of enriched pathways with an FDR of less than 0.25. The majority of the

identified pathways were related to metabolism with the only NTD relevant pathway being cytoskeletal organization which was identified in proteins with higher VPA oxidation at 4 hrs (Figure 3-10). Within this pathway, there were 12 proteins that demonstrated core enrichment for this higher VPA oxidation subset (Table 3-8).

Time Series Oxidation Patterns

There were 102 proteins that were identified in the datasets of all 5 time points. Most of these proteins did not meet the criteria for differential oxidation and showed close to a 1:1 ratio of oxidation in VPA versus control samples (Figure 3-11). Pathway analysis of these proteins shows a similar distribution of pathways to the rest of the data with several developmental and response to stimulus pathways included (Figure 3-12). Hierarchical clustering was performed to identify patterns of VPA/Ctl oxidation percent over time. Figure 3-13 illustrates the results of the clustering with proteins grouped by similar oxidation patterns. The darker the red or blue shading of the rectangle, the greater the fold change in oxidation percent with respect to the control. As supported by Figure 3-11, few of these proteins showed a significant shift in oxidation with VPA exposure, but there are time-specific patterns of oxidation with overall oxidation patterns supporting previously described patterns seen in Figure 3-2 of a shift from higher control oxidation at 2 hrs to higher VPA oxidation at 10 hrs. Despite the limited shifts in oxidation of these proteins identified across the time course there is evidence that proteins with comparable function show equivalent oxidation patterns as demonstrated by the grouping of Mdh1/2 and Rpl3/30. This grouping of functionally similar proteins also supports the data reliability since it demonstrates that oxidation patterns of functionally similar proteins are occurring in predictable patterns. Four proteins (Mif, Cat, Got2 and Adh5) show a more significant shift in oxidation in

the control group at 2 and 10 hrs. These proteins are collectively involved in processes related to metabolism and response to stimuli based on GO-term enrichment.

Discussion

This study aimed to determine if VPA's action as an oxidant extended beyond time-specific changes to cellular redox potential to include reversible oxidative PTM of Cys. We hypothesized that VPA would increase levels of Cys oxidation on proteins and pathways relevant to the process of NTC. A systems level proteomics approach was utilized to test this hypothesis across five time points (mouse GD 8 at 2, 4, 6, 8, and 10 hrs following VPA exposure) of early organogenesis. Enrichment of biological process GO-terms was utilized to identify targets of VPA's oxidation and lead to identification of many developmentally relevant pathways, in addition to several more pathways related to general biological processes that may or may not be directly implicated in failed NTC. This discussion will focus specifically on the pathways of relevance to development, oxidation, and cytoskeletal organization to retain the focus on our hypothesis of VPA's actions related to NTC.

One striking finding of this analysis of VPA's effect on reversible Cys modification is that at four of the five time points there are a greater number of differentially oxidized proteins with higher control oxidation. A larger proportion of differentially affected proteins showing higher VPA oxidation was not seen until the final time point at 10 hrs. Reversible oxidation of Cys residues are believed to act as redox signals, where Cys thiols are temporarily oxidized in the presence of H_2O_2 or other ROS. In the case of oxidation of proteins located in an enzyme's active site or within a receptor binding domain, the action is generally believed to be inhibitory and can only be restored through reduction (Rhee, 2006; Schieber & Chandel, 2014). During the course of development many pathways and molecular signals are attenuated or inhibited

completely in the course of patterning and differentiation to ensure that symmetry, asymmetry, and proper juxtaposition are maintained. Redox signals likely play an important role in these events. While redox signaling through reversible Cys oxidation is an essential process for development and normal biological function, prolonged exposure to oxidants can further oxidize protein Cys residues to sulfinic or sulfonic acid which are mostly irreversible and can lead to permanent changes to protein function or degradation (Figure 3-1) (Go et al., 2015; Schieber & Chandel, 2014). The specific effect of reversible Cys oxidation on a particular protein and the activation or inactivation of function is often protein-specific (Schieber & Chandel, 2014).

An association between reversible Cys oxidation level and lifecycle has been noted in the areas of development and aging. In aging, there is a well-established trend of increasing levels of reversible Cys modification noted across multiple model systems including yeast cells, roundworms, and mice (Brandes et al., 2013; Knoefler et al., 2012; Xiao et al., 2020). A similar effect was noted during the period of development in *C. elegans* with high levels of reversible Cys oxidation during larval development (L2 and L4) that leveled off in adulthood (Days 2-3) and increased again post-reproductive age (Days 8 and 15) (Knoefler et al., 2012). This study in particular may provide an explanation for the higher levels of control oxidation noted in our data for differentially oxidized proteins at 2-8 hrs (Figure 3-2). This would indicate that higher control Cys oxidation is a normal function of developmental process, and that VPA's under-oxidation of the differentially affected proteins may be disrupting the normal course of development leading to altered neurulation. A second possible explanation for the higher levels of differential reversible Cys oxidation in the control is that VPA may promote further oxidation of Cys beyond sulfenic acid. Sulfinic and sulfonic acid modifications are believed to be largely irreversible Cys modifications. Only a single antioxidant, sulfiredoxin, is capable of reducing

sulfinic acid (Findlay et al., 2005). Because IodoTMT only identifies reversible Cys oxidation, it is therefore possible that VPA promoted sulfinic and sulfonic acid oxidation, which would have gone undetected in our analysis. Regardless of the true interpretation for differential reversible Cys oxidation between the control and VPA groups, it is clear that VPA causes patterns of oxidation that differ from the control leading to potential disruption of developmental processes and neural tube closure.

In addition to the unexpected finding of greater oxidation in the control for differentially affected proteins, enrichment of redox relevant pathways was only identified at 10 hrs, but with higher control oxidation across the three identified pathways and 12 proteins (Table 3-6). Given VPA's associations with elevated oxidation, it was unexpected to see redox pathways with higher control oxidation. One of the identified redox proteins was catalase (Cat), which reduces H_2O_2 and showed a 0.4 VPA/Ctl oxidation percentage at 10 hrs. Research studying Cys oxidation of Cat demonstrated decreased activity with increased oxidation (Ghosh et al., 2006). This indicates that although the control group is showing higher levels of Cat oxidation, activity would be higher in the less oxidized VPA-treated group, implying higher antioxidant function under VPA conditions. Many of the other identified oxidation-reduction pathway associated proteins are related to DNA repair and the citric acid (TCA) cycle. The TCA cycle is an aerobic respiration pathway that utilizes the glycolysis byproduct, pyruvate, to produce ATP. Elevated levels of reversible Cys oxidation in mouse ventricles were associated with consumption of a high-fat, high-sucrose western diet leading to the hypothesis that oxidation of the TCA cycle-associated proteins lead to metabolic alterations that manifested in cardiac tissue remodeling and dysfunction (Behring et al., 2014). Glucose metabolism during the organogenesis stage of rat development has been demonstrated to shift from high rates of glycolysis and the pentose

phosphate pathway prior to organogenesis to a more dominant utilization of the TCA cycle and decrease in the other pathways during active organogenesis (Shepard et al., 1970; Tanimura & Shepard, 1970). This switch from predominately anaerobic to oxidative metabolism of glucose is believed to occur as a result of the onset of yolk sac (VYS) circulation (Akazawa et al., 1994). The onset of VYS circulation occurs during the second half of GD 8 in the mouse WEC model used in our study. Several studies of VPA's effects of the TCA cycle have indicated that VPA inhibits TCA cycle activity and promotes glycolysis (Johannessen et al., 2001; Luís et al., 2007; Salsaa et al., 2020; Triyasakorn et al., 2020). This documented effect of VPA's disruption of oxidative glucose metabolism considered in tandem with the observed lower Cys oxidation status of the TCA cycle proteins at 10 hrs in our study could indicate that the higher levels of reversible Cys oxidation in the control are required for TCA cycle function, which is essential to the organogenesis phase of development.

Developmentally relevant biological process GO-terms were identified across all five timepoints (Table 3-5). In most cases, developmentally relevant pathways were enriched in proteins with higher oxidation in the control conceptuses compared to VPA-treated conceptuses. There were several enriched pathways directly related to brain development such as brainstem and nervous system development while others were more peripherally related to general developmental processes such as establishing cell polarity. Two pathways- Nervous System Development and Establishment or Maintenance of Cell Polarity, were recurrently enriched at more than one time point. Each of these pathways maintained the directionality of oxidation response at each occurrence with nervous system development showing elevated control oxidation and establishment or maintenance of cell polarity showing elevated VPA oxidation.

The nervous system development pathway was enriched at 6, 8, 10 hrs in proteins with higher control oxidation. Figure 3-8 displays the proteins that were contained within this pathway at each of these three time points and points to beta-actin (Actb) as the single protein that is common. Beta-Actin is of high developmental relevance to the process of neural tube closure where it is involved in the mechanical mechanism of convergent extension helping to draw the neural folds together at the medial hinge point to form the fused neural tube (Nikolopoulou et al., 2017). The VPA/Ctl oxidation ratios of Actb Cys oxidation were 0.48, 0.75, and 0.75 at 6, 8, and 10 hrs, respectively. The most commonly affected Actb Cys residue was Cys 217 at 6, 8, 10 hrs with Cys 257 and 272 being affected only at 10 hrs. There have been several studies looking at the consequences of Actb oxidative Cys modifications from a perspective of functional change or disease associations. Cys 217, the most commonly labelled Cys in our data, has shown greater oxidation in cataractous human lenses (Wang et al., 2017). S-glutathionylation of Cys 374 has been shown to decrease actin-polymerization (Dalle-Donne et al., 2003; Fiaschi et al., 2006). The association with disease and decreased function following oxidation in these prior studies seems contrary to what would be expected in the higher oxidized control samples. Therefore, it is possible that there is an unknown mechanism related to Cys 217 oxidation that could be required for control function of neural tube closure processes. Additionally, due to IodoTMT labeling not distinguishing between reversible Cys modifications and performing these experiments in whole conceptuses, it is possible that cell and organ type specificity as well as oxidative modification specificity could be key to understanding this phenomenon. Oxidation of Cys 217 of Actb was also noted in the Oximouse database (https://oximouse.hms.harvard.edu) which characterized the cysteine oxidation state of several tissues in young and aged mice through labelling with cysteine-reactive phosphate tags (CPT)

(Xiao et al., 2020). Oxidation at Cys 217 ranged between 2.1 to 14% with the most affected tissues being spleen, kidney, and subcutaneous fat with nearly identical Cys site occupancy in young and old samples (Xiao et al., 2020).

The second pathway with recurring enrichment was establishment or maintenance of cell polarity, which was enriched at 4 and 10 hrs in proteins with higher VPA oxidation (Figure 3-9). Overall there were six proteins across two time points that identified cell polarity as a pathway of interest with one protein, Programmed Cell Death 6 Interacting Protein (Pdcd6ip, also known as Alix), being identified at both 4 and 10 hrs. This protein is involved in processes such as endocytosis, apoptosis, proliferation, and cell polarity. Mouse knock-outs of Pdcd6ip develop a severe form of NTD called microcephaly that is likely caused by increased apoptosis of neural progenitor cells (Laporte et al., 2017). The oxidation sites on Pdcd6ip in our data are at Cys 40 and Cys 691 with total control oxidation percents of 44.5 and 41.9% and VPA oxidation percents of 54 and 54.9% at 4 and 10hrs, respectively, leading to VPA/Ctl oxidation ratios of 1.2 and 1.3. There is no research at present identifying the functional consequences of modification at these oxidation sites. However, Pdcd6ip has previously been uniquely identified in adipose derived stem cells post VPA exposure compared to the control though thereby indicating that its expression patterns may change in addition to its oxidation (Santos et al., 2020). Despite limited evidence of how Pdcd6ip's function may be affected by oxidation, there is additional experimental evidence of cysteine oxidation percent at these sites in the Oximouse database, which identified Cys 691 as being the most affected Cys residue of Pdcd6ip having a percent oxidation ranging from 0 to 26% with the most affected tissues being aged mouse liver and young and aged mouse lung tissue. Cys 40 was the second most affected Cys with percent oxidation ranging from 0.82 to 14% and the most affected tissues being the kidney and spleen of

young mice (Xiao et al., 2020). Future studies will need to be completed to better understand the consequences of the tissue-specific modification of this protein and how it may affect protein function.

GSEA enrichment of the pre-ranked VPA/Ctl oxidation ratios only identified a single developmentally adjacent pathway of 'Cytoskeletal Organization' at 4 hrs with an FDR of less than 0.25 showing higher oxidation following VPA treatment (Table 3-8, Figure 3-9). String analysis of pathway enrichment for the differentially oxidized proteins also identified two cytoskeletal pathways: Actin Cytoskeleton Organization and Cortical Cytoskeleton Organization, which both showed higher oxidation after VPA exposure at 4 hr and 6/10 hrs, respectively (Table 3-7). Cap1was the top hit for GSEA and also identified at 4 hrs in String. Cap1 is an actin monomer binding protein that promotes cellular actin depolymerization (Bertling et al., 2004). Cap1 has previously been identified as upregulated following an analysis of copper's teratogenic properties in a HepG2 cell model (Song et al., 2009). Talin1 (Tln1) is a protein involved in cell adhesion and proliferation that was identified at 4 and 10 hrs. Mutation of Tln1 is associated with decreased proliferation of cranial neural crest cells (CNCC) in the palate development, which could indicate a potential role in proliferation during NTC (Ishii et al., 2018). Cys oxidation of Tln1 has been noted in aged mice as a result of decreased Slc7a11 expression and showed the ability to be reversed upon overexpression of Slc7a11 to restore cellular reduced Cys levels (Zheng et al., 2020). Alpha-actinin 1 (Actn1) is an actin binding protein that showed elevated oxidation following VPA exposure at 6 and 10 hrs (Table 3-7). Actn1 plays an active role in neurulation with protein expression increasing during this stage of development, however overexpression of Actn1 has been demonstrated to inhibit blastopore closure in *Xenopus laevis* (Shawky et al., 2018). Cys oxidation of Actn1 has been reported in several studies, but the

functional consequences of the oxidation are not evident. Following treatment with buthionine sulfoximine to deplete cellular antioxidant GSH, Actn1 expression was shown to decrease under conditions without oxidative stress (Zepeta-Flores et al., 2018). This reveals a potential role for redox-relevant mechanisms of Actn1 expression that could negatively affect neurulation. Alpha-tubulin (Tuba1a), an isoform of tubulin whose mutation has been associated with NTD outcomes, was also identified (Gaitanis & Tarui, 2018). Cys oxidation of purified porcine tubulin has been associated with a decrease in polymerization that can be reversed following reduction of the modified Cys (Landino et al., 2011). Similar to the previously described role of beta-actin, tubulin and microtubules in general are involved in the process of primary neurulation through bending and closure of the neural plate (Cearns et al., 2016). Disruption of polymerization through oxidation could therefore inhibit the neural tube closure process. While many of these proteins have evidence of functional changes following oxidation or importance to neural tube closure, few have clear evidence of both at this time.

Though not strictly developmental in function with a primary role in innate immunity and infection response, the transcription factor nuclear factor-Kappa B (NF-KB) is also essential to development. The pathway, positive regulation of NF-Kappa B transcription factor activity, showed enrichment for higher control oxidation at 10 hrs (Table 3-7). Knockdown of several NF-KB pathway components have been classified as embryonic lethal due to developmental defects (Espín-Palazón & Traver, 2016). The connection of the Cys oxidation in the three identified proteins (Cat, Psma6, and Rps3) to VPA exposure or NTDs is not clear, but there is substantial evidence indicating a role for VPA in disruption of NF-KB signaling. Neurulation is one of many embryonic processes that is impacted by the NF-KB pathway with double knockdown of IKK-alpha and IKK-beta resulting in a hindbrain NTD (Li et al., 2000). A study

of the GD 9 organogenesis mouse conceptuses exposed to VPA *in vivo* demonstrated an acute response of decreased mRNA expression at 1 and 3 hrs of pathway activator Pim-1 and the p65, p105/p50 subunits of the NF-KB heterodimer (Shafique & Winn, 2021). Despite these changes to mRNA expression, there was no change in protein level of the NF-KB heterodimer on GD 9 or 10 (Shafique & Winn, 2021). Differences in protein expression of the NF-KB heterodimer components were present in GD 13 embryo heads with p50 decreased in all VPA-exposed groups, but p65 only exhibited an increase in mice with exencephaly. Nuclear levels of both NF-KB, however remained unchanged (Shafique & Winn, 2021).

Previous investigations into the mechanisms of VPA-induced birth defects, NTDs in particular, have suggested that the anti-epileptic medication causes its deleterious effects through pathways involving increased cellular oxidation (Palsamy et al., 2014; Tung & Winn, 2011). Generalizations of increased cellular oxidation and/or oxidative stress are difficult to reconcile with precise biochemical and molecular mechanisms leading to toxicity because specific affected pathways and their constituent proteins are not identified. The current application of IodoTMT proteomics has allowed for the detection and identification of relevant pathways and proteins differentially oxidized as a result of VPA exposure during the critical period of neurulation in the mouse conceptus. By targeting oxidizable protein Cys sites of reversible post-translational modification temporally in the developing mouse conceptus during organogenesis we have identified several key developmental pathways involving cell polarity and nervous system development that are differentially oxidized under control or VPA-treated conditions. In addition to demonstrating differential oxidation of development-specific pathways, VPA treatment also caused differential oxidation of proteins and pathways relevant to cytoskeletal dynamics and glucose metabolism, which are important processes for neural tube closure and organogenesis.

Future considerations for this work include a spatial assessment of oxidation throughout the conceptus to identify tissue specific targets of VPA-induced protein oxidation. Previous studies have demonstrated distinct differences in the response of the embryo proper and visceral yolk sac to VPA highlighting the need for more work to identify potential differences in Cys oxidation (Chapter 2 and 4). Another future direction for this work includes identification of specific species of reversible oxidative Cys modification. IodoTMT indiscriminately labels reversible Cys modifications making it unable to identify specific species of Cys modification (Figure 3-1). Identifying the specific Cys modifications will improve understanding of how Cys oxidation modifies protein form and function and add a greater depth of knowledge to VPA's differential protein oxidation patterns.

Tables

	126	127	129	130
Sample ID	Ctl Reduced Cysteine	VPA Reduced Cysteine	Ctl Oxidized Cysteine	VPA Oxidized Cysteine

Table 3-1 IodoTMT label assignments: 6-plex Iodoacetyl Tandem Mass Tag (iodoTMT) label assignments for control (Ctl) and valproic acid (VPA) treated samples. These label assignments were used for all 5 time points with one replicate performed for 2, 6, 8, and 10 hr time points and three replicates of the 4 hr time point. All samples were of pooled GD 8 whole mouse conceptuses.

Standard Deviation Distribution			
	Ctl % Ox	VPA % Ox	MEHP % Ox
Mean	7.73	8.50	8.25
Max	21.81	30.08	29.66
75th	11.16	11.70	11.45
Median	6.57	7.75	7.23
25th	4.00	4.13	4.07
Min	0.71	0.34	0.34

Table 3-2 4 hr IodoTMT replicate standard deviation distribution: A standard deviation for percent oxidation was calculated across the three 4 hr replicates to determine data variability. The highest standard deviation for a sample type was 8.5 percentage points, so this was adopted as the threshold of difference required for a protein to be considered differentially oxidized.

		Ctl % Ox	VPA % Ox	Absolute Difference	VPA/Ctl	# Proteins	% Ctl Higher	% VPA Higher
4hr #1	Average	46.3	46.7	4.04	1.02	254	3.9	5.9
	Min	13.2	10.6	0.2	0.3			
	Max	97.3	96.8	28.3	1.7			
4hr #2	Average	46.9	45.1	6.84	0.98	542	20.1	9.8
	Min	5.9	6.1	0	0.22			
	Max	97.4	96.9	32.26	4.98			
4hr #3	Average	46.3	46.9	8.8	1.03	1012	18.1	22.1
	Min	10.0	2.2	0.0	0.08			
	Max	97.0	98.6	51.3	2.83			

Table 3-3 4 hr IodoTMT replicate summary: Data summary table of the three individual 4hr replicate samples highlights the distribution of oxidation percentage, absolute difference between Ctl and VPA oxidation percent, number of identified proteins, and ratio of VPA/Ctl oxidation percent.

		Ctl % Ox	VPA % Ox	Absolute Difference	VPA/Ctl	# Proteins
2hr	Average	47.49	44.02	7.89	0.94	765
	Min	8.41	3.59	0.01	0.25	
	Max	98.66	98.82	61.17	2.94	
4hr	Average	44.70	43.91	4.11	0.97	186
	Min	17.23	12.75	0.07	0.55	
	Max	95.87	96.53	14.73	1.24	
6hr	Average	47.06	46.40	5.70	0.99	299
	Min	14.30	9.55	0.00	0.39	
	Max	98.50	97.60	32.54	1.61	
8hr	Average	44.70	43.98	6.48	1.00	251
	Min	9.15	11.57	0.02	0.21	
	Max	99.63	99.85	49.00	2.24	
10hr	Average	44.26	46.87	8.14	1.09	646
	Min	8.48	8.42	0.02	0.19	
	Max	97.12	96.62	58.28	2.70	

Table 3-4 IodoTMT time course data summary: The IodoTMT data summary includes proteins that had a high confidence FDR and were labelled in Control and VPA samples. The average, minimum, and maximum values are presented for Control Oxidation percent, VPA Oxidation percent, the absolute difference between control and VPA oxidation percent and the VPA/Ctl Oxidation percent ratio.

Enriched Developmental Pathways				
Time	**Direction**	**term_ID**	**description**	**log10 p-value**
2hr	Ctl Ox Higher	GO:0003360	brainstem development	-1.9066
2hr	Ctl Ox Higher	GO:0001701	in utero embryonic development	-1.4342
2hr	Ctl Ox Higher	GO:0060996	dendritic spine development	-1.6556
4hr	Ctl Ox Higher	GO:0001889	liver development	-1.7595
4hr	VPA Ox Higher	GO:0007163	establishment or maintenance of cell polarity	-2.4318
6hr	Ctl Ox Higher	GO:0007399	nervous system development	-1.4461
8hr	Ctl Ox Higher	GO:0010720	positive regulation of cell development	-1.644
8hr	Ctl Ox Higher	GO:0007399	nervous system development	-1.4353
10hr	Ctl Ox Higher	GO:0007275	multicellular organism development	-1.9318
10hr	VPA Ox Higher	GO:0007163	establishment or maintenance of cell polarity	-1.4342
10hr	VPA Ox Higher	GO:0048731	system development	-1.4634
10hr	VPA Ox Higher	GO:0021895	cerebral cortex neuron differentiation	-2.0506

Table 3-5 IodoTMT enriched developmental GO-terms: Enriched biological process GO terms that were identified through String and collapsed by Revigo. Nervous system development (6, 8, 10 hrs higher control oxidation) and establishment or maintenance of cell polarity (4 and 10 hrs higher VPA oxidation) both show recurrent enrichment at more than one time point.

10hr Enriched Oxidation Pathway Proteins	
Protein	***VPA/Ctl Oxidation %***
Citrate Synthase (Cs)	0.6
Alcohol Dehydrogenase (Adh5)	0.4
Malate dehydrogenase, mitchondrial (Mdh2)	0.7
Cytochrome b-c1 complex subunit 1, mitochondrial (Uqcrc2)	0.9
Synaptic vesicle membrane protein (Vat1)	0.8
Phosoglucomutase (Pgm2)	0.6
Serine/threonine-protein phosphatase PP1-gamma catalytic subunit (Ppp1cc)	0.7
Malate dehydrogenase, cytoplasmic (Mdh1)	0.8
NADH dehydrogenase [ubiquinone] flavoprotein 2, mitochondrial (Ndufv2)	0.8
Peptidyl-prolyl cis-trans isomerase F, mitochondrial (Ppif)	0.5
Catalase (Cat)	0.4
40S ribosomal protein S3 (Rps3)	0.6
Haptoglobin (Hp)	0.8
DNA ligase 1 (Lig1)	0.6
Delta-aminolevulinic acid dehydratase (Alad)	0.5

Table 3-6 10 hr IodoTMT enriched oxidation pathway proteins: Response to stimulus pathways relevant to oxidation were exclusively enriched at 10hrs in proteins with higher control oxidation. String enrichment identified three pathway oxidation-relevant pathways including: oxidation-reduction process, response to oxidative stress, and response to hydrogen peroxide. This table identifies the proteins within these pathways alongside their corresponding VPA/Ctl oxidation ratio.

Pathway	Time	Proteins
Actin Cytoskeleton Organization	4hr	Tln1 (1.22), Cap1 (1.24), Pdcd6ip (1.21)
Cortical Cytoskelton Organization	6hr	Coro1c (1.31), Actn1 (1.3)
Cortical Cytoskelton Organization	10hr	Pafah1b1 (1.9), Actn1 (1.9), Vil1 (1.5), Tln1 (1.1), Pdcd6ip (1.3)
Response to Axon Injury	10hr	Arf4 (0.7), Dpysl3 (0.8), Folr1 (0.8)
Positive Regulation of NF-Kappa B Transcription Factor Activity	10hr	Psma6 (0.4), Cat (0.6), Rps3 (0.4)

Table 3-7 IodoTMT cytoskeletal organization, axon injury and NF-Kappa B pathways: Pathways relevant to cytoskeletal organization, axon injury and NF-Kappa B are potentially relevant to the process of neural tube closure, although these processes are not strictly unique to development. Proteins within each of these pathways identified by String are listed alongside their corresponding VPA/Ctl oxidation ratio.

GSEA 4hr Cytoskeletal Organization				
Protein	Uniprot Accession	VPA/Ctl Oxidation Ratio	GSEA Rank Metric Score	Modified Cysteines
CAP1	P40124	1.24	0.310	141, 355, 374, 415, 426,
TLN1	P26039	1.22	0.293	709, 719, 742, 750, 1661, 1671, 1927,
PDCD6IP	Q9WU78	1.21	0.280	38, 691
TUBA1A	P68369	1.14	0.190	295, 315, 316, 347, 376,
TUBB5	P99024	1.12	0.162	12, 127, 129, 238, 303, 354,
FKBP4	P30416	1.12	0.159	103, 107, 189, 202, 342, 396,
DYNC1H1	Q9JHU4	1.11	0.145	631, 976, 1886, 2074, 2637, 2710, 3323, 3710, 4642,
HNRNPU	Q8VEK3	1.10	0.140	365, 367, 384, 449, 473, 538, 570, 583, 624
CFL1	P18760	1.10	0.138	39, 80, 139, 147,
FSCN1	Q61553	1.10	0.136	80, 121, 260, 334, 341, 397, 456, 481
RAN	P62827	1.09	0.121	112, 120
RPS3	D3YV43	1.08	0.117	97, 119, 134

Table 3-8 IodoTMT enriched 4 hr GSEA cytoskeletal organization proteins: GSEA 4 hr Cytoskeletal Organization core enrichment proteins with listing of VPA/Ctl oxidation ratio, GSEA rank metric score, and modified cysteine residues.

Figures

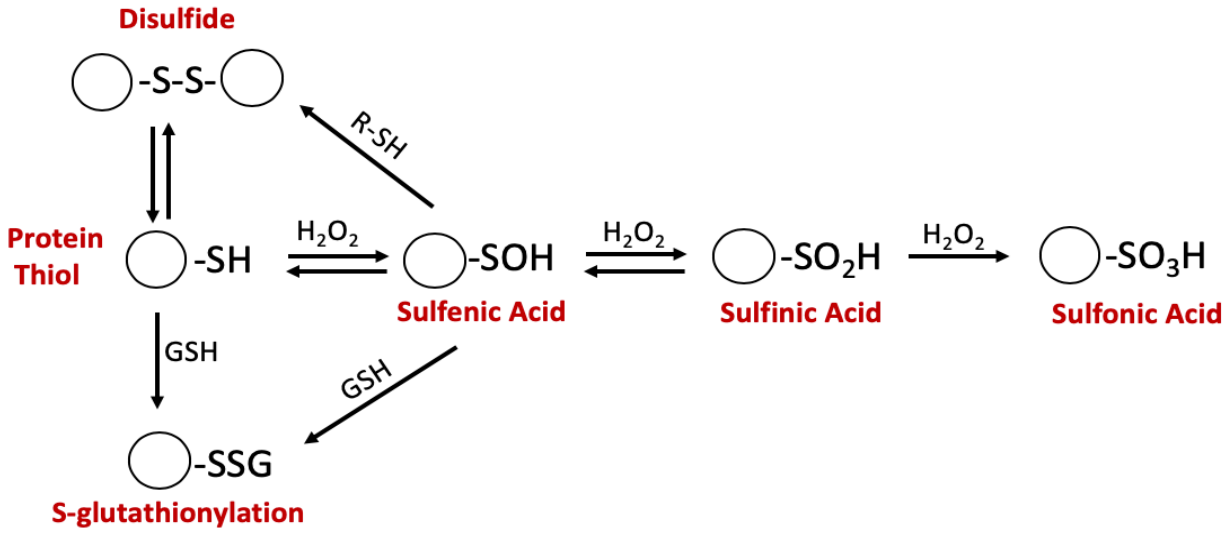

Figure 3-1 Oxidative modifications of cysteine sulfhydryl groups: Thiol groups are highly reactive to oxidation and can exist in several reversible and irreversible states. Reversible modifications, especially sulfenic acid and s-glutathionylation, are hypothesized to act as cellular signaling mechanisms and can be labelled and with IodoTMT.

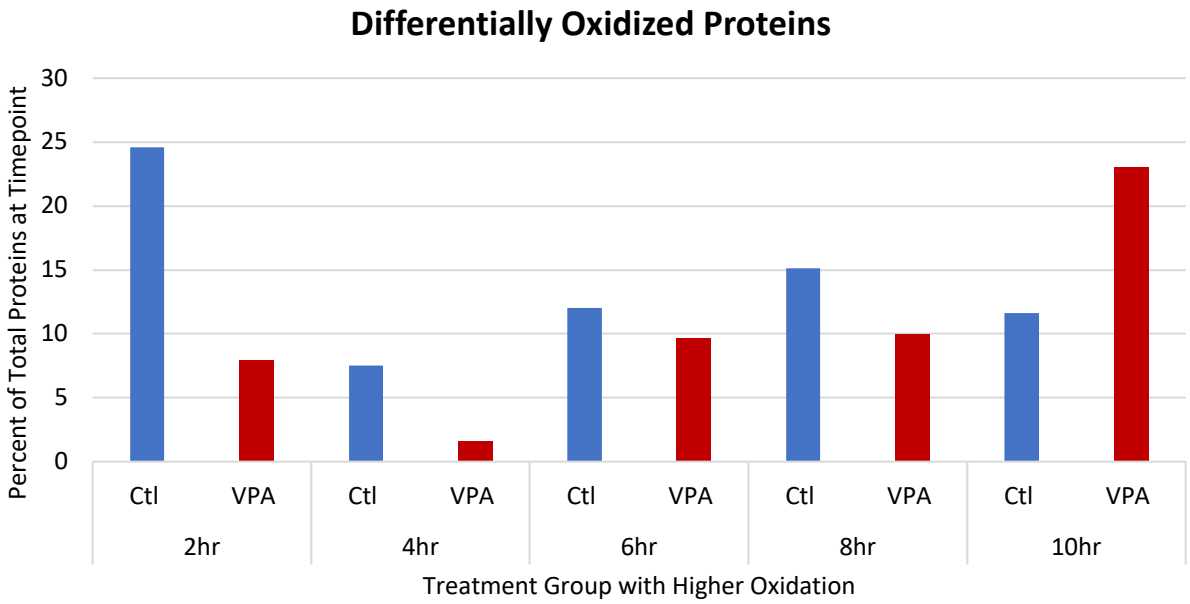

Figure 3-2 IodoTMT differentially oxidized proteins across time course: Proteins with a difference of at least 8.6 percentage points between their control and VPA percent oxidation were deemed differentially oxidized. This figure summarizes the percent of proteins that were differentially oxidized by treatment group and time.

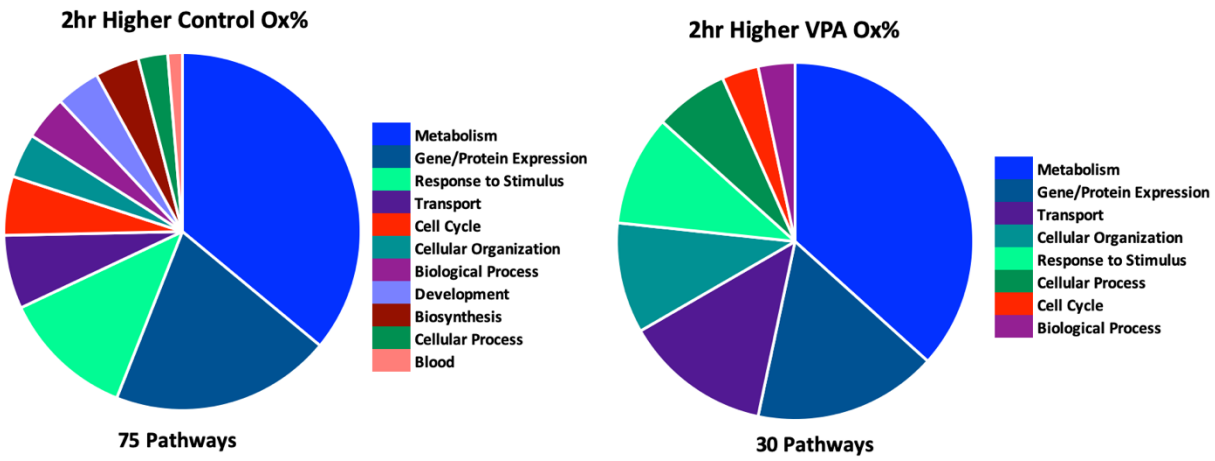

Figure 3-3 IodoTMT 2 hr biological process GO-term enrichment: Enriched biological process GO pathways identified in String and collapsed by Revigo for differentially oxidized proteins at 2hrs. Pie chart divisions correspond to the number of pathways within each category.

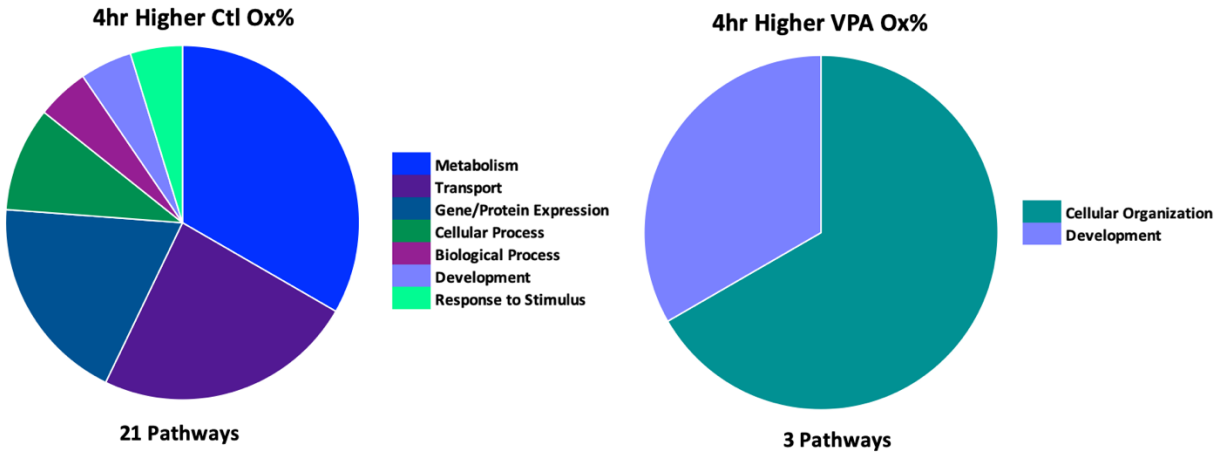

Figure 3-4 IodoTMT 4 hr biological process GO-term enrichment: Enriched biological process GO pathways identified in String and collapsed by Revigo for differentially oxidized proteins at 4hrs. Pie chart divisions correspond to the number of pathways within each category.

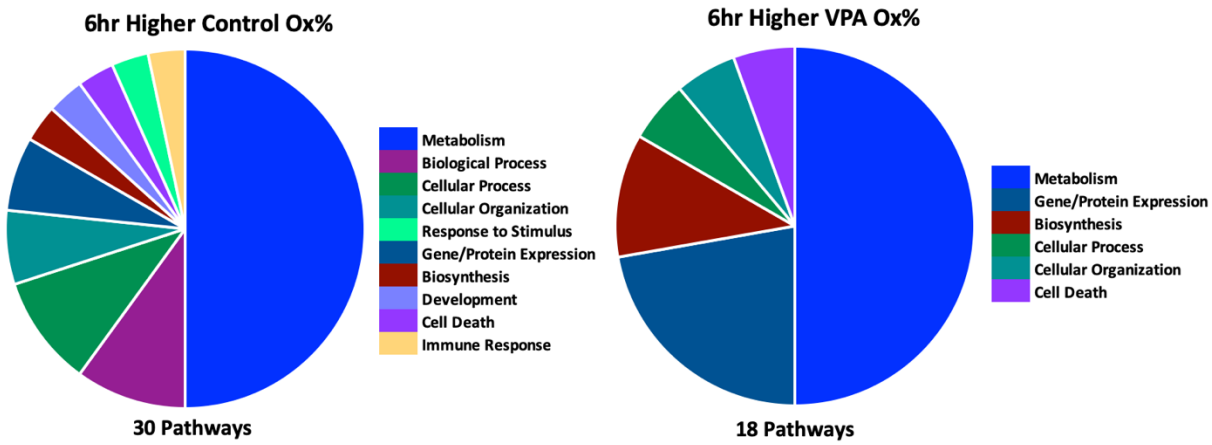

Figure 3-5 IodoTMT 6 hr biological process GO-term enrichment: Enriched biological process GO pathways identified in String and collapsed by Revigo for differentially oxidized proteins at 6hrs. Pie chart divisions correspond to the number of pathways within each category.

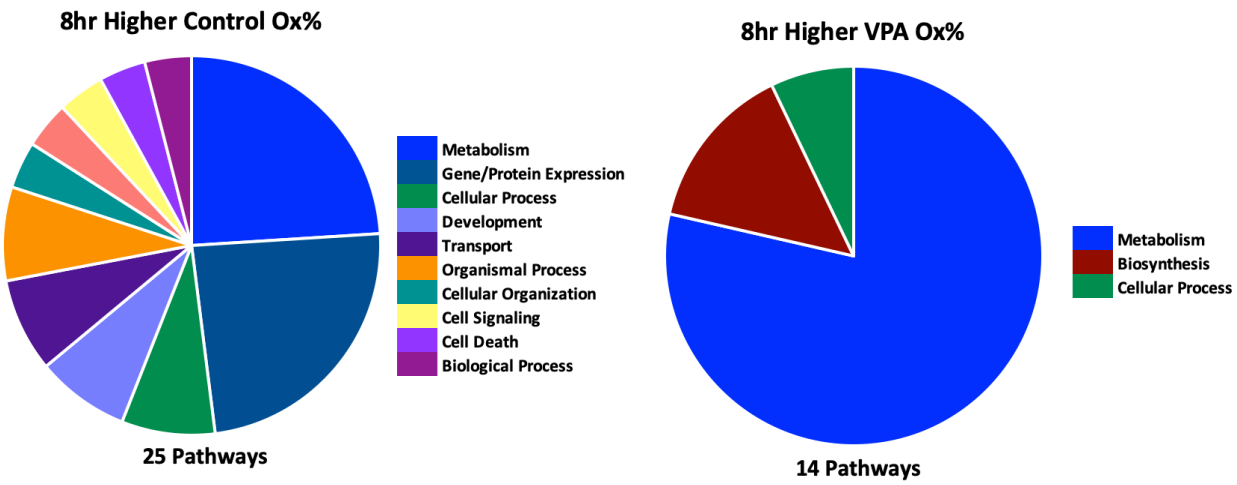

Figure 3-6 IodoTMT 8 hr biological process GO-term enrichment: Enriched biological process GO pathways identified in String and collapsed by Revigo for differentially oxidized proteins at 8hrs. Pie chart divisions correspond to the number of pathways within each category.

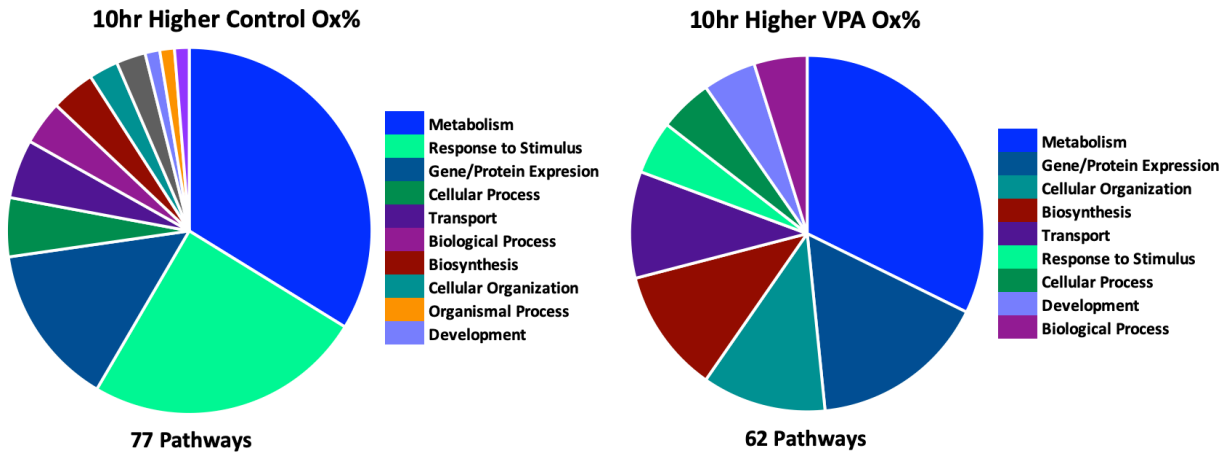

Figure 3-7 IodoTMT 10 hr biological process GO-term enrichment: Enriched biological process GO pathways identified in String and collapsed by Revigo for differentially oxidized proteins at 10hrs. Pie chart divisions correspond to the number of pathways within each category.

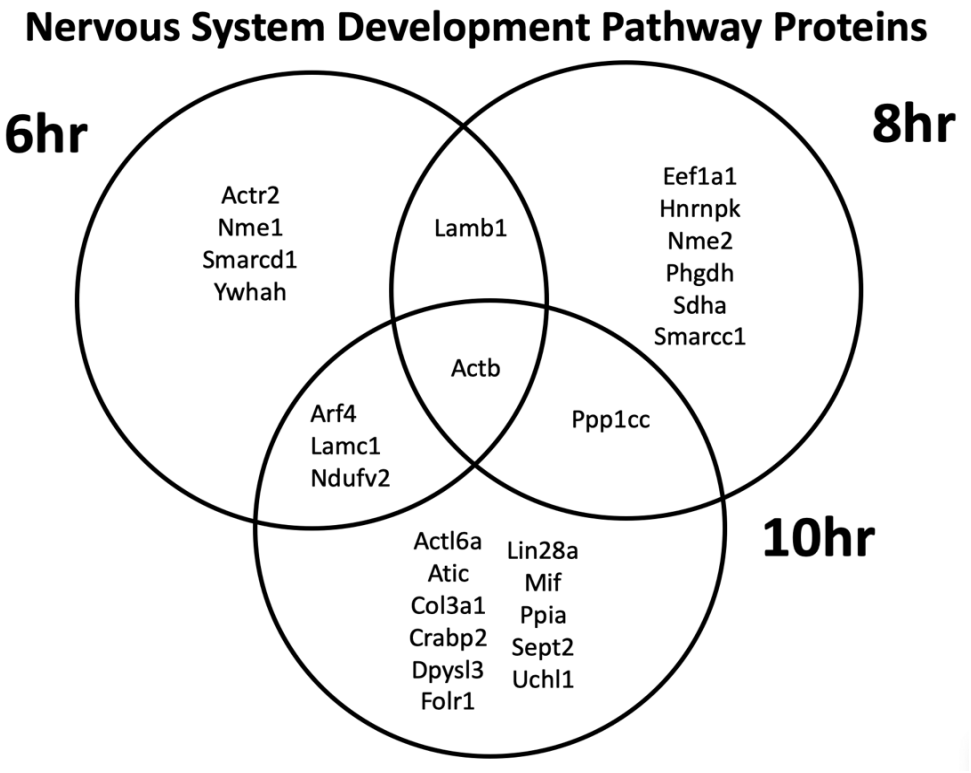

Figure 3-8 Enriched nervous system development proteins at 6, 8, and 10 hrs: The biological process GO term, "Nervous System Development" was enriched in proteins with higher control oxidation at 6, 8, and 10hrs. This Venn diagram displays the proteins identified at each time point that were included in this pathway.

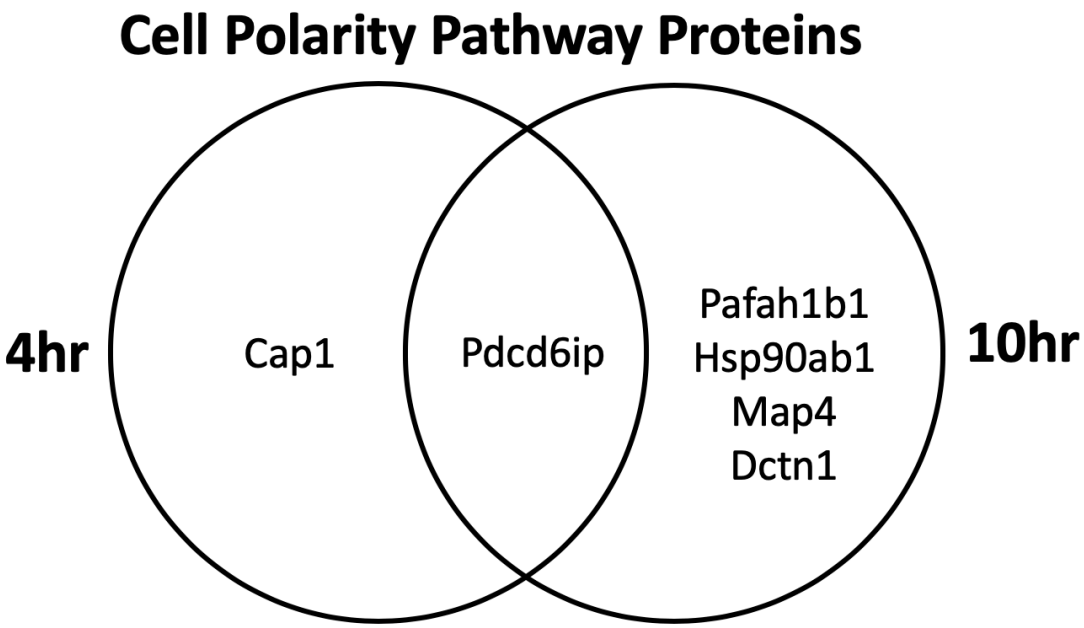

Figure 3-9 Enriched cell polarity proteins at 4 and 10 hrs: The biological process GO-term, "Establishment or maintenance of cell polarity" was enriched in proteins with higher VPA oxidation at 4 and 10 hrs. This Venn diagram displays the proteins identified at each time point that were included in this pathway.

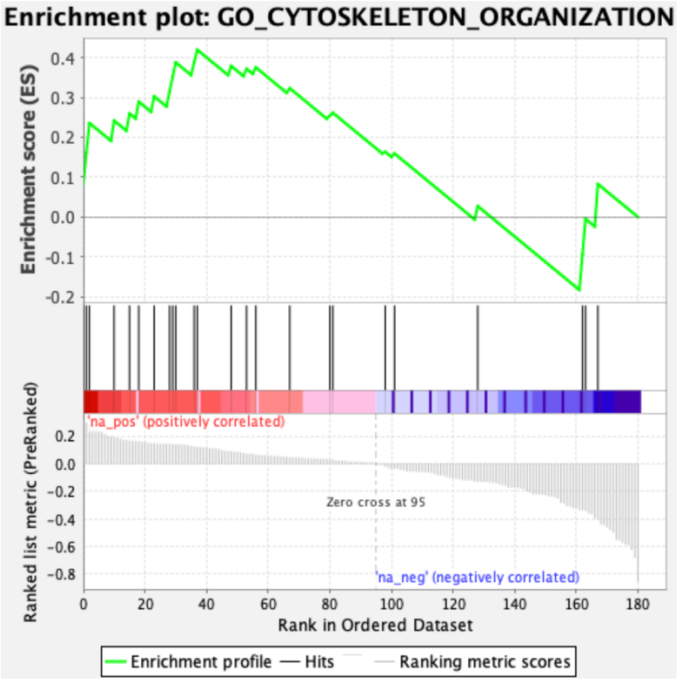

Figure 3-10 4 hr cytoskeletal organization GSEA enrichment plot: GSEA enrichment plot for biological process GO term Cytoskeletal Organization at 4hrs. Enrichment is highest for proteins with higher VPA oxidation when proteins were input as a pre-ranked data set of VPA/Ctl oxidation ratios. 12 proteins were identified as showing core enrichment for this pathway and are identified in Table 8.

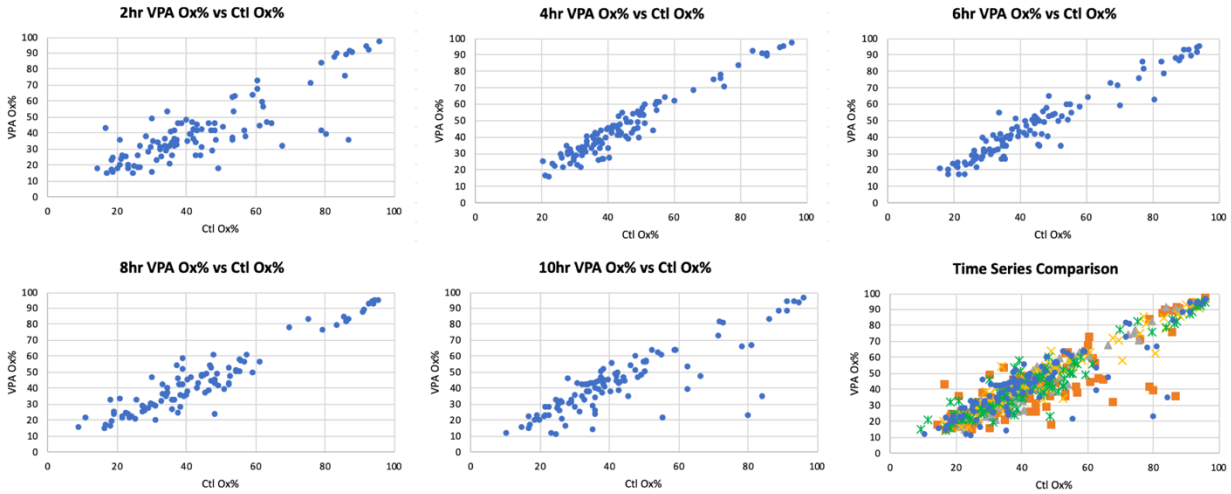

Figure 3-11 Time series VPA versus control percent oxidation: VPA oxidation percent vs. control oxidation percent for 102 proteins that were identified at all 5 time points.

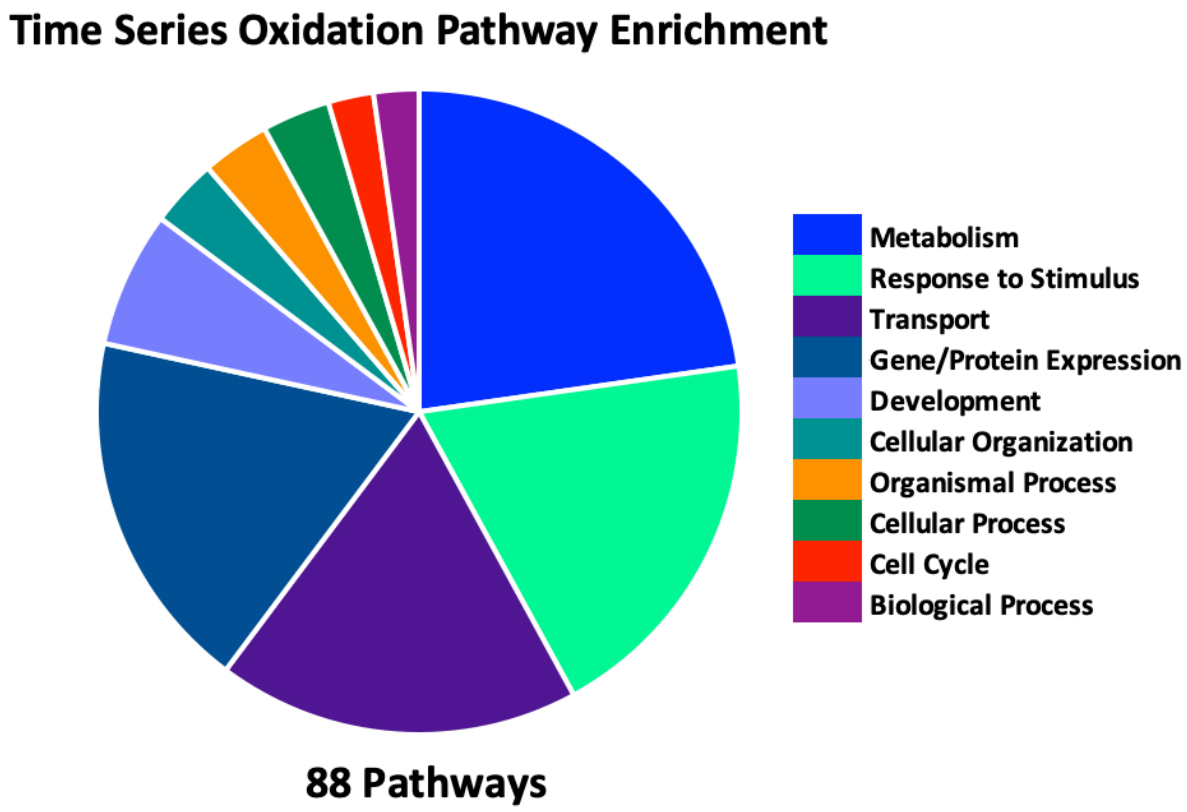

Figure 3-12 IodoTMT time series biological process GO-term enrichment: Biological Process GO term enrichment for the 102 proteins identified at all 5 time points. Enrichment was identified using String and significant pathways (FDR >0.05) were collapsed in Revigo and categorized.

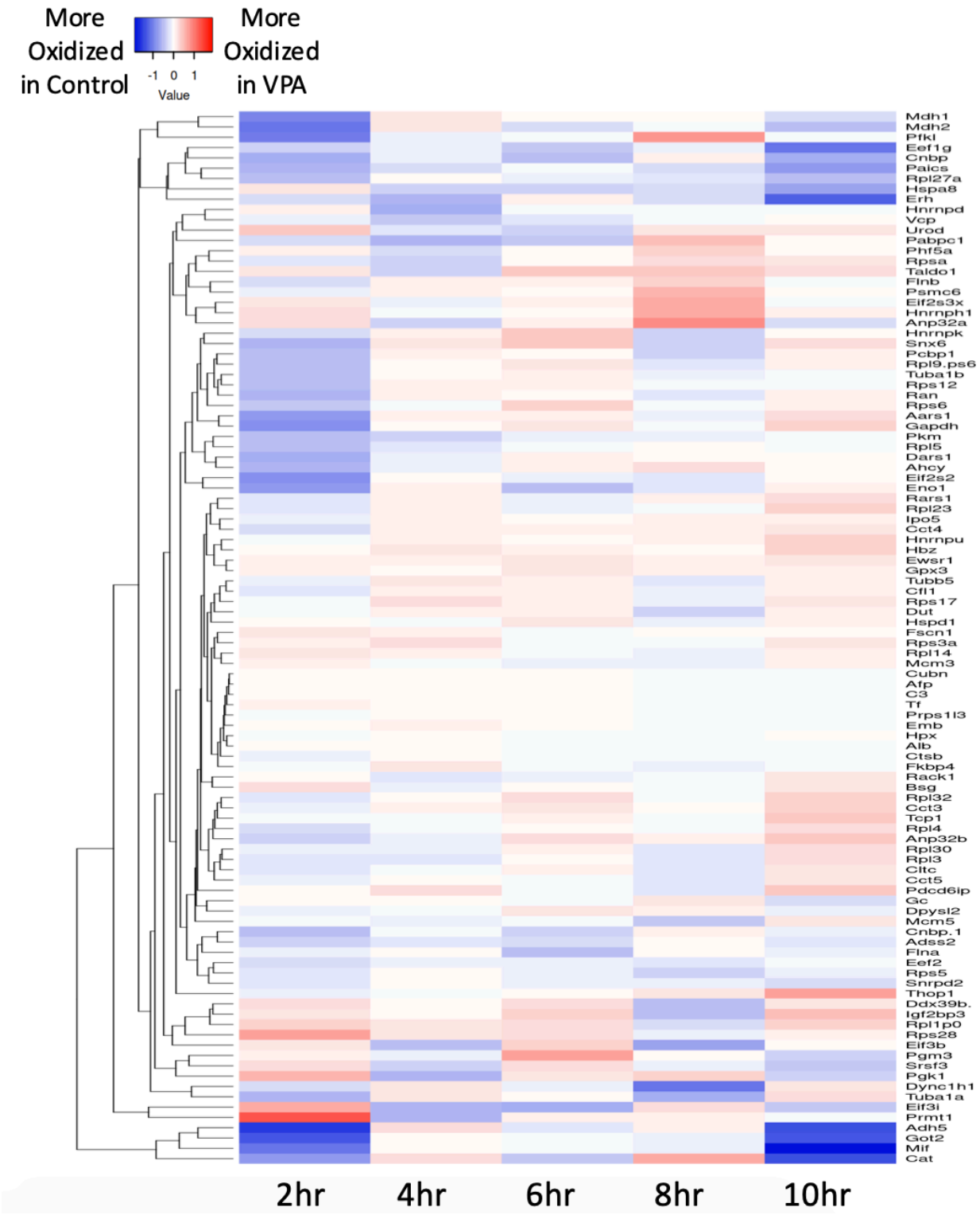

Figure 3-13 Hierarchical clustering of IodoTMT time series proteins: Hierarchical clustering of the 102 proteins that appear at all 5 time points using Euclidean distance and average linkage parameters.

References

Ahangar, N., Naderi, M., Noroozi, A., Ghasemi, M., Zamani, E., & Shaki, F. (2017). Zinc Deficiency and Oxidative Stress Involved in Valproic Acid Induced Hepatotoxicity: Protection by Zinc and Selenium Supplementation. *Biological Trace Element Research*, *179*(1), 102–109. https://doi.org/10.1007/s12011-017-0944-z

Akazawa, S., Unterman, T., & Metzger, B. E. (1994). Glucose metabolism in separated embryos and investing membranes during organogenesis in the rat. *Metabolism*, *43*(7), 830–835. https://doi.org/10.1016/0026-0495(94)90262-3

Babicki, S., Arndt, D., Marcu, A., Liang, Y., Grant, J. R., Maciejewski, A., & Wishart, D. S. (2016). Heatmapper: Web-enabled heat mapping for all. *Nucleic Acids Research*, *44*(W1), W147–W153. https://doi.org/10.1093/nar/gkw419

Bachi, A., Dalle-Donne, I., & Scaloni, A. (2013). Redox Proteomics: Chemical Principles, Methodological Approaches and Biological/Biomedical Promises. *Chemical Reviews*, *113*(1), 596–698. https://doi.org/10.1021/cr300073p

Behring, J. B., Kumar, V., Whelan, S. A., Chauhan, P., Siwik, D. A., Costello, C. E., Colucci, W. S., Cohen, R. A., McComb, M. E., & Bachschmid, M. M. (2014). Does reversible cysteine oxidation link the Western diet to cardiac dysfunction? *The FASEB Journal*, *28*(5), 1975–1987. https://doi.org/10.1096/fj.13-233445

Bertling, E., Hotulainen, P., Mattila, P. K., Matilainen, T., Salminen, M., & Lappalainen, P. (2004). Cyclase-associated Protein 1 (CAP1) Promotes Cofilin-induced Actin Dynamics in Mammalian Nonmuscle Cells. *Molecular Biology of the Cell*, *15*(5), 2324–2334. https://doi.org/10.1091/mbc.e04-01-0048

Brandes, N., Tienson, H., Lindemann, A., Vitvitsky, V., Reichmann, D., Banerjee, R., & Jakob, U. (2013). Time line of redox events in aging postmitotic cells. *ELife*, *2*, e00306. https://doi.org/10.7554/eLife.00306

Cearns, M. D., Escuin, S., Alexandre, P., Greene, N. D. E., & Copp, A. J. (2016). Microtubules, polarity and vertebrate neural tube morphogenesis. *Journal of Anatomy*, *229*(1), 63–74. https://doi.org/10.1111/joa.12468

Chaudhary, S., Ganjoo, P., Raiusddin, S., & Parvez, S. (2015). Nephroprotective activities of quercetin with potential relevance to oxidative stress induced by valproic acid. *Protoplasma*, *252*(1), 209–217. https://doi.org/10.1007/s00709-014-0670-8

Dalle-Donne, I., Giustarini, D., Rossi, R., Colombo, R., & Milzani, A. (2003). Reversible S-glutathionylation of Cys374 regulates actin filament formation by inducing structural changes in the actin molecule. *Free Radical Biology and Medicine*, *34*(1), 23–32. https://doi.org/10.1016/S0891-5849(02)01182-6

Espín-Palazón, R., & Traver, D. (2016). The NF-κB family: Key players during embryonic development and HSC emergence. *Experimental Hematology*, *44*(7), 519–527. https://doi.org/10.1016/j.exphem.2016.03.010

Fiaschi, T., Cozzi, G., Raugei, G., Formigli, L., Ramponi, G., & Chiarugi, P. (2006). Redox Regulation of β-Actin during Integrin-mediated Cell Adhesion. *Journal of Biological Chemistry*, *281*(32), 22983–22991. https://doi.org/10.1074/jbc.M603040200

Findlay, V. J., Tapiero, H., & Townsend, D. M. (2005). Sulfiredoxin: A potential therapeutic agent? *Biomedicine & Pharmacotherapy*, *59*(7), 374–379. https://doi.org/10.1016/j.biopha.2005.07.003

Gaitanis, J., & Tarui, T. (2018). Nervous System Malformations: *CONTINUUM: Lifelong Learning in Neurology*, *24*(1), 72–95. https://doi.org/10.1212/CON.0000000000000561

Ghodke-Puranik, Y., Thorn, C. F., Lamba, J. K., Leeder, J. S., Song, W., Birnbaum, A. K., Altman, R. B., & Klein, T. E. (2013). Valproic acid pathway: Pharmacokinetics and pharmacodynamics. *Pharmacogenetics and Genomics*, *23*(4), 236–241. https://doi.org/10.1097/FPC.0b013e32835ea0b2

Ghosh, S., Janocha, A. J., Aronica, M. A., Swaidani, S., Comhair, S. A. A., Xu, W., Zheng, L., Kaveti, S., Kinter, M., Hazen, S. L., & Erzurum, S. C. (2006). Nitrotyrosine Proteome Survey in Asthma Identifies Oxidative Mechanism of Catalase Inactivation. *The Journal of Immunology*, *176*(9), 5587–5597. https://doi.org/10.4049/jimmunol.176.9.5587

Go, Y.-M., Chandler, J. D., & Jones, D. P. (2015). The cysteine proteome. *Free Radical Biology and Medicine*, *84*, 227–245. https://doi.org/10.1016/j.freeradbiomed.2015.03.022

Gould, N. S., Evans, P., Martínez-Acedo, P., Marino, S. M., Gladyshev, V. N., Carroll, K. S., & Ischiropoulos, H. (2015). Site-Specific Proteomic Mapping Identifies Selectively Modified Regulatory Cysteine Residues in Functionally Distinct Protein Networks. *Chemistry & Biology*, *22*(7), 965–975. https://doi.org/10.1016/j.chembiol.2015.06.010

Greene, N. D. E., & Copp, A. J. (2014). Neural Tube Defects. *Annual Review of Neuroscience*, *37*(1), 221–242. https://doi.org/10.1146/annurev-neuro-062012-170354

Hansen, J. M., Jones, D. P., & Harris, C. (2020). The Redox Theory of Development. *Antioxidants & Redox Signaling*, *32*(10), 715–740. https://doi.org/10.1089/ars.2019.7976

Harris, C. (2012). Rodent Whole Embryo Culture. In C. Harris & J. M. Hansen (Eds.), *Developmental Toxicology* (Vol. 889, pp. 215–237). Humana Press. https://doi.org/10.1007/978-1-61779-867-2_13

Ishii, K., Mukherjee, K., Okada, T., & Liao, E. C. (2018). Genetic Requirement of talin1 for Proliferation of Cranial Neural Crest Cells during Palate Development: *Plastic and Reconstructive Surgery - Global Open*, *6*(3), e1633. https://doi.org/10.1097/GOX.0000000000001633

Jentink, J., Loane, M. A., Dolk, H., Barisic, I., Garne, E., Morris, J. K., & de Jong-van den Berg, L. T. W. (2010). Valproic Acid Monotherapy in Pregnancy and Major Congenital Malformations. *New England Journal of Medicine*, *362*(23), 2185–2193. https://doi.org/10.1056/NEJMoa0907328

Johannessen, C. U., Petersen, D., Fonnum, F., & Hassel, B. (2001). The acute effect of valproate on cerebral energy metabolism in mice. *Epilepsy Research*, *47*(3), 247–256. https://doi.org/10.1016/S0920-1211(01)00308-4

Knoefler, D., Thamsen, M., Koniczek, M., Niemuth, N. J., Diederich, A.-K., & Jakob, U. (2012). Quantitative In Vivo Redox Sensors Uncover Oxidative Stress as an Early Event in Life. *Molecular Cell*, *47*(5), 767–776. https://doi.org/10.1016/j.molcel.2012.06.016

Komulainen, T., Lodge, T., Hinttala, R., Bolszak, M., Pietilä, M., Koivunen, P., Hakkola, J., Poulton, J., Morten, K. J., & Uusimaa, J. (2015). Sodium valproate induces mitochondrial respiration dysfunction in HepG2 in vitro cell model. *Toxicology*, *331*, 47–56. https://doi.org/10.1016/j.tox.2015.03.001

Landino, L. M., Hagedorn, T. D., Kim, S. B., & Hogan, K. M. (2011). Inhibition of tubulin polymerization by hypochlorous acid and chloramines. *Free Radical Biology and Medicine*, *50*(8), 1000–1008. https://doi.org/10.1016/j.freeradbiomed.2011.01.018

Laporte, M. H., Chatellard, C., Vauchez, V., Hemming, F. J., Deloulme, J.-C., Vossier, F., Blot, B., Fraboulet, S., & Sadoul, R. (2017). Alix is required during development for normal growth of the mouse brain. *Scientific Reports*, *7*(1), 44767. https://doi.org/10.1038/srep44767

Li, Q., Estepa, G., Memet, S., Israel, A., & Verma, I. M. (2000). Complete lack of NF-kappaB activity in IKK1 and IKK2 double-deficient mice: Additional defect in neurulation. *Genes & Development*, *14*(14), 1729–1733.

Luís, P. B. M., Ruiter, J. P. N., Aires, C. C. P., Soveral, G., Tavares de Almeida, I., Duran, M., Wanders, R. J. A., & Silva, M. F. B. (2007). Valproic acid metabolites inhibit dihydrolipoyl dehydrogenase activity leading to impaired 2-oxoglutarate-driven oxidative phosphorylation. *Biochimica et Biophysica Acta (BBA) - Bioenergetics*, *1767*(9), 1126–1133. https://doi.org/10.1016/j.bbabio.2007.06.007

Martínez-Acedo, P., Gupta, V., & Carroll, K. S. (2014). Proteomic analysis of peptides tagged with dimedone and related probes: Proteomics insights into dimedone-labeled peptides. *Journal of Mass Spectrometry*, *49*(4), 257–265. https://doi.org/10.1002/jms.3336

McAlister, G. C., Nusinow, D. P., Jedrychowski, M. P., Wühr, M., Huttlin, E. L., Erickson, B. K., Rad, R., Haas, W., & Gygi, S. P. (2014). MultiNotch MS3 Enables Accurate, Sensitive, and Multiplexed Detection of Differential Expression across Cancer Cell Line Proteomes. *Analytical Chemistry*, *86*(14), 7150–7158. https://doi.org/10.1021/ac502040v

Mootha, V. K., Lindgren, C. M., Eriksson, K.-F., Subramanian, A., Sihag, S., Lehar, J., Puigserver, P., Carlsson, E., Ridderstråle, M., Laurila, E., Houstis, N., Daly, M. J., Patterson, N., Mesirov, J. P., Golub, T. R., Tamayo, P., Spiegelman, B., Lander, E. S., Hirschhorn, J. N., … Groop, L. C. (2003). PGC-1α-responsive genes involved in oxidative phosphorylation are coordinately downregulated in human diabetes. *Nature Genetics*, *34*(3), 267–273. https://doi.org/10.1038/ng1180

Nikolopoulou, E., Galea, G. L., Rolo, A., Greene, N. D. E., & Copp, A. J. (2017). Neural tube closure: Cellular, molecular and biomechanical mechanisms. *Development*, *144*(4), 552–566. https://doi.org/10.1242/dev.145904

Palsamy, P., Bidasee, K. R., & Shinohara, T. (2014). Valproic acid suppresses Nrf2/Keap1 dependent antioxidant protection through induction of endoplasmic reticulum stress and Keap1 promoter DNA demethylation in human lens epithelial cells. *Experimental Eye Research*, *121*, 26–34. https://doi.org/10.1016/j.exer.2014.01.021

Phiel, C. J., Zhang, F., Huang, E. Y., Guenther, M. G., Lazar, M. A., & Klein, P. S. (2001). Histone Deacetylase Is a Direct Target of Valproic Acid, a Potent Anticonvulsant, Mood Stabilizer, and Teratogen. *Journal of Biological Chemistry*, *276*(39), 36734–36741. https://doi.org/10.1074/jbc.M101287200

Poole, L. B. (2015). The basics of thiols and cysteines in redox biology and chemistry. *Free Radical Biology and Medicine*, *80*, 148–157. https://doi.org/10.1016/j.freeradbiomed.2014.11.013

Poole, L. B., Furdui, C. M., & King, S. B. (2020). Introduction to approaches and tools for the evaluation of protein cysteine oxidation. *Essays in Biochemistry*, *64*(1), 1–17. https://doi.org/10.1042/EBC20190050

Rhee, S. G. (2006). CELL SIGNALING: H2O2, a Necessary Evil for Cell Signaling. *Science*, *312*(5782), 1882–1883. https://doi.org/10.1126/science.1130481

Salsaa, M., Pereira, B., Liu, J., Yu, W., Jadhav, S., Hüttemann, M., & Greenberg, M. L. (2020). Valproate inhibits mitochondrial bioenergetics and increases glycolysis in Saccharomyces cerevisiae. *Scientific Reports*, *10*(1), 11785. https://doi.org/10.1038/s41598-020-68725-5

Santos, J., Hubert, T., & Milthorpe, B. K. (2020). Valproic Acid Promotes Early Neural Differentiation in Adult Mesenchymal Stem Cells Through Protein Signalling Pathways. *Cells*, *9*(3), 619. https://doi.org/10.3390/cells9030619

Schafer, F. Q., & Buettner, G. R. (2001). Redox environment of the cell as viewed through the redox state of the glutathione disulfide/glutathione couple. *Free Radical Biology and Medicine*, *30*(11), 1191–1212. https://doi.org/10.1016/S0891-5849(01)00480-4

Schieber, M., & Chandel, N. S. (2014). ROS Function in Redox Signaling and Oxidative Stress. *Current Biology*, *24*(10), R453–R462. https://doi.org/10.1016/j.cub.2014.03.034

Shafique, S., & Winn, L. M. (2021). Characterizing the effects of in utero valproic acid exposure on NF-κB signaling in CD-1 mouse embryos during neural tube closure. *Neurotoxicology and Teratology*, *83*, 106941. https://doi.org/10.1016/j.ntt.2020.106941

Shakir, S., Vinh, J., & Chiappetta, G. (2017). Quantitative analysis of the cysteine redoxome by iodoacetyl tandem mass tags. *Analytical and Bioanalytical Chemistry*, *409*(15), 3821–3830. https://doi.org/10.1007/s00216-017-0326-6

Shawky, J. H., Balakrishnan, U. L., Stuckenholz, C., & Davidson, L. A. (2018). Multiscale analysis of architecture, cell size and the cell cortex reveals cortical F-actin density and composition are major contributors to mechanical properties during convergent extension. *Development*, *145*(19), dev161281. https://doi.org/10.1242/dev.161281

Shepard, T. H., Tanimura, T., & Robkin, M. A. (1970). Energy metabolism in early mammalian embryos. *The ... Symposium. Society for Developmental Biology. Symposium*, *29*, 42–58.

Song, M. O., Li, J., & Freedman, J. H. (2009). Physiological and toxicological transcriptome changes in HepG2 cells exposed to copper. *Physiological Genomics*, *38*(3), 386–401. https://doi.org/10.1152/physiolgenomics.00083.2009

Subramanian, A., Tamayo, P., Mootha, V. K., Mukherjee, S., Ebert, B. L., Gillette, M. A., Paulovich, A., Pomeroy, S. L., Golub, T. R., Lander, E. S., & Mesirov, J. P. (2005). Gene set enrichment analysis: A knowledge-based approach for interpreting genome-wide expression profiles. *Proceedings of the National Academy of Sciences*, *102*(43), 15545–15550. https://doi.org/10.1073/pnas.0506580102

Supek, F., Bošnjak, M., Škunca, N., & Šmuc, T. (2011). REVIGO Summarizes and Visualizes Long Lists of Gene Ontology Terms. *PLoS ONE*, *6*(7), e21800. https://doi.org/10.1371/journal.pone.0021800

Szklarczyk, D., Gable, A. L., Lyon, D., Junge, A., Wyder, S., Huerta-Cepas, J., Simonovic, M., Doncheva, N. T., Morris, J. H., Bork, P., Jensen, L. J., & Mering, C. von. (2019). STRING v11: Protein–protein association networks with increased coverage, supporting functional discovery in genome-wide experimental datasets. *Nucleic Acids Research*, *47*(D1), D607–D613. https://doi.org/10.1093/nar/gky1131

Tanimura, T., & Shepard, T. H. (1970). Glucose Metabolism By Rat Embryos in Vitro. *Experimental Biology and Medicine*, *135*(1), 51–54. https://doi.org/10.3181/00379727-135-34985

Thompson, A., Schäfer, J., Kuhn, K., Kienle, S., Schwarz, J., Schmidt, G., Neumann, T., & Hamon, C. (2003). Tandem Mass Tags: A Novel Quantification Strategy for Comparative Analysis of Complex Protein Mixtures by MS/MS. *Analytical Chemistry*, *75*(8), 1895–1904. https://doi.org/10.1021/ac0262560

Triyasakorn, K., Lai, J. C. K., & Awale, P. (2020). Valproic Acid Alters Activities of Key Enzymes of Glucose Oxidative Metabolism, Citric Acid Cycle and Neurotransmitter Synthesis in Embryonic Rat Brain. *The FASEB Journal*, *34*(S1), 1–1. https://doi.org/10.1096/fasebj.2020.34.s1.05917

Tung, E. W. Y., & Winn, L. M. (2011). Valproic Acid Increases Formation of Reactive Oxygen Species and Induces Apoptosis in Postimplantation Embryos: A Role for Oxidative Stress in Valproic Acid-Induced Neural Tube Defects. *Molecular Pharmacology*, *80*(6), 979–987. https://doi.org/10.1124/mol.111.072314

Wang, B., Hom, G., Zhou, S., Guo, M., Li, B., Yang, J., Monnier, V. M., & Fan, X. (2017). The oxidized thiol proteome in aging and cataractous mouse and human lens revealed by ICAT labeling. *Aging Cell*, *16*(2), 244–261. https://doi.org/10.1111/acel.12548

Xiao, H., Jedrychowski, M. P., Schweppe, D. K., Huttlin, E. L., Yu, Q., Heppner, D. E., Li, J., Long, J., Mills, E. L., Szpyt, J., He, Z., Du, G., Garrity, R., Reddy, A., Vaites, L. P., Paulo, J. A., Zhang, T., Gray, N. S., Gygi, S. P., & Chouchani, E. T. (2020). A Quantitative Tissue-Specific Landscape of Protein Redox Regulation during Aging. *Cell*, *180*(5), 968-983.e24. https://doi.org/10.1016/j.cell.2020.02.012

Zepeta-Flores, N., Valverde, M., Lopez-Saavedra, A., & Rojas, E. (2018). Glutathione depletion triggers actin cytoskeleton changes via actin-binding proteins. *Genetics and Molecular Biology*, *41*(2), 475–487. https://doi.org/10.1590/1678-4685-gmb-2017-0158

Zheng, Y., Merchant, M. L., Burke, T. J., Ritzenthaler, J. D., Li, M., Gaweda, A. E., Benz, F. W., Roman, J., & Watson, W. H. (2020). Redox States of Protein Cysteines in Pathways of Protein Turnover and Cytoskeleton Dynamics Are Changed with Aging and Reversed by Slc7a11 Restoration in Mouse Lung Fibroblasts. *Oxidative Medicine and Cellular Longevity*, *2020*, 2468986. https://doi.org/10.1155/2020/2468986

Chapter 4

Spatiotemporal Protein Abundance Dynamics in Early Organogenesis Mouse Conceptuses Treated with Valproic Acid

Abstract

Valproic acid (VPA) is an anti-epileptic medication that increases the risk of neural tube defect (NTD) outcomes in infants exposed during gestation. VPA's mechanism of action related to disruption of neural tube closure (NTC) is not well understood, but it is known that VPA acts as a histone deacetylase (HDAC) inhibitor potentially disrupting the expression of genes essential to NTC. This study evaluates the effects of VPA on protein abundance in the developmentally distinct tissues of the mouse visceral yolk sac (VYS) and embryo proper (EMB) across early organogenesis with the aim of identifying protein pathways relevant to VPA's mechanism of action in failed NTC. Protein abundance was measured across 10 hrs of early organogenesis through tandem mass tag (TMT) labeling followed by liquid chromatography, mass spectrometry. Over 4,800 proteins were identified in the VYS and EMB and tissue-specific responses to VPA were evident through differing response times to VPA with the VYS primarily demonstrating sensitivity to protein abundance changes at 2 and 4 hrs, while the EMB was most affected at 6 and 10 hrs. Limited directional concordance in protein abundance between tissues also supported the conclusion of independent roles for the VYS and EMB in response to VPA. Pathway analysis of proteins with increased or decreased abundance focused on evaluating

enriched pathways with mechanistic relevance to NTC and development leading to identification of cellular differentiation, Wnt Signaling, TOR signaling, cytoskeletal organization and oxidation-reduction process as targets of VPA. Clustering of co-regulated proteins to identify shared patterns of protein abundance over time highlighted 4 hrs and 6/10 hrs as periods of divergent protein abundance between control and VPA-treated samples in the VYS and EMB, respectively. This study greatly increased the breadth of knowledge related to VPA's effects on protein abundance during organogenesis and the importance of temporal and spatial measurements of protein abundance.

Introduction

Valproic acid (VPA) is an anti-epileptic medication that when taken during pregnancy increases the risk of having offspring with a neural tube defect (NTD) (Jentink et al., 2010; Ornoy, 2009). NTDs arise due to failed neural tube closure (NTC) during early organogenesis. This failed closure can lead to a malformations of the brain and spine resulting in a number of NTD conditions of varying severity depending on the timing and location of the failed closure (Sakai, 1989). The mechanism through which VPA increases the risk of NTDs is not known; however, several downstream targets of VPA may be implicated in incomplete NTC. These mechanisms include disruption of redox balance, histone deacetylase (HDAC) inhibition, blocking voltage gated ion channels, and increasing γ-aminobutyric acid (GABA) levels (Ghodke-Puranik et al., 2013; Phiel et al., 2001; Chapter 2; Chapter 3). Through these mechanisms, particularly alteration of redox balance and HDAC inhibition, VPA may cause changes to the developmental proteome which could in turn have functional consequences for the process of NTC.

Many factors can affect protein abundance. The expression activity of protein-encoding genes directly determines the relative abundance of many proteins through translation of mRNA and de novo peptide synthesis. However, despite the connection between mRNA expression and protein translation, it has been frequently demonstrated that there is not a strong correlation between mRNA and protein abundance using both standard and high-throughput experimental techniques (Gygi et al., 1999; Vogel & Marcotte, 2012; D. Wang, 2008). Instead, only about 40% of protein abundance is explained by mRNA expression (Vogel & Marcotte, 2012). Upstream of protein translation and synthesis, gene expression can be regulated at several levels involving the de-condensation of chromatin, release of DNA from histone proteins, assembly of active translation complexes, and a variety of epigenetic mechanisms. Histone protein and transcription complex assembly dynamics are of particular interest with regards to VPA because of its demonstrated role as a histone deacetylase (HDAC) inhibitor (Phiel et al., 2001). Acetylation/deacetylation is an important regulator of both of these processes, making VPA's inhibition of HDAC activities a likely candidate for altering protein abundance. However, it is unknown how this action may directly affect protein abundance. Aside from gene expression there are several other factors affecting protein abundance including, protease activity, post-translational modifications (PTMs), and translational regulation (Vogel & Marcotte, 2012). Proteases are enzymes that degrade proteins through hydrolysis of the peptide bond that play a critical role in biological processes through maintenance or reduction in protein concentrations (López-Otín & Overall, 2002). Controlled rates of protein degradation are often accompanied by poly-ubiquitination, which is a complex and highly regulated process. Protein PTMs can influence a host of protein functions such as enzyme activity, degradation, localization, and protein-protein interactions (Karve & Cheema, 2011). Of particular interest with VPA exposure

are oxidative PTMs due to VPA's association with downstream biomarkers of cellular oxidation. Oxidative PTMs have been demonstrated to affect protein form, function, and abundance which could thereby affect developmental progress (Ghosh et al., 2006; Go et al., 2015). VPA exposure has previously been associated with changes in reversible cysteine oxidation (Chapter 3). Finally, translational regulation plays a role in determining which mRNAs are translated into proteins. Translation can be affected at several different levels including through availability of translational machinery (ribosomes, tRNA, mRNA), frequency of translational initiation, rate of translational elongation, and the process of protein folding (Rodnina, 2016). Due to these many variables that can affect protein abundance, the greater complexity of the proteome compared to the genome, and the slower technological advances in the field of proteomics, there is less research on protein abundance compared to mRNA expression (Sidoli et al., 2017). Understanding protein dynamics and the role of the proteome in biological function, however, remains critically important since proteins are the active molecular contributors to cellular activity and morphological development.

There have been many analyses of gene mutations and gene expression related to NTD occurrence with over 200 genes identified in mice as potential targets in the process of NTC (Copp et al., 2013). Some of the general pathway groupings that these genes belong to include: disturbance of the cytoskeleton, disturbance of cell proliferation or neuronal differentiation, neuroepithelial cell death, transcriptional regulation and chromatin dynamics, and dysregulation of the sonic hedgehog pathway (Copp et al., 2013). One hypothesis for VPA disrupted NTC involves disruption to cellular proliferation of the neuroepithelia which is essential for progression and completion of NTC (Bennett et al., 2000; Walsh & Morris, 1989). This hypothesis has been supported by data that suggests that disruption of the cell cycle leads to

increased neural tube abnormalities in rat embryos (Walsh & Morris, 1989). Additionally, VPA exposure has caused disruption of proliferation through upregulation of growth factor receptors (*ngf*, *ngf-R*, and *trk*) and neurotrophic factors (*bdnf*) in mouse embryo neural tubes at three different times points during closure (Bennett et al., 2000). In addition to supporting the hypothesis that cell proliferation may be altered in embryos affected by NTDs, this data suggests that expression levels of affected genes change over the course of NTC as indicated by the three sampling time points at early, mid, and late NTC (Bennett et al., 2000).

The advancement of omics technologies has drastically altered the way hypotheses related to gene and protein expression are developed and tested. Rather than having to form a hypothesis related to one subset of proteins and test it from the bottom-up, hypotheses can instead be generated and tested through a top-down systems biology framework. Tandem Mass Tags (TMT) are a set of 10 isobaric protein labels that are amine reactive and therefore capable of labeling the global proteome of a system (McAlister et al., 2012; Thompson et al., 2003). The isobaric masses of the 10 TMT labels paired with their unique mass reporter group allows for simultaneous analysis of protein abundance across ten unique groupings for a comparative analysis of protein abundance. There have only been few studies looking at the proteome of mouse embryos, one of these studies in pre-implantation mouse embryos, highlighted that the mouse proteome from zygote to blastocyst stages is highly dynamic over time with proteins of high abundance and enrichment being associated with different pathways across developmental stages (Gao et al., 2017). A study of organogenesis-stage rat embryo proper (EMB) and visceral yolk sac (VYS) tissue demonstrated that these two tissues have unique patterns of protein expression and that within a tissue, there were few changes in proteins identified across two time points, but that quantity of proteins did differ over time (Usami et al., 2007). There are not any

known global proteome studies evaluating changes in protein abundance throughout mouse organogenesis, though this stage would also likely show highly dynamic temporal changes in protein abundance over time due to the myriad of morphological and physiological processes operating in the embryo.

Most of the research to date, evaluating changes in gene or protein expression following VPA exposure, has been a product of reductionist molecular studies dedicated to specific sets of genes related to a central hypothesis for VPA's NTD mechanism. Systems-wide global genome or proteome studies have yet to be undertaken. This study will evaluate changes in global protein quantity following VPA exposure in order to determine patterns of protein abundance in early development. Pathway analysis of proteins affected by VPA exposure will aid in determining protein networks and biological processes that may be part of VPA's mechanism in causing NTDs. This will be accomplished through a time and tissue specific assessment of protein abundance following VPA exposure during the period of NTC using 10-plex TMT labels with protein identification through liquid chromatography and mass spectrometry. Through these methods it is hypothesized that patterns of tissue and time specific protein abundance following VPA exposure will differ from the patterns in control conceptuses revealing potential pathways involved in mouse NTC and implicated in VPA's mechanism of action.

Materials and Methods

Animals

Experiments were conducted using mouse whole embryo culture (mWEC) to culture conceptuses from gestational days (GD) 8-9 in time-mated pregnant CD-1 mice (Charles River Laboratories, Raleigh, NC). Gestational day 0 was measured as the morning following mating

with a positive vaginal plug. Animals were housed in groups of 6 or fewer in ventilated cages. All animal methodology was approved by the University of Michigan Institutional Animal Care and Use Committee.

Culture Conditions

Pregnant GD 8 dams were euthanized by CO^2 asphyxiation and uteri were removed and placed in Tyrode's solution (pH 7.4, HiMedia; Mumbai, India). Implantation sites were dissected with watchmaker's forceps and iridectomy scissors. Maternal tissues including the decidua and Reichert's membrane were removed to reveal intact conceptuses. Conceptuses were cultured in groups of 2-6 per bottle of 2mL of immediately centrifuged female rat serum with 4.3 µl/mL penicillin, streptomycin (10,000 units penicillin and 10 mg streptomycin per mL, Sigma Aldrich; St. Louis, MO). All culture conditions were at 37 °C with gas concentrations at 5% O_2, 5% CO_2, 90% N_2 for 6 hrs then 20% O_2, 5% CO_2, 75% N_2 for the remainder of the culture period (C. Harris, 2012).

Time Course Exposures and Sampling for Tandem Mass Tag Labeling

VPA (600 µM in H_2O) was added *in vitro* to the female rat serum two hours following the start of culture. Samples were collected 2, 4, 6, 8, and 10 hrs following the addition of VPA. At the designated end of culture, conceptuses were rinsed 3times with 1x Hank's Balanced Salt Solution (HBSS, pH 7.4, Thermo Fisher Scientific; Waltham, MA). The ecto-placental cone was removed and discarded and then conceptuses were dissected into the visceral yolk sac (VYS) and embryo proper (EMB). VYS and EMB were collected as pooled samples consisting of tissue from up to 10 conceptuses to ensure high enough protein content for further analysis. Samples were collected in 100 µL RIPA buffer (pH 7.4; 50 mM Tris-HCl, 1% NP-40 v/v, 1:100 HALT

Protease/Phosphatase Inhibitor, 150 mM NaCl, 1mM EGTA, 1mM NaF, 0.25% Na Deoxycholate w/v, and 0.1% SDS w/v), then sonicated to disrupt tissue and homogenize the solution. Homogenized samples were centrifuged for 10 min at 12,000 x g before being frozen at -80 °C.

Tandem Mass Tag Labeling

A bicinchoninic acid (BCA) assay was performed to determine protein concentration of samples. 100 µg of protein was added to a new microfuge tube with volume brought up to 100 µL with 1x Tetraethylammonium bromide (TEAB, Thermo Fisher Scientific; Waltham, MA). Samples were reduced with 5 µL 200 mM tris(2-carboxyethyl)phosphine (TCEP, Thermo Fisher Scientific; Waltham, MA) for 1 hr at 55 °C then alkylated with 5 µL 375 mM iodoacetamide (Sigma Aldrich; St. Louis, MO) and incubated at room temperature in the dark for 30 minutes. Protein was then precipitated overnight in ice-cold acetone at 4 °C then resuspended in 100 µL 1x TEAB. 2.5 µg trypsin was added to each sample for overnight protein digestion at 37 °C . The next day, 41 µL anhydrous acetonitrile was added to each of the 10-plex TMT labels and vortexed and centrifuged (Thermo Fisher Scientific; Waltham, MA). Each label was then combined with the corresponding sample (Table 4-1) and incubated for 1 hr at room temperature. The labeling reaction was quenched with 8 µL hydroxylamine (Thermo Fisher Scientific; Waltham, MA) for 15 minutes. Following labeling, all 10-plex labels were combined into one sample and dried in a centrifugal vacuum concentrator. Pierce reverse-phase high pH fractionation was performed following manufacturer's instructions to split each 10-plex labelled sample into 8 fractions (Thermo Scientific; Waltham, MA).

Liquid Chromatography, Mass Spectrometry

Liquid chromatography, mass spectrometry, and protein identification were performed by the Proteomics Resource Facility at the University of Michigan. Multinotch-MS3 was utilized to obtain superior accuracy which minimizes the reporter ion ratio distortion resulting from fragmentation of co-isolated peptides during MS analysis(McAlister et al., 2014). Orbitrap Fusion (Thermo Fisher Scientific; Waltham, MA) and RSLC Ultimate 3000 nano-UPLC (Dionex; Sunnyvale, CA) was used to acquire the data. 2 µl of the sample was resolved on a PepMap RSLC C18 column (75 µm i.d. x 50 cm; Thermo Scientific) at a flow-rate of 300 nl/min using 0.1% formic acid/acetonitrile gradient system (2-22% acetonitrile in 150 min; 22-32% acetonitrile in 40 min; 20 min wash at 90% followed by 50 min re-equilibration) and directly sprayed into the mass spectrometer using an EasySpray source (Thermo Fisher Scientific; Waltham, MA). The mass spectrometer was set to collect one MS1 scan (Orbitrap; 120K resolution; AGC target $2x10^5$; max IT 100ms) followed by data-dependent, "Top Speed" (3 sec) MS2 scans (collision induced dissociation; ion trap; NCE 35; AGC $5x10^3$; max IT 100ms). For multinotch-MS3, the top 10 precursors from each MS2 were fragmented by HCD followed by Orbitrap analysis (NCE 55; 60K resolution; AGC $5x10^4$; max IT 120ms, 100-500 m/z scan range).

Protein identification in Proteome Discoverer

Proteome Discoverer (v2.4; Thermo Fisher Scientific; Waltham, MA) was used for data analysis. MS2 spectra were searched against the Uniprot mouse protein database (reviewed and unreviewed; 94044 entries; downloaded on 06/20/2019) using the following search parameters: MS1 and MS2 tolerance were set to 10 ppm and 0.6 Da, respectively; carbamidomethylation of cysteines (57.02146 Da) and TMT labeling of lysine and N-termini of peptides (229.16293 Da)

were considered static modifications; oxidation of methionine (15.9949 Da) and deamidation of asparagine and glutamine (0.98401 Da) were considered variable. Identified proteins and peptides were filtered to retain only those that passed ≤1% FDR threshold. Quantitation was performed using high-quality MS3 spectra (Average signal-to-noise ratio of 10 and <30% isolation interference).

Protein Inclusion & Differential Abundance Determination

Proteins were included in downstream analysis when they were identified with high FDR confidence in both replicates and showed labeling with all 10 TMT labels. Included proteins had a VPA/Ctl abundance ratio calculated using normalized abundance values from the appropriate TMT channels (Table 4-1). The average difference in VPA/Ctl abundance ratio for a single protein across replicates was 0.25, so this value was adopted as the threshold of difference required for proteins to be determined differentially expressed between VPA and Control samples. Therefore, proteins with a VPA/Ctl log2 ratio of 0.33 or greater were indicative of increased expression following VPA treatment, whereas VPA/Ctl log2 ratios of -0.33 or less were indicative of decreased expression following VPA treatment.

Co-regulation Clustering

Co-regulated protein clustering was performed using *Clust* (Abu-Jamous & Kelly, 2018). Clustering was completed separately for EMB protein abundances and VYS protein abundances. Default *Clust* settings were applied for this analysis.

Pathway Analysis

Pathway analysis was conducted for each list of proteins that met the cut-off criteria for inclusion described in the Variability section as well as each co-regulated protein cluster.

DAVID Bioinformatics Database functional annotation tool was used to designate enriched Biological Process Gene Ontology (GO) terms (Huang et al., 2009b, 2009a). Protein lists were searched against the full list of proteins identified for the specific tissue as background to adjust for the presence of higher abundance proteins being overly represented in mass spectrometry data. GO-terms were deemed significant if the p-value was less than 0.05.

Transcription Factor Enrichment

Enrichment of transcription factors was measured using Enrichr (Chen et al., 2013; Kuleshov et al., 2016). Uniprot IDs were converted to Entrez gene names which were compared against the database ENCODE and ChEA Consensus TFs from ChIP-X (Davis et al., 2018; ENCODE Project Consortium, 2012). An adjusted p-value less than 0.05 was used as the cut-off for inclusion in the results. Within each set of tissue specific co-regulated clusters, lists of significant TFs were compared to identify TFs unique to that cluster.

Gene Set Enrichment Analysis

Gene Set Enrichment Analysis (GSEA) was performed to identify pathways that showed differential enrichment between proteins with higher or lower abundance following VPA exposure without the need to use the pre-determined threshold inclusion criteria (Mootha et al., 2003; Subramanian et al., 2005). Data were input into the GSEA software (v. 4.1.0) as a .rnk file containing Uniprot accession numbers and VPA/Ctl abundance ratios and run as a pre-ranked dataset with 1000 permutations and collapsing redundant accession numbers to a single gene name. Proteins were searched against the Biological Process Gene Ontology (GO) term database (v 7.2). Pathways with an FDR value of less than 25% were included in the results.

Targeted Analysis- Antioxidant and Neural Tube Defect Associated Proteins

For targeted analysis of antioxidant relevant proteins, EMB and VYS datasets were searched for proteins that were linked to the molecular function GO term "antioxidant activity." Targeted analysis of NTD associated proteins searched the EMB and VYS TMT datasets for proteins that were reviewed by Copp and Greene as being associated with the process of NTC (Copp & Greene, 2010). Inclusion criteria for the targeted analysis required proteins to fit the designated search criteria and be significantly increased or decreased following VPA exposure in at least one tissue and time point. Significance cut-off criteria were as described in the Variability section.

Results

Data Summary

In the VYS 4,815 proteins were identified across both replicates with high FDR confidence and identification of all 10 TMT labels, whereas in the EMB there were 4,897 proteins that met these criteria. Comparing the two tissue datasets, there were 4,238 proteins that appeared in both VYS and EMB (Table 4-2).

Variability

Each tissue (EMB and VYS) determination and comparison were based on two biological replicates. Variability of the VPA/control (Ctl) abundance ratio for each tissue and time point is summarized in Figure 4-1. Proteins that showed variability of greater than 300% between replicate VPA/Ctl abundance ratios at least one time point were excluded from this dataset and included ten proteins identified in the EMB and seven proteins in the VYS. In the EMB, median variability ranges from 8.7% to 34.1%, while the VYS variability median is between 5.9% and

22.6%. In the EMB, the most variable time points across the two replicates were at 6 and 10 hr, while in the VYS, the most variable time points were at 2 and 4 hrs.

Tissue Comparison Summary- Embryo vs Visceral Yolk Sac

4,238 proteins were identified and labeled in both the EMB and VYS datasets with high FDR confidence and identification in both biological replicates. Figure 4-2 compares the VPA/Ctl abundance ratios for each protein between the EMB and VYS and illustrates that there is a strong similarity between EMB and VYS abundance ratios, especially at 2, 4, and 8 hrs. EMB and VYS ratios showed less similarity at 6 and 10 hrs, mostly due to higher variation in the EMB, but there still remained a large number of proteins that exhibited close to equivalence between their VYS and EMB ratios. The VYS shows the widest spread in abundance ratios at 2 and 4 hrs, whereas the EMB shows the widest spread at 6 and 10 hrs. Patterns of concordance and discordance related to increases and decreases in abundance between the EMB and VYS are shown in Table 4-7. At all time points the majority of proteins were unchanged following VPA exposure in both EMB and VYS. At 2 and 4 hrs, the next largest subset of proteins was only changed in response to VPA in the VYS with 21.4 and 31.71% of proteins falling into this category respectively. Proteins that were exclusively affected in the EMB comprised 22.91 and 28.34% of the total proteins at 6 and 10 hrs respectively. The 8 hr timepoint had the highest proportion of proteins that were unchanged at 92.66% with roughly an equal number of proteins affected exclusively in the VYS or EMB.

Embryo Time Series

There were 4,897 proteins identified in the EMB at all five time points (Table 4-2). Within each of these time points proteins were categorized by increased or decreased abundance

following VPA exposure using the inclusion criteria described in the methods (Table 4-3). 6 and 10 hr time points contained the highest number of affected proteins. At all time points in the EMB, with the exception of 6 hrs, there were more proteins increased in abundance following VPA exposure than were decreased in abundance.

Pathway analysis was carried out for each time-specific group of increased or decreased proteins and enrichment of biological process GO-terms was identified for all groups (Figure 4-3). While the majority of categorical pathway groups enriched within each time point are similar, there are several points of interest. Enrichment of developmentally relevant pathways is found at all time points except 4 hr increased abundance and 8 hr decreased abundance. Table 4-4 identifies the enriched developmentally relevant pathways at each time point. There were 8 unique developmental pathways enriched in proteins with increased abundance and 9 unique pathways in those that were decreased (Table 4-4). Significant transcription factor (TFs) enrichment was mostly found at time points with a large number of increased or decreased proteins. TFs that are unique to either increased or decreased proteins within a specific time point are listed in Table 4-6. The EMB showed enrichment of TFs in increased proteins at 4, 6, and 10 hrs and in decreased proteins at 4, 6, and 10 hrs.

In addition to pathway analysis based on categorization of proteins into groups increased and decreased by VPA exposure, pre-ranked Gene Set Enrichment Analysis (GSEA) was also performed. In the EMB, GSEA identified 46 developmentally relevant pathways that were more enriched in proteins that increased in abundance following VPA exposure and seven pathways that were more enriched in decreased proteins (Table 4-10). There was no enrichment of developmental pathways at 4 hrs for increased proteins, or 6, 8, and 10 hrs for decreased proteins.

Visceral Yolk Sac Time Series

There were 4,815 proteins identified in the VYS at all 5 time points. Within each of these timepoints proteins were categorized by increased or decreased abundance following VPA exposure using the inclusion criteria described in the methods (Table 4-3). 2 and 4 hrs showed the highest number of proteins that were affected by VPA exposure. At all time points, with the exception of 2 hrs, there were more proteins with increased abundance than decreased abundance.

Pathway analysis identified significantly enriched GO-terms in categories except 6 hr and 8hr decreased (Figure 4-4). Developmentally relevant pathways were enriched in both increased proteins at 2, 4, 8, and 10 hrs and in decreased proteins at 4, 6, 8, and 10 hrs. Table 4-5 identifies the developmental pathways enriched in the VYS. Significant transcription factor enrichment was primarily identified at 2 hr and 4 hr timepoints in the VYS, but there was also enrichment for decreased proteins only at 6 and 8 hrs (Table 4-6). The groups of increased proteins at these time points were more enriched for TFs than the decreased timepoints.

Pre-ranked GSEA in the VYS identified 28 developmentally relevant pathways that were enriched in proteins with increased abundance following VPA exposure and 12 pathways that were enriched in proteins with decreased abundance (Table 4-11). There was no developmental enrichment at 6 and 8 hrs for increased abundance proteins and at 2 and 4 hrs for decreased abundance proteins.

Co-regulated protein clustering

Clustering of EMB abundance data lead to two co-regulated protein clusters of 624 (EMB Cluster 0) and 536 (EMB Cluster 1) proteins each (Figure 4-5). The main time points of difference between control and VPA in these clusters are at 6 and 10 hrs. Pathway analysis of

enriched biological process gene ontology (GO) terms was conducted for each EMB and VYS co-regulated abundance cluster. EMB Cluster 0 showed significant enrichment for 11 biological process GO-terms (Figure 4-6). Of these 11 terms there was enrichment for two developmentally relevant terms including, epidermal growth factor signaling and forebrain development. EMB Cluster 1 was enriched for 21 biological process GO-terms (Figure 4-7). None of these pathways were specifically related to development, but negative regulation of apoptotic process and oxidation-reduction process are still noteworthy due to apoptosis serving as an important mechanism of programmed cell death during development and VPA's association with oxidative endpoints.

Clustering of VYS data also lead to two distinct clusters of 738 (VYS Cluster 0) and 601 (VYS Cluster 1) proteins respectively (Figure 4-8). For the two VYS clusters, the single time point of divergence between the Ctl and VPA samples occurred at 4 hrs in both clusters. VYS Cluster 0 had 14 significantly enriched pathways biological process GO-terms (Figure 4-9). None of these pathways were directly relevant to development, although cardiac muscle cell apoptosis may be partly related to heart development. VYS Cluster 1 showed significant enrichment for 31 biological process pathways with several relevant to development or oxidation (Figure 4-10). Developmental pathways included the following: skeletal muscle tissue differentiation, cerebral cortex neuron differentiation, and axon extension. Oxidation relevant pathways included oxidation-reduction process, cellular response to hypoxia, and response to reactive oxygen species (ROS).

EMB Cluster 0 and EMB Cluster 1 were significantly enriched for 65 and 64 transcription factors (TFs), respectively. Of these enriched TFs, 6 were unique to EMB Cluster 0 and 5 were unique to EMB Cluster 1 (Table 4-8). The TFs unique to EMB Cluster 0 had 4

developmentally relevant TFs, while EMB Cluster 1 had 2 TFs of developmental relevance and two related to VPA's function as an HDAC inhibitor. In the VYS abundance clusters, there were 64 significantly enriched TFs in VYS Cluster 0 and 65 in VYS Cluster 1 (Table 4-9). VYS Cluster 0 was enriched for 7 TFs that were unique compared to 8 unique TFs for VYS Cluster 1. Five of the enriched TFs for VYS Cluster 0 are developmentally relevant and 4 of the enriched TFs for VYS Cluster 1 are developmentally relevant. Transcription factor ZKSCAN1, which is enriched uniquely in VYS Cluster 1, is relevant to VPA's function as an HDAC inhibitor.

Targeted Analysis-Antioxidant and NTD associated proteins

There were 22 significantly altered antioxidant proteins identified in the VYS and 17 in the EMB (Table 4-12). In the VYS, the most sensitive time point to changes in antioxidant protein abundance was 4 hrs with 19 of the 22 proteins either increased or decreased following VPA exposure. In the EMB the most sensitive time periods to changes in antioxidant protein abundance were 6 and 10 hrs with 9 and 13 increased or decreased proteins, respectively.

There were 14 significantly altered NTD associated proteins in the VYS and 11 in the EMB (Table 4-13). In the VYS, the most sensitive time point was 4 hrs with 13 proteins significantly increased following VPA exposure. There was only a single decreased protein at this time point (vasodilator stimulated phosphoprotein). In the EMB, 6 and 10 hr time points showed the greatest change with 8 proteins each with a roughly equal mix of increased and decreased abundance following VPA exposure. None of the NTD relevant proteins showed changes in abundance at 2 and 4 hrs in the EMB and only a single protein was affected in the VYS at 8 and 10 hrs (apoptotic protease-activating factor 1).

Discussion

The aim of this study was to evaluate changes in protein abundance following VPA exposure that are time and tissue-specific with the goal of identifying proteins that may be involved in VPA's mechanism of disrupting neural tube closure (NTC). The analysis identified over 4,800 proteins in each tissue with hundreds of these proteins exhibiting differential abundance between control and VPA treated samples. The TMT labeling methodology with protein identification through LC-MS^3 is biased toward analyzing proteins of the greatest abundance. To account for this methodological bias, pathway analysis in DAVID was conducted using the full tissue-specific data set as background for determining enrichment. While this method helped to reduce the inclusion of extraneous pathways unrelated to the direct question of neural tube closure, such as those belonging to more general homeostatic biological processes such as metabolism, transport, gene/protein expression, and biosynthesis, there are still more pathways identified than can be adequately evaluated in detail in this analysis. Alterations in these common pathways for maintenance of cellular homeostasis, however, cannot be wholly excluded from involvement in complete mechanisms of VPA toxicity. For this reason, we have focused attention on pathways of greatest relevance to general developmental processes, neural tube closure, and oxidation-reduction to specifically address VPA's effects on redox-mediated disruption of NTC. Future studies may benefit from utilizing the data from this paper to assess VPA's effect on other pathways such as metabolism, immune response, and transport which also exhibited high levels of enrichment.

Studies of developmental biology and toxicology frequently focus exclusively on the cells and tissues of the embryo proper, ignoring the shared vascular system and functional dependence of the VYS that make up the intact and viable conceptus of early organogenesis.

Paucity of EMB tissue and complexities related to developmental dynamics precluded closer inspection of individual EMB tissue types but did allow for comparison of EMB and VYS. The observed differences between EMB and VYS, as interdependent developmental tissues, result from many factors including their germline origins (EMB → female; VYS → male), different types of environmental interface and overall developmental juxtaposition within the conceptus. As such, tissue specificity was a key component of the analysis with EMB and VYS protein abundance measured independently. The independent assessment of EMB and VYS is due to the unique roles played by these tissues. While the EMB will form into the fetal and eventually adult mouse, the VYS is a uniquely developmental tissue. The VYS performs many roles that are essential for the development of the EMB proper including germ cell maintenance and release, hematopoiesis (blood islands), vasculogenesis, angiogenesis, nutritional uptake prior to placentation, a source of mesenchymal stem cells and as an essential environmental interface for signaling and regulation (Aires et al., 2015; Halbach et al., 2020; Ross & Boroviak, 2020; Zohn & Sarkar, 2010). Due to these critical roles played by the VYS during early organogenesis, it is essential to include a separate assessment of the EMB and VYS to identify any distinct responses to, and consequences of, VPA exposure even though our downstream stream mechanism of interest of neural tube closure (NTC) appears to lie solely within the EMB proper.

It is generally understood that the VYS reaches its metabolic and functional maturity earlier than the cells and tissues of the EMB proper but roles played by the VYS in regulating EMB growth, differentiation and morphogenesis remain obscure (Donovan & Bordoni, 2020). Comparative analysis of protein abundance at the 2 hr time point where the process of neurulation is still in its early stages shows no enrichment in the EMB but both increased and decreased enrichment in the VYS. At this stage of neurogenesis the neural plate is being

polarized and established. Neural folds are beginning to elevate and the first fusions are occurring near the point of dorsal embryonic flexion. The cranial neuropore and posterior spinal cord, however, are still completely open. This phase of development, therefore, marks the time of optimal sensitivity for disruption of neurulation by chemical and environmental insults (Burggren & Mueller, 2015; Choi et al., 2012). Of high interest, is our discovery that changes in protein abundance, which should indicate active regulation of new protein synthesis, occurs primarily in the VYS during the critical, early 2 and 4 hr phases of development (Table 4-3) with only a limited number of EMB proteins affected. By almost all enrichment identification measures (DAVID and GSEA pathway analysis and transcription factor enrichment), the VYS shows enrichment of increased and decreased developmental and VPA-associated proteins at 4 hrs that were previously decreased at 2 hrs. As the conceptus enters the 6 hr phase, enrichment-related activity and control appears to be transferred to the EMB and the VYS relinquishes regulatory control. The significance of an apparent pause in enrichment at 8 hrs cannot be explained currently but is known to occurs during the developmental phase where an active heartbeat is being established and several important physiological changes are occurring in the conceptus.

In comparing the proteins identified in each tissue-specific data set, a significant overlap of 4,238 protein was identified. Evaluation of the directional concordance of protein abundance within each tissue showed few similarities as noted in Table 4-7. While the majority of proteins at each time point showed no change in abundance in both the VYS and EMB, the share of proteins with concordant increases or decreases in abundance was small with less than 1% of all proteins falling into these categories. Of the categories indicating directional changes in abundance, the largest share of proteins was categorized at a given time point as only changing

in the VYS or the EMB. The independent response of the VYS and EMB to VPA is further supported by the distribution of differentially abundant proteins across the time course where the VYS had the greatest number of affected proteins at 2 and 4 hrs, while the EMB showed the greatest effect at 6 and 10 hrs (Table 4-3). Together the directional concordance and differential abundance distribution indicate that protein abundance and directional response to VPA are independently regulated in the VYS and EMB.

Examination of protein abundance with respect to the potential alterations to developmental process and neurulation will begin by focusing on pathways of developmental relevance with an emphasis on those associated with brain development. In the EMB, there is increased abundance of proteins related to pathways of substantia nigra development (6, 10 hrs), animal organ morphogenesis (6, 10 hrs), tissue morphogenesis (6 hrs), and neural nucleus development (6 hrs). Multicellular organism development (10 hrs) was enriched for proteins with decreased abundance following VPA exposure. Compared to the EMB, the VYS shows less enrichment for brain and general organogenesis pathways, which is expected due to its lesser, supportive role in NTC. Of the two enriched pathways that were found in the VYS, both were proteins with increased abundance and were mapped to cerebral cortex development (10 hrs) and animal organ morphogenesis (4 hrs). Between both the EMB and VYS, the pathways most relevant to the brain included the following: substantia nigra development, cerebral cortex development, and neural nucleus development and were all enriched in sets of proteins that were increased following VPA exposure and limited to the time periods of 6 and 10 hrs. This suggests that VPA's action on larger networks of proteins relevant to brain development may be limited to specific developmental phases and that at other time points VPA may be causing limited changes to individual proteins rather than modifying a full or partial network. The enrichment of these

brain-relevant pathways in increased proteins seems counterintuitive, but there is a possibility that the increase may be an adaptive mechanism to counterbalance other changes VPA has made to mechanistic pathways.

One mechanistic pathway that is essential to development that showed frequent enrichment was cellular differentiation, which plays an important role in neural development and NTC. In mice, NTDs have been associated with improper differentiation of Notch pathway genes, Hes1, Hes3, and RBP-Jk, although none of these specific proteins were identified in our data (M. J. Harris & Juriloff, 2010). Ethionine, an analog of amino acid methionine, has been demonstrated to disrupt neural stem cell differentiation into neurons and astrocytes and induce ROS generation leading to increased NTD outcomes (Zhang et al., 2020). This provides evidence that oxidation and disruption of differentiation may be associated with NTD outcomes. In this study of VPA exposure, various differentiation pathways were decreased in the EMB at 2 and 10 hrs and in increased proteins at 6 and 10 hrs when combining the lists of enriched developmental pathways across DAVID and GSEA analyses (Tables 4-4 and 4-8). The increased differentiation pathways in the EMB included stem cell, osteoclast and hematopoietic stem cells while the decreased differentiation cell types included osteoblast, keratinocyte, epidermal, epithelial, and general cell differentiation. In the VYS, differentiation was enriched in both increased and decreased proteins across the time course with cell type being associated with directional changes (Tables 4-5 and 4-9). Keratinocyte and epidermal cell differentiation were enriched for decreased proteins at 6, 8, 10 hrs. At 4 hrs in the VYS, there were several additional differentiation pathways enriched in increased proteins including: hematopoietic, stem cell, epidermal and epithelial. At 10 hrs, three immune system relevant cell types, megakaryocyte, lymphocyte, and T-cell showed enrichment in increased protein abundance. Of these cell types

showing altered differentiation, the most relevant for forming the neural tube are stem cells, osteoclasts & osteoblasts, epidermal and epithelial cells.

Another mechanistic theme present among enriched pathways was growth and proliferation. As discussed in the introduction, NTC relies on proliferation of the neuroepithelia for proper closure and VPA has been associated with alterations to the proliferation through growth factor pathways (Bennett et al., 2000; Walsh & Morris, 1989). In the VYS, increased growth pathways included target of rapamycin (TOR) signaling at 4 hrs and decreased growth pathways included epidermal growth factor signaling and smooth muscle cell proliferation at 4 hrs and TOR signaling at 8 and 10 hrs (Tables 4-5 and 4-9). In the EMB, growth related pathways were only enriched in proteins with increased abundance and included negative regulation of growth at 6 and 10 hrs, negative regulation of cell growth at 6 hrs, and positive regulation of developmental growth at 8 hrs (Tables 4-4 and 4-8).

TOR signaling is a process that promotes cell growth and proliferation in response to nutritional cue and has been shown to be critical to mouse development (Wullschleger et al., 2006). Homozygous mammalian TOR mutants die early in development due to decreased cell proliferation in a manner similar to EMB starved of amino acids (Gangloff et al., 2004; Martin & Sutherland, 2001; Murakami et al., 2004). This has been further supported by rapamycin exposure in early development similarly preventing cell proliferation supporting the importance of active TOR signaling to mouse growth and development (Martin & Sutherland, 2001). In our data, TOR signaling enrichment was specific to the VYS, which holds a critical role in nutritional uptake prior to formation of the placenta after organogenesis. TOR Signaling pathways were enriched in elevated proteins at 4 hrs, but in decreased proteins at 8 and 10 hrs

indicating a potential dip in nutrient availability which is supported by the histiotrophic nutrition assessment from Chapter 2.

In contrast to the VYS, which only showed one time point with elevated growth and proliferation pathways, the EMB was exclusively enriched for growth and proliferation pathways in proteins that increased in abundance following VPA exposure. However, at least two of these pathways were related to negative regulation of cell growth and more broadly tissue growth in general at 6 and 10 hrs with the only positive regulation of growth occurring at 8 hrs. This anomaly at 8 hrs could potentially be an adaptive mechanism following extended VPA exposure to try to make up for decreased growth patterns enriched at other time points. Overall, it is clear from the patterns of enrichment from the EMB and VYS, that VPA most commonly decreases growth and proliferation pathways, which may lead to failed NTC.

Wnt Signaling and cell polarity relevant pathways were heavily enriched across EMB and VYS and always within proteins that showed increased abundance following VPA exposure. In the EMB, Wnt and Cell Polarity pathways were enriched for increased proteins at 6 and 10 hrs and in the VYS Wnt and cell polarity pathways were enriched for increased proteins at 4 hrs. A fully functioning non-canonical Wnt/Planar Cell Polarity (PCP) signaling pathway is a necessity for completion of the convergent extension (CE) process involved in NTC (M. Wang et al., 2019). PCP is responsible for establishing and maintaining cell polarity and movement to establish tissue organization. In the context of CE, the PCP pathway directs the reshaping of the neural epithelium through sequential resolution of the anteroposterior cell junction and extension along the mediolateral junction followed by intercalation of the newly shaped cells guided by actin protrusions (Butler & Wallingford, 2017; M. Wang et al., 2019). This process of cellular re-shaping and movement is what drives the folding of the neural plate into the neural tube. Based

on VPA's role in disrupting normal neurulation, it would be expected that it might cause a decrease in abundance of Wnt/PCP proteins, however, these pathways were exclusively enriched in increased proteins. There has been research that has indicated that VPA promotes neural stem cell differentiation into neurons through the canonical Wnt signaling pathway as measured through Wnt3a and β-catenin expression which could explain the increase in abundance seen in our data (L. Wang et al., 2015). VPA is also implicated in activating the canonical Wnt signaling pathway in a VPA treated rat model of autism spectrum disorder where it elevated expression levels of β-catenin and phospho-GS3Kb (Qin et al., 2016). Despite the support for VPA's induction of the canonical Wnt signaling pathway, there is little evidence that VPA increases or decreases activity of the non-canonical Wnt signaling pathway that is responsible for NTC. It is therefore possible, that due to the large overlap in proteins contained within the canonical versus non-canonical Wnt pathways that both pathways were highlighted as increased when in reality VPA is not increasing the non-canonical Wnt pathway that is primarily responsible for NTC.

β-catenin is the main differentiating component between the canonical and non-canonical Wnt pathways and was identified at all 5 time points in both EMB and VYS. β-catenin abundance ratio values for the VYS were 0.84, 1.29, 0.99, 0.92, and 0.96 in order of occurrence, whereas in the EMB the abundance ratios were 0.99, 0.97, 1.2, 0.99, and 1.29. The increases at 4 hrs in the VYS and 6 and 10 hrs in the EMB are reflective of the Wnt pathway enrichment results. Although the canonical, β-catenin-dependent Wnt pathway is not the primary driver of neural tube closure, there is known crosstalk between the canonical and non-canonical/PCP pathways with protein mediators (Lrp6 and Ptk7) that cause simultaneous activation and inactivation of the dual Wnt pathways. Ptk7 is an activator of the non-canonical/PCP Wnt pathway while also serving as a repressor of the canonical Wnt pathway (M. Wang et al., 2019).

Ptk7 was identified in the EMB (0.99, 1.01, 0.99, 1.0, 1.06) and VYS (0.91, 1.12, 1.20, 1.06, 1.14) at all five time points, but showed limited changes in abundance relative to the control indicating that VPA is not causing over or under-activation of the non-canonical Wnt/PCP pathway. While it is clear that VPA is causing changes in the abundance of Wnt associated proteins, this systems level view of the changes will not be able to determine a direct mechanism. Further molecular studies should be undertaken to better define VPA's role in Wnt signaling disruption.

Measurements of protein abundance were made across 10 hours of early organogenesis from a fully open neural tube to the time period of active closure (Sakai, 1989). Differing patterns of differential protein abundance and pathway enrichment between the VYS and EMB revealed tissue-specific windows of sensitivity to VPA with the VYS generally showing effects of VPA exposure earlier than in the EMB. Clustering of co-regulated proteins revealed that during the 4 hr phase in the VYS and 6 and 10 hr phases in the EMB periods of distinct divergence in protein abundance were seen in control compared to the VPA-treated samples. In addition to the initiation of NTC occurring during this timeframe, there are many other developmental processes occurring including angiogenesis, heart beat initiation, axial rotation, and eye, ear, and limb bud development (C. Harris, 2012). The 4 hr time point in the VYS occurring around shortly after the mid-way point of GD 8 is around the time of heartbeat initiation and circulation (Nishii & Shibata, 2006). Though not discussed here in detail, there were many development pathways relevant to smooth muscle development, rhythmic process, heart process, and hematopoiesis supporting the idea that VPA may be affecting cardiac development. Mouse embryos exposed to VPA *in vivo* have shown decreased cardiac contractility by GD 19 compared to controls (Philbrook et al., 2019). The 6 and 10 hr time points

in the EMB may be related to the events of neurulation occurring near those times including the initiation of the third neural tube fusion and the closure of the telencephalic neuropore (Sakai, 1989). The brain development pathways previously discussed showed their greatest periods of enrichment at 6 and 10 hrs in the EMB.

Enrichment of the pathway oxidation-reduction process was noted in addition to enrichment of developmentally relevant pathways. This enrichment may link changes in protein abundance to VPA's perturbations of cellular and protein oxidation (Chapter 2 and 3). In the VYS, oxidation-reduction process was enriched at 2 hrs in proteins with lower abundance following VPA exposure and at 4 hrs in proteins with higher abundance based on the DAVID pathway analysis. In the EMB, oxidation-reduction process was enriched for increased proteins at 10 hrs. The proteins identified for the oxidation-reduction pathway for each of these tissues and time points are listed in Figure 4-11. The two time points with increased abundance of oxidation-reduction proteins at 4hrs in the VYS and 10 hrs in the EMB show the greatest overlap in protein identities. This pattern of an increase in the VYS mirrored by a later increase in the EMB is also noted with other pathways. Of the four proteins that are present in all occurrences of the oxidation-reduction process pathway, two are peroxiredoxin antioxidants and two (Uqcr10 and Sdhc) are related to the process of glucose metabolism and ATP production. The time and direction of divergence is also reflected in EMB Cluster 1 and VYS Cluster 1 (Figure 4-7 and 4-10). The time delayed increase in the oxidation-reduction process pathway at 4 and 10 hrs in the VYS and EMB respectively supports the results of VPA's effect on cellular oxidation and antioxidant concentrations being time dependent (Chapter 2).

The findings of this study are the result of a single acute exposure to VPA during an early period of organogenesis. Whole embryo culture experiments conducted *in vivo* as well as *in vitro*

confirm the ability of VPA to elicit NTDs as a result of a single dose (Tung & Winn, 2011). Due to the limited exposure window, it is not possible to determine whether our results are specific to the length of exposure or a combination of the timing and length of exposure to VPA. Future studies may benefit from performing earlier *in vivo* dosing of VPA in dams with measurement of protein abundance at these same time points within organogenesis to determine whether the timing or duration of the exposure is more critical for the response. *In vivo* dosing provides the benefit of assessing the roles of maternal transport and metabolism to the experimental design, which are lacking in the whole embryo culture model. Despite this, it is evident that proteins exhibit a dynamic response to VPA exposure over time and do not perpetually remain in a state of increased or decreased expression, thus emphasizing the importance of temporal measurements when evaluating a compound for safety during pregnancy. An additional future direction for this research would be to separately analyze organ and cell type responses to VPA exposure. By treating the whole EMB proper as a single "tissue," it is not possible to definitely conclude whether instances of altered differentiation or proliferation for example are directly related to the process of neural tube closure or instead relevant to VPA's effects on a separate organ or tissue system.

We present strong evidence to show that the EMB and VYS respond to VPA in an independent and temporally specific manner with the VYS responding to VPA during the earlier phases of organogenesis as compared to the later response in the EMB. This shift in regulatory activity/control from VYS to EMB proper over the time course has important implications for understanding potential mechanisms and targets of chemical action and the role of the VYS environmental interface during organogenesis. This study has demonstrated that VPA is causing time and tissue specific alterations to mechanistic pathways of importance to development and

NTC such as Wnt signaling (planar cell polarity, convergent extension), differentiation, cytoskeletal dynamics, proliferation, growth, and oxidation-reduction. These results bolster previous findings of time and tissue-specific cellular redox and protein oxidation resulting from VPA exposure (Chapter 2 and 3). VPA's mechanism of disrupting NTC, therefore, is likely the combinatorial result of disruption across cellular oxidation, protein oxidation, and protein abundance. Integration of VPA's time-specific effects on each of these measurements will help reveal the interaction between redox regulation, NTC, and VPA exposure during organogenesis that results in NTDs.

Tables

	126	**127N**	**127C**	**128N**	**128C**	**129N**	**129C**	**130N**	**130C**	**131**
Sample ID	Ctl 2hr	VPA 2hr	Ctl 4hr	VPA 4hr	Ctl 6hr	VPA 6hr	Ctl 8hr	VPA 8hr	Ctl 10hr	VPA 10hr

Table 4-1 TMT label assignments: 10-plex Tandem Mass Tag (TMT) label assignments for control (Ctl) and valproic acid (VPA) exposed tissues. These label assignments were the same for visceral yolk sac (VYS) and embryo proper (EMB) labeling. In total, there were two biological replicates for each tissue.

	Embryo	Visceral Yolk Sac	Embryo + Visceral Yolk Sac
# Proteins	4,897	4,815	4,238

Table 4-2 TMT data summary: Summary of the number of identified proteins in the VYS or EMB and the proteins identified across both datasets. Criteria for inclusion were a high FDR confidence level, identification across both biological replicates, and identification of all 10 TMT labels.

	Embryo					Visceral Yolk Sac				
	2hr	4hr	6hr	8hr	10hr	2hr	4hr	6hr	8hr	10hr
Number Increased	113	96	556	115	767	444	934	137	86	66
Number Decreased	89	80	666	61	748	606	646	69	54	110

Table 4-3 Summary of differential protein abundance: Directional changes in protein abundance following VPA treatment compared to the control in EMB and VYS from 2-10hrs. The threshold for increased and decreased abundance is described in the "Protein Inclusion & Differential Abundance Determination," section.

Timepoint	Embryo Enriched Biological Process GO Terms- DAVID			
	Increased		Decreased	
	Pathway	P-Value	Pathway	P-Value
2hr	In Utero Embryonic Development	0.024	Epidermis Development	0.006
	Rhythmic Process	0.033	Cell Differentiation Involved in Embryonic Placenta Development	0.046
	Muscle Organ Development	0.047		
4hr	No Enrichment		Epidermis Development	0.005
6hr	Substantia Nigra Development	0.001	Response to Transforming Growth Factor Beta	0.019
			Labyrinthine Layer Development	0.034
			Eyelid Development in Camera-Type Eyes	0.034
8hr	Epidermis Development	0.000	No Enrichment	
	Keratinocyte Development	0.009		
	Positive Regulation of Developmental Growth	0.042		
10hr			Positive Regulation of Cell Differentiation	0.036
	Substantia Nigra Development	0.031	Multicellular Organism Development	0.044
	Epithelial Tube Branching Involved in Lung Morphogenesis	0.042	Somatic Stem Cell Population Maintenance	0.049
			Negative Regulation of Osteoblast Differentiation	0.049

Table 4-4 EMB enriched developmentally relevant biological process GO-terms: Developmentally relevant biological process GO terms enriched within the increased or decreased category of EMB proteins as defined by significant ($p<0.05$) DAVID pathway analysis results using the full EMB dataset as background.

Timepoint	Visceral Yolk Sac Enriched Biological Process GO Terms- DAVID			
	Increased		Decreased	
	Pathway	P-Value	Pathway	P-Value
2hr	Lung Development Embryonic Process Involved in Female Pregnancy	0.004 0.041	No Enrichment	
4hr	Skeletal Muscle Tissue Development	0.018	Epidermal Growth Factor Receptor Signaling Pathway Negative Regulation of Osteoblast Differentiation Spermatogenesis Angiogenesis Positive Regulation of Smooth Muscle Cell Proliferation Osteoblast Development	0.008 0.020 0.024 0.039 0.045 0.046
6hr	No Enrichment		Cell Differentiation Involved in Embryonic Placenta Development	0.044
8hr	Male Gonad Development	0.048	Organ Regeneration	0.020
10hr	Cerebral Cortex Development	0.026	Regulation of Spongiotrophoblast Cell Proliferation	0.037

Table 4-5 VYS enriched developmentally relevant biological process GO-terms: Developmentally relevant biological process GO terms enriched within the increased or decreased category of VYS proteins as defined by significant ($p<0.05$) DAVID pathway analysis results using the full VYS dataset as background.

	Embryo		Visceral Yolk Sac	
	Increased	Decreased	Increased	Decreased
2hr	No Enrichment	No Enrichment	CHD1, ETS1, FOXP2, NFIC, NR2C2, SIX5, SMC3, SOX2, SRF, TCF7L2, ZBTB7A	EGR1, PBX3, PML, SP2, SPI1, TAF7, USF2
4hr	YY1	POU5F1	CEBPB, CTCF, EGR1, ERG, HNF4A, IRF1, NFIC, PPARG, RFX5, RUNX1, SRF, ZKSCAN1	ATF3, BCL3, ETS1, FOXM1, FOXP2, GATA2, NANOG, NELFE, PPARD, SOX2
6hr	CEBPB, CTCF, ETS1, FOS, HNF4A, IRF1, IRF3, KLF4, NFIC, PPARG, STAT3, TCF7L2	AR, BHLHE40, CEBPD, KAT2A, NANOG, RELA, RUNX1, SPI1, SRF, VDR, YY1, ZBTB7A	No Enrichment	FOSL2, YY1
8hr	No Enrichment	No Enrichment	No Enrichment	ATF2, BRCA1, CREB1, E2F1, E2F4, IRF3, MAX, MYC, NFYA, SP1, ZMIZ1
10hr	CTCF, ERG, FOS, HDAC2, IRF1, NFIC, PPARD, PPARG, RFX5, TCF7L2, YY1	BCL3, EGR1, FOXA1, FOXM1, RELA, RUNX1, SALL4, SRF, VDR	No Enrichment	No Enrichment

Table 4-6 EMB and VYS unique transcription factor enrichment: Transcription factor enrichment of increased and decreased proteins within each tissue and time point from the ENCODE and CHEA consensus transcription factors in Enrichr. Listed TFs are significant (adjusted $p<0.05$) and specific to the directional category within the tissue and time point. Red indicates relevance to developmental processes and blue represents relevance to VPA's known mechanisms. No enrichment indicates that no unique TFs were identified within that tissue and time point.

	Percent of Total				
	2hr	4hr	6hr	8hr	10hr
Concordant Upregulation	0.64	0.78	0.57	0.31	0.38
Concordant Downregulation	0.26	0.57	0.50	0.09	0.33
Discordant EMB Up, VYS Down	0.24	0.35	0.24	0.09	0.50
Discordant EMB Down, VYS Up	0.09	0.28	0.42	0.05	0.61
Concordant No Change	74.71	64.56	72.56	92.66	67.72
EMB Increase Only	1.46	0.94	11.02	2.29	15.20
EMB Decrease Only	1.16	0.80	11.89	1.34	13.14
VYS Increase Only	8.99	18.17	1.79	2.03	1.13
VYS Decrease Only	12.41	13.54	0.99	0.61	0.99

Table 4-7 EMB and VYS protein abundance directional concordance: Concordant and discordant directional changes in protein abundance following VPA exposure in VYS and EMB. The threshold for increased and decreased abundance is described in the "Protein Inclusion & Differential Abundance Determination," section.

	Enriched Cluster-specific Transcription Factors
EMB Cluster 0	KAT2A, RELA, BCL3, NANOG, POU5F1, FOXM1
EMB Cluster 1	FOS, RFX5, ZKSCAN1, PPARD, HDAC2

Table 4-8 EMB cluster unique transcription factor enrichment: Transcription factors (TFs) uniquely enriched in one of the two co-regulated embryo abundance clusters. TFs are listed in order of significance, which required an adjusted p-value less than 0.05. Red indicates relevance to developmental processes and blue represents relevance to VPA's known mechanisms.

	Enriched Cluster-specific Transcription Factors
VYS Cluster 0	KAT2A, FOXM1, NELFE, NANOG, VDR, SOX2, TRIM28
VYS Cluster 1	ERG, IRF1, ZKSCAN1, NFIC, RFX5, HNF4A, GATA1, CEBPB

Table 4-9 VYS cluster unique transcription factor enrichment: Transcription factors (TFs) uniquely enriched in one of the two co-regulated visceral yolk sac abundance clusters. TFs are listed in order of significance, which required an adjusted p-value less than 0.05. Red indicates relevance to developmental processes and blue represents relevance to VPA's known mechanisms.

Timepoint	Embryo GSEA Developmental Pathway Enrichment					
	Increased			Decreased		
	Pathway	NES	FDR	Pathway	NES	FDR
2hr	Body Morphogenesis	1.788	0.249	Keratinocyte Differentiation	-2.698	0
				Epidermal Cell Differentiation	-2.581	0
				Skin Development	-2.562	0
				Epidermis Development	-2.505	0
				Epithelial Cell Differentiation	-2.178	0.008
4hr	No Enrichment			Negative Regulation of Muscle Tissue Development	-1.897	0.125
				Negative Regulation of Developmental Growth	-1.776	0.215
6hr	Establishment of Tissue Polarity	2.4613	0.000	No Enrichment		
	Regulation of Animal Organ Morphogenesis	2.3354	0.000			
	Morphogenesis of a Polarized Epithelium	2.3247	0.000			
	Non-canonical Wnt Signaling Pathway	2.2792	0.000			
	Regulation of Stem Cell Differentiation	2.2688	0.000			
	Positive Regulation of Canonical Wnt Signaling	2.2645	0.000			
	Regulation of Morphogenesis of an Epithelium	2.2528	0.000			
	Hematopoietic Stem Cell Differentiation	2.2342	0.000			
	Negative Regulation of Canonical Wnt Signaling	2.1445	0.001			
	Positive Regulation of Wnt Signaling	2.0896	0.002			
	Negative Regulation of Growth	1.9977	0.006			
	Negative Regulation of Wnt Signaling	1.9006	0.016			
	Canonical Wnt Signaling Pathway	1.8836	0.017			
	Stem Cell Differentiation	1.8139	0.033			
	Osteoclast Differentiation	1.7343	0.059			
	Negative Regulation of Myeloid Cell Differentiation	1.7159	0.068			
	Endothelial Cell Development	1.6637	0.099			
	Negative Regulation of Cell Growth	1.6517	0.107			
	Regulation of Wnt Signaling Pathway	1.6342	0.111			
	Substantia Nigra Development	1.6037	0.133			
	Morphogenesis of an Epithelium	1.5843	0.148			
	Regulation of Embryonic Development	1.5362	0.181			
	Endothelium Development	1.5316	0.182			
	Tissue Morphogenesis	1.5164	0.188			
	Heart Process	1.4818	0.211			
	Neural Nucleus Development	1.4487	0.242			
8hr	Regulation of Body Fluid Levels	1.744	0.111	No Enrichment		
	Stem Cell Differentiation	1.626	0.229			
10hr	Establishment of Tissue Polarity	2.398	0.000	No Enrichment		
	Regulation of Animal Organ Morphogenesis	2.310	0.000			
	Regulation of Hematopoietic Stem Cell Differentiation	2.285	0.000			
	Regulation of Morphogenesis of an Epithelium	2.237	0.000			
	Non-canonical Wnt Signaling Pathway	2.218	0.000			
	Morphogenesis of a Polarized Epithelium	2.180	0.000			
	Positive Regulation of Canonical Wnt Signaling	2.100	0.001			
	Negative Regulation of Canonical Wnt Signaling	2.073	0.002			
	Positive Regulation of Wnt Signaling	2.019	0.005			
	Negative Regulation of Wnt Signaling	1.899	0.021			
	Cell-Cell Signaling by Wnt	1.836	0.036			
	Hematopoietic Progenitor Cell Differentiation	1.818	0.039			
	Regulation of Wnt Signaling Pathway	1.685	0.096			
	Stem Cell Differentiation	1.649	0.116			
	Canonical Wnt Signaling Pathway	1.834	0.035			
	Negative Regulation of Growth	1.784	0.051			
	Osteoclast Differentiation	1.951	0.012			

Table 4-10 EMB GSEA developmental pathway GO-term enrichment: Developmentally relevant enriched Biological Process GO-terms with an FDR <0.25 in a pre-ranked GSEA of VPA/Ctl abundance ratios in the EMB. “No enrichment” is specific to developmental pathways only.

Timepoint	Visceral Yolk Sac GSEA Developmental Pathway Enrichment					
	Increased			Decreased		
	Pathway	NES	FDR	Pathway	NES	FDR
2hr	No Enrichment			No Enrichment		
4hr	Regulation of Hematopoietic Progenitor Cell Differentiation	1.978	0.008	No Enrichment		
	Hematopoietic Stem Cell Differentiation	1.942	0.011			
	Regulation of Hematopoietic Cell Differentiation	1.947	0.011			
	Positive Regulation of Wnt Signaling	1.892	0.017			
	Establishment of Tissue Polarity	1.871	0.022			
	Keratinocyte Differentiation	1.854	0.024			
	Regulation of Animal Organ Morphogenesis	1.856	0.024			
	Positive Regulation of Canonical Wnt Signaling	1.841	0.027			
	Regulation of Morphogenesis of an Epithelium	1.814	0.036			
	Morphogenesis of a Polarized Epithelium	1.780	0.047			
	Rhythmic Process	1.774	0.049			
	Circadian Rhythm	1.757	0.057			
	Non-Canonical Wnt Signaling Pathway	1.739	0.063			
	Regulation of Stem Cell Differentiation	1.721	0.073			
	Hematopoietic Progenitor Cell Differentiation	1.705	0.085			
	Regulation of TOR Signaling	1.642	0.145			
	Epithelium Development	1.602	0.180			
	Regulation of Circadian Rhythm	1.590	0.190			
	Stem Cell Differentiation	1.562	0.208			
	Negative Regulation of Canonical Wnt Signaling	1.564	0.209			
	Epidermal Cell Differentiation	1.550	0.219			
	Epithelial Cell Differentiation	1.539	0.234			
	Nephron Development	1.537	0.234			
	Positive Regulation of TOR Signaling	1.536	0.235			
	Smooth Muscle Cell Proliferation	1.534	0.236			
6hr	No Enrichment			Keratinocyte Differentiation	-2.053	0.096
8hr	No Enrichment			Keratinocyte Differentiation	-2.217	0.002
				Epidermal Cell Differentiation	-2.146	0.005
				Skin Development	-2.112	0.006
				Epidermis Development	-1.974	0.022
				Regulation of TOR Signaling	-1.732	0.196
10hr	Regulation of MegaKaryocyte Differentiation	1.759	0.1849	Keratinocyte Differentiation	-2.276	0.000
	Lymphocyte Differentiation	1.679	0.2066	Skin Development	-2.219	0.001
	T Cell Differentiation	1.697	0.2217	Epidermal Cell Differentiation	-2.116	0.005
				Positive Regulation of TOR Signaling	-2.075	0.008
				Regulation of TOR Signaling	-2.012	0.015
				Epidermis Development	-1.938	0.029

Table 4-11 VYS GSEA developmental pathway GO-term enrichment: Developmentally relevant enriched Biological Process GO-terms with an FDR <0.25 in a pre-ranked GSEA of VPA/Ctl abundance ratios in the VYS. “No enrichment” is specific to developmental pathways only.

	Visceral Yolk Sac					Embryo				
	2hr	4hr	6hr	8hr	10hr	2hr	4hr	6hr	8hr	10hr
Alpha-globin	-0.18	-0.2	0.1	0.1	0.33	0.32	-0.25	0.38	-0.71	0.75
Beta-globin	-0.4	-1.02	-0.8	-0.37	0.45	-0.52	0.4	-0.11	-0.35	-0.18
Catalase	-0.2	0.33	-0.07	-0.05	-0.05	-0.08	0.02	0.1	-0.02	0.13
Copper chaperone for superoxide dismutase	0.11	0.36	0.06	0.2	-0.09	-0.19	-0.05	0.77	-0.24	0.96
Fatty acid-binding protein, liver	-0.18	0.73	0.16	0.08	-0.23					
Glutathione peroxidase						0.43	-0.17	0.8	-0.11	0.64
Glutathione peroxidase 1	0.08	0.78	0.03	0.07	-0.04					
Glutathione peroxidase 3	-0.48	0.03	-0.07	-0.07	-0.31	-0.16	-0.1	0.29	0.42	0.3
Probable glutathione peroxidase 8	2.8	-3.5	-0.6	0.35	-0.68					
Haptoglobin	0.29	-0.27	0.54	-0.11	-0.37	-0.05	-0.46	0.05	0.91	-0.18
Microsomal glutathione S-transferase 3	0.56	0.97	0.16	-0.04	-0.36					
Peroxiredoxin-4	-0.13	0.85	-0.09	-0.05	0.08	-0.08	0	0.78	0.15	0.74
Peroxiredoxin-6	-0.5	0.37	0.03	0.05	0.15	-0.14	0.15	0.29	-0.01	0.41
Peroxiredoxin-like 2A	-0.77	0.89	-0.07	-0.08	0.00	-0.13	0.1	0.11	-0.01	0.37
Phospholipid hydroperoxide glutathione peroxidase	-0.27	0.75	-0.03	-0.09	-0.08	-0.07	0.16	0.25	-0.02	0.30
Prostamide/prostaglandin F synthase						0.08	-0.05	0.07	-0.06	0.46
Protein SCO1 homolog, mitochondrial	-0.05	-0.78	-0.34	0.03	0.16	0.11	0.1	-0.47	0.04	-0.38
Protein SCO2 homolog, mitochondrial	0.45	-0.56	-0.07	-0.22	-0.02	0.48	-0.05	-0.72	-0.06	-1.01
Selenoprotein F	0.04	0.59	0.13	0.09	0.33	0.09	0.2	0.36	-0.06	0.39
Sestrin-2						0.47	-0.37	-0.46	-0.01	-1.54
Superoxide dismutase [Cu-Zn]	0.76	-1.37	-0.37	-0.4	0.02					
Superoxide dismutase [Mn], mitochondrial	-0.18	0.51	0.18	-0.03	-0.05	-0.05	0.01	0.21	-0.17	0.18
Thioredoxin	0.03	0.16	-0.12	-0.04	0.17	-0.09	0.1	0.2	0.04	0.35
Thioredoxin domain-containing protein 17	0.45	-0.71	-0.02	-0.02	0.04	0.07	-0.16	-0.18	0.12	-0.36
Thioredoxin reductase 2, mitochondrial	-0.09	0.52	-0.14	0.08	-0.06	0.1	0.02	-0.25	0.09	0.29
Thioredoxin reductase-like selenoprotein T	-0.27	0.59	0.06	-0.08	0.02	0.02	0.27	0.47	-0.16	0.09

Log 2 Ratios >0.33 <-0.33

Table 4-12 Antioxidant protein abundance in VYS and EMB: Antioxidant proteins that showed a significant increase or decrease in protein abundance following VPA exposure in at least one tissue and time point. Cells highlighted red were decreased in abundance and cells highlighted in green were increased in abundance.

	Visceral Yolk Sac					Embryo				
	2hr	4hr	6hr	8hr	10hr	2hr	4hr	6hr	8hr	10hr
Disturbance of Cytoskeleton										
Cofilin-2	-0.43	0.65	-0.16	-0.02	-0.05	-0.06	0.17	0.03	-0.06	0.25
Mitogen-activated protein kinase	-0.17	0.55	-0.02	0.17	-0.11	-0.15	0.07	0.13	0.00	0.16
Mitogen-activated protein kinase	0.25	0.43	-0.54	0.14	-0.15					
Profilin	-0.54	0.57	-0.10	-0.01	0.05	-0.21	0.11	0.44	0.00	0.40
Vasodilator-stimulated phosphoprotein	0.21	-0.40	-0.11	0.06	0.05	0.10	-0.11	-0.60	-0.06	-0.62
Vinculin	0.00	0.56	0.05	0.00	-0.04	-0.06	0.04	0.60	0.09	0.72
Disturbance of Cell Proliferation or Neuronal Differentiation										
Numb-like protein	-0.66	1.27	0.22	-0.05	-0.21	0.08	-0.06	-0.34	0.16	-0.20
Alterations in Neuroepithelial Cell Death										
AP-2 complex subunit alpha	-0.14	0.39	-0.01	0.00	-0.07	-0.10	0.13	0.29	0.03	0.46
Apoptotic protease-activating factor 1	0.10	0.53	0.26	0.42	-0.34	0.08	0.19	0.06	0.34	0.30
B-cell leukemia/lymphoma 10	0.16	0.10	0.01	-0.19	0.05	0.20	-0.12	-0.88	-0.35	-1.03
Growth arrest and DNA damage-inducible proteins-interacting protein 1	0.31	-0.21	0.24	0.09	-0.12	-0.06	0.28	-0.64	-0.10	-0.18
Uncharacterized protein (Fragment)						-0.03	-0.31	-0.32	0.13	-0.38
Transcriptional Regulation and Chromatin Dynamics										
Activity-dependent neuroprotector homeobox protein	0.10	0.33	0.20	0.05	0.05	0.00	-0.04	0.19	-0.13	0.12
Cat eye syndrome critical region protein 2 homolog						0.18	-0.15	-0.34	0.02	-0.49
Histone acetyltransferase p300	-0.12	0.45	0.11	0.01	-0.04	0.15	0.04	-0.23	-0.03	-0.16
RING1 and YY1-binding protein	0.32	0.38	0.06	0.03	0.00	-0.10	-0.01	0.07	0.13	0.20
Dysregulation of Sonic Hedgehog Signaling										
cAMP-dependent protein kinase catalytic subunit alpha	-0.40	0.52	-0.02	-0.04	0.00	-0.17	0.05	0.75	-0.03	0.90
cAMP-dependent protein kinase catalytic subunit beta	0.14	0.18	0.40	0.07	0.29	0.13	0.05	0.05	0.05	0.01

Log 2 Ratios >0.33 <-0.33

Table 4-13 Neural tube defect associated protein abundance in VYS and EMB: Neural Tube Defect (NTD) associated proteins identified by Copp et al. (2010) that showed a significant increase or decrease in protein abundance following VPA exposure in at least one tissue and time point. Cells highlighted red were decreased in abundance and cells highlighted in green were increased in abundance.

Figures

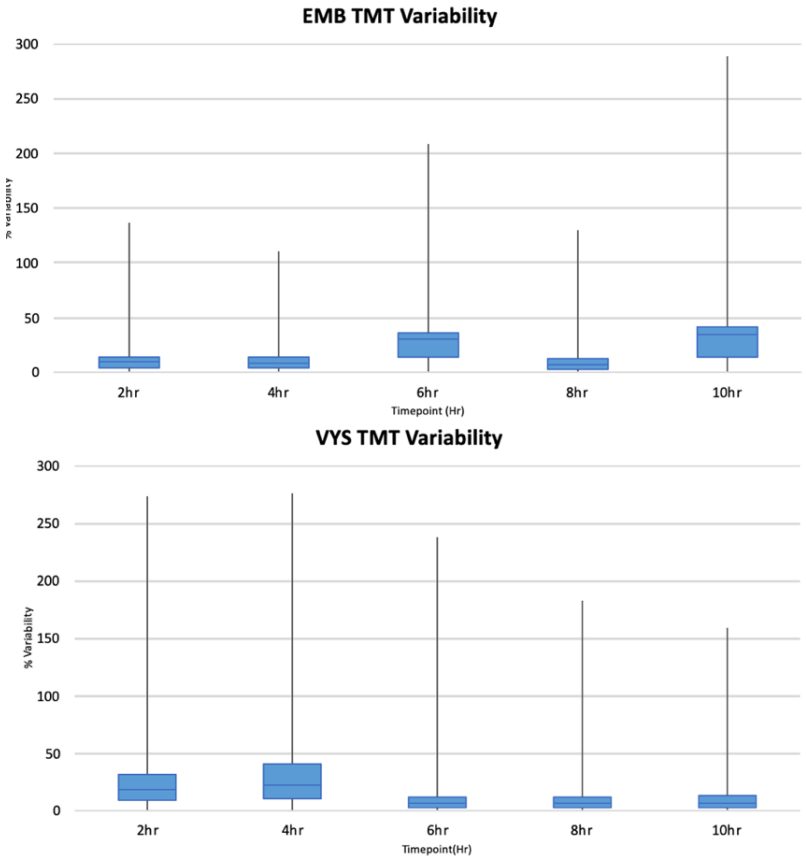

Figure 4-1 Variability of VPA/Ctl protein abundance ratios in EMB and VYS: Variability range of the VPA/Ctl abundance ratios identified between the 1st and 2nd biological replicates for VYS and EMB. Whiskers represent maximum and minimum variability measurement, while the upper and lower limits of the box represent the 25th and 75th percentile with the separating line indicating the median variability.

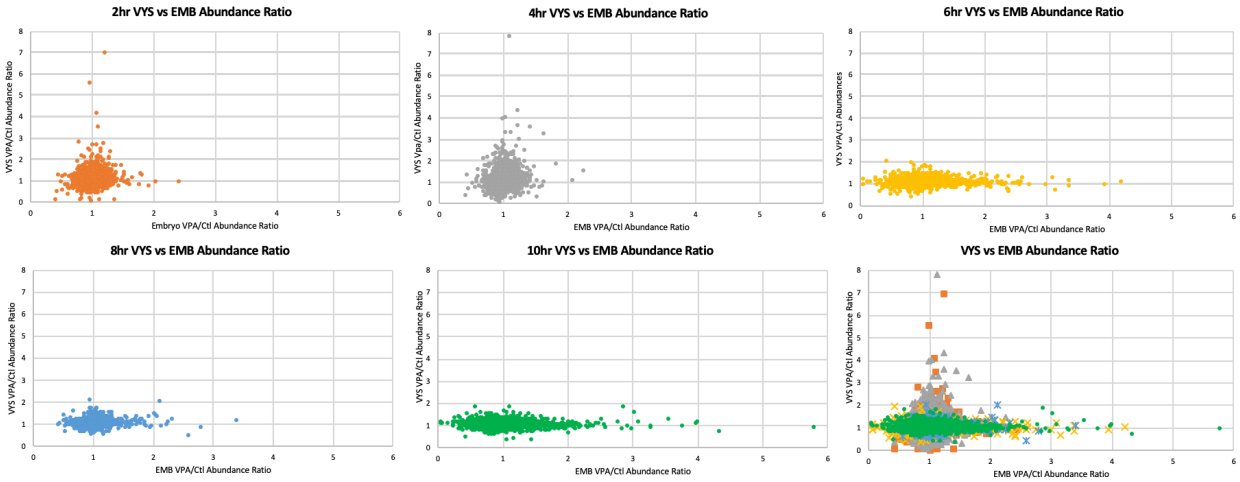

Figure 4-2 VYS vs. EMB VPA/Ctl protein abundance ratios: VYS vs EMB VPA/Ctl abundance ratios of the 4,238 proteins that were identified across both tissue-specific datasets. Proteins with an abundance ratio >8 were removed as outliers for this figure.

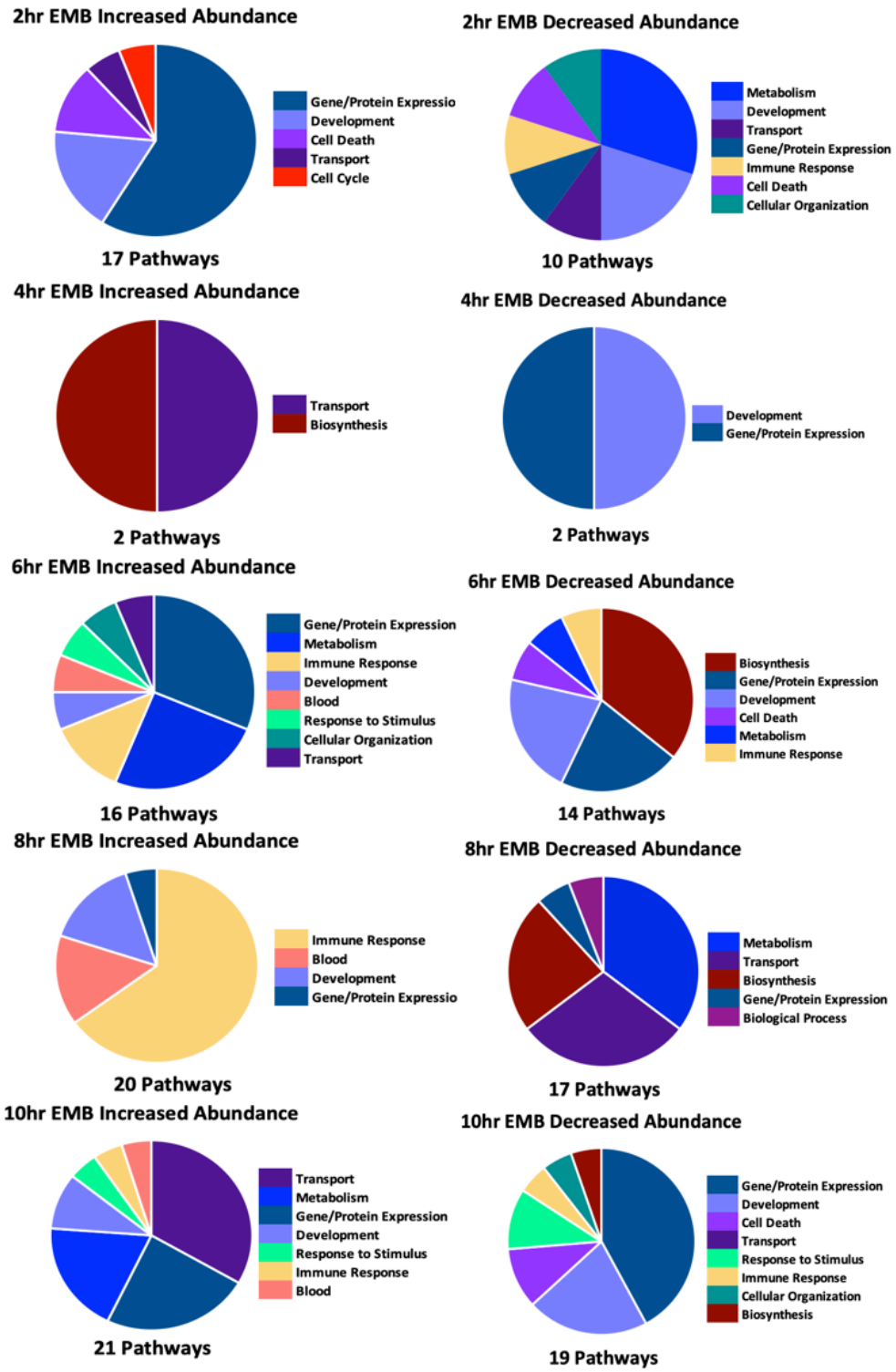

Figure 4-3 EMB biological process GO-term enrichment: Biological process GO-term enrichment in the EMB using the DAVID database with the total list of identified EMB proteins as background. The number of proteins in each category is listed in Table 3. Size of pie-chart division corresponds to the number of significant GO terms within each category.

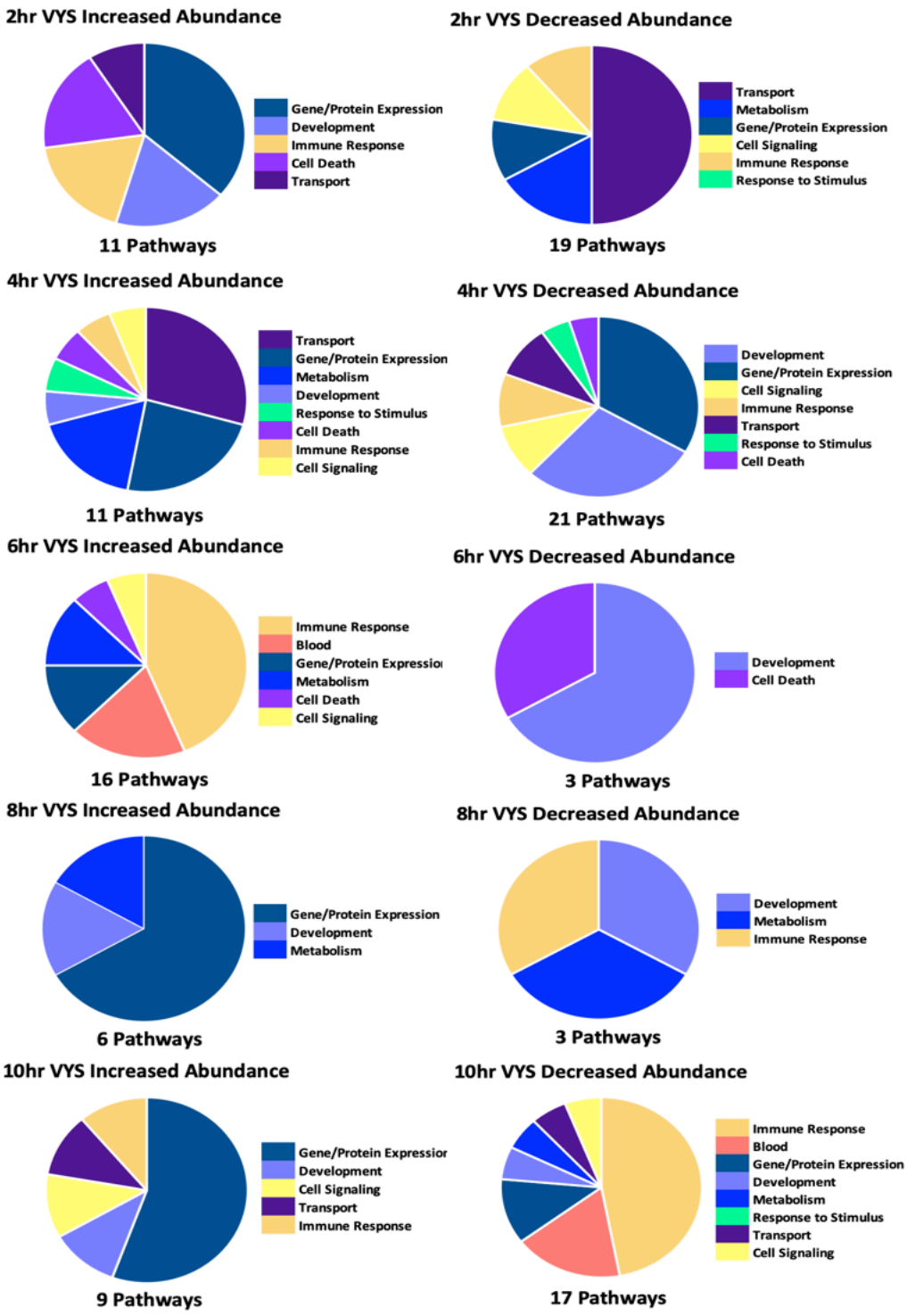

Figure 4-4 VYS biological process GO-term enrichment: Biological process GO-term enrichment in the VYS using the DAVID database with the total list of identified VYS proteins as background. Included pathways had a p-value <0.05. The number of proteins in each category is listed in Table 3. Size of pie-chart division corresponds to the number of significant GO-terms within each category.

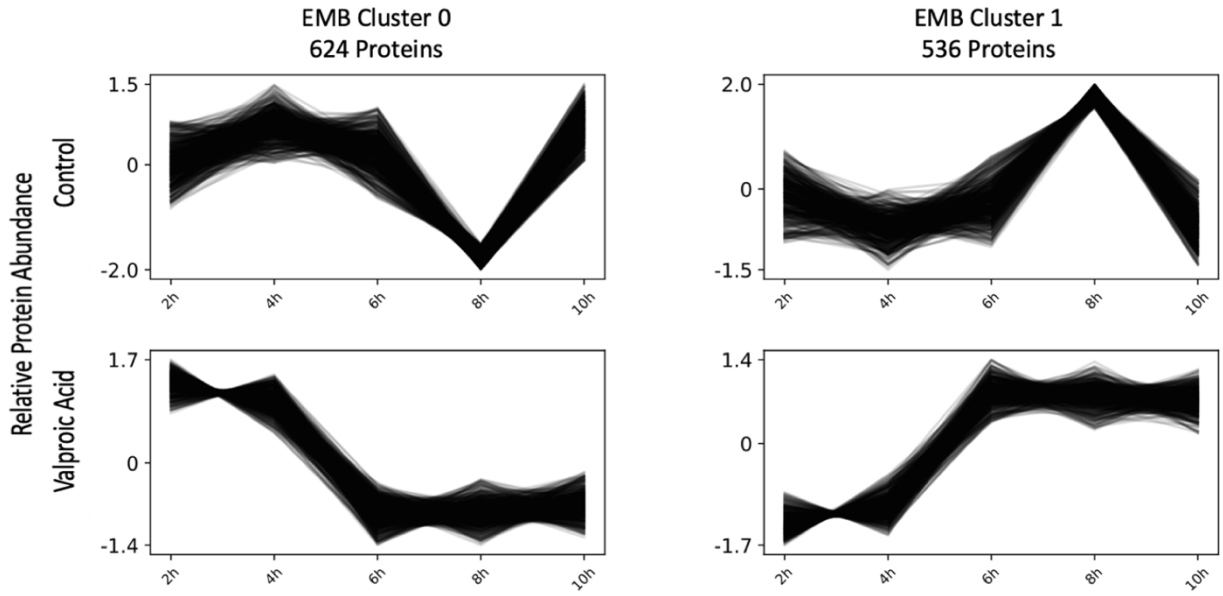

Figure 4-5 EMB co-regulated protein clusters: Co-regulated protein clustering of EMB protein abundance values in *Clust* identified two unique clusters of proteins that showed similar expression patterns within a given treatment group.

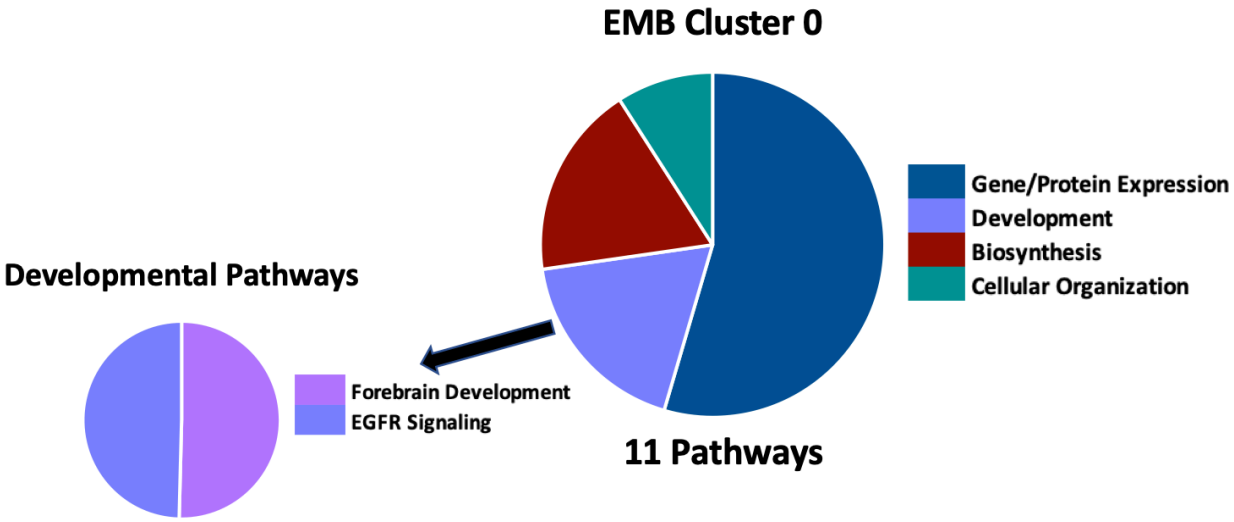

Figure 4-6 EMB cluster 0 biological process GO-term enrichment: EMB abundance cluster 0 biological process GO-term pathway enrichment in DAVID identified 11 enriched pathways with a p-value < 0.05 using the full EMB protein list as background. Pie chart division is based on the total number of pathways in each category in the main figure with division based on the pathway's -log10 p-value in the highlighted developmental pathways.

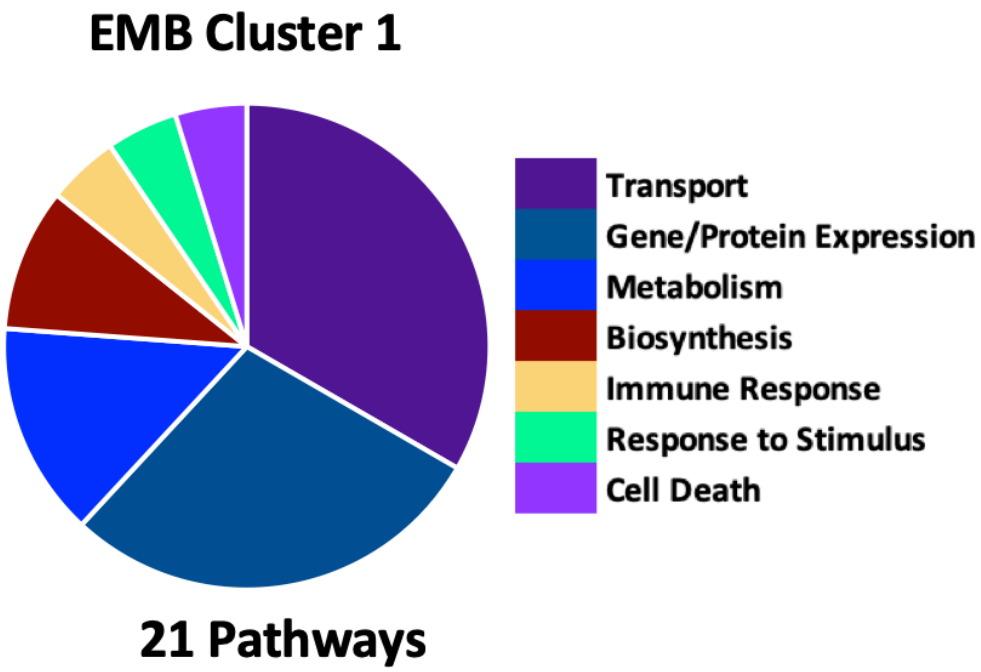

Figure 4-7 EMB cluster 1 biological process GO-term enrichment: EMB Abundance Cluster 1 biological process GO-term pathway enrichment in DAVID identified 31 enriched pathways with a p-value < 0.05 using the full EMB protein list as background. Pie chart division is based on the total number of pathways in each category.

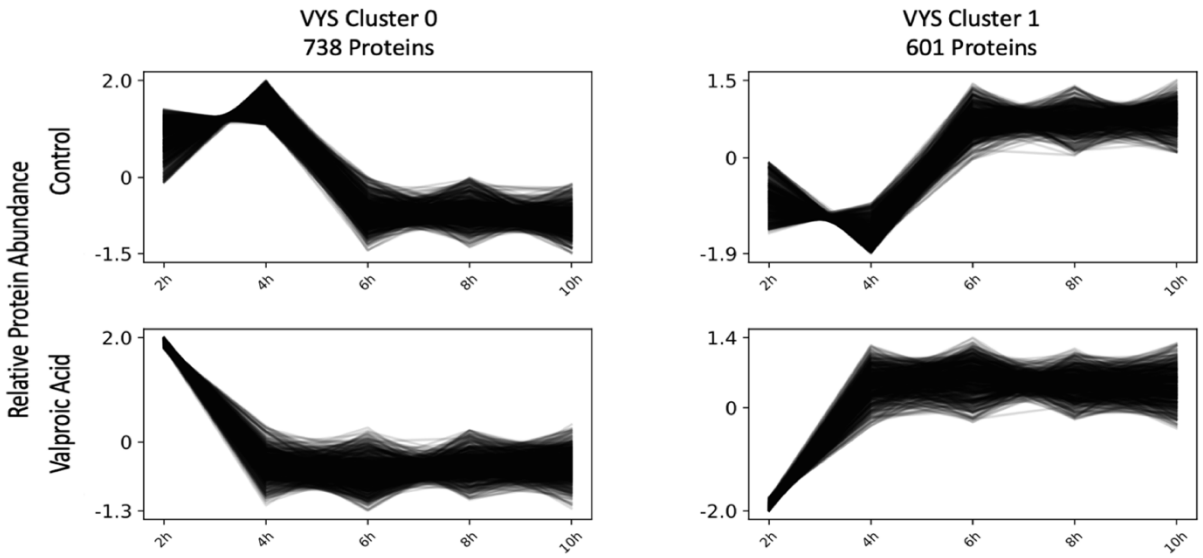

Figure 4-8 VYS co-regulated protein clusters: Co-regulated protein clustering of VYS protein abundance values in *Clust* identified two unique clusters of proteins that showed similar expression patterns within a given treatment group.

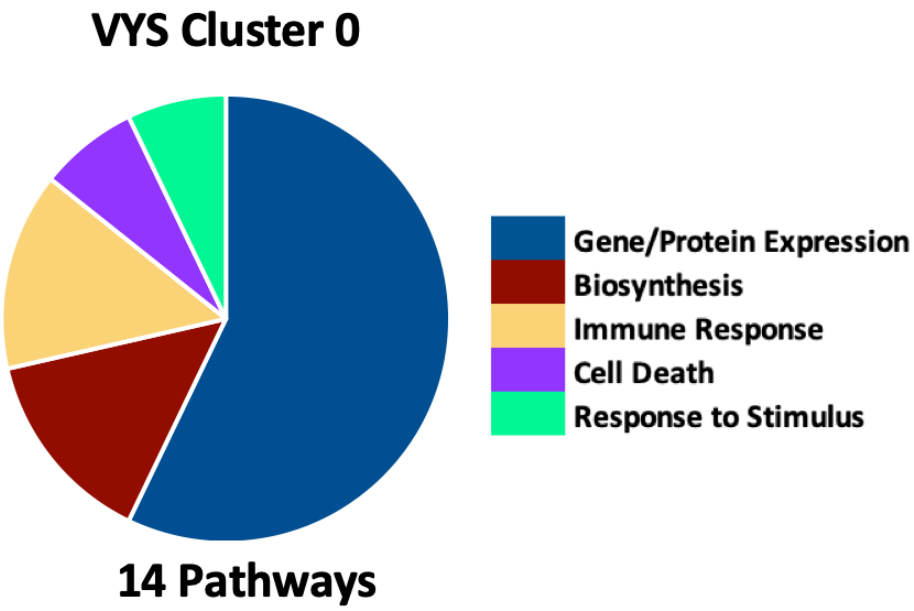

Figure 4-9 VYS cluster 0 biological process GO-term enrichment: VYS Abundance Cluster 0 biological process GO-term pathway enrichment in DAVID identified 14 enriched pathways with a p-value < 0.05 using the full VYS protein list as background. Pie chart division is based on the total number of pathways in each category.

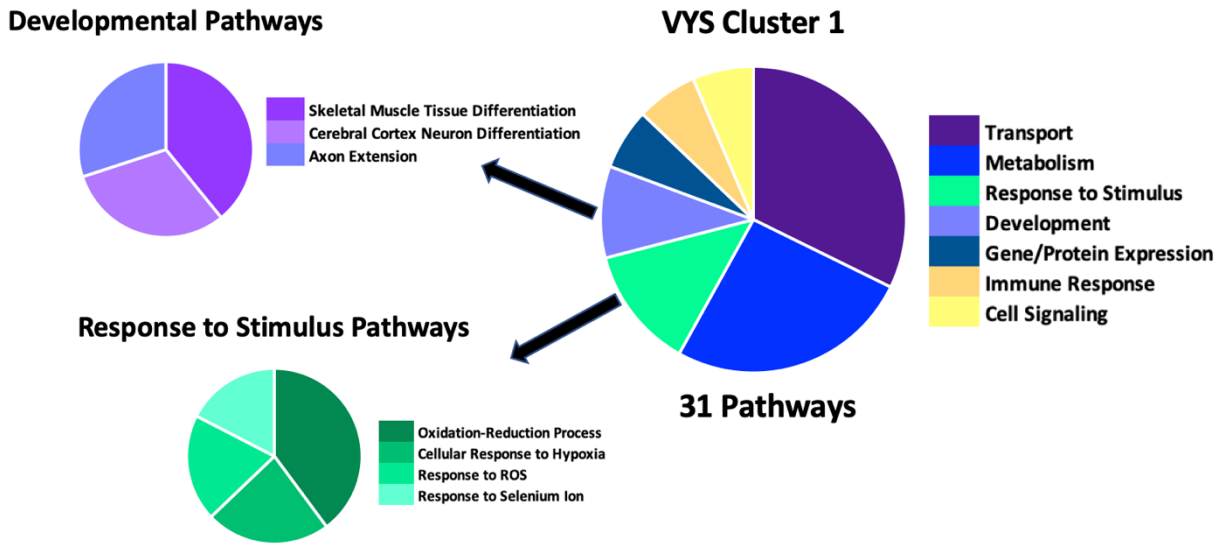

Figure 4-10 VYS cluster 1 biological process GO-term enrichment: VYS Abundance Cluster 1 biological process GO-term pathway enrichment in DAVID identified 31 enriched pathways with a p-value < 0.05 using the full VYS protein list as background. Pie chart division is based on the total number of pathways in each category in the main figure with division based on the pathway's -log10 p-value in the highlighted developmental and response to stimulus pathways.

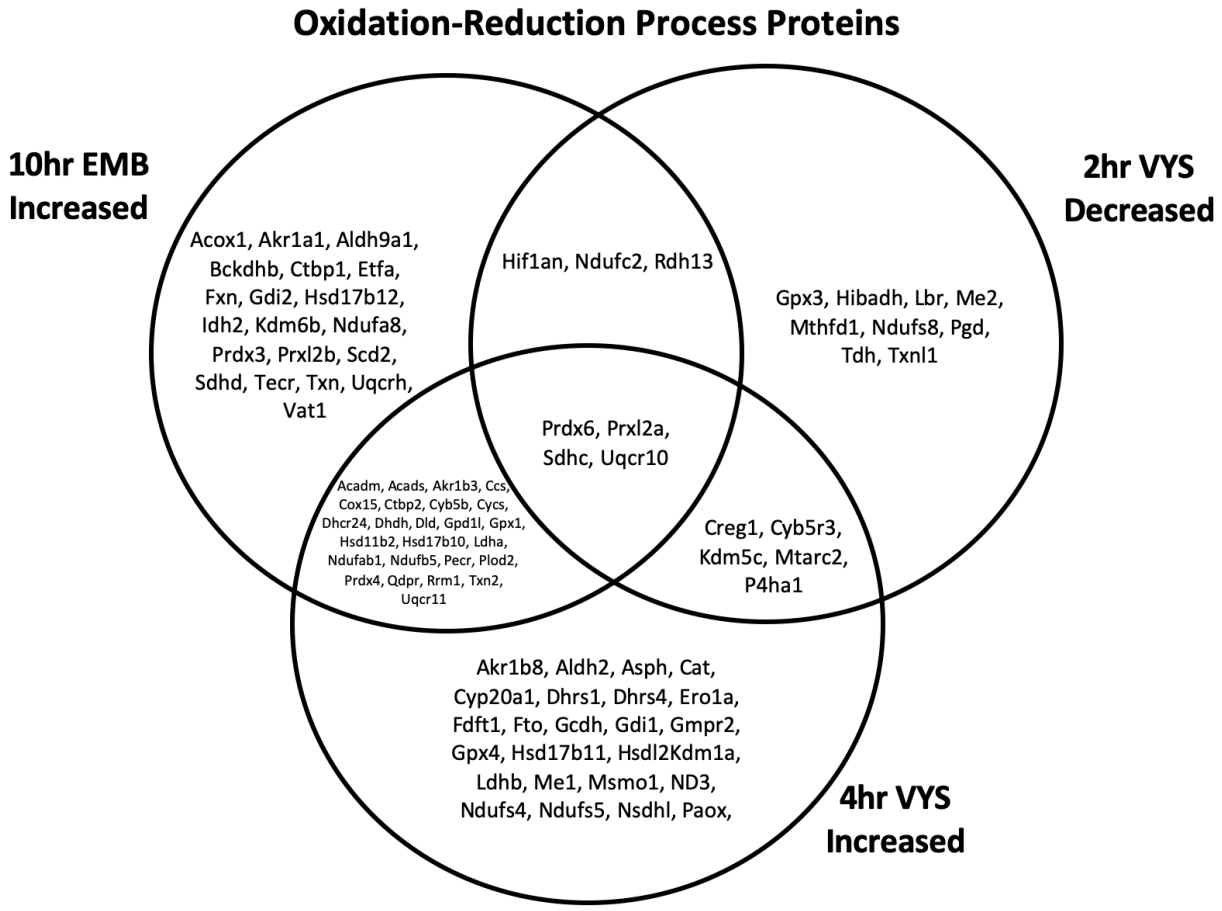

Figure 4-11 Oxidation-reduction process pathway proteins: Oxidation-Reduction Process was enriched at 2 and 4 hrs in the VYS and 10 hrs in the EMB. Proteins identities and overlaps of each of these tissue and time points are displayed.

References

Abu-Jamous, B., & Kelly, S. (2018). Clust: Automatic extraction of optimal co-expressed gene clusters from gene expression data. *Genome Biology*, *19*(1), 172. https://doi.org/10.1186/s13059-018-1536-8

Aires, M. B., Santos, J. R. A., Souza, K. S., Farias, P. S., Santos, A. C. V., Fioretto, E. T., & Maria, D. A. (2015). Rat visceral yolk sac cells: Viability and expression of cell markers during maternal diabetes. *Brazilian Journal of Medical and Biological Research*, *48*(8), 676–682. https://doi.org/10.1590/1414-431x20154739

Bennett, G. D., Wlodarczyk, B., Calvin, J. A., Craig, J. C., & Finnell, R. H. (2000). Valproic acid-induced alterations in growth and neurotrophic factor. *Reproductive Toxicology*, *14*(1), 1–11. https://doi.org/10.1016/S0890-6238(99)00064-7

Burggren, W. W., & Mueller, C. A. (2015). Developmental Critical Windows and Sensitive Periods as Three-Dimensional Constructs in Time and Space. *Physiological and Biochemical Zoology*, *88*(2), 91–102. https://doi.org/10.1086/679906

Butler, M. T., & Wallingford, J. B. (2017). Planar cell polarity in development and disease. *Nature Reviews Molecular Cell Biology*, *18*(6), 375–388. https://doi.org/10.1038/nrm.2017.11

Chen, E. Y., Tan, C. M., Kou, Y., Duan, Q., Wang, Z., Meirelles, G., Clark, N. R., & Ma'ayan, A. (2013). Enrichr: Interactive and collaborative HTML5 gene list enrichment analysis tool. *BMC Bioinformatics*, *14*(1), 128. https://doi.org/10.1186/1471-2105-14-128

Choi, H., Wang, L., Lin, X., Spengler, J. D., & Perera, F. P. (2012). Fetal Window of Vulnerability to Airborne Polycyclic Aromatic Hydrocarbons on Proportional Intrauterine Growth Restriction. *PLoS ONE*, *7*(4), e35464. https://doi.org/10.1371/journal.pone.0035464

Copp, A. J., & Greene, N. D. (2010). Genetics and development of neural tube defects: Genetics and development of neural tube defects. *The Journal of Pathology*, *220*(2), 217–230. https://doi.org/10.1002/path.2643

Copp, A. J., Stanier, P., & Greene, N. D. E. (2013). Neural tube defects: Recent advances, unsolved questions, and controversies. *The Lancet. Neurology*, *12*(8), 799–810. https://doi.org/10.1016/S1474-4422(13)70110-8

Davis, C. A., Hitz, B. C., Sloan, C. A., Chan, E. T., Davidson, J. M., Gabdank, I., Hilton, J. A., Jain, K., Baymuradov, U. K., Narayanan, A. K., Onate, K. C., Graham, K., Miyasato, S. R., Dreszer, T. R., Strattan, J. S., Jolanki, O., Tanaka, F. Y., & Cherry, J. M. (2018). The Encyclopedia of DNA elements (ENCODE): Data portal update. *Nucleic Acids Research*, *46*(D1), D794–D801. https://doi.org/10.1093/nar/gkx1081

Donovan, M. F., & Bordoni, B. (2020). Embryology, Yolk Sac. In *StatPearls*. StatPearls Publishing. http://www.ncbi.nlm.nih.gov/books/NBK555965/

ENCODE Project Consortium. (2012). An integrated encyclopedia of DNA elements in the human genome. *Nature*, *489*(7414), 57–74. https://doi.org/10.1038/nature11247

Gangloff, Y.-G., Mueller, M., Dann, S. G., Svoboda, P., Sticker, M., Spetz, J.-F., Um, S. H., Brown, E. J., Cereghini, S., Thomas, G., & Kozma, S. C. (2004). Disruption of the mouse mTOR gene leads to early postimplantation lethality and prohibits embryonic stem cell development. *Molecular and Cellular Biology*, *24*(21), 9508–9516. https://doi.org/10.1128/MCB.24.21.9508-9516.2004

Gao, Y., Liu, X., Tang, B., Li, C., Kou, Z., Li, L., Liu, W., Wu, Y., Kou, X., Li, J., Zhao, Y., Yin, J., Wang, H., Chen, S., Liao, L., & Gao, S. (2017). Protein Expression Landscape of Mouse Embryos during Pre-implantation Development. *Cell Reports*, *21*(13), 3957–3969. https://doi.org/10.1016/j.celrep.2017.11.111

Ghodke-Puranik, Y., Thorn, C. F., Lamba, J. K., Leeder, J. S., Song, W., Birnbaum, A. K., Altman, R. B., & Klein, T. E. (2013). Valproic acid pathway: Pharmacokinetics and pharmacodynamics. *Pharmacogenetics and Genomics*, *23*(4), 236–241. https://doi.org/10.1097/FPC.0b013e32835ea0b2

Ghosh, S., Janocha, A. J., Aronica, M. A., Swaidani, S., Comhair, S. A. A., Xu, W., Zheng, L., Kaveti, S., Kinter, M., Hazen, S. L., & Erzurum, S. C. (2006). Nitrotyrosine Proteome Survey in Asthma Identifies Oxidative Mechanism of Catalase Inactivation. *The Journal of Immunology*, *176*(9), 5587–5597. https://doi.org/10.4049/jimmunol.176.9.5587

Go, Y.-M., Chandler, J. D., & Jones, D. P. (2015). The cysteine proteome. *Free Radical Biology and Medicine*, *84*, 227–245. https://doi.org/10.1016/j.freeradbiomed.2015.03.022

Gygi, S. P., Rochon, Y., Franza, B. R., & Aebersold, R. (1999). Correlation between Protein and mRNA Abundance in Yeast. *Molecular and Cellular Biology*, *19*(3), 1720–1730. https://doi.org/10.1128/MCB.19.3.1720

Halbach, K., Ulrich, N., Goss, K.-U., Seiwert, B., Wagner, S., Scholz, S., Luckenbach, T., Bauer, C., Schweiger, N., & Reemtsma, T. (2020). Yolk Sac of Zebrafish Embryos as Backpack for Chemicals? *Environmental Science & Technology*, *54*(16), 10159–10169. https://doi.org/10.1021/acs.est.0c02068

Harris, C. (2012). Rodent Whole Embryo Culture. In C. Harris & J. M. Hansen (Eds.), *Developmental Toxicology* (Vol. 889, pp. 215–237). Humana Press. https://doi.org/10.1007/978-1-61779-867-2_13

Harris, M. J., & Juriloff, D. M. (2010). An update to the list of mouse mutants with neural tube closure defects and advances toward a complete genetic perspective of neural tube closure. *Birth Defects Research Part A: Clinical and Molecular Teratology*, *88*(8), 653–669. https://doi.org/10.1002/bdra.20676

Huang, D. W., Sherman, B. T., & Lempicki, R. A. (2009a). Bioinformatics enrichment tools: Paths toward the comprehensive functional analysis of large gene lists. *Nucleic Acids Research*, *37*(1), 1–13. https://doi.org/10.1093/nar/gkn923

Huang, D. W., Sherman, B. T., & Lempicki, R. A. (2009b). Systematic and integrative analysis of large gene lists using DAVID bioinformatics resources. *Nature Protocols*, *4*(1), 44–57. https://doi.org/10.1038/nprot.2008.211

Jentink, J., Loane, M. A., Dolk, H., Barisic, I., Garne, E., Morris, J. K., & de Jong-van den Berg, L. T. W. (2010). Valproic Acid Monotherapy in Pregnancy and Major Congenital Malformations. *New England Journal of Medicine*, *362*(23), 2185–2193. https://doi.org/10.1056/NEJMoa0907328

Karve, T. M., & Cheema, A. K. (2011). Small Changes Huge Impact: The Role of Protein Posttranslational Modifications in Cellular Homeostasis and Disease. *Journal of Amino Acids*, *2011*, 1–13. https://doi.org/10.4061/2011/207691

Kuleshov, M. V., Jones, M. R., Rouillard, A. D., Fernandez, N. F., Duan, Q., Wang, Z., Koplev, S., Jenkins, S. L., Jagodnik, K. M., Lachmann, A., McDermott, M. G., Monteiro, C. D., Gundersen, G. W., & Ma'ayan, A. (2016). Enrichr: A comprehensive gene set enrichment analysis web server 2016 update. *Nucleic Acids Research*, *44*(W1), W90–W97. https://doi.org/10.1093/nar/gkw377

López-Otín, C., & Overall, C. M. (2002). Protease degradomics: A new challenge for proteomics. *Nature Reviews Molecular Cell Biology*, *3*(7), 509–519. https://doi.org/10.1038/nrm858

Martin, P. M., & Sutherland, A. E. (2001). Exogenous Amino Acids Regulate Trophectoderm Differentiation in the Mouse Blastocyst through an mTOR-Dependent Pathway. *Developmental Biology*, *240*(1), 182–193. https://doi.org/10.1006/dbio.2001.0461

McAlister, G. C., Huttlin, E. L., Haas, W., Ting, L., Jedrychowski, M. P., Rogers, J. C., Kuhn, K., Pike, I., Grothe, R. A., Blethrow, J. D., & Gygi, S. P. (2012). Increasing the Multiplexing Capacity of TMTs Using Reporter Ion Isotopologues with Isobaric Masses. *Analytical Chemistry*, *84*(17), 7469–7478. https://doi.org/10.1021/ac301572t

McAlister, G. C., Nusinow, D. P., Jedrychowski, M. P., Wühr, M., Huttlin, E. L., Erickson, B. K., Rad, R., Haas, W., & Gygi, S. P. (2014). MultiNotch MS3 Enables Accurate, Sensitive, and Multiplexed Detection of Differential Expression across Cancer Cell Line Proteomes. *Analytical Chemistry*, *86*(14), 7150–7158. https://doi.org/10.1021/ac502040v

Mootha, V. K., Lindgren, C. M., Eriksson, K.-F., Subramanian, A., Sihag, S., Lehar, J., Puigserver, P., Carlsson, E., Ridderstråle, M., Laurila, E., Houstis, N., Daly, M. J., Patterson, N., Mesirov, J. P., Golub, T. R., Tamayo, P., Spiegelman, B., Lander, E. S., Hirschhorn, J. N., … Groop, L. C. (2003). PGC-1α-responsive genes involved in oxidative phosphorylation are coordinately downregulated in human diabetes. *Nature Genetics*, *34*(3), 267–273. https://doi.org/10.1038/ng1180

Murakami, M., Ichisaka, T., Maeda, M., Oshiro, N., Hara, K., Edenhofer, F., Kiyama, H., Yonezawa, K., & Yamanaka, S. (2004). MTOR is essential for growth and proliferation in early mouse embryos and embryonic stem cells. *Molecular and Cellular Biology*, *24*(15), 6710–6718. https://doi.org/10.1128/MCB.24.15.6710-6718.2004

Nishii, K., & Shibata, Y. (2006). Mode and determination of the initial contraction stage in the mouse embryo heart. *Anatomy and Embryology*, *211*(2), 95–100. https://doi.org/10.1007/s00429-005-0065-x

Ornoy, A. (2009). Valproic acid in pregnancy: How much are we endangering the embryo and fetus? *Reproductive Toxicology*, *28*(1), 1–10. https://doi.org/10.1016/j.reprotox.2009.02.014

Phiel, C. J., Zhang, F., Huang, E. Y., Guenther, M. G., Lazar, M. A., & Klein, P. S. (2001). Histone Deacetylase Is a Direct Target of Valproic Acid, a Potent Anticonvulsant, Mood Stabilizer, and Teratogen. *Journal of Biological Chemistry*, *276*(39), 36734–36741. https://doi.org/10.1074/jbc.M101287200

Philbrook, N. A., Nikolovska, A., Maciver, R. D., Belanger, C. L., & Winn, L. M. (2019). Characterizing the effects of in utero exposure to valproic acid on murine fetal heart development. *Birth Defects Research*, *111*(19), 1551–1560. https://doi.org/10.1002/bdr2.1610

Qin, L., Dai, X., & Yin, Y. (2016). Valproic acid exposure sequentially activates Wnt and mTOR pathways in rats. *Molecular and Cellular Neuroscience*, *75*, 27–35. https://doi.org/10.1016/j.mcn.2016.06.004

Rodnina, M. V. (2016). The ribosome in action: Tuning of translational efficiency and protein folding: The Ribosome in Action. *Protein Science*, *25*(8), 1390–1406. https://doi.org/10.1002/pro.2950

Ross, C., & Boroviak, T. E. (2020). Origin and function of the yolk sac in primate embryogenesis. *Nature Communications*, *11*(1), 3760. https://doi.org/10.1038/s41467-020-17575-w

Sakai, Y. (1989). Neurulation in the mouse: Manner and timing of neural tube closure. *The Anatomical Record*, *223*(2), 194–203. https://doi.org/10.1002/ar.1092230212

Sidoli, S., Kulej, K., & Garcia, B. A. (2017). Why proteomics is not the new genomics and the future of mass spectrometry in cell biology. *Journal of Cell Biology*, *216*(1), 21–24. https://doi.org/10.1083/jcb.201612010

Subramanian, A., Tamayo, P., Mootha, V. K., Mukherjee, S., Ebert, B. L., Gillette, M. A., Paulovich, A., Pomeroy, S. L., Golub, T. R., Lander, E. S., & Mesirov, J. P. (2005). Gene set enrichment analysis: A knowledge-based approach for interpreting genome-wide expression profiles. *Proceedings of the National Academy of Sciences*, *102*(43), 15545–15550. https://doi.org/10.1073/pnas.0506580102

Thompson, A., Schäfer, J., Kuhn, K., Kienle, S., Schwarz, J., Schmidt, G., Neumann, T., & Hamon, C. (2003). Tandem Mass Tags: A Novel Quantification Strategy for Comparative Analysis of Complex Protein Mixtures by MS/MS. *Analytical Chemistry*, *75*(8), 1895–1904. https://doi.org/10.1021/ac0262560

Tung, E. W. Y., & Winn, L. M. (2011). Valproic Acid Increases Formation of Reactive Oxygen Species and Induces Apoptosis in Postimplantation Embryos: A Role for Oxidative Stress in Valproic Acid-Induced Neural Tube Defects. *Molecular Pharmacology*, *80*(6), 979–987. https://doi.org/10.1124/mol.111.072314

Usami, M., Mitsunaga, K., & Nakazawa, K. (2007). Comparative proteome analysis of the embryo proper and yolk sac membrane of day 11.5 cultured rat embryos. *Birth Defects Research Part B: Developmental and Reproductive Toxicology*, *80*(5), 383–395. https://doi.org/10.1002/bdrb.20127

Vogel, C., & Marcotte, E. M. (2012). Insights into the regulation of protein abundance from proteomic and transcriptomic analyses. *Nature Reviews Genetics*, *13*(4), 227–232. https://doi.org/10.1038/nrg3185

Walsh, D. A., & Morris, V. B. (1989). Heat shock affects cell cycling in the neural plate of cultured rat embryos: A flow cytometric study. *Teratology*, *40*(6), 583–592. https://doi.org/10.1002/tera.1420400606

Wang, D. (2008). Discrepancy between mRNA and protein abundance: Insight from information retrieval process in computers. *Computational Biology and Chemistry*, *32*(6), 462–468. https://doi.org/10.1016/j.compbiolchem.2008.07.014

Wang, L., Liu, Y., Li, S., Long, Z.-Y., & Wu, Y.-M. (2015). Wnt signaling pathway participates in valproic acid-induced neuronal differentiation of neural stem cells. *International Journal of Clinical and Experimental Pathology*, *8*(1), 578–585.

Wang, M., Marco, P. de, Capra, V., & Kibar, Z. (2019). Update on the Role of the Non-Canonical Wnt/Planar Cell Polarity Pathway in Neural Tube Defects. *Cells*, *8*(10). https://doi.org/10.3390/cells8101198

Wullschleger, S., Loewith, R., & Hall, M. N. (2006). TOR Signaling in Growth and Metabolism. *Cell*, *124*(3), 471–484. https://doi.org/10.1016/j.cell.2006.01.016

Zhang, L., Li, D., Zhang, J., Yan, P., Liu, X., Wang, L., Khan, A., Liu, Z., Mu, J., Xu, J., Niu, B., & Xie, J. (2020). Excessive apoptosis and ROS induced by ethionine affect neural cell viability and differentiation. *Acta Biochimica et Biophysica Sinica*, *52*(10), 1156–1165. https://doi.org/10.1093/abbs/gmaa093

Zohn, I. E., & Sarkar, A. A. (2010). The visceral yolk sac endoderm provides for absorption of nutrients to the embryo during neurulation. *Birth Defects Research Part A: Clinical and Molecular Teratology*, *88*(8), 593–600. https://doi.org/10.1002/bdra.20705

Chapter 5

Construction of a Spatiotemporal Model of Valproic Acid Perturbed Developmental Pathways in the Early Organogenesis-Stage Mouse Conceptus

Abstract

Exposure to anti-epileptic medication valproic acid (VPA) has been associated with time and tissue specific changes to cellular redox, protein abundance, and protein oxidation state in the early organogenesis mouse conceptus. This integrative analysis evaluates the relationship between these metrics to develop a spatiotemporal timeline of perturbed pathways following VPA exposure during early mouse organogenesis that may explain its mechanism of failed neural tube closure (NTC). Spatiotemporal patterns of recurrent enrichment of developmental pathways were drawn from IodoTMT protein Cys oxidation and TMT protein abundance data at 2, 4, 6, 8, and 10 hrs following VPA exposure. The culminating timeline of VPA perturbation revealed an interconnected role of protein oxidation and abundance in cell polarity as well as tandem tissue specific pathway connections relevant to developmental growth. General and cell type specific differentiation also showed promise as a downstream target of VPA exposure. Cellular glutathione redox potential was associated with alterations to the oxidation-reduction process pathway. Future studies should build off this timeline of VPA perturbed developmental pathways to identify the specific proteins that are oxidatively modified at accessible Cys sites to define the complete and precise mechanisms of redox-mediated mechanisms of VPA developmental toxicity.

Introduction

Valproic acid (VPA) is an anti-epileptic medication that is associated with an increased risk of neural tube defects (NTDs) in infants exposed during pregnancy (Vajda et al., 2013). Substantial research efforts have gone into uncovering the mechanism of VPA-induced NTDs, but a definitive mechanism has not yet been resolved. While a defined mechanism is not yet available, there have been significant advances in understanding the physiological effects of VPA exposure. Previous research has demonstrated that VPA acts as a histone deacetylase (HDAC) inhibitor, blocker of sodium gated ion channels, regulator of GABA levels, and disruptor of reduction-oxidation (redox) balance (Ghodke-Puranik et al., 2013; Palsamy et al., 2014; Phiel et al., 2001). Embryonic development relies on a highly regulated redox environment with tightly controlled oxygen and antioxidant concentrations serving as developmental signals (Hansen et al., 2020; Schafer & Buettner, 2001). For this reason, VPA's perturbation of the redox environment is viewed as a likely contributor to the process of failed neural tube closure (NTC).

Several studies have been undertaken in the organogenesis-stage mouse conceptus to explore the potential link between VPA's actions as an oxidant and the downstream effects on redox balance, morphology, and alterations to developmental protein pathways (Chapters 2, 3, 4). Through this work, VPA has been shown to act in temporally and spatially specific manner with developmental timing and conceptal tissue playing a role in the response. An investigation into cellular redox status across 24 hours of mouse organogenesis in 4 distinct embryonic compartments revealed that VPA does not act as a consistent, global oxidant. Instead, VPA caused oxidation that was compartment and time specific with only a few instances of global conceptal oxidation (Chapter 2). Despite VPA's lower than anticipated cellular oxidation burden,

VPA caused time specific alterations to protein oxidation through the process of reversible oxidative post-translational modification (PTM) of cysteine (Cys) residues. Here it was revealed that VPA induced higher oxidation in only a fraction of the proteins showing differential oxidation patterns between the control and VPA at early timepoints prior to a shift in oxidative burden at 10 hrs to increase the proportion of differentially affected proteins with higher VPA oxidation. Proteins with differential oxidation status exhibited differences between control and VPA-treated samples with respect to pathways relevant to neural tube closure (NTC) such as nervous system development, cell polarity, and oxidation-reduction process (Chapter 3). One of VPA's known molecular functions is as an inhibitor of histone deacetylases (HDAC) which can change chromatin conformation to direct transcriptional availability. Due to this function, it was anticipated that VPA might cause changes to protein abundance in pathways associated with NTDs. Tandem mass tag (TMT) protein abundance data revealed that VPA caused time specific alterations in developmental pathways with distinct sensitivity times and affected pathways by tissue. Several developmental mechanisms were identified that were altered by VPA at two or more time points including Wnt signaling, growth and proliferation, and differentiation. VPA was also associated with spatiotemporal increases of the oxidation-reduction process pathway (Chapter 4).

Utilizing and integrating data from previous studies of VPA's redox impact on the organogenesis-stage mouse conceptus, this study will identify patterns in oxidation outcomes and pathway enrichment to construct of timeline of VPA's recurrent developmental perturbation events. Creating a timeline of developmental VPA perturbation events related to protein abundance and oxidation and linking them to cellular glutathione response will aid in understanding how the cellular redox environment is associated with altered downstream

pathways and proteins sensitive to VPA exposure. Patterns of pathway perturbation and enrichment may reveal mechanistic targets of VPA's actions relevant to failed neural tube closure.

Materials & Methods

Data Sources

The iodoacetyl tandem mass tag (IodoTMT) protein oxidation and tandem mass tag (TMT) protein abundance data were sourced from previous experiments (Chapters 3 and 4). Each of these data sets analyzed control and VPA (600 μM) treated samples at 2, 4, 6, 8, and 10 hrs on mouse GD 8. TMT data was collected in separate EMB and VYS samples, while IodoTMT data was based on whole conceptuses. Cellular glutathione (GSH), glutathione disulfide (GSSG) redox potential (E_h) data in Tables 5-4 and 5-5 was sourced from previous experiments using the same dosing strategy described above (Chapter 2).

Data Integration

Time specific IodoTMT protein lists were compared to tissue and time specific TMT protein abundance lists for matches. Following successful combination of the two datasets, previously defined cut-offs were applied to identify proteins that changed in both abundance and oxidation status following VPA exposure. For TMT the threshold required a log2 VPA/Ctl ratio of greater than 0.33 or less than -0.33 (Chapter 4). For IodoTMT, the threshold required an absolute difference of 8.6 or more percentage points between the oxidation percentages of VPA and control proteins (Chapter 3). Pathway analysis was performed on the list of proteins identified to meet this criteria for the VYS and EMB using String to identify enriched Biological Process Gene Ontology (GO) terms (FDR<0.05) (Szklarczyk et al., 2019). Individual proteins

that were identified as meeting the criteria for altered abundance and oxidation were categorized as being associated with development, redox, or VPA mechanisms based on biological process GO-terms affiliated with the protein in the Uniprot database (The UniProt Consortium, 2019).

Timeline Evaluation

Pathway Analysis data identifying enriched Biological Process GO-terms was sourced from previous TMT and IodoTMT studies identified above to identify patterns in protein abundance and oxidation over time that were time or tissue specific (Chapter 3 and 4). Gene set enrichment analysis (GSEA) and DAVID pathway analysis was utilized for TMT data (Huang et al., 2009, 2009; Mootha et al., 2003; Subramanian et al., 2005). Protein oxidation data was sourced exclusively from String and Revigo enrichment results due to the lack of developmentally relevant pathways in the GSEA data (Supek et al., 2011; Szklarczyk et al., 2019). Developmentally relevant pathways with at least two appearances were categorized by time to identify patterns in directional abundance changes or oxidation status in response to VPA treatment. Cellular GSH E_h values for the EMB and VYS were also included (Chapter 2).

Results

Data Integration Summary

Figure 5-1 plots the VPA/Control (Ctl) protein abundance ratios against the VPA Oxidation Percent/Ctl Oxidation Percent ratio. Here it can be seen that the spread in protein abundance between the EMB and VYS samples differs across time with the VYS showing the greatest spread in abundance at 2 and 4 hrs whereas the EMB shows the largest range in abundance at 6, 8, and 10 hrs. The time points with the greatest change in oxidation percent in VPA compared to the control were 2, 8, and 10 hrs. By applying the threshold criteria described

in the methods, Table 5-1 identifies the number that were differentially affected by VPA exposure in abundance and oxidation status. In the EMB, 34 proteins met the inclusion criteria for abundance and oxidation with the majority of those occurring at 10 hrs. Sixteen of the 31 proteins in this category at 10 hrs showed an increase in abundance accompanied by an increase in oxidation following VPA exposure. In the VYS, there are 31 proteins affected by both oxidation and abundance changes with 28 of these being at 2 hrs. Of these 28 proteins, 22 show lower abundance and lower oxidation.

EMB- Abundance and Redox Sensitive Proteins

Table 5-3 identifies the 34 proteins that showed a change in EMB abundance and whole conceptus oxidation following VPA exposure. Based on Uniprot biological process GO-terms associated with each protein, 14 of the proteins have relevance to development, 5 are related to redox mechanisms, and 1 is related to VPA's action as an HDAC inhibitor. Pathway analysis results of these proteins revealed 25 pathways after enrichment with String and list condensation by Revigo (Figure 5-2). Nervous system development was the single developmental pathway enriched within this set of 34 proteins and contained 8 of the 31 proteins at 10 hrs (Table 5-4). Of these 8 nervous system development proteins, 3 showed a concordant increase in abundance and oxidation, 1 showed a concordant decreased in abundance and oxidation and the other 4 had discordant oxidation and abundance levels following VPA exposure.

VYS-Abundance and Redox Sensitive Proteins

Table 5-4 identifies the 31 proteins that were altered in abundance and oxidation in response to VPA in the VYS and whole conceptus. Pathway analysis of these 31 proteins did not identify enrichment of any biological process GO-terms. Proteins were categorized by their

associated biological process GO-terms. Of these proteins, 9 show relevance to development, 2 are related to redox regulation, and 1 has relevance to VPA's mechanism as an HDAC inhibitor.

VYS & EMB Redox Potential and Protein Abundance Changes

Tissue-specific differences in the response of the mouse conceptus VYS and EMB proper to VPA has been studied in terms of cellular GSH:GSSG redox potential and protein abundance changes in response to VPA (Chapter 2 and 4). By comparing these two datasets, tissue-specific periods of sensitivity to VPA can be confirmed. In the EMB the time periods of greatest redox potential oxidation caused by VPA was at 4, 6, and 10 hrs, while the time periods of greatest change to protein abundance were at 6 and 10 hrs (Table 5-5). In the VYS, 2, 4, and 10 hrs demonstrated the greatest oxidizing shift in redox potential, while 2 and 4 hrs showed the highest number of proteins affected by changes in abundance (Table 5-6).

Timeline of VPA Actions

Enriched development pathways were categorized by time point and directional change across protein abundance and protein oxidation data sets with differentiation of tissues by color (Tables 5-7 to 5-11). Pathways with at least two appearances that may hold mechanistic or organ system relevance to neural tube closure were organized into a timeline of developmental perturbation events caused by VPA exposure (Figure 5-3).

Discussion

The timeline of developmental VPA perturbation events identifies several patterns related to time, tissue, abundance, and oxidation patterns of proteins identified during early organogenesis. Beginning with patterns related to tissue and time, there is a clear split in directionality of abundance data in the EMB and VYS that shifts over time (Figure 5-3). At 2 and

4 hrs, highlighted EMB developmental pathways are all decreased in abundance, whereas at 6, 8, 10 hrs highlighted EMB developmental pathways are mostly increased in abundance with the exception of osteoblast differentiation at 6 and 10 hrs. The converse is true in the VYS, where development pathways at 4 hrs are mostly increased in abundance and pathways at 8 and 10 hrs are decreased in abundance. This implies a distinct spatiotemporal response to VPA in the mouse conceptus with independent regulation of the EMB and VYS response. During the period of organogenesis, the major morphological events in the EMB include heart development and heartbeat activation, neural tube closure, limb bud development, and formation of the otic vesicle and optic cup occur during the latter half of the time course. In contrast, the VYS is actively involved in the process of histiotrophic nutrition, angiogenesis, and hematopoiesis beginning at the earliest time points (Beckman et al., 1990; Harris, 2012; Lloyd et al., 1998). The distinct spatiotemporal differences in the enrichment of developmental pathways in the EMB and VYS could therefore be relative to the level of developmental activity in a tissue during a given time point. This would imply that VPA is more likely to increase pathways of developmental relevance during periods of high tissue activity and decrease pathways of developmental relevance during periods of lower tissue activity.

Across both EMB and VYS, stem cell differentiation is a pathway that is always increased in response to VPA. In the VYS, it is elevated at 4 hrs, while in the EMB it is elevated at 6 and 8 hrs. VPA's effects on cellular differentiation have been noted in multiple studies with its action as an HDAC inhibitor often implicated in the findings. In a study of rat mesenchymal stem cell (MSC) differentiation into neurons, it was noted that exposure to VPA decreased markers of early stage neural cells and increased expression of gene markers of mature neurons (Fila-Danilow et al., 2017). In addition to promoting differentiation of MSCs, VPA exposure has

also been shown to increase rat MSC migration through upregulation of Cxcr4 through HDAC inhibition pathways (Tsai et al., 2010).

In addition to VPA's effects on general stem cell populations, it was also noted that differentiation of several specific cell types was affected by VPA exposure. Keratinocyte differentiation was exclusively enriched within VYS proteins decreased by VPA exposure and identified at 6, 8, and 10 hrs and in decreased EMB proteins at 2 hrs (Figure 5-3). In a model of mouse wound healing, VPA administration to an open wound lead to a faster rate of healing with increased cell proliferation and where markers of keratinocyte differentiation were observed and believed to be due to VPA's activation of the canonical Wnt signaling pathways (Lee, Zahoor, et al., 2012). Osteoblast differentiation was decreased at 4 hrs in the VYS and 6 and 10 hrs in the EMB, while osteoclast differentiation was increased in the EMB at 6 and 10 hrs. Osteoclasts and osteoblasts work in tandem to promote the resorption and replacement of mature bone (osteoclasts) with new bone (osteoblasts) (Pitetzis et al., 2017). VPA has been shown to increase proliferation and differentiation of osteoblasts, but may suppress activity of mature osteoblasts to explain VPA's association with increased fracture risk (Pitetzis et al., 2017). The decrease in osteoblast differentiation and increase in osteoclast differentiation seen in our data could support VPA's association with bone fragility due to a decrease in the buildup of new bone to replace mature bone. The application of VPA exposure to osteoclast and osteoblast differentiation during organogenesis is not clear since bone ossification doesn't occur until much later in development beginning around GD 15 through the post-natal period (Patton & Kaufman, 1995). It is possible therefore, that while VPA is affecting osteoblast and osteoclast differentiation that the effects of the changes would not be applicable to neural tube closure, but may instead affect downstream skeletal integrity.

Epithelial differentiation was decreased in the EMB at 2 hrs, but increased in the VYS at 4 hrs. VPA has been noted to increase differentiation of epithelial cells in a study of epithelial origin submandibular salivary gland cells that showed increased hepatocyte markers following VPA exposure (Petrakova et al., 2015). The contradiction in directionality of our EMB results could be due to our tissue being of embryonic origin, whereas the salivary gland cells originated from adult mice. Epidermal cell differentiation was decreased in the EMB at 2 hrs, increased in the VYS at 4 hrs, and then decreased in the VYS at 8 and 10 hrs indicating the most dynamic abundance change profile of a cell type specific differentiation pathway. In a mouse model of alopecia, topical VPA application was shown to induce hair growth and increase markers of epidermal cell differentiation (Lee, Yoon, et al., 2012). Epithelial and epidermal tissues are both important contributors to the process of neurulation. The epidermal ectoderm and neuroepithelium both participate in the process of convergent extension with fold elevation and fusion of the neural plate to form the neural tube. The two tissues jointly participate in the folding, but progressively delaminate from one another as the process of neural plate elevation and folding progresses (Martins-Green, 1988). Therefore, failed or decreased differentiation of either of these tissues could affect the process of neural tube closure.

Polarity pathways show an interesting pattern of occurrence across the timeline with cell polarity showing increased oxidation in response to VPA treatment two hours prior to increased abundance of tissue polarity pathways in the EMB at 4 and 6 hrs, with a concurrent appearance of increased oxidation and increased abundance noted at 10 hrs. The closely timed appearances of increased oxidation and increased abundance indicate a potential link between protein abundance and oxidation. VPA has previously been implicated in disruption of the planar cell polarity (PCP) pathway in cardiomyocytes through inhibition of HDAC3 leading to decreased

expression of PCP genes Vangl2 and Scrib (Duan et al., 2018). PCP genes are critically important for NTC and mutation of PCP genes has been associated with NTD risk (Copp & Greene, 2010). Our abundance data for Vangl2 and Scrib indicate an increase in Vangl2 at 6 and 10 hrs (1.35 and 1.19 respectively) and a concurrent decrease in Scrib (0.74 and 0.72 respectively). Neither Vangl2 or Scrib were identified in IodoTMT oxidation data at either 6 or 10 hrs. Although these proteins were not specifically identified by IodoTMT labeling, this does not preclude their involvement in a redox-mediated mechanism. Many signaling pathways are redox-regulated through targeted oxidation of an upstream protein that then activates or inactivates downstream targets. An example of this style of upstream redox regulation is the Nrf2/Keap1 antioxidant pathway, where oxidation of Keap1 activates the translocation of Nrf2 to the nucleus, despite Nrf2 not being directly affected by the oxidation event (Tonelli et al., 2018).

Another potential link between two pathways exists in the interplay between target of rapamycin (TOR) signaling and developmental growth. TOR signaling promotes cellular growth and proliferation in response to nutritional cues (Wullschleger et al., 2006). Inactivation of TOR signaling has been associated with embryonic lethality in early development (Gangloff et al., 2004). Figure 5-3 shows that developmental growth and TOR signaling are jointly enriched at 4 hrs and 8 hrs in both cases with developmental growth in the EMB and TOR signaling in the VYS. In both of these instances, the directionality of these pathways is the reverse of one another. The tissue specific directional opposition of these pathways may be supporting TOR's role in growth, where TOR increases in abundance when growth is depressed but decreases in abundance when growth is high creating a system of checks and balances. The tissue-specificity of these pathways is also interesting since TOR is known to take cues from the nutritional environment which is part of the role of the VYS (Lloyd et al., 1998). It therefore appears that

the VYS is helping to orchestrate developmental growth of the EMB through TOR signaling that respond to VPA alterations of developmental growth.

In addition to recurrent enrichment of developmental mechanisms in response to VPA exposure, there was also recurrent enrichment of the pathway oxidation-reduction process. Oxidation-reduction process was decreased in abundance in the VYS at 2 hrs, with increase in abundance at 4 and 10 hrs in the VYS and EMB, respectively. At 10 hrs, there was also differential oxidation of this pathway with lower oxidation in VPA-treated samples (Figure 5-3). Cellular GSH redox potential of the VYS and EMB was also affected at these same timepoints with the VPA treated VYS oxidized compared to the control at 2 hrs. At 4 and 10 hrs, both the EMB and VYS exhibited higher oxidation following VPA treatment. While there is some degree of VYS oxidation at all timepoints compared to the control, the magnitude of difference between control and VPA oxidation is greatest at 2, 4, and 6 hrs. Conversely, the VPA treated EMB is actually reduced compared to the control at 2, 6 and 8 hrs with the only times of oxidation being at 4 and 10 hrs. Therefore, the time points with the least difference in cellular oxidation are also the two timepoints without enrichment of the oxidation-reduction process pathway. 10 hrs is a particularly interesting timepoint for oxidation since there is an increase in abundance of oxidation-reduction process proteins, but a decrease in protein oxidation compared to the control despite a more reduced GSH redox potential in the control. This discordant finding between cellular redox and redox status of oxidation-reduction process proteins confirms that VPA selectively affects cellular redox status independently from protein redox.

This integrative systems level approach to understanding VPA's effects on the organogenesis-stage mouse conceptus has highlighted several potential pathways and windows of sensitivity to VPA perturbation. Unlike traditional reductionist methods in developmental

biology, this systems level approach identified an impressive breadth of developmental processes in the differentially affected pathways. However, while the breadth of the analysis was expansive, the depth of knowledge into the underlying mechanisms of VPA's activity still requires significant research to determine how the specific proteins within each affected pathway and their abundances and oxidation states are related to neural tube closure. One limitation of this analysis is that the IodoTMT protein oxidation labeling was performed only on whole conceptuses compared to TMT labeling which was performed separately in the EMB and VYS. This reduces the spatial distinctions that can be made in terms of oxidation to compare to the tissue specific protein abundance data. Additionally, while the use of IodoTMT labeling is useful due to the built in quantitation aspect of the labels, the inability to distinguish reversible Cys modifications from one another make drawing mechanistic conclusions regarding pathway or protein oxidation status difficult. Despite these limitations, this analysis has provided strong evidence for VPA's perturbation of the developmental mechanisms of differentiation, cell polarity, and proliferation/growth, all of which have known connections to the process of neurulation and neural tube closure. It has also uniquely demonstrated the importance of tissue specific assessment of EMB and VYS outcomes to understand the important interplay of these distinct developmental entities. Future studies should make use of the breadth of this systems analysis of VPA perturbations to focus on specific pathways and proteins that show promise as being downstream targets of VPA exposure that may be implicated in the mechanism of failed neural tube closure.

Tables

	Embryo					Visceral Yolk Sac				
	2hr	4hr	6hr	8hr	10hr	2hr	4hr	6hr	8hr	10hr
Total Matched Proteins	415	119	168	125	363	430	123	168	126	370
Differentially Affected Proteins	0	0	2	1	31	28	0	0	0	3
Higher Abundance, Higher Oxidation	0	0	0	0	16	1	0	0	0	0
Higher Abundance, Lower Oxidation	0	0	1	1	8	0	0	0	0	0
Lower Abundance, Higher Oxidation	0	0	0	0	1	2	0	0	0	0
Lower Abundance, Lower Oxidation	0	0	1	0	6	25	0	0	0	3

Table 5-1 Summary of proteins affected by changes to oxidation and abundance: Number of protein matches identified across the TMT protein abundance and iodoTMT protein oxidation data sets as well as number of proteins that were differentially affected in both the oxidation and abundance.

Time	Accession	Protein Name	Ctl Ox %	VPA Ox%	VPA/Ctl Ox%	VPA/Ctl Abundance
6hr	P68510	14-3-3 protein eta	64.9	55.7	0.86	1.39
6hr	Q9CX86	Heterogeneous nuclear ribonucleoprotein A0	24.8	9.6	0.39	0.77
8hr	Q61646	Haptoglobin	79.9	69.0	0.86	1.88
10hr	A0A1W2P7X0	Costars family protein ABRACL (Fragment)	14.8	28.0	1.89	2.16
10hr	P00493	Hypoxanthine-guanine phosphoribosyltransferase	32.9	49.6	1.51	1.78
10hr	Q64727	Vinculin	29.3	39.9	1.36	1.65
10hr	Q4VBE8	WD repeat-containing protein 18	36.4	56.8	1.56	1.64
10hr	Q9DAK9	14 kDa phosphohistidine phosphatase	18.9	28.7	1.52	1.59
10hr	Q8BY71	Histone acetyltransferase type B catalytic subunit	33.5	49.7	1.48	1.58
10hr	Q9WVJ2	26S proteasome non-ATPase regulatory subunit 13	14.1	30.5	2.17	1.49
10hr	Q8QZY1	Eukaryotic translation initiation factor 3 subunit L	22.5	36.8	1.63	1.39
10hr	Q6P4T2	U5 small nuclear ribonucleoprotein 200 kDa helicase	34.8	50.7	1.46	1.35
10hr	Q9ERK4	Exportin-2	27.5	39.9	1.45	1.34
10hr	Q99PV0	Pre-mRNA-processing-splicing factor 8	46.0	57.6	1.25	1.33
10hr	Q9D8W5	26S proteasome non-ATPase regulatory subunit 12	40.6	60.2	1.48	1.31
10hr	Q9DC51	Guanine nucleotide-binding protein G(i) subunit alpha	41.9	53.5	1.28	1.29
10hr	O08528	Hexokinase-2	48.4	57.0	1.18	1.29
10hr	Q6DFW4	Nucleolar protein 58	53.1	78.4	1.48	1.28
10hr	P10639	Thioredoxin	46.9	72.0	1.54	1.28
10hr	A6ZI44	Fructose-bisphosphate aldolase	30.9	11.6	0.38	0.78
10hr	Q9WTP6	Adenylate kinase 2, mitochondrial	79.4	35.5	0.45	0.78
10hr	Q99J08	SEC14-like protein 2	58.5	45.3	0.78	0.78
10hr	P21614	Vitamin D-binding protein	78.6	65.4	0.83	0.73
10hr	P22935	Cellular retinoic acid-binding protein 2	47.7	37.3	0.78	0.72
10hr	Q99KR7	Peptidyl-prolyl cis-trans isomerase F, mitochondrial	78.7	42.3	0.54	0.72
10hr	P37913	DNA ligase 1	48.8	27.1	0.56	1.79
10hr	P62317	Small nuclear ribonucleoprotein Sm D2	81.3	66.5	0.82	1.51
10hr	P34884	Macrophage migration inhibitory factor	80.3	22.0	0.27	1.37
10hr	Q91WG4	Elongator complex protein 2	49.2	34.1	0.69	1.34
10hr	Q9CWJ9	Bifunctional purine biosynthesis protein PURH	66.7	54.2	0.81	1.34
10hr	F8VQJ3	Laminin subunit gamma-1	94.1	76.4	0.81	1.32
10hr	P61750	ADP-ribosylation factor 4	38.8	28.5	0.73	1.27
10hr	Q5SWN2	Replication protein A subunit	48.7	23.7	0.49	1.26
10hr	A0A140LHY7	DNA polymerase delta subunit 3	42.8	51.4	1.20	0.77

Development Redox Regulation Development & Redox Regulation VPA Mechanisms

Table 5-2 EMB proteins affected by changes to oxidation and abundance: Proteins differentially affected by VPA treatment in abundance and oxidation state in the EMB categorized by role in development, redox regulation, or a known VPA mechanism based on associated biological process gene ontology terms.

Time	Accession	Protein Name	Ctl Ox %	VPA Ox%	VPA/Ctl Ox%	VPA/Ctl Abundance
2hr	Q9DBD0	Inhibitor of carbonic anhydrase	75.8	85.1	1.12	1.39
2hr	Q9QYJ0	DnaJ homolog subfamily A member 2	43.3	71.7	1.66	0.73
2hr	Q9D8W5	26S proteasome non-ATPase regulatory subunit 12	23.4	48.9	2.08	0.72
2hr	Q80ZQ9	Protein Abitram	56.7	48.1	0.85	1.45
2hr	Q9QYA2	Mitochondrial import receptor subunit TOM40 homolog	69.8	43.3	0.62	1.33
2hr	P97315	Cysteine and glycine-rich protein 1	57.5	47.6	0.83	1.30
2hr	A0A087WQS2	Basic leucine zipper and W2 domain-containing protein 1	53.1	33.7	0.64	0.72
2hr	D3YU12	NmrA-like family domain-containing protein 1	45.5	25.7	0.56	0.70
2hr	Q922B2	Aspartate--tRNA ligase, cytoplasmic	53.6	34.7	0.65	0.69
2hr	Q80VD1	Protein FAM98B	49.2	38.3	0.78	0.62
2hr	P61965	WD repeat-containing protein 5	52.9	27.4	0.52	0.56
2hr	P84084	ADP-ribosylation factor 5	40.2	27.3	0.68	0.53
2hr	Q99LE6	ATP-binding cassette sub-family F member 2	48.0	37.5	0.78	0.75
2hr	Q8BTS4	Nuclear pore complex protein Nup54	42.0	21.3	0.51	0.75
2hr	O88685	26S proteasome regulatory subunit 6A	28.5	17.0	0.60	0.75
2hr	P27048	Small nuclear ribonucleoprotein-associated protein B	70.8	59.1	0.83	0.76
2hr	P50516	V-type proton ATPase catalytic subunit A	63.3	43.9	0.69	0.77
2hr	Q9R0P3	S-formylglutathione hydrolase	28.6	20.4	0.71	0.77
2hr	P08752	Guanine nucleotide-binding protein G(i) subunit alpha-2	34.1	24.8	0.73	0.77
2hr	P97310	DNA replication licensing factor MCM2	32.2	23.0	0.71	0.77
2hr	P80313	T-complex protein 1 subunit eta	43.3	32.7	0.76	0.77
2hr	Q9QUR6	Prolyl endopeptidase	30.3	20.8	0.69	0.77
2hr	P62317	Small nuclear ribonucleoprotein Sm D2	86.0	75.0	0.87	0.78
2hr	P68369	Tubulin alpha-1A chain	26.2	17.7	0.67	0.78
2hr	Q3UDE2	Tubulin--tyrosine ligase-like protein 12	58.7	43.4	0.74	0.79
2hr	J3QN89	Angio-associated migratory protein	43.9	30.9	0.70	0.79
2hr	P06745	Glucose-6-phosphate isomerase	75.8	41.0	0.54	0.79
2hr	Q9CWJ9	Bifunctional purine biosynthesis protein PURH	41.7	30.3	0.73	0.79
10hr	P07759	Serine protease inhibitor A3K	49.4	39.2	0.79	0.75
10hr	Q61646	Haptoglobin	79.6	65.0	0.82	0.77
10hr	P21614	Vitamin D-binding protein	78.6	65.4	0.83	0.73

Development | Redox Regulation | Development & Redox Regulation | VPA Mechanisms | Development + VPA Mechanisms

Table 5-3 VYS proteins affected by changes to oxidation and abundance: Proteins differentially affected by VPA treatment in abundance and oxidation state in the EMB categorized by role in development or a known VPA mechanism based on associated biological process gene ontology terms.

Nervous System Development 10hr EMB	*Abundance*	*Oxidation*
Gnai3	1.29	1.3
Crabp2	0.721	0.8
Vcl	1.69	1.4
Arf4	1.27	0.7
Hprt	1.78	1.5
Atic	1.34	0.8
Lamc1	1.32	0.8
Mif	1.4	0.3

Table 5-4 10 hr EMB nervous system development proteins: Nervous system development was the only developmental pathway enriched within the list of 34 EMB and whole conceptus proteins affected by oxidation and abundance changes. The VPA/Ctl abundance and percent oxidation ratios are listed here for the 8 proteins that were identified to comprise this pathway at 10 hrs.

EMB	0hr	2hr		4hr		6hr		8hr		10hr	
	Ctl	Ctl	VPA	Ctl	VPA	Ctl	VPA	Ctl	VPA	Ctl	VPA
GSH E_h	-196.47	-175.16	-186.81	-201.50	-181.93	-189.24	-191.86	-176.35	-198.94	-190.18	-170.99
Proteins Increased	-	113		96		556		115		767	
Proteins Decreased	-	89		80		666		61		748	

Table 5-5 EMB summary of glutathione redox potential and protein abundance:
GSH:GSSG E_h from 0-10 hrs in the EMB compared to the number of proteins showing increased or decreased abundance at the corresponding time as measured through TMT labeling.

VYS	0hr	2hr		4hr		6hr		8hr		10hr	
	Ctl	Ctl	VPA	Ctl	VPA	Ctl	VPA	Ctl	VPA	Ctl	VPA
GSH E_h	-178.13	-189.51	-174.13	-184.13	-173.77	-188.09	-180.19	-187.10	-180.20	-171.91	-130.70
Proteins Increased	-	444		934		137		86		66	
Proteins Decreased	-	606		646		69		54		110	

Table 5-6 VYS summary of glutathione redox potential and protein abundance:
GSH:GSSG E_h from 0-10 hrs in the VYS compared to the number of proteins showing increased or decreased abundance at the corresponding time as measured through TMT labeling.

	2hr Developmental VPA Perturbations			
	Increased		Decreased	
	Pathway	P-value/FDR	Pathway	P-value/FDR
DAVID Protein Abundance	In Utero Embryonic Development	0.024		
	Rhythmic Process	0.033	Epidermis Development	0.006
	Muscle Organ Development	0.047	Cell Differentiation Involved in Embryonic Placenta Development	0.046
	Lung Development	0.004		
	Embryonic Process Involved in Female Pregnancy	0.041		
GSEA Protein Abundance			Keratinocyte Differentiation	0.000
			Epidermal Cell Differentiation	0.000
	Body Morphogenesis	0.249	Skin Development	0.000
			Epidermis Development	0.000
			Epithelial Cell Differentiation	0.008
Protein Oxidation	No Enrichment		Brainstem Development	0.012
			In Utero Embryonic Development	0.037
			Dendritc Spine Development	0.022

Table 5-7 2 hr developmental pathways affected by changes to protein abundance or oxidation: 2 hr enrichment of biological process GO-term developmental pathways affected by VPA exposure through changes in protein abundance or protein oxidation. Blue pathways are specific to the EMB. Orange pathways are specific to the VYS and black pathways are whole conceptus. DAVID and protein oxidation pathways are listed with p-values and GSEA pathways are listed with FDR values.

	4hr Developmental VPA Perturbations			
	Increased		Decreased	
	Pathway	P-value/FDR	Pathway	P-value/FDR
DAVID Protein Abundance	Skeletal Muscle Tissue Development	0.018	Epidermis Development	0.005
GSEA Protein Abundance	Regulation of Hematopoietic Progenitor Cell Differentiation	0.008		
	Hematopoietic Stem Cell Differentiation	0.011		
	Regulation of Hematopoietic Cell Differentiation	0.011		
	Positive Regulation of Wnt Signaling	0.017		
	Establishment of Tissue Polarity	0.022		
	Keratinocyte Differentiation	0.024		
	Regulation of Animal Organ Morphogenesis	0.024		
	Positive Regulation of Canonical Wnt Signaling	0.027		
	Regulation of Morphogenesis of an Epithelium	0.036		
	Morphogenesis of a Polarized Epithelium	0.047		
	Rhythmic Process	0.049	Negative Regulation of Muscle Tissue Development	0.125
	Circadian Rhythm	0.057	Negative Regulation of Developmental Growth	0.215
	Non-Canonical Wnt Signaling Pathway	0.063		
	Regulation of Stem Cell Differentiation	0.073		
	Hematopoietic Progenitor Cell Differentiation	0.085		
	Regulation of TOR Signaling	0.145		
	Epithelium Development	0.180		
	Regulation of Circadian Rhythm	0.190		
	Stem Cell Differentiation	0.208		
	Negative Regulation of Canonical Wnt Signaling	0.209		
	Epidermal Cell Differentiation	0.219		
	Epithelial Cell Differentiation	0.234		
	Nephron Development	0.234		
	Positive Regulation of TOR Signaling	0.235		
	Smooth Muscle Cell Proliferation	0.236		
Protein Oxidation	Establishment or Maintenance of Cell Polarity	0.004	Liver Development	0.017

Table 5-8 4 hr developmental pathways affected by changes to protein abundance or oxidation: 4 hr enrichment of biological process GO-term developmental pathways affected by VPA exposure through changes in protein abundance or protein oxidation. Blue pathways are specific to the EMB. Orange pathways are specific to the VYS and black pathways are whole conceptus. DAVID and protein oxidation pathways are listed with p-values and GSEA pathways are listed with FDR values.

	6hr Developmental VPA Perturbations			
	Increased		Decreased	
	Pathway	P-value/FDR	Pathway	P-value/FDR
DAVID Protein Abundance	Substantia Nigra Development	0.001	Response to Transforming Growth Factor Beta Labyrinthine Layer Development Eyelid Development in Camera-type Eye Cell Differentiation involved in Embryonic Placenta Development	0.019 0.034 0.034 0.044
GSEA Protein Abundance	Establishment of Tissue Polarity Regulation of Animal Organ Morphogenesis Morphogenesis of a Polarized Epithelium Non-canonical Wnt Signaling Pathway Regulation of Stem Cell Differentiation Positive Regulation of Canonical Wnt Signaling Regulation of Morphogenesis of an Epithelium Hematopoietic Stem Cell Differentiation Negative Regulation of Canonical Wnt Signaling Positive Regulation of Wnt Signaling Negative Regulation of Growth Negative Regulation of Wnt Signaling Canonical Wnt Signaling Pathway Stem Cell Differentiation Osteoclast Differentiation Negative Regulation of Myeloid Cell Differentiation Endothelial Cell Development Negative Regulation of Cell Growth Regulation of Wnt Signaling Pathway Substantia Nigra Development Morphogenesis of an Epithelium Regulation of Embryonic Development Endothelium Development Tissue Morphogenesis Heart Process Neural Nucleus Development	0.000 0.000 0.000 0.000 0.000 0.000 0.000 0.000 0.001 0.002 0.006 0.016 0.017 0.033 0.059 0.068 0.099 0.107 0.111 0.133 0.148 0.181 0.182 0.188 0.211 0.242	Keratinocyte Differentiation	0.096
Protein Oxidation	No Enrichment		Nervous System Development	0.036

Table 5-9 6 hr developmental pathways affected by changes to protein abundance or oxidation: 6 hr enrichment of biological process GO-term developmental pathways affected by VPA exposure through changes in protein abundance or protein oxidation. Blue pathways are specific to the EMB. Orange pathways are specific to the VYS and black pathways are whole conceptus. DAVID and protein oxidation pathways are listed with p-values and GSEA pathways are listed with FDR values.

	8hr Developmental VPA Perturbations			
	Increased		Decreased	
	Pathway	P-value/FDR	Pathway	P-value/FDR
DAVID Protein Abundance	Epidermis Development Keratinocyte Development Positive Regulation of Developmental Growth Male Gonad Development	0.000 0.009 0.042 0.048	Organ Regeneration	0.02
GSEA Protein Abundance	Regulation of Body Fluid Levels Stem Cell Differentiation	0.111 0.229	Keratinocyte Differentiation Epidermal Cell Differentiation Skin Development Epidermis Development Regulation of TOR Signaling	0.002 0.005 0.006 0.022 0.196
Protein Oxidation	No Enrichment		Positive Regulation of Cell Development Nervous System Development	0.023 0.012

Table 5-10 8 hr developmental pathways affected by changes to protein abundance or oxidation: 8 hr enrichment of biological process GO term developmental pathways affected by VPA exposure through changes in protein abundance or protein oxidation. Blue pathways are specific to the EMB. Orange pathways are specific to the VYS and black pathways are whole conceptus. DAVID and protein oxidation pathways are listed with p-values and GSEA pathways are listed with FDR values.

	10hr Developmental VPA Perturbations			
	Increased		Decreased	
	Pathway	P-value/FDR	Pathway	P-value/FDR
DAVID Protein Abundance	Substantia Nigra Development	0.031	Positive Regulation of Cell Differentiation	0.036
	Epithelial Tube Branching Involved in Lung Morphogenesis	0.042	Multicellular Organism Development	0.044
	Cerebral Cortex Development	0.026	Somatic Stem Cell Population Maintenance	0.049
			Negative Regulation of Osteoblast Differentiation	0.049
			Regulation of Spongiotrophoblast Cell Proliferation	0.037
GSEA Protein Abundance	Establishment of Tissue Polarity	0.000		
	Regulation of Animal Organ Morphogenesis	0.000		
	Regulation of Hematopoietic Stem Cell Differentiation	0.000		
	Regulation of Morphogenesis of an Epithelium	0.000		
	Non-canonical Wnt Signaling Pathway	0.000		
	Morphogenesis of a Polarized Epithelium	0.000	Keratinocyte Differentiation	0.000
	Positive Regulation of Canonical Wnt Signaling	0.001	Skin Development	0.001
	Negative Regulation of Canonical Wnt Signaling	0.002	Epidermal Cell Differentiation	0.005
	Positive Regulation of Wnt Signaling	0.005	Positive Regulation of TOR Signaling	0.008
	Negative Regulation of Wnt Signaling	0.021	Regulation of TOR Signaling	0.015
	Cell-Cell Signaling by Wnt	0.036	Epidermis Development	0.029
	Hematopoietic Progenitor Cell Differentiation	0.039		
	Regulation of Wnt Signaling Pathway	0.096		
	Stem Cell Differentiation	0.116		
	Canonical Wnt Signaling Pathway	0.035		
	Negative Regulation of Growth	0.051		
	Osteoclast Differentiation	0.012		
	Regulation of MegaKaryocyte Differentiation	0.185		
	Lymphocyte Differentiation	0.207		
	T Cell Differentiation	0.222		
Protein Oxidation	Establishment or Maintenance of Cell Polarity	0.037		
	System Development	0.034	Multicellular Organ Development	0.012
	Cerebral Cortex Neuron Differentiation	0.009		

Table 5-11 10 hr developmental pathways affected by changes to protein abundance or oxidation: 10 hr enrichment of biological process GO-term developmental pathways affected by VPA exposure through changes in protein abundance or protein oxidation. Blue pathways are specific to the EMB. Orange pathways are specific to the VYS and black pathways are whole conceptus. DAVID and protein oxidation pathways are listed with p-values and GSEA pathways are listed with FDR values.

Figures

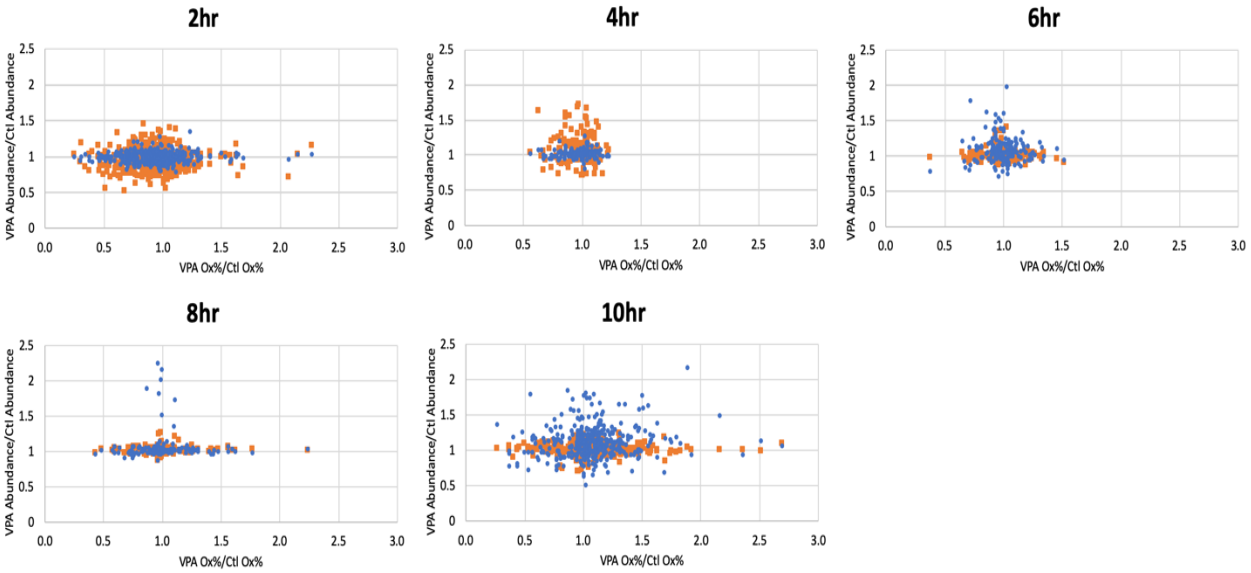

Figure 5-1 VPA/Ctl protein abundance vs. VPA/Ctl protein oxidation in the EMB and VYS: VPA/Ctl protein abundance vs VPA/Ctl protein oxidation percent for proteins identified in both TMT protein abundance and iodoTMT protein oxidation data sets. EMB in blue and VYS in orange.

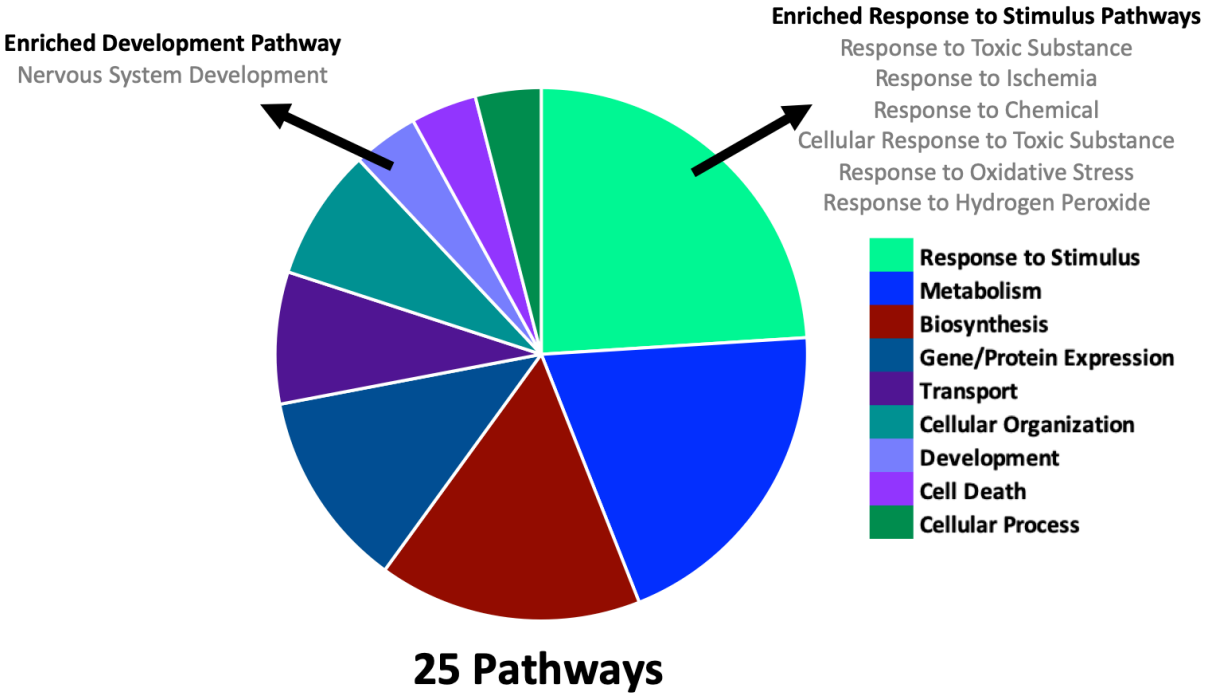

Figure 5-2 Enrichment of biological process GO-terms for EMB proteins with changes to protein oxidation and abundance: Enriched biological process GO-terms identified in String for Table 5-2 EMB proteins showing alterations in abundance and oxidation were collapsed by Revigo and categorized by primary function. Division of the pie chart is based on the number of pathways within each category.

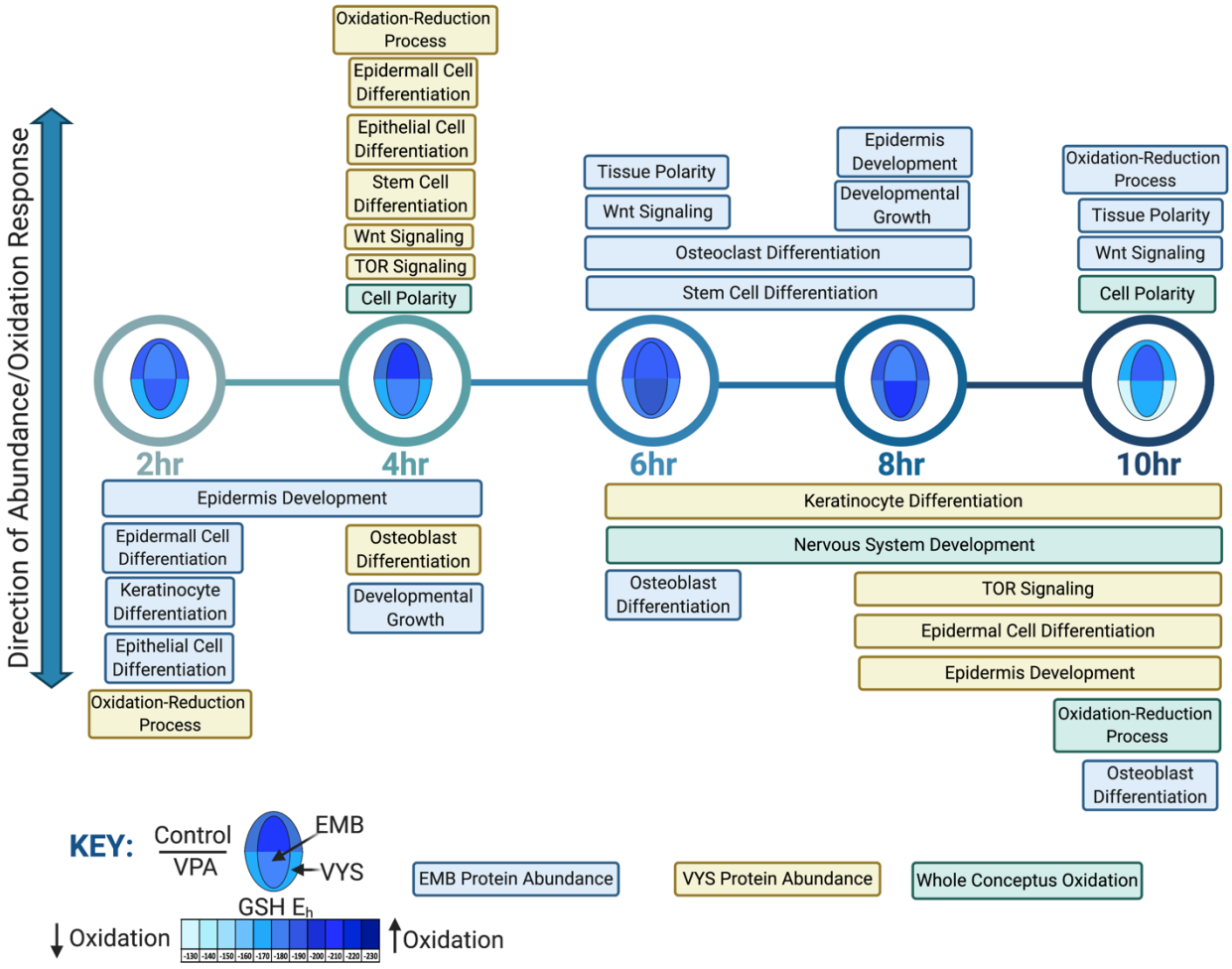

Figure 5-3 Summary timeline of recurrent VPA perturbation events: Timeline of developmental VPA perturbation events categorized by directional change and tissue. Displayed pathways showed recurrent enrichment related to protein abundance or oxidation. Protein abundance and cellular GSH E_h are tissue-specific and protein oxidation is for whole conceptus. Cellular GSH E_h is displayed as a split bubble model of the mouse conceptus with the outer ring representing the VYS and the inner oval representing the EMB proper. The horizontal dividing line separates the upper control measurement from the lower VPA measurement. Adapted from "Timeline (5 Segments, Horizontal)", by BioRender.com (2020). Retrieved from https://app.biorender.com/biorender-templates

References

Beckman, D. A., Koszalka, T. R., Jensen, M., & Brent, R. L. (1990). Experimental manipulation of the rodent visceral yolk sac. *Teratology*, *41*(4), 395–404. https://doi.org/10.1002/tera.1420410405

Copp, A. J., & Greene, N. D. (2010). Genetics and development of neural tube defects: Genetics and development of neural tube defects. *The Journal of Pathology*, *220*(2), 217–230. https://doi.org/10.1002/path.2643

Duan, H.-Y., Zhou, K.-Y., Wang, T., Zhang, Y., Li, Y.-F., Hua, Y.-M., & Wang, C. (2018). Disruption of Planar Cell Polarity Pathway Attributable to Valproic Acid-Induced Congenital Heart Disease through Hdac3 Participation in Mice. *Chinese Medical Journal*, *131*(17), 2080–2088. https://doi.org/10.4103/0366-6999.239311

Fila-Danilow, A., Borkowska, P., Paul-Samojedny, M., Kowalczyk, M., & Kowalski, J. (2017). The influence of TSA and VPA on the in vitro differentiation of bone marrow mesenchymal stem cells into neuronal lineage cells: Gene expression studies. *Postepy Higieny I Medycyny Doswiadczalnej (Online)*, *71*(0), 236–242. https://doi.org/10.5604/01.3001.0010.3809

Gangloff, Y.-G., Mueller, M., Dann, S. G., Svoboda, P., Sticker, M., Spetz, J.-F., Um, S. H., Brown, E. J., Cereghini, S., Thomas, G., & Kozma, S. C. (2004). Disruption of the mouse mTOR gene leads to early postimplantation lethality and prohibits embryonic stem cell development. *Molecular and Cellular Biology*, *24*(21), 9508–9516. https://doi.org/10.1128/MCB.24.21.9508-9516.2004

Ghodke-Puranik, Y., Thorn, C. F., Lamba, J. K., Leeder, J. S., Song, W., Birnbaum, A. K., Altman, R. B., & Klein, T. E. (2013). Valproic acid pathway: Pharmacokinetics and pharmacodynamics. *Pharmacogenetics and Genomics*, *23*(4), 236–241. https://doi.org/10.1097/FPC.0b013e32835ea0b2

Hansen, J. M., Jones, D. P., & Harris, C. (2020). The Redox Theory of Development. *Antioxidants & Redox Signaling*, *32*(10), 715–740. https://doi.org/10.1089/ars.2019.7976

Harris, C. (2012). Rodent Whole Embryo Culture. In C. Harris & J. M. Hansen (Eds.), *Developmental Toxicology* (Vol. 889, pp. 215–237). Humana Press. https://doi.org/10.1007/978-1-61779-867-2_13

Huang, D. W., Sherman, B. T., & Lempicki, R. A. (2009). Bioinformatics enrichment tools: Paths toward the comprehensive functional analysis of large gene lists. *Nucleic Acids Research*, *37*(1), 1–13. https://doi.org/10.1093/nar/gkn923

Lee, S.-H., Yoon, J., Shin, S. H., Zahoor, M., Kim, H. J., Park, P. J., Park, W.-S., Min, D. S., Kim, H.-Y., & Choi, K.-Y. (2012). Valproic Acid Induces Hair Regeneration in Murine Model and Activates Alkaline Phosphatase Activity in Human Dermal Papilla Cells. *PLoS ONE*, *7*(4), e34152. https://doi.org/10.1371/journal.pone.0034152

Lee, S.-H., Zahoor, M., Hwang, J.-K., Min, D. S., & Choi, K.-Y. (2012). Valproic acid induces cutaneous wound healing in vivo and enhances keratinocyte motility. *PloS One*, *7*(11), e48791. https://doi.org/10.1371/journal.pone.0048791

Lloyd, J. B., Beckman, D. A., & Brent, R. L. (1998). Nutritional role of the visceral yolk sac in organogenesis-stage rat embryos. *Reproductive Toxicology*, *12*(2), 193–195. https://doi.org/10.1016/S0890-6238(97)00148-2

Martins-Green, M. (1988). Origin of the dorsal surface of the neural tube by progressive delamination of epidermal ectoderm and neuroepithelium: Implications for neurulation and neural tube defects. *Development (Cambridge, England)*, *103*(4), 687–706.

Mootha, V. K., Lindgren, C. M., Eriksson, K.-F., Subramanian, A., Sihag, S., Lehar, J., Puigserver, P., Carlsson, E., Ridderstråle, M., Laurila, E., Houstis, N., Daly, M. J., Patterson, N., Mesirov, J. P., Golub, T. R., Tamayo, P., Spiegelman, B., Lander, E. S., Hirschhorn, J. N., … Groop, L. C. (2003). PGC-1α-responsive genes involved in oxidative phosphorylation are coordinately downregulated in human diabetes. *Nature Genetics*, *34*(3), 267–273. https://doi.org/10.1038/ng1180

Palsamy, P., Bidasee, K. R., & Shinohara, T. (2014). Valproic acid suppresses Nrf2/Keap1 dependent antioxidant protection through induction of endoplasmic reticulum stress and Keap1 promoter DNA demethylation in human lens epithelial cells. *Experimental Eye Research*, *121*, 26–34. https://doi.org/10.1016/j.exer.2014.01.021

Patton, J. T., & Kaufman, M. H. (1995). The timing of ossification of the limb bones, and growth rates of various long bones of the fore and hind limbs of the prenatal and early postnatal laboratory mouse. *Journal of Anatomy*, *186 (Pt 1)*, 175–185.

Petrakova, O. S., Ashapkin, V. V., Shtratnikova, V. Y., Kutueva, L. I., Vorotelyak, E. A., Borisov, M. A., Terskikh, V. V., Gvazava, I. G., & Vasiliev, A. V. (2015). Valproic Acid Increases the Hepatic Differentiation Potential of Salivary Gland Cells. *Acta Naturae*, *7*(4), 80–92.

Phiel, C. J., Zhang, F., Huang, E. Y., Guenther, M. G., Lazar, M. A., & Klein, P. S. (2001). Histone Deacetylase Is a Direct Target of Valproic Acid, a Potent Anticonvulsant, Mood Stabilizer, and Teratogen. *Journal of Biological Chemistry*, *276*(39), 36734–36741. https://doi.org/10.1074/jbc.M101287200

Pitetzis, D. A., Spilioti, M. G., Yovos, J. G., & Yavropoulou, M. P. (2017). The effect of VPA on bone: From clinical studies to cell cultures—The molecular mechanisms revisited. *Seizure*, *48*, 36–43. https://doi.org/10.1016/j.seizure.2017.03.013

Schafer, F. Q., & Buettner, G. R. (2001). Redox environment of the cell as viewed through the redox state of the glutathione disulfide/glutathione couple. *Free Radical Biology and Medicine*, *30*(11), 1191–1212. https://doi.org/10.1016/S0891-5849(01)00480-4

Subramanian, A., Tamayo, P., Mootha, V. K., Mukherjee, S., Ebert, B. L., Gillette, M. A., Paulovich, A., Pomeroy, S. L., Golub, T. R., Lander, E. S., & Mesirov, J. P. (2005). Gene set enrichment analysis: A knowledge-based approach for interpreting genome-wide expression profiles. *Proceedings of the National Academy of Sciences*, *102*(43), 15545–15550. https://doi.org/10.1073/pnas.0506580102

Supek, F., Bošnjak, M., Škunca, N., & Šmuc, T. (2011). REVIGO Summarizes and Visualizes Long Lists of Gene Ontology Terms. *PLoS ONE*, *6*(7), e21800. https://doi.org/10.1371/journal.pone.0021800

Szklarczyk, D., Gable, A. L., Lyon, D., Junge, A., Wyder, S., Huerta-Cepas, J., Simonovic, M., Doncheva, N. T., Morris, J. H., Bork, P., Jensen, L. J., & Mering, C. von. (2019). STRING v11: Protein–protein association networks with increased coverage, supporting functional discovery in genome-wide experimental datasets. *Nucleic Acids Research*, *47*(D1), D607–D613. https://doi.org/10.1093/nar/gky1131

The UniProt Consortium. (2019). UniProt: A worldwide hub of protein knowledge. *Nucleic Acids Research*, *47*(D1), D506–D515. https://doi.org/10.1093/nar/gky1049

Tonelli, C., Chio, I. I. C., & Tuveson, D. A. (2018). Transcriptional Regulation by Nrf2. *Antioxidants & Redox Signaling*, *29*(17), 1727–1745. https://doi.org/10.1089/ars.2017.7342

Tsai, L.-K., Leng, Y., Wang, Z., Leeds, P., & Chuang, D.-M. (2010). The mood stabilizers valproic acid and lithium enhance mesenchymal stem cell migration via distinct mechanisms. *Neuropsychopharmacology: Official Publication of the American College of Neuropsychopharmacology*, *35*(11), 2225–2237. https://doi.org/10.1038/npp.2010.97

Vajda, F. J., O'Brien, T. J., Graham, J. E., Lander, C. M., & Eadie, M. J. (2013). Dose dependence of fetal malformations associated with valproate. *Neurology*, *81*(11), 999–1003. https://doi.org/10.1212/WNL.0b013e3182a43e81

Wullschleger, S., Loewith, R., & Hall, M. N. (2006). TOR Signaling in Growth and Metabolism. *Cell*, *124*(3), 471–484. https://doi.org/10.1016/j.cell.2006.01.016

Chapter 6

Conclusion

Conclusions

Despite many years of study, the cause of a majority of anatomical and functional birth defects remains unknown and even where causes are well documented, the description of definitive biochemical and molecular mechanisms are lacking. Challenges related to biological inaccessibility, paucity of tissue for study, and the extraordinary challenges of superimposing effects of significant toxicological and environmental insults over an already complex and poorly understood developmental program have combined to slow progress in this field of study. Recent advances in high throughput "omics" technologies have made possible more detailed and comprehensive analyses than have heretofore been applied to yield a better understanding of relevant developmental mechanisms. One area of investigation showing increased importance for the regulation of embryonic development is that of redox regulation and control through protein cysteine-centered redox signaling. The principal logic for this assertion has been laid out in *"The Redox Theory of Development"* and forms the basis for investigating mechanisms of VPA-induced NTDs based on observations that developmental toxicity is elicited through the increased production of ROS (Hansen et al., 2020).

The task of describing developmental mechanisms during embryogenesis is hindered by the acknowledgement that, during development, patterns of gene expression are changing rapidly,

both temporally and spatially, to accommodate the differentiation of new cell types and the creation of new tissues and organs. In terms of cellular responses to increased oxidation, the widespread notion of "oxidative stress" predicts that cellular oxidation (increase of oxidants over antioxidants) of any type and magnitude is sufficient to alter cellular function and activity to cause toxicity (Jones, 2006; Sies et al., 2017). Redefinition of "oxidative stress" to focus on the disruption of redox signaling and control as the critical target of oxidative damage means that emphasis of the global cellular redox status is less important mechanistically than the evaluation and understanding of the selective oxidative posttranslational modification of proteins that make up susceptible pathways. It is from this perspective that the current dissertation was undertaken, using biochemical and proteomics approaches to characterize the redox environment of the GD8 organogenesis-stage mouse conceptus under control and VPA-perturbed conditions to explore a potential connection between VPA-induced neural tube defects (NTDs) and altered redox state. This was accomplished through a spatiotemporal analysis of cellular redox, reversible protein cysteine redox, and protein abundance following VPA exposure across three specific aims:

1) Characterization of the spatial, temporal and stage-specific redox status of early, mid- and late neurulation in control and treated gestational day (GD) 8-9 mouse conceptuses in response to VPA and D3T was conducted through measurement of cellular thiol redox pairs glutathione/glutathione disulfide and cysteine/cystine. This investigation demonstrated that VPA does not cause widespread, global oxidation of the mouse conceptus, but rather affects individual tissue compartments (EMB, VYS, YSF, AF) independently of one another. It had been hypothesized that pre-treatment of conceptuses with D3T and subsequent induction of the Nrf2 antioxidant pathways would alleviate oxidation caused by VPA. While this effect was noted in some tissues and time points,

there was not an overall reduction seen with D3T treatment, despite clear evidence that D3T was inducing the Nrf2 antioxidant pathway.

2) Chapters 3 and 4 identified changes in protein abundance and oxidative reversible Cys modification across early organogenesis through TMT and IodoTMT labeling. Chapter 3 identified whole conceptus time-specific patterns of reversible oxidative modifications of Cys and noted that control conceptuses showed greater sensitivity to oxidation early in the time course with a transition to higher VPA oxidation levels by 10 hrs. Pathways of cell polarity indicated higher VPA oxidation at two time points (4 and 10 hrs), while the pathway of nervous system development showed higher control oxidation at 6, 8, 10 hrs. Cytoskeletal proteins were identified to be differentially affected through GSEA pathway identification and as components of the nervous system development pathway. Chapter 4 evaluated tissue specific (VYS vs EMB) changes to protein abundance as a result of VPA exposure. Protein abundance patterns were shown to be distinct to tissue type and time with enrichment of unique upstream transcription factors related to developmental processes and known mechanisms of VPA action also demonstrated to be sensitive to tissue and temporality. Many pathways of developmental significance were identified as enriched in proteins with increased or decreased abundance following VPA exposure including pathways relevant to the mechanisms of differentiation, tissue polarity, and growth/proliferation.

3) Chapter 5 developed an integrative omics analysis incorporating data on protein quantity and redox modifications across developmental time and space. By combining

protein oxidation and protein abundance data sets and looking for patterns in the enrichment of developmentally relevant pathways a timeline of VPA perturbations was developed that summarizes the tissue and mechanism specific effects of VPA across the time course. This timeline of VPA perturbations can serve as a blueprint for future studies in evaluating VPA's effects on the organogenesis-stage mouse conceptus in causing NTDs.

Further conclusions of VPA's effects on the organogenesis-stage mouse conceptus can be categorized as temporal, spatial, or systems-wide.

Temporal

Temporality was an important aspect in the design of this study. Unlike during adulthood, where systems work to maintain a continuous homeostasis, development is a period of the lifecycle with frequent and dynamic shifts in biological activity, cell differentiation, and growth. Therefore, to understand the role of VPA in causing NTDs, it was essential to evaluate the effects of VPA as a time course because even a few hours in developmental time can make a sizable difference in the physiological and morphological response to a toxicant. Figure 6-1 summarizes the GD 8 mouse conceptus's VPA response through measurement of whole conceptus Cys oxidation, and tissue specific cellular GSH redox potential (E_h) and protein abundance.

Reversible Cys oxidation differentially affected control and VPA-treated proteins most significantly at 2 and 10 hrs with over 30% of proteins showing an increased or decreased Cys oxidation response compared to the control (Figure 6-1). The percent of proteins with differential

Cys oxidation status decreased substantially at 4 hrs and then followed a trend of modest increase up through 10 hrs to again reach the levels seen at 2 hrs. Interestingly the timing of the increases in oxidation do not show a direct correlation with cellular GSH E_h. For example: at both 2 and 4 hrs, the VPA-treated VYS is oxidized compared to the control, while the EMB is only oxidized in response to VPA at 4 hrs. The differential Cys oxidation status in the whole conceptus, however, is much higher at 2 hrs where there is a lower oxidative burden in the combined EMB and VYS compared to 4 hrs where both tissues exhibited cellular oxidation. These findings indicate that cellular GSH E_h is only one aspect of the full redox environment of an organism or tissue and that VPA can independently affect redox at the cellular or protein level.

Patterns of protein abundance were strongly associated with time. At 2 and 4 hrs in the VYS, ~22 and 33% of proteins, respectively, were changed in abundance compared to the control following VPA exposure (Figure 6-1). From 6-10 hrs, however, there were fewer than 5% of proteins changed in abundance in the VYS. Conversely, changes to protein abundance in the EMB were highest at 6 and 10 hrs, affecting ~20 and 25% of proteins, whereas the EMB showed little change at 2, 4, and 8 hrs.

Figure 6-2 reveals the recurrently enriched developmentally relevant protein pathways at each time point, which further reveals temporal patterns in the response to VPA. Certain pathways including keratinocyte development, nervous system development, TOR signaling, epidermal cell differentiation, osteoclast differentiation, and stem cell differentiation show at least once continuous streak of enrichment over 2 or more time points, however, all of the other enriched pathways are either enriched at non-sequential timepoints or show changes in the directionality of their enrichment over time.

Spatial

Considering the developing mouse conceptus as multiple embryonic compartments rather than a single entity was one of several innovative strategies utilized in this dissertation. The compartmental redox state of the conceptus was defined in two tissue (EMB and VYS) and two fluid (YSF and AF) compartments, while protein abundance was analyzed for EMB versus VYS. In the previous section, the tissue-specific patterns of protein abundance were discussed highlighting the early (2-4 hr) VYS response to VPA compared to the later (6/10 hr) EMB response to VPA. Figure 6-2 highlights the differential enrichment of developmentally relevant pathways in the EMB versus VYS. The directionality of the protein abundance changes induced by VPA exposure is evident in the VYS. The VYS is only enriched for recurrent developmental pathways with increased abundance at 4 hrs, with all other enrichment in pathways with decreased abundance. Epithelial cell differentiation, stem cell differentiation, Wnt signaling, osteoblast differentiation, and keratinocyte differentiation are all exclusively enriched for increased or decreased proteins in the VYS. All other enriched VYS pathways, showed time-specific directional changes in abundance. The EMB was enriched only for pathways with decreased protein abundance at 2 and 4 hrs. In contrast, there was almost exclusive enrichment of pathways with increased protein abundance from 6-10 hrs with the exception of osteoblast differentiation at 6 hrs. Compared to the VYS, the EMB was enriched for fewer pathways with continuous, sequential enrichment, but also had fewer pathways that shifted their directional response to VPA over time. Of the eleven unique developmental pathways with recurrent enrichment in the EMB, only two, developmental growth and epidermal development, showed a shift in directionality from lower to higher abundance.

Compartmental GSH E_h of the VYS and EMB rarely exhibited concurrent directionality in their responses to VPA compared to the control. Of the five time points in Figure 6-2, only 4 and 10 hrs show higher simultaneous oxidation in the EMB and VYS. At 2, 6, and 8 hrs, the VPA-treated EMB is reduced compared to the control, while the VYS is oxidized. These results demonstrate that response to VPA is dependent on the target tissue and that each of these tissues may hold a unique role in VPA teratogenesis.

Systems-wide/Integrative

As a whole, these results demonstrated that VPA causes time and tissue-sensitive changes to cellular redox and protein oxidation. Interestingly, only a few proteins experienced changes in protein redox state and protein abundance, indicating that VPA's ability to alter the redox environment is not the only mechanism at play in the etiology of NTDs and that most of the changes to protein abundance are occurring independently of redox status or are indirectly distanced from redox-regulated events. The large number of developmental pathways affected in abundance by VPA exposure, suggest an important role for VPA's function as an HDAC inhibitor, which has previously been shown to affect pluripotency of embryonic stem cells (Hezroni et al., 2011). The unique results of protein abundance and protein oxidation experiments, therefore, indicate that NTD outcomes may arise due to a combinatorial effect of separate and unique changes to protein oxidation and protein abundance. Figure 6-3 further collapses and categorizes the developmental pathways highlighted in Figure 6-2 to provide a summary of the mechanisms that this dissertation has proposed as potential mechanisms disrupted by VPA that could affect neural tube closure. The processes that have proved sensitive to VPA exposure include the following: growth, differentiation, Wnt/planar cell polarity (PCP) signaling, oxidation-reduction process, cellular redox, and nervous system development

(including cytoskeletal dynamics). Two of these proposed mechanisms, Wnt/PCP signaling and oxidation-reduction process showed differential responses between control and VPA-treated samples in terms of protein abundance and protein oxidation (Figure 6-3). The dual effect of VPA on these pathways emphasizes the importance of using an integrative experimental approach to understanding VPA's effects on a system. Future studies should focus on specifically defining VPA's effects on these pathways through targeted molecular and proteomic studies of specific gene and protein targets. The interplay of these processes under normal and VPA-perturbed conditions should also be evaluated further to gain a better understanding of VPA's effects at a systems biology, rather than, a pathway level.

Significance

This study of VPA's effects on cellular redox, protein abundance, and reversible Cys oxidation in the context of mouse organogenesis has contributed many significant findings to the understanding of VPA teratogenesis and more broadly the organogenesis-stage mouse conceptus. These findings include:

VPA's Mechanism

- VPA's effects on the cellular GSH redox potential are dependent on tissue and time. The EMB proper was the least affected by fluctuations in cellular GSH redox potential, despite being the tissue of origin for neural tube defects.
- VPA produces selective alterations to the state of reversible Cys oxidation in proteins with a recurrent impact on the specific processes/pathways of cell polarity and nervous system development.

- Cellular redox status does not directly correlate with levels of Cys oxidation indicating independent mechanisms for VPA's effects on cellular and protein redox state.
- Differentiation, growth, Wnt signaling, tissue polarity, and oxidation-reduction processes were all impacted by tissue-specific changes in protein abundance in response to VPA. These processes all contribute significantly to the successful process of neurulation in the developing embryo and the complete closure of the neural tube.
- Few proteins were differentially affected by changes to abundance and oxidation. This may indicate separate, parallel mechanisms of VPA's response. Due to the very large number of proteins, pathways, and associated genes involved in the complete process of neurogenesis and neural tube closure it is expected that numerous secondary and tertiary regulator events are overlapping to affect outcomes that would be difficult to assess in terms of protein oxidation or abundance changes.

The Mouse Conceptus

- The EMB proper and VYS of the GD 8 mouse conceptus respond independently to VPA as measured by cellular GSH redox potential and protein abundance. Based on the findings of this dissertation and many other observations from the emerging field of redox signaling and control, we would expect that the constellation of individual proteins within their respective biological pathways would exhibit profound differences in differential oxidation for the greater than 200,000 reversibly oxidizable Cys loci, based on their respective differences structure and microenvironment. Although, great progress is being made in understanding factors within the microenvironment that serve to differentiate the Cys redox response to affect signaling, much less is known about the broader environmental and chemical signals that act far upstream to initiate and direct the

execution of the genomic developmental program. The structural anatomy of the mouse conceptus consists of a developing embryo proper surrounded by a trophoblast-derived VYS which is physiologically inseparable from the EMB through shared vascular, nutritional, metabolic, and signaling connections. It has been proposed that the process of development, specifically, and of reproduction, more generally, have evolved to be initiated and subsequently regulated by the conceptal/embryonic environment and represent the logic behind a *Redox Theory of Development* (Hansen et al., 2020). Within this theory, the VYS has been identified as the critical environmental interface that senses ambient conditions and transmits regulatory signals to the embryo. This spatial and temporal relationship between the VYS and EMB is also critical for mediating the perturbations produced by chemical toxicants such as VPA. Therefore, we can expect independent responses of VYS and EMB to VPA in terms of altered redox potential and protein abundance.

- There are temporal differences in response to VPA with the VYS responding earlier than the EMB. The discovery in this dissertation of protein abundance enrichment and discreet changes in redox states occurring in the VYS at the earliest time points (2 and 4 hrs) before any similar changes in the EMB were observed is significant. It asserts that the earliest developmental source of regulatory stimuli and signals that initiate critical processes in the EMB, such as neurulation and neural tube closure may originate in the tissues of the VYS and not within the embryo itself. Within the limited temporal window that we have investigated in the present report, we have observed a decreased developmental pathway protein enrichment in the VYS at 2 hr, followed by an increased enrichment of most of the same proteins at 4 hr and then a mixed enrichment of increased

and decreased abundance in the EMB at 6 hr. Of interest to the study of birth defects is the fact that this apparent switch from VYS to EMB control occurs during the peak times of sensitivity for eliciting anatomical and functional birth defects with chemicals and environmental perturbations.

Toxicological

- Timing and/or length of exposure to a toxicant defines the response. Toxicological assessment of developmental exposures should utilize multiple temporal endpoints to ensure identification of windows of sensitivity due to the highly dynamic and time-specific processes of development.
- Valproic acid exposure (600 μM) of rodent embryos in whole embryo culture, as a single dose, has been shown to elicit a full spectrum of failed neural tube closure when given during the 0 hr to 2 hr phase of early organogenesis (4-8 somites) (Harris et al., 1988). Administration of the same VPA concentrations during the 4 hr-6 hr phase caused no observable toxicity and resulted in normal neural tube closure (Harris et al., 1988). The results of this dissertation are in line with these results and may suggest that developmental pathways of planar cell polarity, actin cytoskeleton, differentiation, and growth may be more selectively sensitive to the effects of VPA exposure than the more general pathways affecting growth and viability later on. Although not addressed in this dissertation, questions of how maternal metabolism and toxicokinetics affect VPA's toxicity should be considered. These considerations would include an understanding of maternal and conceptal metabolism and their effects on the concentration of VPA that reaches the conceptuses. VPA is a fatty acid that is predominately protein bound leading to a low clearance rate of 6-20 ml/h/kg (Ghodke-Puranik et al., 2013). The main routes of

VPA metabolism include: glucuronidation, β-oxidation in the mitochondria and cytochrome P-450 mediated oxidation (Ghodke-Puranik et al., 2013). An analysis of VPA's stability in culture and ability to reach the embryo proper found that VPA's concentration in serum was stable over the course of 48 hrs in culture for a GD 9.5-11.5 rat conceptus (H. Nau et al., 1988). In addition to being measured in the culture serum, VPA was also present in the embryo, membranes, and sub-embryonic fluid under conditions of the 300 of 600 μM *in vitro* dose (H. Nau et al., 1988). Given that the longest duration of a VPA exposure used in this dissertation was 24 hrs at a 600 μM concentration, it is therefore safe to assume that VPA was present in culture and able to reach the cultured conceptuses for the entirety of the culture period.

This still leaves the open question of whether an *in vitro* dosing strategy is comparable to the effects of *in vivo* maternal dosing. In Sprague-Dawley rats compared to humans, it is known that the half-life of VPA is considerably different at 0.3-4 hrs and 9 to 18 hrs, respectively (Binkerd, 1988). Due to the short half-life of *in vivo* VPA administration in rodents, the extended life of *in vitro* VPA dosing might more closely approximate what is happening under human conditions. There have been efforts to maintain a stable plasma concentration of VPA in rodents, but these experiments require constant administration and a higher dose than it takes to see effects under *in vitro* conditions (H. Nau et al., 1981; Heinz Nau, 1985). In addition to differences in dosing required for an *in vitro* vs *in vivo* VPA exposure, it has been demonstrated that VPA shows greater teratogenicity than its metabolite (2-en-VPA) indicating that a slower rate of metabolism as indicated by the human VPA half-life and *in vitro* dose stability may be necessary for teratogenic outcomes (Lewandowski et al., 1986).

Innovation

In the field of developmental biology reductionist, bottom-up approaches are most commonly used to explore questions of developmental origin. This dissertation utilized an innovative proteomics technology to study changes to the developmental mouse proteome in terms of reversible Cys oxidation and protein abundance over time. The major advantage of this experimental strategy was that instead of targeting a small number of genes or proteins with known associations with VPA, we were instead able to generate a database of thousands of protein targets of VPA. Many of these identified proteins were associated with biological processes and pathways with known relevance to development, neural tube closure, or VPA exposure, which allowed us to propose these processes as potential mechanisms of VPA-induced NTD teratogenesis (Figure 6-3). Some of these proposed mechanisms have been the subject of significant research studies linking the biological process to NTD outcomes or VPA exposure; but for some, the mechanistic connection between exposure and outcome is not yet clear. The proteomics level data is, therefore, only able to aid in generating new hypotheses regarding the interplay of these pathways with VPA exposure and NTD occurrence. The remaining proteins and pathways that were not directly relevant to developmental processes were not analyzed in depth in this dissertation, but the data generated through these experiments may prove useful in defining VPA's effects of more general biological processes such as metabolism, transport, and gene/protein expression.

This project was also innovative through the assessment of the mouse conceptus as separate tissue and fluid compartments and in demonstrating the importance of the VYS to embryonic development. In the study of rodent conceptuses, the VYS is often discarded or analyzed jointly with the EMB. Despite differing anatomy of the VYS between rodents and

humans, the role of the VYS as a mediator of histiotrophic nutrition is shared and remains the main source of embryonic nutrition throughout the period of neurulation and organogenesis in both species (Zohn & Sarkar, 2010). Our cellular redox and protein abundance data clearly illustrate that the VYS responds to VPA independently of the EMB in terms of windows of sensitivity and affected pathways and many pathways of relevance to neural tube closure were identified in the VYS, despite the morphological process of closure occurring exclusively in the EMB proper. These findings suggest that in addition to the accepted roles of the VYS in hematopoiesis, angiogenesis, and histiotrophic nutrition, that the VYS may play a role in protein synthesis and transport as well as response to external stressors.

Another innovation in this dissertation was the time course assessment of VPA. While the time course analysis on its own, is not necessarily an innovative experimental design, there are few studies encompassing the period of mouse organogenesis that have taken as many finely spaced measurements of multiple outcomes as were completed in this study. Through these observations, we can begin to better appreciate the rapidity with which molecular, biochemical, and physiological events transpire during organogenesis, and the logistical difficulties that are created for our ability to understand mechanisms. The temporal aspects of this dissertation were instrumental in understanding VPA's effects on development. Within each measured outcome, there were periods of higher and lower sensitivity to VPA. Had this research been conducted at only a single time point, the results and conclusions would have been greatly impacted. While toxicological assessments during adulthood may not be as deeply affected by the issue of temporality, this study has demonstrated that the developmental period is highly sensitive to time and that toxicological assessments during this period should be conducted with multiple temporal endpoints.

Future Considerations

The experiments performed in this dissertation were all conducted as mouse whole embryo culture (mWEC) experiments on GD 8-9 mouse conceptuses and all VPA exposures were conducted as *in vitro* dosing directly in the culture serum of the conceptuses. While this dosing strategy is a common, accepted practice of mWEC technique, it is a limitation in applying these results to human pregnancy due to the differences in metabolism, time duration of embryogenesis, and anatomical structure. Further molecular and systems-level investigations of the critical affected proteins and pathways identified in this work should significantly assist in the efforts to answer these questions.

One general question of interest that arose throughout this study is whether the changes to cellular and protein redox states and protein abundance are an adverse reaction of VPA exposure or an adaptive or artifact response. In toxicology, an adverse outcome is generally considered one in which harm to the test subject is present (Pandiri et al., 2017). In the case of a developmental study, "harm" may encompass endpoints such as embryotoxicity, morphological or physiological abnormalities. Due to the limited duration of this study examining only organogenesis stage conceptuses it is difficult to determine whether the specific changes to cellular redox, protein abundance, or protein oxidation definitively caused harm to the developing mouse conceptuses. Under an additional working definition of adversity for non-clinical studies developed by the European Society of Toxicologic Pathology (ESTP), an adverse effect is defined as, "a test item-related change in the morphology, physiology, growth, development, reproduction or life span of the animal model that likely results in an impairment of functional capacity to maintain homeostasis and/or an impairment of the capacity to respond to an additional challenge," (Palazzi et al., 2016). This more flexible definition of adversity

makes it easier to define disruptions in developmental process as adverse events since the downstream morphological and physiological outcomes are not necessary for making the call.

Events caused by VPA exposure that are not believed to fall under the definition of an adverse outcome may be non-adverse, adaptive, an artifact, or a combination of more than one of these categories. One definition of an adaptive response from the Health and Environmental Science Institute (HESI) was, "the process whereby a cell or organism responds to a xenobiotic so that the cell or organism will survive in the new environment that contains the xenobiotic without impairment of function," (Keller et al., 2012). An example of how this definition of adaptive responses may fit in the context of our data could be the changes in abundance of the oxidation-reduction pathway. The main hypothesis of this dissertation was that VPA was acting through a redox mechanism to cause NTDs. In Chapter 4, we saw that VPA caused time and tissue-specific increases and decreases of the oxidation-reduction pathway which rather than being an adverse reaction of VPA exposure, may be considered an adaptive response to help the shift the redox state back to homeostatic conditions. Unfortunately, due to the systems biology level framework used to assess VPA's effects on the GD 8 mouse conceptus, it is difficult to definitively categorize the effects seen in this study as adverse, non-adverse, or adaptive. Additional mechanistic studies should be completed to determine whether the alterations to cell polarity, oxidation-reduction, Wnt signaling, differentiation, and growth/proliferation might lead to disruption of developmental processes.

The wide breadth of data obtained through proteomic evaluation of protein abundance and protein oxidation in response to VPA identified hundreds of contender pathways for VPA's mechanism of neural tube teratogenesis. One advantage of systems level methodology, such as

this is the ability to not only test known hypotheses for VPA's disruption of neural tube closure, but also to generate additional hypotheses related to neural tube closure and other physiological processes. The proposed mechanisms for VPA-disrupted development highlighted in Figure 6-3 should be followed up through methods such as knockout models or protein immunoprecipitation to verify the timing and findings seen in this study. While many of these pathways, with the exclusion of Wnt/Cell polarity and oxidation-reduction, were only affected by a single measurement of disruption (reversible Cys oxidation or protein abundance), these pathways might be affected by more than one method of disruption. For this reason, complementary omics methodology such as RNAseq may also be applied to this question to confirm proteomics findings in addition to applying other methods for measuring specific types of reversible and irreversible Cys oxidation. Together these methods will aid in determining whether protein abundance is being affected through pre- or post-transcriptional regulators of protein expression and whether VPA favors a particular type of oxidative Cys modification.

IodoTMT labeling demonstrated the varying levels of reversible oxidative post-translational modifications of Cys in response to VPA exposure, however we were unable to distinguish between the classes of reversible oxidative PTMs. Future studies should utilize labeling processes that differentiate by modification type to understand whether VPA specifically affects one type of modification over another. Some examples of labels that may serve this purpose through western blot or proteomic applications include: BioGEE (S-glutathionylation), DCP-bio1/DCP-rho1 (sulfenic acid), and dimedone (sulfenic acid) (Klomsiri et al., 2010; Martínez-Acedo et al., 2014; Sullivan et al., 2002). Further research also needs to be done to perform an in-depth characterization of the control-state of the oxidative Cys proteome in the developing mouse conceptus, which will eventually allow for a better understanding of

how this control-state is perturbed following toxicant exposures. Current work is underway to accomplish this goal using cysteine-reactive phosphate tags (CPT) which can be used to label reversible cysteine modification using similar methodology to the IodoTMT experiments presented in Chapter 3. The usage of CPT labels in lieu of IodoTMT for the characterization of the control-state Cys proteome is due to the substantial improvements in proteome coverage demonstrated with CPT labels through the use of immobilized metal affinity chromatography (IMAC) to selectively enrich for the phosphorylated CPT labels with up to a 99% yield (Xiao et al., 2020). This outcome has been demonstrated through the use of CPT labels to characterize the reversible oxidative Cys proteome in young and aging mice, where over 9,400 proteins and 34,000 unique cysteine sites were identified providing the most in-depth quantitative analysis of the redox-regulated Cys proteome to date (Xiao et al., 2020). Utilizing this labeling strategy over the course of mouse development would vastly improve the level of detail currently available regarding protein Cys-level redox regulation in the mouse which could then be compared across mouse lifecycle stages from the embryonic through aging period using the Oximouse database (Xiao et al., 2020). The significantly greater magnitude of detail provided through this labeling strategy would be instrumental in defining the role of Cys-mediated redox signaling across the lifecycle (Go et al., 2015; Xiao et al., 2020).

A final future direction would be to further characterize tissue differences by analyzing separate tissue, organ, or cell types within the EMB proper. This dissertation provided strong evidence for the differences in the VYS and EMB responses to VPA, but it is not yet known whether specific organs, tissues, or cell types uniquely respond over developmental time. In assessing the teratogenicity of VPA, it would be especially compelling to isolate developing neural tissue to see whether VPA has differential effects on this target tissue compared to the

EMB as a whole. A temporal evaluation of VPA's effects of species-specific Cys oxidation paired with protein abundance in neural tissue pre and post NT closure may help to more specifically define the mechanisms proposed in Figure 6-3 and test their specific relevance to neural tube closure. The enrichment of Wnt signaling and cell polarity-based pathways in protein abundance and Cys oxidation results and the known connection of these pathways to the process of convergent extension makes these pathways strong contenders for further evaluation in the context of neural tissue. Timing of VPA exposure and its associated outcomes over developmental time can also be expanded through future work. This dissertation focused on the period of organogenesis due to sensitivity during this time for birth defects with dosing and measurement limited to this small window of time. In human pregnancy, gestational VPA exposure does not occur in the form of an acute, single dose exposure, but rather through repeated exposure for the duration of the pregnancy in some cases. For this reason, it would be interesting to apply a study of repeated, *in vivo* dosing of VPA throughout mouse development to see whether the addition of maternal metabolism and repeat dosing changes the outcomes measured in this study. Periods of interest to study in this context could include the GD 7 pre-organogenesis EMB, the GD 9 post-organogenesis EMB, and the neonatal mouse pup.

Overall, it is clear that VPA differentially targets the organogenesis-stage EMB and VYS through time and tissue-specific alterations to cellular redox, reversible Cys oxidation, and protein abundance. The combinatorial downstream effects of these changes on developmental pathways of recurrent enrichment (Figure 6-2) are likely to contribute to VPA's mechanism of failed neural tube closure. In the context of the organogenesis-stage mouse conceptus, we propose that VPA's mechanism of action in causing NTDs is related to temporal and spatial disruption of pathways related to embryonic growth, oxidation-reduction process, Wnt/PCP

signaling, cellular differentiation, and cytoskeletal dynamics of nervous system development. Our original hypothesis postulated that selective protein oxidation caused by VPA-induced ROS generation would disrupt normal redox signaling and control and that this would be the major factor in mechanisms of failed neural tube closure. We instead found that events involving oxidative PTMs of protein Cys are likely, but that other redox-independent stimuli are also in play.

Figures

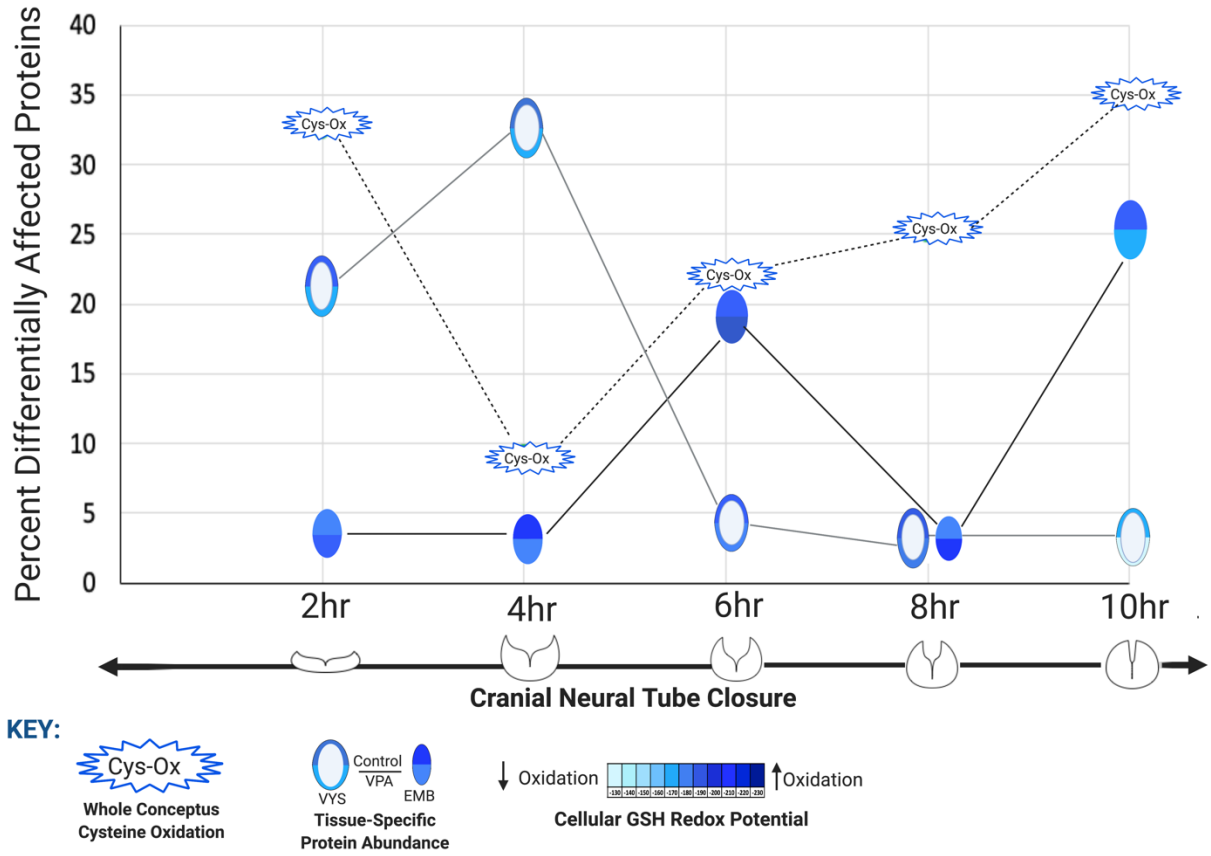

Figure 6-1 Quantitative patterning of cellular redox, protein abundance, and Cys oxidation: This figure summarizes the temporal responses of the whole conceptus or EMB and VYS to changes in cellular glutathione (GSH) redox potential, protein abundance, and reversible oxidative modification of Cys. The GSH E_h is displayed separately for EMB and VYS with a horizontal division dividing the upper control E_h from the lower VPA E_h. Protein abundance was evaluated in EMB and VYS. The percent of proteins within each tissue-specific data set that were differentially increased or decreased following VPA exposure compared to the control it noted by placement of the EMB or VYS symbol at the appropriate percentage. The percent of proteins that showed differential Cys oxidation at each time point is noted by the Cys-Ox symbol. For both protein abundance and Cys oxidation, the direction of change is not indicated, but rather a summary value of the total percentage of proteins at each time point that was increased or decreased in abundance or oxidation. Figure created using Biorender.com

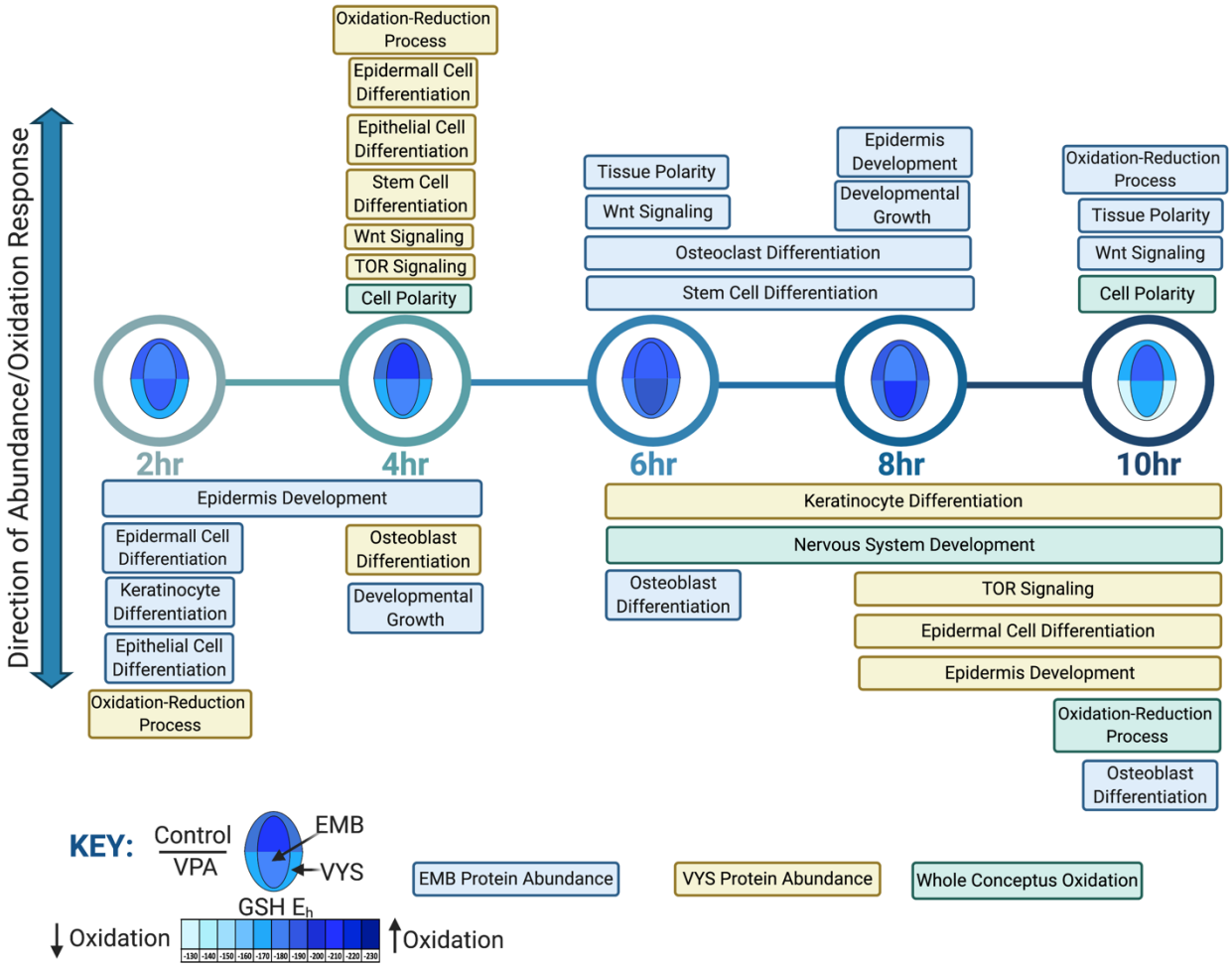

Figure 6-2 Summary timeline of recurrent VPA perturbation events: Timeline of developmental VPA perturbation events categorized by directional change and tissue. Displayed pathways showed recurrent enrichment related to protein abundance or oxidation. Protein abundance and cellular GSH E_h are tissue-specific and protein oxidation is for whole conceptus. Cellular GSH E_h is displayed as a split bubble model of the mouse conceptus with the outer ring representing the VYS and the inner oval representing the EMB proper. The horizontal dividing line separates the upper control measurement from the lower VPA measurement. Adapted from "Timeline (5 Segments, Horizontal)", by BioRender.com (2020). Retrieved from https://app.biorender.com/biorender-templates

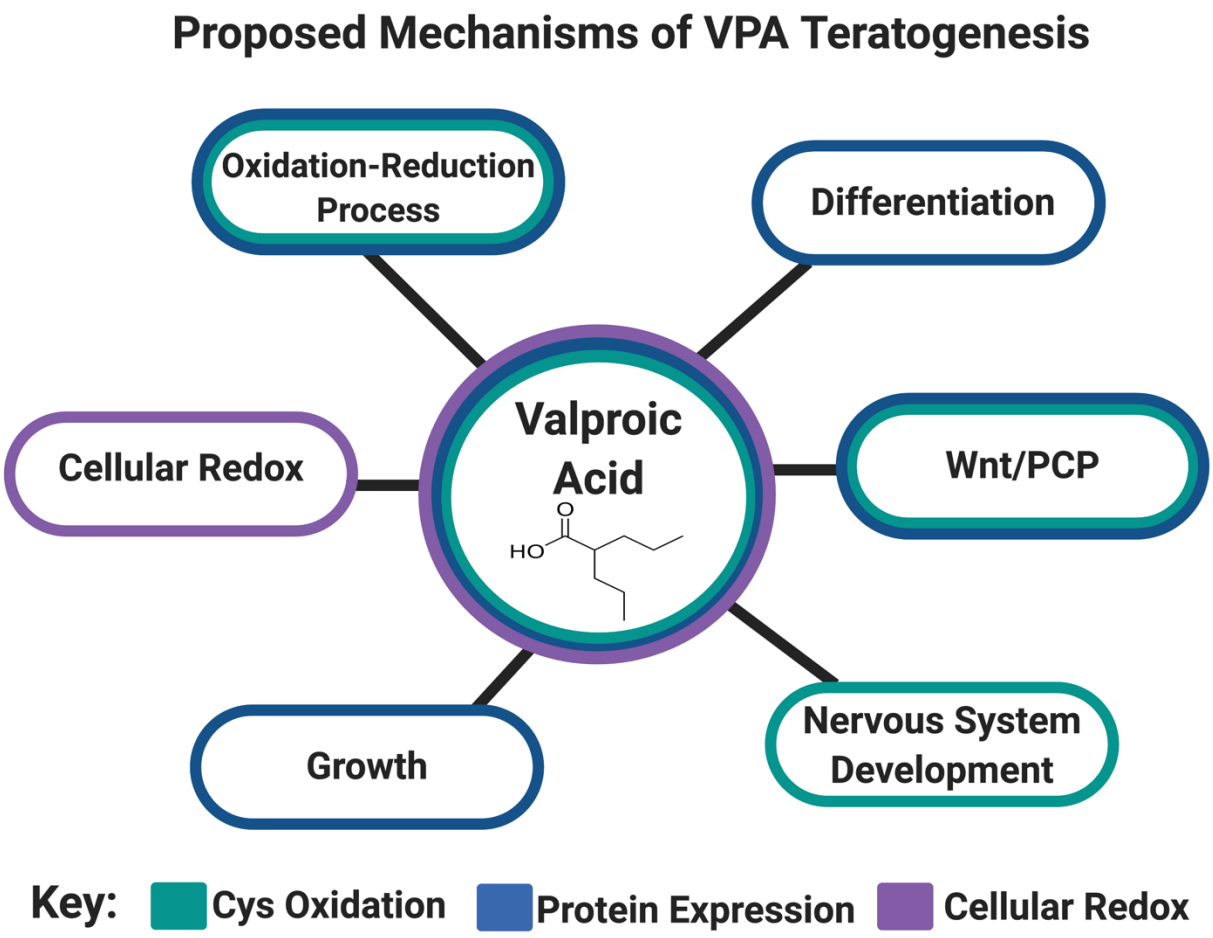

Figure 6-3 Proposed mechanisms of VPA teratogenesis: The systems-level analysis of the effects of VPA on the organogenesis stage mouse conceptus revealed several recurrent pathway themes that are proposed as likely targets of VPA teratogenesis implicated in neural tube defects. Each proposed mechanism was identified as being differentially affected by VPA in relation to reversible Cys oxidation status, protein expression, or cellular redox. The directional changes and affected time and tissues are noted in Figure 6-2. Created with Biorender.com

References

Binkerd, P. (1988). Evaluation of valproic acid (VPA) developmental toxicity and pharmacokinetics in Sprague-Dawley rats. *Fundamental and Applied Toxicology*, *11*(3), 485–493. https://doi.org/10.1016/0272-0590(88)90112-1

Ghodke-Puranik, Y., Thorn, C. F., Lamba, J. K., Leeder, J. S., Song, W., Birnbaum, A. K., Altman, R. B., & Klein, T. E. (2013). Valproic acid pathway: Pharmacokinetics and pharmacodynamics. *Pharmacogenetics and Genomics*, *23*(4), 236–241. https://doi.org/10.1097/FPC.0b013e32835ea0b2

Go, Y.-M., Chandler, J. D., & Jones, D. P. (2015). The cysteine proteome. *Free Radical Biology and Medicine*, *84*, 227–245. https://doi.org/10.1016/j.freeradbiomed.2015.03.022

Hansen, J. M., Jones, D. P., & Harris, C. (2020). The Redox Theory of Development. *Antioxidants & Redox Signaling*, *32*(10), 715–740. https://doi.org/10.1089/ars.2019.7976

Harris, C., Stark, K. L., & Juchau, M. R. (1988). Glutathione status and the incidence of neural tube defects elicited by direct acting teratogens in vitro. *Teratology*, *37*(6), 577–590. https://doi.org/10.1002/tera.1420370607

Hezroni, H., Sailaja, B. S., & Meshorer, E. (2011). Pluripotency-related, Valproic Acid (VPA)-induced Genome-wide Histone H3 Lysine 9 (H3K9) Acetylation Patterns in Embryonic Stem Cells. *Journal of Biological Chemistry*, *286*(41), 35977–35988. https://doi.org/10.1074/jbc.M111.266254

Jones, D. P. (2006). Redefining Oxidative Stress. *Antioxidants & Redox Signaling*, *8*(9–10), 1865–1879. https://doi.org/10.1089/ars.2006.8.1865

Keller, D. A., Juberg, D. R., Catlin, N., Farland, W. H., Hess, F. G., Wolf, D. C., & Doerrer, N. G. (2012). Identification and Characterization of Adverse Effects in 21st Century Toxicology. *Toxicological Sciences*, *126*(2), 291–297. https://doi.org/10.1093/toxsci/kfr350

Klomsiri, C., Nelson, K. J., Bechtold, E., Soito, L., Johnson, L. C., Lowther, W. T., Ryu, S.-E., King, S. B., Furdui, C. M., & Poole, L. B. (2010). Use of Dimedone-Based Chemical Probes for Sulfenic Acid Detection. In *Methods in Enzymology* (Vol. 473, pp. 77–94). Elsevier. https://doi.org/10.1016/S0076-6879(10)73003-2

Lewandowski, C., Klug, S., Nau, H., & Neubert, D. (1986). Pharmacokinetic aspects of drug effects in vitro: Effects of serum protein binding on concentration and teratogenicity of valproic acid and 2-en-valproic acid in whole embryos in culture. *Archives of Toxicology*, *58*(4), 239–242. https://doi.org/10.1007/BF00297113

Martínez-Acedo, P., Gupta, V., & Carroll, K. S. (2014). Proteomic analysis of peptides tagged with dimedone and related probes: Proteomics insights into dimedone-labeled peptides. *Journal of Mass Spectrometry*, *49*(4), 257–265. https://doi.org/10.1002/jms.3336

Nau, H., Lewandowski, C., Klug, S., & Neubert, D. (1988). Pharmacokinetic aspects of drug effects in vitro (II) placental transfer to the embryo and activity of some carboxylic acids structurally related to valproic acid in whole embryos in culture. *Toxicology in Vitro*, *2*(3), 169–174. https://doi.org/10.1016/0887-2333(88)90004-5

Nau, H., Zierer, R., Spielmann, H., Neubert, D., & Gansau, Ch. (1981). A new model for embryotoxicity testing: Teratogenicity and pharmacokinetics of valproic acid following constant-rate administration in the mouse using human therapeutic drug and metabolite concentrations. *Life Sciences*, *29*(26), 2803–2813. https://doi.org/10.1016/0024-3205(81)90541-5

Nau, Heinz. (1985). Teratogenic valproic acid concentrations: Infusion by implanted minipumps vs conventional injection regimen in the mouse. *Toxicology and Applied Pharmacology*, *80*(2), 243–250. https://doi.org/10.1016/0041-008X(85)90081-X

Palazzi, X., Burkhardt, J. E., Caplain, H., Dellarco, V., Fant, P., Foster, J. R., Francke, S., Germann, P., Gröters, S., Harada, T., Harleman, J., Inui, K., Kaufmann, W., Lenz, B., Nagai, H., Pohlmeyer-Esch, G., Schulte, A., Skydsgaard, M., Tomlinson, L., … Yoshida, M. (2016). Characterizing "Adversity" of Pathology Findings in Nonclinical Toxicity Studies: Results from the 4th ESTP International Expert Workshop. *Toxicologic Pathology*, *44*(6), 810–824. https://doi.org/10.1177/0192623316642527

Pandiri, A. R., Kerlin, R. L., Mann, P. C., Everds, N. E., Sharma, A. K., Myers, L. P., & Steinbach, T. J. (2017). Is It Adverse, Nonadverse, Adaptive, or Artifact? *Toxicologic Pathology*, *45*(1), 238–247. https://doi.org/10.1177/0192623316672352

Sies, H., Berndt, C., & Jones, D. P. (2017). Oxidative Stress. *Annual Review of Biochemistry*, *86*(1), 715–748. https://doi.org/10.1146/annurev-biochem-061516-045037

Sullivan, D. M., Levine, R. L., & Finkel, T. (2002). Detection and Affinity Purification of Oxidant-Sensitive Proteins Using Biotinylated Glutathione Ethyl Ester. In *Methods in Enzymology* (Vol. 353, pp. 101–113). Elsevier. https://doi.org/10.1016/S0076-6879(02)53040-8

Xiao, H., Jedrychowski, M. P., Schweppe, D. K., Huttlin, E. L., Yu, Q., Heppner, D. E., Li, J., Long, J., Mills, E. L., Szpyt, J., He, Z., Du, G., Garrity, R., Reddy, A., Vaites, L. P., Paulo, J. A., Zhang, T., Gray, N. S., Gygi, S. P., & Chouchani, E. T. (2020). A Quantitative Tissue-Specific Landscape of Protein Redox Regulation during Aging. *Cell*, *180*(5), 968-983.e24. https://doi.org/10.1016/j.cell.2020.02.012

Zohn, I. E., & Sarkar, A. A. (2010). The visceral yolk sac endoderm provides for absorption of nutrients to the embryo during neurulation. *Birth Defects Research Part A: Clinical and Molecular Teratology*, *88*(8), 593–600. https://doi.org/10.1002/bdra.20705